The Structure and Performance of Collagen Biomaterials

A thesis presented in partial fulfilment of the requirements for the degree of

Doctor of Philosophy

In

Engineering

Massey University, Palmerston North, New Zealand

Hannah Wells

2016

Abstract

Type I collagen materials are used in a wide range of industrial applications. Some examples include leather for shoes and upholstery, acellular dermal matrix (ADM) materials for surgical applications, and bovine pericardium for the fabrication of heart valve replacements. The structure of these materials is based on a matrix of collagen fibrils, largely responsible for the physical properties and strength of the materials. How the collagen fibrils themselves contribute to the overall bulk properties of these materials is not fully understood.

The first part of this work investigates a collagen structure defect in leather, known as looseness. Looseness occurs in around 5-10% of bovine leather, and is a result of the collagen fibril layers separating during processing from raw skin to leather. A greater understanding of why looseness develops in leather and a method of detecting looseness early in processing is needed to save tanners a significant amount on wasted processing time and costs. In addition, an environmentally safe method of disposing of defect and waste leather is sort after since the current method of disposing to landfill is causing environmental concern due to the possibility of chromium leaching from leather into the soil as it biodegrades.

Synchrotron based small angle X-ray scattering (SAXS) revealed that loose leather has a more aligned and layered collagen fibril arrangement, meaning there is less fibril overlap, particularly in the grain-corium boundary region. This results in larger gaps in the internal structure of loose leather compared with tight. These gaps could be detected using ultrasonic imaging in partially processed pickle and wet-blue hides as well as leather. Incorporating an ultrasound system into the leather processing line could be a viable method for identifying hides deemed to develop looseness earlier in processing, and these could be diverted down a separate processing line or removed.

Disposing of waste leather by first forming biochar prior to land fill proved to be an effective way of reducing chromium from leaching into the environment. XAS revealed that heating leather to temperatures above 600°C in the absence of oxygen formed a char where chromium was bound in the stable form of chromium carbide. The stability of this structure makes chromium less available to form the toxic hexavalent form in the environment and presents a possible alternative option for environmentally safe disposal of leather.

The second part to this work looks at the correlation between collagen fibril structure in a range of biomaterials in relation to material strength. Leather, ADM and pericardium are three type I collagen based materials which rely on sufficient strength to carry out their

industrial and medical applications. These three materials were studied to try and identify collagen fibril characteristics that relate to high material strength.

SAXS on a range of leather samples from various species revealed that collagen fibril diameter had only a small influence over material strength in bovine leather, and no correlation to strength in leather from other species. Therefore it can be said that the influence of fibril orientation on leather strength takes precedence over that of fibril diameter.

Fibril diameter, d-spacing and orientation were studied in pericardium using SAXS while simultaneously applying strain. It was revealed collagen materials undergo two distinct stages of deformation when strain is applied and incrementally increased. The first stage, at low strain, involves a re-orientation of fibrils to become more aligned. When strain is increased further, the fibrils themselves take up the strain, causing fibrils to stretch and decrease in diameter. The Poisson ratio of the collagen fibrils was calculated to be 2.1 ± 0.7. This high Poisson's ratio indicates the fibrils decrease in diameter at a faster rate than they elongate with strain, and as a result the volume of the fibrils decreases. This feature of collagen could help explain some of the unique behaviours and strength of collagen based materials and could be useful for optimizing industrial applications of collagen materials.

ADM materials, derived from human, porcine and bovine skin was the third collagen material studied. SAXS revealed that each species of ADM material had a slightly different collagen fibril arrangement when viewing the samples perpendicular to the surface. Human ADM was highly isotropic in arrangement, porcine was largely anisotropic, and bovine was somewhere in between the two. Bovine has a more layered fibril arrangement edge on and was the strongest material, followed by human ADM, and porcine was significantly weaker. Bovine was also the most porous material of the three. The discovery of the variations in strength, porosity and fibril arrangement between the three types of ADM materials may help medical professionals select the most suitable material for specific surgical procedures and could lead to a greater number of successful surgeries taking place.

Acknowledgements

There are a number of people whom I would like to thank for their guidance and support during this project.

Firstly, I would like to thank my supervisor, Professor Richard Haverkamp. The advice and encouragement that Richard provided was invaluable. His knowledge in science and research is inspirational, and his enthusiasm contagious. The opportunities presented during this project were far greater than I expected, and it was through these opportunities that I was able to experience and explore science and research internationally, as well as here in New Zealand. I wish Richard the very best for future research projects, and I hope to work with him again sometime in the future.

Thank you to the New Zealand Leather and Shoe Research Association (LASRA) for co-funding the project through the grant LSRX1301, supported by the Ministry of Business, Innovation and Employment. I would like to thank Geoff Holmes, Richard Edmonds, and Sue Cooper of LASRA for providing advice and sharing their expertise in the leather industry throughout my project.

A significant portion of the synchrotron based data collection was undertaken at the Australian Synchrotron, Victoria, Australia. The SAXS work was carried out on the SAXS/WAXS beamline and Drs Nigel Kirby, Adrian Hawley and Stephen Mudie are thanked for assistance with SAXS data collection. The XAS data collection was also carried out at the Australian Synchrotron, Victoria, Australia. The NZ Synchrotron Group and the Australian Synchrotron is acknowledged for travel funding and accommodation. Katie Sizeland, Melissa Basil-Jones, Hanan Kayed, and Richard Haverkamp are thanked for their assistance in data collection for this research at the Australian Synchrotron.

SAXS data was also collected at NSRRC in Taiwan, and Dr. U-Ser Cheng is thanked for his assistance with preliminary synchrotron studies here. The Royal Society of New Zealand provided travel funding for myself to Taiwan through the Royal Society of New Zealand NZ-Taiwan Nanotechnology Research Student Travel grant.

Doug Hopcroft, Jordan Taylor and Niki Murray of the Manawatu Microscopy Centre are thanked for their assistance in TEM and SEM sample preparation and imaging.

The ultrasound device used for ultrasonic measurements during this project was the Dermascan C USB device, purchased from Cortex Technologies in Denmark. Susanne Holst

Borre and Klaus Ahlbech, Cortex Technologies, Denmark, are thanked for their assistance in creating a custom gain profile for leather and their assistance with the ultrasound measurements.

Clive Bardell and John Edwards, Massey University, are thanked for building the high-temperature reactor required for the work in chapter 4: Stabilizing Chromium from Leather Waste in Biochar.

The work for chapter 7 was supported by a grant from TEI Biosciences. Bret Jessee and Vladimir Russakovsky of TEI Biosciences provided the samples and the motivation for this work.

Sue Hallas of Nelson assisted with editing the manuscripts, chapters 1 – 7, before the manuscripts were submitted for publishing.

Lastly, I would like to thank those that supported me from outside the academia environment. Thank you to my friends, training partners and my coach, Brendan, for your support, encouragement, and friendships over the years.

To my family; Mum, Dad and Jemma, thank you for your never ending love and support and for always believing in me.

Table of Contents

List of Figures

Figure 9: a) An SEM image taken of the entire cross-sectional structure of a bovine leather sample, showing the collagen structure. Bundle size and overall structure is visible however the fibrils are too small at this magnification. Scale bar is 1 mm. B) An SEM taken at a much higher magnification of bovine leather, both collagen fibril and bundle structures can be seen. Scale bar is 10 μm.

Figure 10: Examples of images achieved using TEM of collagen within a leather sample. The figure on the left is an example of an image taken end-on to the fibrils, from which the fibril diameter can be observed. The figure on the right shows an image taken perpendicular to the long axis of the collagen fibrils, from which d-spacing can be observed. Scale bar is 500 nm.

Figure 11: A schematic demonstrating the basic idea of how ultrasound can be used to detect flaws, such as air gaps, in a material for non-destructive testing.

Figure 12: Photo of the transducer probe used for the analysis on leather and ADM materials. This transducer was purchased along with the Dermascan C USB device from Cortex Technologies in Denmark.

Figure 1.1: Comparison of the break in (a) tight leather with a break of 1 and (b) loose leather with a break of 7. Photos were taken during the break test of the concave surface of the grain). Scale bar is 2 mm.

Figure 1.2: Examples of orientation index (OI) of (a) tight leather and (b) loose leather.

Figure 1.3: Ultrasonic image of (a, c, e, g) tight leather and (b, d, f, h) loose leather (scale bar 1 mm). The grain is at the top of each image and the image was taken from the grain side. Some of the bottom part of the leather (corium) is not visible as the ultrasonic signal is greatly attenuated as it passes through the sample. Positions of these samples with their looseness scores are: tight – a (2) OSP, c (2) OSP, e (2) OSP, g (2.5) upper axilla; loose – b

(7) lower axilla, d (6) lower axilla, f (5) belly, h (6.5) lower axilla. Samples a and b are the same as those displayed in the SAXS, SEM and TEM figures below.

Figure 1.4: Representative SEM images of cross-sections of (a, c) tight and (b, d) loose leather from the grain - corium boundary region. Scale bar (a, b) is 2 mm, (c, d) 300 μm.

Figure 1.5: Representative TEM images of cross-sections though the fibre bundles of (a, b) tight leather and (c, d) loose leather. Grain (a, c) and corium (b, d). Scale bar is 5 μm.

Figure 2.1: Ultrasonic images (B-scans) of A, tight pickle, B, loose pickle, C, tight wet blue, D, loose wet blue, E, tight leather, F, loose leather. The grain is on the left, corium on the right. Scale bar is 0.5 mm. The colour scale represents signal intensity from black (minimum intensity) to white (maximum intensity).

Figure 2.2: Display of the portion with intensity below 7.8% of the maximum intensity of reflected ultrasonic signal (in red) for a selected region 0.378 mm wide (defined by the white line) at the grain. A, tight pickle, B, loose pickle, C, tight wet blue, D, loose wet blue, E, tight leather, F, loose leather. These are the same datasets as in Figure. 2.1.

Figure 2.3: A-scans of tight (solid line) and loose (dashed line) leather. Each plot is an average of 20 scans, representing a total of 1.0 mm movement across the surface of the leather. These are taken from recordings similar to, but not identical to, the images from Figure. 2.1 and 2.2, e and f.

Figure 2.4: SEM images of cross sections of tight (a, b) and loose (c, d) leather. Grain is at the top. The enlargements (b, d) are near the grain–corium boundary. Scale bar (a, c) 1 mm, (b, d) 400 μm.

Figure 3.1: Representative scattering patterns of a) poorly aligned leather with a low OI, b) leather under tension and therefore highly aligned with a high OI. 76x34 mm (300 x 300 DPI).

Figure 3.2: SAXS OI data from cross sections of loose and tight hide and leathers. a) tight pickled hide; b) loose pickled hide; c) tight wet blue; d) loose wet blue; e) tight leather; f) loose leather. The two lines in each plot represent duplicate measurements (at different positions).

Figure 3.3: d-spacing measured edge-on through cross sections of a) tight pickled hide; b) loose pickled hide; c) tight wet blue; d) loose wet blue; e) tight leather; f) loose leather. The two lines in each plot represent duplicate measurements at different positions.

Figure 3.4: OI and d-spacing measured edge-on during strain (average values). Solid lines: tight materials, dashed lines: loose. a, b) pickled hide; c, d) wet blue; e, f) leather. The two lines in each plot represent duplicate measurements at different positions.

Figure 3.5: OI and d-spacing measured normal to the surface during strain. Solid lines: tight materials, dashed lines: loose. a, b) pickled hide; c, d) wet blue; e, f) leather. The two lines in each plot represent duplicate measurements at different positions.

Figure 3.6: Illustration of the different behaviour of loose and tight leathers during processing.

Figure 4.1: XAS of standards. Cr metal (——), Cr_3C_2 (— —), $Cr(O_2C_5H_7)_3$ (▪▪▪), Cr_2O_3 (——), $CrCO_6$ (— —), $Cr_2(SO_4)_3$ (▪▪▪).

Figure 4.2: XANES of dry leather (——) and $Cr_2(SO_4)_3.xH_2O$ (——).

Figure 4.3: XANES of leather and leather biochar heated to different temperatures. Leather standard (——); heated in the large vessel: 500°C (— —), 600°C (——); heated in the small vessel: 600°C (····), 800°C (— —), 1000°C (▪▪▪▪).

Figure 4.4: XANES of standards tested for linear combination fit. $Cr_2(SO_4)_3$ (——), Cr_3C_2 (— —), Cr metal (——), Cr_2O_3 (— —).

Figure 4.5: XANES Linear combination fit of biochar prepared at a) 500°C; b) 600°C; c) 800°C; d) 1000°C. Cr_3C_2 (— —), Dry leather (— —), data (——), fit (——).

Figure 4.6: EXAFS of biochar produced at a) 800 °C; b) 1000 °C. Circles $k^2\chi(k)$, solid line fitted model.

Figure 5.1: SEM images of a) bovine and b) ovine leather, with the aligned collagen fibrils visible and organized in bundles. Figure a reproduced from *J. Agric. Food Chem.* (2011) **59**, 9972−9979 © American Chemical Society.

Figure 5.2: SAXS patterns for a) ovine and b) bovine leather, showing the region of the patterns selected for fibril diameter analysis.

Figure 5.3: SAXS profiles of examples of a) ovine leather; and b) bovine leather. The profile at two azimuthal angle ranges are shown with the solid lines at the azimuthal angle range where the D-spacing diffraction peaks are maximum (typically a range ψ = –30 to 30°) and the dashed lines at right angles to this, typically ψ = 60 to 120°. The data shown in the dashed lines represent that used for the fibril diameter analysis.

Figure 5.4: Collagen fibril diameter versus tear strength for a) ovine leather; b) bovine leather; c) a range of other animals. Bovine r^2 = 0.59, P = 0.009 (for slope); ovine r^2 = 0.0077, P = 0.75 (for slope); other animals r^2 = 0.080, P = 0.46 (for slope). Each point is the average value from 12–20 diffraction patterns.

Figure 5.5: Orientation index versus fibril diameter for a) ovine and b) bovine leather, showing a lack of correlation between these properties. Ovine r^2 = 0.011, P = 0.6747 (for slope); bovine r^2 = 0.28, P = 0.22 (for slope).

Figure 6.1: Transmission electron microscopy of pericardium.

Figure 6.2: Representative integrated scattering pattern of pericardium. Solid line – at an azimuthal angle segment centred 90°, which is used for assessing d-spacing, dashed line – at an azimuthal angle segment centred on 0°, which is used for fibril diameter.

Figure 6.3: Stress-strain curve measured on pericardium during in-situ SAXS measurements.

Figure 6.4: d-spacing (long dash, blue), fibril diameter (short dash, red) and OI (solid, green) changes with increasing strain. Lines are a guide for the eye only.

Figure 7.1: Experimental setup for SAXS analysis.

Figure 7.2: Examples of scattering patterns taken with the X-ray beam edge-on to the samples: a) fetal bovine; b) 3 mm thick neonatal bovine; c) porcine; d) human ADM materials.

Figure 7.3: Variation in intensity of the 5th diffraction peak with azimuthal angle (measured with the X-ray beam edge-on to the surface) to illustrate the nature of the fibril orientation: a) fetal bovine ADM material; b) 3 mm thick neonatal bovine; c) porcine; d) human. These plots correspond with the diffraction patterns in Fig. 39.

Figure 7.4: Variation in intensity of the 5th diffraction peak with azimuthal angle (measured with the X-ray beam edge-on to the surface) and distance through the sample (equivalent to a series of plots of the type in Fig. 3) to illustrate the nature of the fibril orientation through

the sample thickness: a) fetal bovine ADM material; b) 3 mm thick neonatal bovine; c) porcine; d) human. These plots are just for 90° either side of the origin to simplify the images because the information is duplicated in the region for 90 to 180° and -90 to -180°.

Figure 7.5: Variation in intensity of the 5th diffraction peak with azimuthal angle (measured with the X-ray beam perpendicular to the surface) to illustrate the nature of fibril orientation: a) fetal bovine ADM material; b) 3 mm thick neonatal bovine; c) porcine; d) human.

Figure 7.6: Variation in OI through the thickness of the materials: a) fetal bovine ADM material; b) 1.7 mm thick neonatal bovine; c) 2 mm thick neonatal bovine; d) 3 mm thick neonatal bovine; e) 4 mm thick neonatal bovine; f) porcine; g) human.

Figure 7.7: Variation in d-spacing through the thickness of ADM materials: a) fetal bovine; b) 1.7 mm thick neonatal bovine; c) 2 mm thick neonatal bovine; d) 3 mm thick neonatal bovine; e) 4 mm thick neonatal bovine; f) porcine; g) human.

Figure 7.8: Tear (left) and tensile (right) strength and OI for ADM materials measured with the X-ray beam edge-on to the samples. Line for linear correlation for just the neonatal bovine ADM of varying thickness (tear r^2 = 0.97, P = 0.002 for α = 0.05; tensile r^2 = 0.44, P = 0.22 for α = 0.05).

Figure 7.9: Tear (left) and tensile (right) strength and OI for ADM materials measured with the X-ray beam perpendicular to the samples. Unmarked points are bovine neonatal ADM.

Figure 7.10: Tear strength and fibril diameter. Unmarked points are bovine neonatal ADM.

Figure 7.11: Scanning electron microscopy images through the thickness of the ADM materials: a) fetal bovine; b) neonatal bovine 2 mm thick; c) neonatal bovine 3 mm thick; d) neonatal bovine 4 mm thick; e) porcine; f) human. All at the same magnification; bar is 500 μm.

Figure 7.12: Scanning electron microscopy images at higher magnification through the thickness of the ADM materials: a) porcine; b) human. Both at the same magnification; bar is 200 μm.

Figure 7.13: Illustration of the difference between ADM material that is: a) poorly oriented when measured with the X-ray beam edge-on; b) highly oriented when measured with the X-ray beam edge-on.

Figure 7.14: Illustration of the difference between ADM material that is: a) highly oriented in two orthogonal directions when measured with the X-ray beam perpendicular to the sample face, such as in porcine material; b) partly oriented when measured with the X-ray beam perpendicular to the sample face, such as in bovine material; c) largely isotropic when measured with the X-ray beam perpendicular to the sample face, such as in human material.

List of Tables

Table 11. Tensile test results for ADM materials.

Table 12. Strain (approximate) of different sample types.

Table 13. Orientation index for collagen from SAXS measured with the X-ray beam edge-on.

Table 14. Orientation index for collagen from SAXS measured with the X-ray beam perpendicular to the surface.

Table 15. Average diameter of collagen fibrils from SAXS analysis.

Table 16. Average d-spacing for collagen from SAXS analysis (on hydrated materials).

List of Publications

Published Journal Articles

1. H. R. Kayed, K. H. Sizeland, **H. C. Wells**, N. Kirby, A. Hawley, S. T. Mudie, R. G. Haverkamp. “Age differences in gluteraldehyde cross linking on collagen fibril orientation in bovine pericardium”. *Submitted to Connect Tissue Res* (**2016**).

2. **H. C. Wells**, G. Holmes, J. U-Ser, W. Wei-Ru, N. Kirby, A. Hawley, S. Mudie, R. G. Haverkamp. “A Small Angle X-ray Scattering Study of the Structure and Development of Looseness in Bovine Hides and Leather” **(2016)** *J. Sci. Agri.Food. (Preliminary acceptance).*

3. **H. C. Wells**, G. Holmes, R. G. Haverkamp “Early Detection of Looseness in Bovine Hides using Ultrasonic Imaging” *J. Am. Leather Chem. Assoc.* **(2016)** 111 (3).

4. **H. C. Wells**, K. H. Sizeland, N. Kirby, A. Hawley, S. Mudie, R. G. Haverkamp “Collagen Fibril Structure and Strength in Acellular Dermal Matrix Materials of Bovine, Porcine and Human Origin” **(2015)** *ACS Biomat. Sci. Eng.* 1 (10), 1026-1038.

5. **H. C. Wells,** G. Holmes, R. G. Haverkamp, “Looseness in bovine leather: microstructural characterization” **(2016)** *J. Sci. Food Agric.* 96 (8), 2731-2736.

6. K. H. Sizeland, **H. C. Wells,** G. Norris, R. Edmonds, N. Kirby, A. Hawley, S. Mudie, R. Haverkamp, “Collagen D-spacing and the Effect of Fat Liquor Addition” (**2015)** *J. Am. Leather Chem. Assoc.* **110** (2) 43-53.

7. **H. C. Wells**, K. H. Sizeland, H. R. Kayed, N. Kirby, A. Hawley, S. T. Mudie, R. G. Haverkamp, “Poisson's Ratio of Collagen Fibrils Measured by Small Angle X-ray Scattering of Strained Bovine Pericardium” **(2015)** *J. Appl. Phys.* **117** (4), 044701.

8. **Wells, H. C.**; Sizeland, K. H.; Edmonds, R. L.; Aitkenhead. W.; Kappen, P.; Glover, C.; Johannessen, B.; Haverkamp, R. G. (**2014**). “Stabilizing Chromium from Leather Waste in Biochar.” *ACS Sustainable Chem. Eng.* **2**: 1864-1870.

9. Sizeland, K. H.; **Wells, H. C.**; Higgins, J.; Cunanan, C. M.; Kirby, N.; Hawley, A.; Mudie, S. T.; Haverkamp, R. G. (**2014**). “Age Dependent Differences in Collagen Alignment of Gluteraldehyde Fixed Bovine Pericardium.” *BioMed Res.Int.* vol.2014, Article ID 189197, 10 pages.

10. **Wells, H. C.**; Edmonds, R. L.; Kirby, N.; Hawley, A.; Mudie, S. T.; Haverkamp, R. G. "Collagen Fibril Diameter and Leather Strength." (**2013**) *J. Agric. Food Chem.* **61** (47) ,11524-11531.

Conference Papers, Presentations and Posters

Hannah C. Wells, Katie H. Sizeland, Hanan Kayed, Nigel Kirby, Adrian Hawley, Stephen Mudie, Richard G. Haverkamp, "Poisson Ratio of Collagen Fibrils under Tension." Poster presented at The International Chemical Congress of Pacific Basin Societies, 15-20th December **2015,** Honolulu, Hawaii.

Katie H. Sizeland, **Hannah C. Wells**, John Higgins, Crystal M Cunanan, Nigel Kirby, Adrian Hawley, Stephen Mudie & Richard G. Haverkamp, "Structure and Strength of Neonatal Pericardium for Heart Valve Applications." Poster presented at The International Chemical Congress of Pacifichem Basin Societies, 15-20th December **2015**, Honolulu, Hawaii.

Richard G. Haverkamp, **Hannah C. Wells**, Katie H. Sizeland, Richard L. Edmonds, Nigel Kirby, Adrian Hawley, Stephen Mudie, "Collagen Structure and strength in leather." Conference paper presented at the XXXIII International Congress of IULTCS **2015**, 24-27th November, Novo Hamburgo, Brazil.

H. C. Wells, G. Holmes, R. G. Haverkamp, " Microstructural Characterisation of Looseness in Bovine Leather using Ultrasound." Poster and conference paper presented at the XXXIII International Congress of IULTCS **2015**, 24-27th November, Novo Hamburgo, Brazil.

Hannah C. Wells, Katie H. Sizeland, Nigel Kirby, Adrian Hawley, Stephen Mudie & Richard G. Haverkamp, "A Comparison of Strength and Collagen Structure in Bovine, Porcine and Human Acellular Dermal Matrix Materials for Surgical Applications." Poster presented at the 9th Annual CIGR Section VI International Technical Symposium, 16th – 20th November 2015, Massey University, Albany Campus, Auckland, New Zealand.

K. H. Sizeland, H. R. Kayed, **H. C. Wells**, N. Kirby, A. Hawley, S. Mudie, R. L. Edmonds, R. G. Haverkamp. "Nanostructural Analysis of Bioengineered Tissues for Enhanced Performance." Poster presented at the 9th Annual CIGR Section VI International Technical

Symposium, 16th – 20th November 2015, Massey University, Albany Campus, Auckland, New Zealand.

Hannah C. Wells, Richard G. Haverkamp, "Mechanical Behaviour of Collagen Fibrils with Strain." Poster presented at the Advanced Materials World Congress, 23-26 August, **2015,** Stockholm Sweden. *This poster was chosen for the IAAM Young Scientist of the Year Award for 2015.*

Hannah C. Wells, Geoff Holmes, Richard G. Haverkamp, "Microstructure and Looseness in Bovine Leather." Poster presented at the Advanced Materials World Congress, 23-26 August **2015,** Stockholm, Sweden.

Hannah C. Wells & Richard G. Haverkamp, "An Investigation into Looseness in Bovine Hides and Leather." Symposium presented at the 66th Annual Leather and Shoe Research Association Conference, 24th August **2015,** Queenstown, New Zealand.

Haverkamp, R. G., Sizeland, K. H., **Wells, H. C.,** Kayed, H. R., Edmonds, R. L., Kirby, N., Hawley, A., & Mudie, S. "Strength in Collagen Biomaterials." Poster presented at the Fourth International Conference on Multifunctional, Hybrid and Nanomaterials, 9-13th March **2015**, Sitges, Spain.

Hannah C. Wells, Katie H. Sizeland, Hanan R. Kayed, Nigel Kirby, Adrian Hawley, Stephen T. Mudie, Richard G. Haverkamp, "Poisson Ratio of Collagen Fibrils Measured by SAXS." Poster presented at the Fourth International Conference on Multifunctional, Hybrid and Nanomaterials, 9-13th March **2015**, Sitges, Spain.

Hannah C. Wells, Katie H. Sizeland, Richard L. Edmonds, Nigel Kirby, Adrian Hawley, Stephen Mudie, Richard G. Haverkamp, "Poisson Ratio of Collagen Fibrils." Poster presented at the 1st MBE (Matrix Biology Europe) conference (XXIVth FECTS meeting), 21 - 24 June **2014**, Rotterdam.

Hannah C. Wells, Katie H. Sizeland, Richard L. Edmonds, William Aitkenhead, Peter Kappen, Chris Glover, Bernt Johannessen, Richard G. Haverkamp "Biochar from Leather - the Fate of Chromium." Symposium presented at SLTC 117th Annual Conference 26th April **2014**, Northampton, UK.

Hannah C. Wells, Katie H. Sizeland, Richard L. Edmonds, William Aitkenhead, Peter Kappen, Chris Glover, Bernt Johannessen, Richard G. Haverkamp. "Forming Biochar from Leather Waste to Reduce Leaching of Chromium into the Environment." Symposium presented at 65th Annual Leather and Shoe Research Association Conference, 13th August **2014**, Wellington, New Zealand.

Sizeland, K. H., **Wells, H. C.,** Norris, G. E., Edmonds, R. L., & Haverkamp, R. G. "Collagen D-spacing Modification by Fat Liquor Addition." Symposium Presented at the 65th Annual Leather and Shoe Research Association Conference, Wellington, New Zealand, 13th August **2014.**

Richard G. Haverkamp, Katie H. Sizeland, **Hannah C. Wells**, Hanan Kayed, Melissa M. Basil-Jones, Richard L. Edmonds, Nigel Kirby, Adrian Hawley, Stephen Mudie "Collagen Structure in Useful Biomaterials." Symposium presented at 12th International Conference on Frontiers of Polymers and Advanced Materials Auckland, December 8-13, **2013.**

Hannah C. Wells, Katie H. Sizeland, Richard L. Edmonds, Nigel Kirby, Adrian Hawley, Stephen Mudie, Richard G. Haverkamp, "Collagen Fibril Diameter and Strength." Poster presented at the 12th International Conference on Frontiers of Polymers and Advanced Materials, Auckland, December 8-13, **2013**.

Patent Applications

Hannah C. Wells, Richard G. Haverkamp (2015) "Tissue Analysis Using Ultrasonography" Massey University, NZ Patent application no. 707963

Hannah C. Wells, Richard G. Haverkamp (2015) “Method of Analysing Leather” Massey University, NZ Patent application no. 707978

Client and Technical Reports

K. H. Sizeland, **H. C. Wells**, M. M. Basil-Jones, R. L. Edmonds, R. G. Haverkamp “Leather Nanostructure and Performance” *International Leather Maker* **2014** Sept/Oct p30-34

Richard G. Haverkamp, **Hannah C. Wells**, Katie H. Sizeland “Preliminary Comparison of the Collagen Fibril Structure of Bovine and Porcine Derived Acellular Dermal Matrix Materials” Pilot study report for TEI Biosciences Inc., Boston, USA **(2014).**

Introduction

This thesis titled “Structure and Performance of Collagen Biomaterials” describes a study of collagen structure, strength and deficiencies in strength in a range of collagen based materials. The aim of the project has been to gain a better understanding of the underlying structural properties of collagen, and the structural mechanisms that relate to strength in dermal materials, including leather, acellular dermal matrix (ADM) materials for medical applications, and heart pericardium.

Collagen is a long fibrous protein that is responsible for providing strength and stability in various connective tissues in the body. Collagen is the most abundant protein in the animal kingdom, making up approximately one third of the total protein content in the human body. There are around 16 different types of collagen, with collagen types I, II, and III making up 80-90 % of the collagen in the body (*3*). Collagen type I is the main structural protein in skin, tendon, ligaments and pericardium, and is the focus of this research.

This report has been divided into two sections.

- Section A discusses, in detail, research carried out to better understand a collagen structure defect that occurs specifically in leather during processing, called looseness.
- Section B looks at the nano-structural characteristics of collagen fibrils and fibres within dermal materials and heart pericardium, and the correlation between these characteristics and bulk material strength. A range of collagen based materials were used during these studies including leather, acellular dermal matrix (ADM) materials and pericardium.

The research questions for this project were;

1) What is the structural motif that describes looseness?
2) How do we detect looseness in leather?
3) Can we look at the structural basis of looseness using X-rays?
4) Is there a structural characteristic of skin that can be identified, that leads to looseness in finished leather?
5) When we know the structural characteristic of skin that leads to loose leather, can we modify the processing procedure to incorporate a system to more easily identify loose hide/leather?

6) Is there a method of safely disposing of leathers deemed too loose for use, and other unwanted leather materials that have been chrome tanned, that ensures little or no Cr^{3+} leaching into the environment?
7) How does the collagen fibril size relate to strength?
8) How do collagen fibrils behave when strain is applied to a bulk material?
9) How do the collagen structures within ADM materials differ and compare in bovine, porcine and human ADM?

Research questions 1- 6 are covered in section A of the report. Looseness in leather is an important topic for leather industries here in New Zealand and around the world. Leather is desirable material for many applications since it is a biomaterial that is flexible, durable, tear resistant, partially water resistant and breathable. These characteristics make leather a useful material for the production of footwear, upholstery, and clothing. Leather can be produced from a range of animal skins, however bovine hide is the most commonly used raw material (*4*). Leather is a major by-product of the meat industry making it economically significant around the world, with an estimated global annual trade value of US$100 billion (*5*). The visual appearance of leather is important, and has a major influence on the selling price and usability of leather, with many applications requiring top quality material. Any defects or imperfections on finished leather, such as looseness, will result in a significant reduction in value. Looseness is a structural defect that occurs when the collagen fibre layers within finished leather separate causing the leather to appear wrinkled, which is aesthetically undesirable. Looseness largely affects bovine and deer leathers, with around 5-10% of finished bovine hides produced in tanneries being deemed loose (*6*). These hides then become second grade or waste materials and are worth a fraction of the price of first grade leather. Until now, the structural mechanisms and features relating to looseness have not been well understood.

Section B covers research questions 7 – 9, and investigates the nanostructure and behaviour of collagen within dermal materials, including bovine pericardium and ADM materials. Leather, pericardium and ADM material all share similar collagen structures, and therefore have comparable characteristics and behaviours. Strength is an important property for the applications of each of these materials; leather requires strength for durability to be able to withstand continual ‘wear and tear’ when made into clothing garments, shoes and upholstery, and failures can be costly to distributors. ADM materials used for surgical applications and pericardium used for heart valve replacement require strength to be able to endure the pressures inside the body when manipulated into place during surgical procedures, and failures can be fatal. The way in which collagen contributes to a material’s strength and properties was not well understood until now. Various analytical techniques

have been used to characterise the structures of collagen within dermal materials, including synchrotron base small angle X-ray scattering, scanning and transmission electron microscopy and ultrasonic imaging. Collagen properties such as fibril diameter, orientation and the size of d-spacing regions were measured, and physical structures of materials have been compared using imaging techniques. The collagen structures were investigated while under strain and tear tests were performed to relate structural characteristics to material strength.

Literature Review

Collagen – General Overview

Skin, skin based materials, such as leather and ADM, and heart pericardium are all mostly composed of type I collagen. Type I Collagen is a fibrous structural protein that is responsible for maintaining structure and providing mechanical stability in tissues (*7*). When animal hide or skin is processed into leather or ADM material, the collagen matrix is maintained structurally, however is exposed to a number of chemical and physical processes that slightly alter the structure. The distinct hierarchical structure of type I collagen, from the molecular structure up to fibril bundle, is described below.

1) Molecular Structure

Collagen has a distinct molecular structure, consisting of a long chain of a repeating $(Gly\text{-}X\text{-}Y)_n$ amino acids sequence, where 'Gly' refers to the amino acid Glycine and X and Y can be any other amino acid. A high proportion of the amino acids in the X and Y positions are the imino acids proline and hydroxyproline. Hydroxyproline is an imino acid formed from enzymatic action during protein synthesis, where proline is hydrolysed to form hydroxyproline. The three amino acids glycine, proline and hydroxyproline make up over half of the total amino acid content in tropocollagen (*8*). The number of repeats in a collagen polypeptide chain usually ranges from 100-400 units, which forms a long left-handed helical chain structure (*9*).

2) Tropocollagen (Collagen Molecule)

A collagen molecule, or tropocollagen, consists of three left-handed helical polypeptide α-chains arranged in a right-handed super helix. Collagen type I contains two identical α-chains and a third α-chain which has a unique amino acid sequence to the others. The molecule is approximately 280 nm long and 1.5 nm wide and has a molecular weight of 300,000 Daltons (*10*). This arrangement is known as the coiled-coil configuration. Non-helical polypeptide sequences exist at both ends of the molecule, called the carboxyl (C) and amino (N) terminal

ends. These end sequences are approximately 15 to 25 amino acids long (*11*). Hydrogen bonds between hydroxylated residues in polypeptide chains stabilise the 3D structure of tropocollagen. Three polypeptide chains spontaneously take the shape of a right-handed triple helix due to initial disulphide bonding between the N- and C- terminal ends of the polypeptide chains. The configuration is further stabilised through cross-links between glycine's in each Gly-X-Y triplet and the adjacent polypeptide chains in the helical structure(*12*). When proline is not in the 'X' position of the Gly-X-Y triplets, an additional hydrogen bond is able to exist, mediated by a water molecule, between the X position residue and the Glycine on an adjacent chain. The residual groups of the amino acids in sequence point outwards from the centre of the helix to reduce any sterical hindrance within the molecule, giving further stability (*13*).

3) Collagen Microfibril and Fibril Structure

To form a collagen microfibril, five tropocollagen molecules arrange side by side in a quarter staggered array. Microfibrils arrange themselves into larger structures to form fibrils. The axes of each of the collagen molecules run parallel to the direction of the fibril direction. The staggering of molecules within fibrils results in gap and overlap regions of adjacent molecules. These overlapping and gap regions within the fibril result in regions of high and low density which when fired with X-rays, form a characteristic banding pattern in X-ray diffraction patterns (*8*). This collagen banding pattern has an axial spacing of approximately D = 67nm by x-ray diffraction or 234 amino acid residues by sequence analysis, and is referred to as the d-spacing. Another important feature of collagen fibrils is the enzymatic covalent cross-links between the molecules and help to hold the structure together. This crosslink formation is initiated by the enzyme lysyl oxidase which acts on lysine groups in the molecules. This forms allysine, which can then react with another lysine group in the helical region of a neighbouring molecule to form a divalent intermolecular bond. It is through the formation of these covalent bonds that the collagen fibril is stabilised(*14*).

4) Collagen Fibre Structure

In collagen based biological tissues such as skin, leather and pericardium, multiple collagen fibrils bundle together in various bundle-sizes to form collagen fibres. Collagen fibres can range in diameter from 30-300nm and lengths up to the millimetre range, depending on the

number of fibrils present (*11*). These bundles of fibrils, called fibres, are formed and held in place through the existence crosslinks. These can be either physical lysine-based crosslinks or proteoglycan crosslinks composing of glucosaminoglycans (GAGs) (*12*). In nature, the cross-links between fibrils are provided by proteoglycan bridges. These proteoglycan bridges are mostly made of decoran, a proteoglycan that contains either the glucosaminoglycan dermatan sulphate or chrondroitin sulphate. (*12, 15*) These crosslinking bridges can influence the mechanical properties of the structure, although the extent of their role is debated. Some believe the role of collagen cross-links in the mechanical behaviour of collagen fibrils and fibril bundles is insignificant, while other studies believe they have a significant influence. Among those that believe cross-link play a major role, there are further debates in how these cross links function. There have been suggestions that GAGs allow for shear forces to be transferred via their connections between fibrils, forcing fibrils to stretch when force is applied, rather than slide(*16-18*).

Synthetic crosslinks can also be introduced to a biomaterial to alter the mechanical properties of collagen structures. The cross-linking of collagen can alter the arrangement of the fibrils within collagen fibres, which can ultimately influence the behaviour and strength of the collagen material(*19*). A commonly used cross-linking agent is gluteraldehyde which is capable of not only forming cross-links between fibrils (forming fibril bundles or fibres), but also can form crosslinks within the fibrils themselves(*20, 21*). Synthetic cross-linking of collagen can be used as a technique to alter the mechanical properties of biomaterials, such as pericardium for heart valves replacements, and skin/hide in the production of leather and/or surgical scaffolds (*22*).

A schematic view of the hierarchical features of collagen is shown below (figure 1). Approximate lengths of each hierarchy is given, ranging from the amino acid sequence level to the collagen fibre level (*23*).

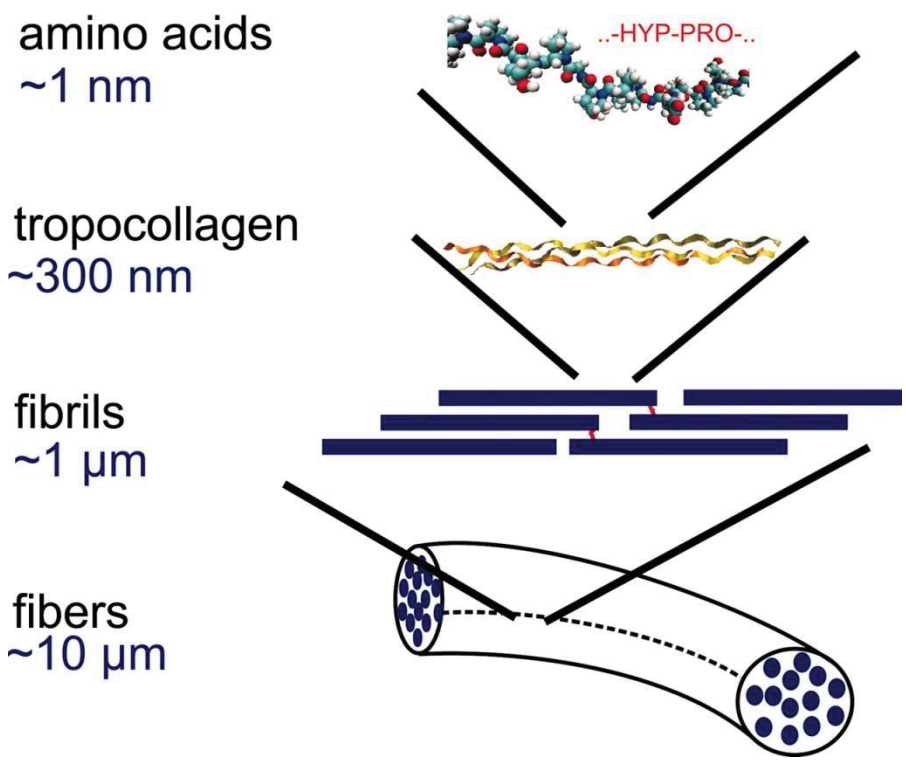

FIGURE1. SCHEMATIC IMAGE OF SOME OF THE HIERARCHICAL FEATURES OF COLLAGEN, RANGING FROM THE AMINO ACID SEQUENCE LEVEL AT THE NANOSCALE UP TO THE SCALE OF COLLAGEN FIBERS WITH LENGTHS ON THE ORDER OF 10. IMAGE SOURCED FROM MARKUS J. BUEHLER PNAS 2006,103: 12285-12290.

An Introduction to Leather

Leather is produced from raw animal hides and skins through multiple chemical and physical processes. A fundamental property of leather that is achieved through processing is the resistance to bacterial degradation. Another important property of leather is that when leather dries the material remains soft, flexible and strong, whereas skin or hide is known to dry hard and brittle.

During the preparation stages of leather processing, the epidermis and subcutaneous tissue layers of the hides are both removed, leaving only the fibrous dermis layer. The dermis consists of a network of fibres that is primarily made up of collagen, elastin and crosslinks including glycosaminoglycans, proteoglycans and glycoproteins (*24*). The dermis layer of leather can be further separated into two distinct layers which show differing structures and properties. These two layers are the grain corium layers, which are separated by the grain-corium junction (*25*). The grain layer is the outer-most layer, under the epidermis, and contains the hyaline layer consisting of hair pores, giving a patterned effect on the leather surface. The collagen fibres in the grain layer are smaller fibres that are densely packed. The corium is the second and bottom layer within the dermis, and consists of a network of larger collagen fibre bundles and makes up the bulk of the derma (*26*). The corium has coarser structure than the grain layer and provides the bulk of the strength to skin and leather. The corium layer of skin also contains blood vessels, adipose cells and sweat glands present which are removed during leather processing (*27*). Also during processing, most of the crosslinking agents and proteins in skin other than collagen and elastin are removed from the dermis.

The final quality and appearance of leather will be influenced by the condition of the animal the raw hide was sourced from. For instance, how and why the animal was reared, how it was slaughtered, its age, breed, sex and environment will influence the quality and characteristics of hide and therefore leather. Leather quality is also affected by the presence of any defects, which can occur prior or during processing. Hide defects can be caused by parasites, diseases, malnutrition, brand marks and scratches to the animal, which go on to devalue leather (*28*). Once the animal is dead, poor stripping of the skin, handling of the hides and storage will also influence the final leather quality. Good animal management and hide preservation is vital for the leather industry, since without good quality hides, good quality leather cannot be produced.

Once hides reach a leather tannery, numerous processing factors and stages can influence quality and characteristics of the leather produced. One of the most important processing

stages during leather production is the tanning process. The purpose of leather tanning is to retain the hide's desirable natural properties while stabilising the structure and protecting the hide from putrefaction after the animal dies (*29*). When skin or hide is alive, the collagen fibres are able to move and flex in relation to one another, however when the animals dies and metabolic processes are stopped, the collagen fibres have a tendency to stick together and shrink, causing the hide to become stiff and hard. The additives used during tanning aim to lubricate the fibres and permanently fix the fibres apart from one another through chemical treatment. To ensure properly preserved and quality leather, correct tanning is vital. There are a variety of tanning agents and additives that can be used and each result in slightly different properties of leather. Chrome tanning agents are the most common tanning agents used, however vegetable tanning is also carried out using plant polyphenols. Other synthetic, oil and aldehyde and organic tanning agents exist although are not as commonly used(*30*). The variability in available tanning agents allows tanners to manipulate the processing stages to give a specific final appearance or property to suit the intended end application of the leather (*29*).

A full leather production protocol has been followed and discussed below, this is the protocol outlined in the World Leather Journal (*27*). It is important to note that protocol followed for leather production is unique to every tannery in accordance to specific customer requirements, raw material availability, as well as environmental and plant limitations. Tanning processes are therefore forever evolving with changes in customer demands, legislations, environmental demands and new emerging technologies/research findings.

Leather Preparation Process

Step 1: Soaking

The animal hides are soaked in water with the aim of rehydrating the skin to its original condition after being preserved during storage/transportation. This removes salt, dirt, blood and other residues. Water is also important for proper penetration of chemicals and is therefore necessary for the processes to follow (*31*).

Step 2: Un-hairing and Liming Processes

This can be carried out using alkali solutions such as sodium sulphide and hydrosulphide under conditions which allows for the hair to be dissolved without affecting skin structure.

The alkali solution breaks down the structure of the hair at its weakest point, the root, which removes the hair from the skin. It is also possible to add lime to the float at the same time to carry out liming simultaneously, however if the hair is of value then the hair removal and liming processes are carried out separately. Liming helps to remove the epidermis skin layer, swells the skin and modifies the collagen structure to a more open structure for later chemical treatments. Liming also helps to break down complex sugars, and non-structured proteins within the collagen structure (*27*).

Step 3: Fleshing

The fleshing machine is used to cut away any residual tissue from the corium. In doing this, the fleshing operation also helps to squeeze out any debris and grease within the grain layer and helps to relax the hide.

Step 4: Splitting

The purpose of this step is to even-out any variations in the thickness of hides by feeding the hide against a moving band knife. Through splitting, a thinner hide is achieved, which allows for better chemical penetration in later processing and gives a more relaxed grain structure.

Step 5: Deliming and Bating

Deliming de-swells the hides, using ammonium sulphate or carbon dioxide gas. A change in pH is seen as a result, to a more acidic state. Bating is an enzymes digestion process that involves using specialised enzymes to help soften and relax the hide.

Step 6: Degreasing

This stage involves removing as much of the grease from the hide as possible. In order to achieve this, hides can be drummed with paraffin oil and detergents to soften and remove the grease. The hides are now prepared for the tanning process.

Step 7: Pickling

To bring the hides to a moderately acidic state (required for tanning), sulphuric and formic acid can be added into a drum along with the hide. This ensures a more controlled tanning process. Adding acids can however cause the hides to swell and therefore to counteract this common salt is added as well.

Step 8: Tanning

Tanning is the main stabilising process of leather production. The tanning agent used is often either a chrome or vegetable tanning agent(*31*); however other tanning materials can be used depending on the final desired characteristics of the leather. Tanning stabilizes the raw hide to prevent the material from decomposing. After tanning, the hide will dry to a soft and flexible material, rather than a dry hard material. Chrome tanning agents, such as trivalent chromium sulphate, are the most commonly used agents and result in a pale blue tanned leather, known as 'wet-blue.' Chromium sulphate is produced from the following reaction:

$$Na_2Cr_2O_7 + 3SO_2 + H_2SO_4 \rightarrow Na_2SO_4 + H_2O + Cr_2(SO_4)_3$$

Chromium is a useful element in the tanning process because the complexes that are formed are of intermediate stability allowing for the exchange of ligands, and chromium is capable of forming polynuclear complexes that involve Cr-O-Cr bridges through oxolation. This process is not easily reversed. The occurrence of many of these polynuclear complexes bridges the gaps between collagen chains, results in the tanning action.

The length of time of the tanning process can also be altered according to the desired product. Generally speaking, the chrome tanning process is around 2 – 3 hours for thin skins, and can be up to 24 hours for thicker skins(*32*).

Step 9: Sammying, blue splitting and shaving

Surplus water from tanning is squeezed from the tanned hides via the sammying process, usually involving passing the hide through two rollers. Grading of the leather takes place according to potential thickness and quality. The hides are then split in their wet-blue state to reduce variation in thickness. Thickness is then again reduced through the process of shaving where spiral knives are used to shave the leather to a very precise and accurate thickness (*27*).

The tanned hides or leathers are now ready for dyeing, re-tanning and/or softening stages of the process.

Step 10: Neutralisation

In preparation for dyeing, re-tanning and softening, the pH of the leather is increased through the addition of mild alkalis. This allows chemicals and agents to penetrate the skins more effectively.

Step 11: Dyeing

The most common dyes to use to treat leathers are anionic dyes, however many different types of dyes exist, in many colours. In order to achieve the desired colour, several additions of dye can be added to increase colour intensity. Prior to the addition of dye, fixatives can be added to lock-in the colour.

Step 12: Re-tanning

Re-tanning can be carried out on skins to further soften and plump the material. The agents used are usually very specific and have a significant effect on the final leather properties. The structure of the leather is modified during re-tanning and any empty regions between the grain and corium can be filled (*31*).

Step 13: Leather Softening

Leather softening is a step added into the process to further prevent the leather fibres from sticking together when the leather is dried. A number of products are used for this purpose, including fat liquor, soluble acrylic polymers and modified acrylic polymers. Fat liquor is an oil based product that penetrates the leather and attaches to the fibre structure to act as a fibre lubricant, producing a softer material. A negative impact of fat liquoring is that the leather can become more prone to course breaking. Soluble acrylic polymers can be used for polymeric softening of the leather. These polymers can combine with collagen in leather to improve physical properties and provide heat resistance. Modified acrylic polymers can be used to develop waterproofing in the leather and provide further softening (*27*).

Step 14: Preparation for drying – samm/setting

After leather softening, leathers are removed from the processing vessel and are prepared for drying. This involves removing excess water through either sammying or centrifuge systems. The skins then go through an operation known as setting. Setting involves stretching the skins using a blunt angled blade on a rotating cylinder to remove any wrinkles or creases.

Step 15: Drying

There are a number of methods of drying that can be carried out on the leathers, the technique selected is usually based on what final properties are wanted in that particular leather. Drying methods include hand drying, toggle drying, vacuum drying and paste drying. Removing water from leathers helps to stabilise and fix the chemical properties and structures within the leather and it is at this stage the final properties of the leather are determined (*31*).

Step 16: Conditioning and Staking

Conditioning helps to relax the structure of the leather after drying and involves lightly dampening the leather and leaving them in piles to reach equilibrium. Staking involves stretching and flexing the leather after conditioning to loosen any sticking fibres, giving softer leather. The leathers are usually slowly dried slightly after this step to reduce moisture content to around 16%. The leathers are now ready to undergo the steps involved in leather finishing.

Step 17: Finishing

Leathers are buffed against a rotating emery board to produce an even smoother finish. An acrylic resin is applied to the buffed grain layer to fill the junction between the grain and corium. Then, a surface coating can be applied to ensure even texture and colour and improve the leathers wear, or embossing can be done to obtain a three dimensional print on the leathers surface (*32*). This can be followed with the application of a water resistant finish to the leather. The leathers are now ready for final inspection and dispatch.

Environmental and processing conditions, such as temperature and pH, as well as processing time are all important for each step. For this reason, the entire process is closely monitored. For leather tanning to be complete, specific conditions must be met and the leather must be correctly prepared in the preparatory stages for the agents to fully penetrate the hide. For example, the pH during the liming stages of hide processing needs to be maintained slightly alkali for a period of time in order to ensure the structure becomes "opened-up" enough to allow for dyes and agents to fully penetrate the leather. If not, the proteins within the hides may not be fully stabilized and the leather could spoil over time. It is important that the hide is evenly exposed to agents and additives and therefore hides are often processed in drums. Processes such as the stretching and drying can also degrade leather quality of not carried out correctly (*27*). All processing stages play an important role in producing a desired material. Because of the large number of processing stages, and specific conditions required for each stage, the chance of defects occurring during processing (as well as prior to) is quite high. One of the most common defects to occur during processing is looseness in leather. Looseness occurs when the layers within leather begin to separate which results in a wrinkling effect on the leather surface which cannot be detected until late in processing. It is unknown at what stage (or stages) looseness is caused. Gaining a better understanding of looseness and developing a method of detecting looseness easily earlier in processing could help to improve leather quality and reduce defects, thereby increasing revenues for the leather industry; this project looks more closely at looseness to achieve this.

Looseness in leather

Looseness occurs mostly in bovine and deer leather and is when the layers within the leather structure (corium and grain) separate. This causes the appearance of wrinkles on the surface of leather when it is bent or folded inwards with the grain surface up, (figure 2) and significantly lowers the leather quality and value.

FIGURE 2: PHOTOS COMPARING THE SURFACE APPEARANCE OF TIGHT (LEFT) AND LOOSE (RIGHT) LEATHER WHEN BEING FOLDED INWARDS SLIGHTLY WITH THE GRAIN SIDE UP. THE SCALE BAR IS 2 CM.

Looseness has been linked to a reduction in toughness of leather and cannot be identified in leather until the end stages of processing. It is estimated that around 5-10% of total bovine leather is deemed loose currently(*6*). This means tanners are spending a significant amount of money on tanning and treating hides that end up as second grade and lower priced materials (*33*).

As well as a visible gap between the corium and grain layers within the leather, microscopic investigations have shown some differences in the fibrous structure in the grain layer of loose leather. In tight leather, the grain consists of tightly packed small fibre bundles, whereas in loose leather, the fibres are arranged in a more “sheet-like” structure with larger bundles (*33*). Looseness is thought it appear sometime during processing and one pre-existing theory was that looseness occurred upon the removal of non-collagen proteins, proteoglycans and other components of the hide structure during processing. The removal of these components could create holes or voids within the thickness of leather, particularly at the corium-grain junction. Processing factors such as fat liquor penetration, bacterial degradation in the raw stock, mechanical stressing, drying and moisture content have been believed to contribute to looseness in leather. However, the exact process or reason for looseness occurring is not understood by tanners. Once leather becomes ‘loose’ or the layers of the leather begin to separate, further processing could result in even further enlarging of these voids or gaps, resulting in severely loose leather (*34*). Looseness is first evident in hides after the chrome tanning stage where the collagen structure is fixed using chemical additives. After this stage, the tanning process cannot be reversed and if any looseness is present, the hides value will be significantly decreased (*35*). This thesis discusses a more in depth look into the structural properties of loose leather to determine a

more accurate explanation of the cause looseness. Multiple research techniques have been used to investigate looseness including small angle X-ray scattering (SAXS), scanning and transmission electron microscopy (SEM and TEM), ultrasonic imaging and tear and tensile testing. These techniques are also discussed in more detail further on.

An Introduction to Acellular Dermal Matrix Materials

Acellular dermal matrix (ADM) materials are used as biological scaffolds for a variety of reconstructive surgical applications including breast reconstructions(*36*), abdominal wall reconstructions(*37*), hernia repair(*38*) and skin burn repair(*39*). ADM is a collagen matrix produced through decellularization of dermal tissues. Bovine, porcine and human dermal tissues are commonly used tissues of origin. The aim of the decellularization process is to effectively remove all cellular and nuclear material from the dermis, while preserving as much of the native collagen ultrastructure and composition of the matrix as possible. Preserving the dermal structure will minimise the chance of inflammatory response or immune-mediated rejection of the tissue when it is implanted into the patient(*40*). Decellularization methods used vary depending on the species of origin, tissue thickness and density, and the intended use of the scaffold; however the most effective protocols are those that include a combination of physical, chemical and enzymatic treatments(*41*). It should be understood that any process intended to remove cells will alter the three-dimensional architecture of the dermis matrix to some degree, therefore minimising disruption rather than avoiding disruption is the aim when carrying out decellularization.

Prior to the decellularization process, skins are thoroughly cleaned, de-haired using sodium sulphide, and the subcutaneous fat layers are cut off(*42*). An example of a decellularization protocol is discussed in more detail below. This is just one method of many possible variations to decellularize extracellular matrix materials. This particular method has been shown to be effective for thicker laminates such as dermis(*41*).

ADM Production Process

Step 1: Freezing

Freeze-thawing will effectively lysis cells within tissue due to intracellular ice crystals forming and disrupting cell membranes(*40*). The contents of the cells will remain within the tissue however, unless removed by subsequent processing. Multistage freeze-thaw processing can be carried out without significantly increasing the loss or damage to the matrix proteins, as long as the rate of freezing is controlled(*41*).

Step 2: Enzymes

Enzymes such as nucleases, trypsin, collagenase, lipase, dispase, thermolysin, and α-galactosidase can be used as methods of tissue decellularization. Trypsin is the most commonly used enzymatic agent for decellularization of dermal tissues, and is a highly specific agent capable of cleaving peptide bonds(*41*). Trypsin can disrupt tissue ultrastructure for effective decellularization, and in doing so also improves the penetration of other decellularization agents used subsequently. For this reason, treatment with trypsin is often included as an initial step in tissue decellularization, particularly for dense tissues such as dermis(*43*). However, the use of trypsin for decellularization can have an adverse effect upon the extracellular matrix (ECM). Proteins such as collagen and elastin have limited resistance to trypsin, and therefore prolonged exposure can damaged the collagen matrix. The overexposure of trypsin can result in changes in mechanical properties of the ECM and significantly reduce the tensile strength of the tissue, by up to 50%(*40*). For this reason, the duration of exposure to trypsin should be limited and controlled. Complete cell removal using trypsin is unlikely, and any enzyme residue within the matrix after treatment can effect recellularization later on or trigger an immune response. Therefore subsequent processing is often required(*41*).

Step 3: Addition of alcohol

Alcohols help to remove lipids from tissue, and have shown to be more effective at doing so than lipase(*44*). Methanol with chloroform has been used for delipidation of porcine skin to successfully produce acellular matrix materials(*45*) as well as other tissues(*41*). Alcohols need to be used with caution when treating tissues however, since they are capable of precipitating proteins and damaging the collagen matrix(*41*).

Step 4: Adding acid or base

Modifying pH to either extreme (alkali or acidic) in tissues solubilizes the cytoplasmic components of cells, disrupting and removing nucleic acids(*40*). Peracetic acid is one acid that is commonly used in decellularization protocols to remove DNA and RNA, and also acts as disinfectant for the tissue. Peracetic acid has a minimal effect on the composition and structure of the ECM when used correctly. Other acids such as acetic acid can be used but are not as common due to their tendency to damage and remove collagen from the ECM structure(*41*). Bases such as sodium sulphide and sodium hydroxide are used to remove hair

from skins and hides in both ADM and leather production. Bases are also able to aid in the removal of nucleic acids from tissues however can disrupt collagen crosslinks and cleave collagen fibrils, resulting in a change in the mechanical properties of the ECM which is not desired. For this reason enzymatic agents may be favoured over bases for the removal of nucleic acids in decellularization(*41*).

Step 5: Applying Detergent

Detergents remove cell components by solubilizing cell membranes and dissociating DNA from proteins in tissues. The effectiveness of detergents in the decellularization of tissues is dependent on exposure time, tissue type, thickness, and age; and over exposure to detergents can result in an adverse effect on the ECM due to protein disruption and dissociation(*41*). The two most commonly used detergents are Triton X-100 and sodium dodecyl sulphate (SDS). Triton X-100 is a non-ionic detergent, whereas SDS is ionic. SDS is more effective at removing cellular components from dense tissues than Triton X-100, and compared to other detergents, is able to achieve a more complete removal of nuclei and cytoplasmic proteins(*43*). However the drawback of using SDS in the decellularization protocol is that it is disruptive to the ECM by decreasing the GAG concentration in the tissue, resulting in a loss of collagen integrity(*40*).

The decellularization protocol described above is just one example of a method used to decellularize dermis tissue to produce ADM surgical scaffold material, as described by Crapo *et al.* (2011). Subsequent treatment is usually required to remove any residual chemicals or agents from the tissue after decellularization. These remaining chemicals may be toxic to host cells, invoking an adverse immune response when implanted in vivo. Assays are used after decellularization to firstly quantitatively analyse the extent of decellularization achieved, and to quantify the level of residual chemicals and enzymes remaining in the material after decellularization(*40*). Decellularization level has not be quantitatively defined by metrics, however Crapo *et al.* (2011) defines the minimum criteria to be:

1) <50 ng dsDNA per mg ECM dry weight
2) <200 bp DNA fragment length
3) No visible nuclear material in the tissue when it is stained with 4’,6-diamidino-2-phenylindole (DAPI) or H&E

The tissue type, age and decellularization protocol used all influence the mechanical properties and ultrastructure features of ADM materials. The desired characteristics of the material depend on the intended use, but have in depth knowledge of ADM materials and properties will be beneficial in the field of tissue engineering and regenerative medicine. This thesis discusses more in depth, the structural and strength differences of three ADM materials; Strattice Firm porcine ADM (LifeCell Corporation, US), Alloderm human ADM (LifeCell Corporation, US) and SurgiMend bovine ADM (TEI Biosciences, US).

An Introduction to Pericardium and Heart Valves

Heart valve disease is a growing health problem around the world due to an increase in degenerative heart disease along with an aging population. It is estimated that over 800,000 heart valve replacement procedures will be required annually by 2050(*46*).Tissue-based heart valves were developed in the late 1960's, beginning with human tissue and developing to use animal tissue(*47*). Bioprosthetic tissue heart valves offer an alternative option to mechanical valves, with different advantages and side effects existing for each. Mechanical heart valves are made up of entirely synthetic materials such as polymers or carbon, whereas the bioprosthetic valves consist of biological tissues mounted onto a stent. The development of biological tissue heart valves has provided patients with more options, and in recent years, there has been more of an inclination towards using these bioprosthetic valves due to the significant improvements and new technologies in the area(*46*).

The biological tissue used to fabricate the heart valve bioprosthesis is a collagen based biomaterial, with the most common tissues used being porcine aortic valve, bovine pericardium, dura mater, fascia lata and autologous pericardium(*48*). The tissue studied as part of the characterisation of collagen based materials in this project was the bovine pericardium. This tissue is of interest due to its desirable characteristics and availability for the production of replacement heart valves.

Bovine pericardium is an inelastic protective sac that surrounds the heart of a cow. Its purpose is to protect the heart from infection or inflammation from surrounding structures in the body, to hold the heart in place, and to lubricate the heart to allow for sufficient movement upon contraction. It is made up of two layers; an outer pericardium that attaches and secures the heart to the diaphragm and blood vessel, and an inner serous pericardium which is more delicate. The inner serous pericardium is a double membrane itself, consisting of an outer parietal layer and an inner visceral layer. The two layers of the serous pericardium are separated by the pericardial cavity containing serous fluid, which works as the lubricant to allow to heart to move when beating(*49*).

The outer pericardium is a fibrous and tough tissue, comprised of mostly collagen fibres woven together in a matrix much like skin. It is this pericardium tissue that is useful for fabricating bioprosthetic valves.

Producing Heart Valves from Bovine Pericardium

Pericardium tissue is harvested from neonatal or adult bovine and is usually processed within 24 hours after the animal dies. The pericardium is cleaned and the surrounding adipose tissue is removed. If required, the pericardium can be cryopreserved until the following stages are carried out. Cryopreservation involves rapidly freezing the tissue in liquid nitrogen(*50*).

Step 1: Fixation in Gluteraldehyde

The bovine pericardium undergoes treatment with gluteraldehyde to reduce calcification. Calcification is a significant issue in bioprosthetic heart valves and is thought be the main mechanism for valve degeneration. The occurrence of calcification after surgery will significantly affect the durability of pericardial heart valves, and patients may require further replacement procedures after only a few years(*51*). Schoen *et al* demonstrated that gluteraldehyde treated tissues implanted into a rat model will calcify according to the amount of gluteraldehyde present in the tissue, and that those tissue containing more gluteraldehyde experience less calcification (*52-54*). Fixation with gluteraldehyde causes cross-linking of collagen; and prevents the production of calcium, further preventing the formation of calcium crystal upon the interaction with membrane phospholipids. It is these calcium crystals that result in valve failure due to tear and stenosis(*50*).

Step 2: Anti-mineralization Treatment

Further treatment of the pericardium tissue to reduce calcification can be carried out through anti-mineralization processes. This involves treatment of the tissue with agents such as alpha-oleic acid and ethanol, and surfactants. These anti-mineralization agents prevent calcification by binding covalently to the tissue preventing calcium influx(*50*).

Step 3: Valve design and construction

An intravascular stent is used to insert and mount the bovine pericardial replacement heart valve. The stent is either balloon expandable or self-expanding, and the biological tissue valve is sutured to the interior of the stent(*55*). The first generation of stent-valves was the Cribier-Edwards PHV, shown in figure 2, which consisted of three leaflets of fabricated tissue sewn onto a stainless steel stent. Since then, the design has been modified and improved,

with multiple configurations and valve diameters possible. The material of choice for the stent depends on the type of stent; balloon-expandable stents (Figure 3) are made of materials such as steel, platinum, and alloys containing plastic balloons inside the stent, self-expanding stents are made of memory materials such as nitinol(*56*).

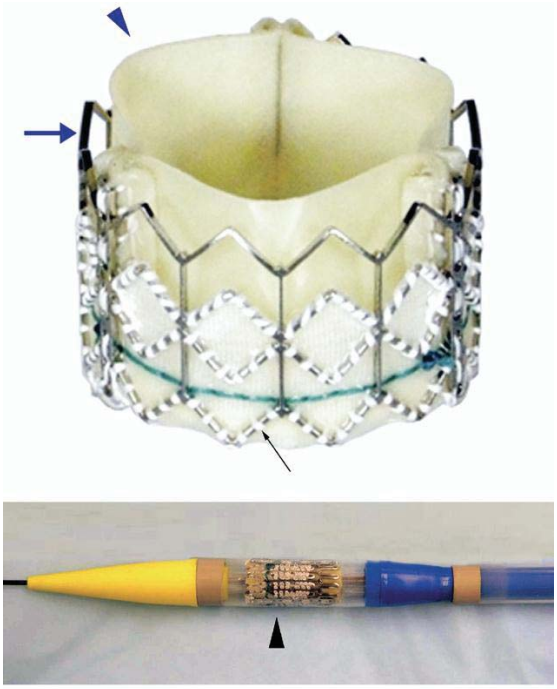

FIGURE 3: AN EXAMPLE OF A BALLOON EXPANDABLE VALVE DESIGN, THE EDWARDS-SAPIEN PERCUTANEOUS HEART VALVE. TOP: BOVINE PERICARDIUM LEAFLET (BLUE ARROWHEAD) INSIDE THE FRAME OF A STAINLESS STEEL STENT (BLUE ARROW). BOTTOM: A DELIVERY CATHETER WITH A VALVE LOADED (BLACK ARROWHEAD) (EDWARDS LIFESCIENCES INC., CALIFORNIA). IMAGE SOURCED FROM P. T. L. CHIAM & C. E. RUIZ (2008) "PERCUTANEOUS TRANS CATHETER AORTIC VALVE IMPLANTATION: ASSESSING RESULTS, JUDGING OUTCOMES, AND PLANNING TRIALS" JACC: CARDIOVASCULAR INTERVENTIONS (1), 4, 341-350.

Step 4: Implantation into heart valves

Initially, open heart surgery was required for valve replacement however in recent years trans catheter aortic valve replacement using a delivery device has appeared as a less invasive method. This involves delivering the bioprosthetic valves through catheters to the replacement site via transarterial or transapical approaches(*56*). The transarterial approach involves feeding the catheter through an artery to deliver the replacement valve, whereas transapical involves going through the wall of the heart. Once the collagenous pericardium tissue is mounted on to the delivery device, it is carefully placed using one of the techniques mentioned, and sutured into the area of the valve that needs replacing.

Methods for Characterising the Structure of Collagen Materials

The properties and characteristics of bulk materials largely depend on the structure and behaviour of the material at the nanoscale level. For this reason, to understand the behaviours of each of the materials studied; leather, ADM and pericardium, we aimed to measure the properties of these materials on a very small scale. A number of techniques can be used to characterise the nanostructure of collagenous materials such as leather, ADM and heart pericardium. This thesis discusses the use of, synchrotron based small angle X-ray scattering (SAXS), scanning and transmission electron microscopy (SEM and TEM), ultrasonic imaging, and tear and tensile testing to characterise the collagen matrix and the individual collagen fibrils that make up the matrix structure of collagen biomaterials. These techniques are discussed further below.

Synchrotron based small Angle X-ray Scattering (SAXS)

Synchrotron based SAXS was used as opposed to laboratory based SAXS since the synchrotron offers much higher x-ray intensities allowing for faster data collection, and higher spatial resolutions. The beam can be focused much sharper allowing for multiple data analysis points in one material cross section. This allows the structural differences throughout the thickness of the samples to be compared, something which has been important for the studies on leather looseness. Laboratory based SAXS systems have lower flux than synchrotron based SAXS systems and therefore samples need to be exposed to x-rays for much longer to achieve a diffraction pattern fit for data analysis. Samples could be affected by longer exposure times to the x-rays, or could dry out during longer data collection times, which could affect results. For these reasons, synchrotron based SAXS was chosen over the laboratory systems for this work.

Synchrotron radiation is electromagnetic radiation that is generated by accelerating charged particles (electrons) close to the speed of light around a large curved synchrotron ring. Electrons are generated in the centre of a large storage ring by an electron gun which heats a tungsten matrix cathode and fires thermionic emissions into a linear accelerator. The linear accelerator accelerates the generated electron beam to an energy of 100MeV over 10 metres. After the first metre of acceleration, the electrons are already travelling at around 99.99% of the speed of light. The beam then enters the booster ring. The Australian

synchrotron booster ring is 130 meters in circumference. The electron energy is increased significantly in the booster ring by the ramping of magnets located around the ring. An electron will spend about half a second in the booster ring before it enters the storage ring, and during this time it will complete over one million laps of the ring. The electrons are then injected into the storage ring with energy of around 3 GeV and an expected beam life time of 20 hours. The Australian synchrotron storage ring is 216 meters in circumference and can hold 200mA of stored current. The electrons travel continuously around the ring controlled by a series of magnetics placed around the storage ring. The electrons do not travel in a perfect circle around the ring, but instead undergo multiple changes in path in one direction, until they return back to the starting position. At the Australian synchrotron there are 14 sections that make up the ring, consisting of 4.4 metres of straight section and 11 meters of arc each. The arc sections contain dipole magnets. Each time the electrons are forced to change path around the arc by the dipole magnets, a beam of synchrotron light is emitted tangentially from their path. This beam is the synchrotron radiation that is directed and focused into a piece of analytical equipment located around the large ring. Each of these pieces of equipment is a different beamline station, each with specific capabilities and technical specifications. The radiation emitted from a synchrotron ranges from infrared through to hard X-rays, making it a useful research tool for a wide variety of purposes and materials.

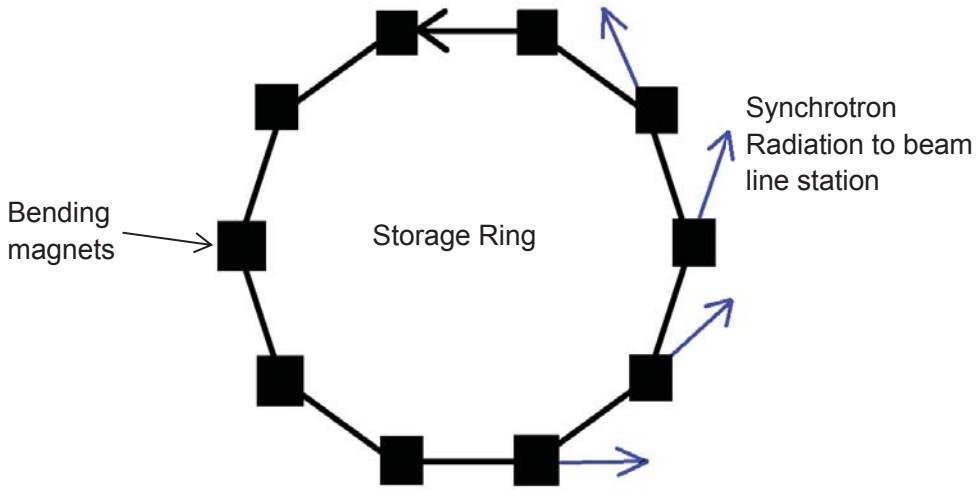

FIGURE 4: SCHEMATIC DIAGRAM OF A SYNCHROTRON STORAGE RING SHOWING THE TANGENTIAL OUTPUT OF SYNCHROTRON RADIATION

The Australian Synchrotron is the closest synchrotron to us here in New Zealand, and was used for most of the synchrotron based analysis of collagen based biomaterials for this project. Some research on leather was also carried out at the National Synchrotron Radiation Research Centre (NSRRC) in Taiwan. The Australian Synchrotron is located in Melbourne,

Victoria, and currently has nine beam line stations; Imaging and Medical beamline, infrared microspectroscopy, terahertz/far-infrared, macromolecular crystallography, powder diffraction, small and wide angle X-ray scattering (SAXS/WAXS), X-ray absorption spectroscopy, and X-ray fluorescence microscopy. The small angle X-ray scattering (SAXS) beamline has been used for the analysis of collagen structure in this project.

SAXS is able to provide structural information on complex materials through observing diffraction patterns when utilising a high-intensity undulator source **(*57*)**. SAXS can provide information at extremely high resolutions and has been shown previously to be useful for determining collagen structure and characteristics in a number of biomaterials. For example, SAXS has been used to successfully study the collagen structure in leather samples(*19, 57-59*), tendon(*17, 60-62*), cartilage(*63-65*), bone(*66-68*) and pericardium(*69, 70*).

The basic layout and component parts of the SAXS beamline, in order from top to bottom from the radiation source or storage ring, are shown in the figure below.

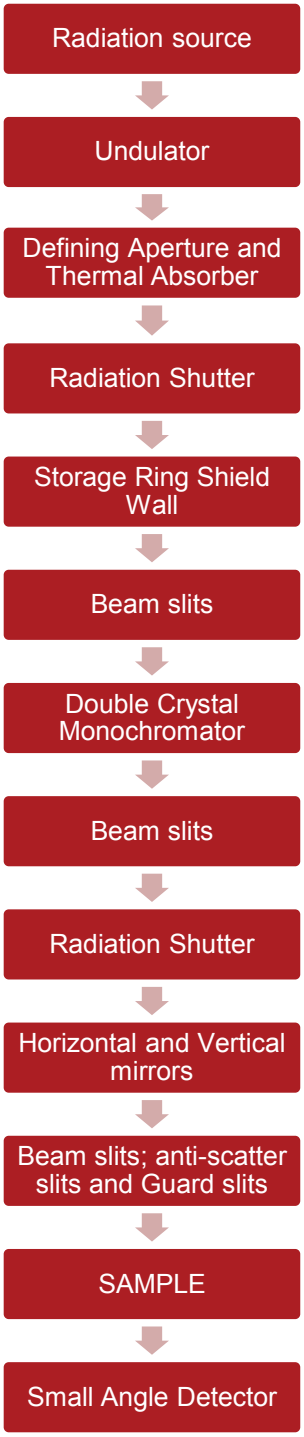

FIGURE 5: FLOW CHART SHOWING THE COMPONENT PARTS OF A SAXS BEAMLINE FROM UNDULATOR SOURCE THROUGH TO DETECTOR.

The top or front end of the main beam line is designed to protect the ultra-high vacuum of the storage ring and also deliver synchrotron radiation to the beam line chambers. Radiation enters the beamline from the storage ring to the undulator. An undulator is a series of dipole magnets which forces the incoming particles to oscillate, radiating energy in concentrated

narrow beam. The beam then travels through the defining aperture to determine the size of the beam and the thermal absorbers which are designed to protect the beam line chambers by absorbing up to 90% of the synchrotron radiation power generated by the magnets(*71*). The radiation shutters are in place for safety and to control the entry of radiation into the beam line chamber. The storage ring shield wall is a thick wall that separates the ring from the experimental area of the beamline. Beam slits are used to focus the beam down further before entering the double crystal monochromator. By using crystal monochromators, it is possible for researchers to select and transmit the desired wavelength from the incident synchrotron radiation beam for analysis(*72*). The energy can be selected by rotating the crystals while they are parallel to each other, varying the Bragg angle. From the monochromator, the beam travels through more splits and shutters to the sample. When the beam hits the sample, X-rays are diffracted and/or reflected and those that travel through the sample and are collected at the detector. It is possible to study the structure of molecules anywhere from 1 – 500 nm in size using SAXS, making it an ideal tool to study the complex hierarchical structure of collagen.

Below is a simplified SAXS experimental set-up for the analysis of leather. A similar set up was used for ADM and pericardium.

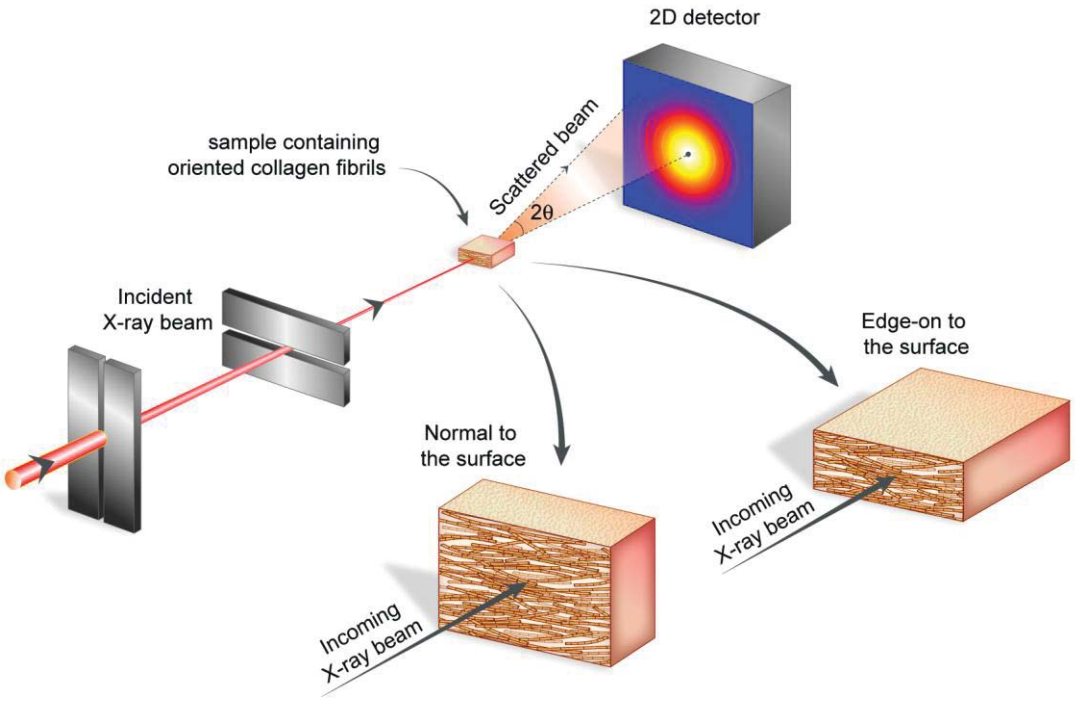

FIGURE 6: THE SAXS EXPERIMENTAL SET-UP FOR ANALYSING LEATHER PARALLEL AND PERPENDICULAR TO THE GRAIN SURFACE. A SIMILAR SET-UP WAS USED FOR ADM AND PERICARDIUM.

Small angle X-ray scattering (SAXS) is a technique that is based around the diffraction of a monochromatic X-ray beam upon the interaction with a sample. SAXS was developed in the early-20th century where A. Guinier developed a method to retrieve information on the sizes and shapes of particles in lattices, as well as the internal structure of disordered and partially ordered structures(*73*). When X-rays are fired at a sample, most will pass through with no interaction, however some will be diffracted; these are collected and used to form a scattering pattern that contains information on the molecular structure of the sample including pore size, distribution and shape.

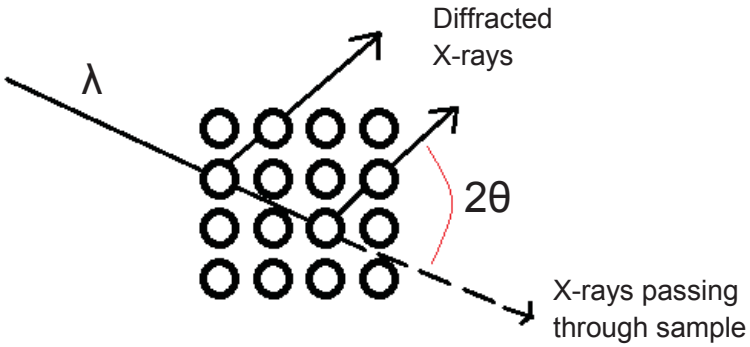

FIGURE 7: THE DIFFRACTION OF X-RAYS WHEN PASSING THROUGH A LATTICE. 2Θ = SCATTERING ANGLE, Λ = INCIDENT WAVELENGTH

For SAXS, the scattering pattern is recorded at very low angles, typical from 0.1 – 10°, giving a modest resolution that is capable of determining the size and shape of macromolecules, nanoparticles and large molecules, but not the atomic structure of materials. A two dimensional detector, such as the detectors at the Australian Synchrotron and NSRRC, allows an full 360° scattering pattern to be collected at once, as shown in Figures 5.

The 2D detector records the diffraction patterns which require the collection of two patterns when the sample is randomly orientated such as in a collagen based biomaterials; one of the collagen sample and one of a background solution or buffer. This is because the scattering pattern represents an average of the scattering from all possible orientations. The scattering intensity is recorded as a function of the scattering vector (k);

$$k = 4\pi \sin(\theta) / \lambda.$$

Where 2θ is defined as the scattering angle and λ is the wavelength of the incident X-ray beam.

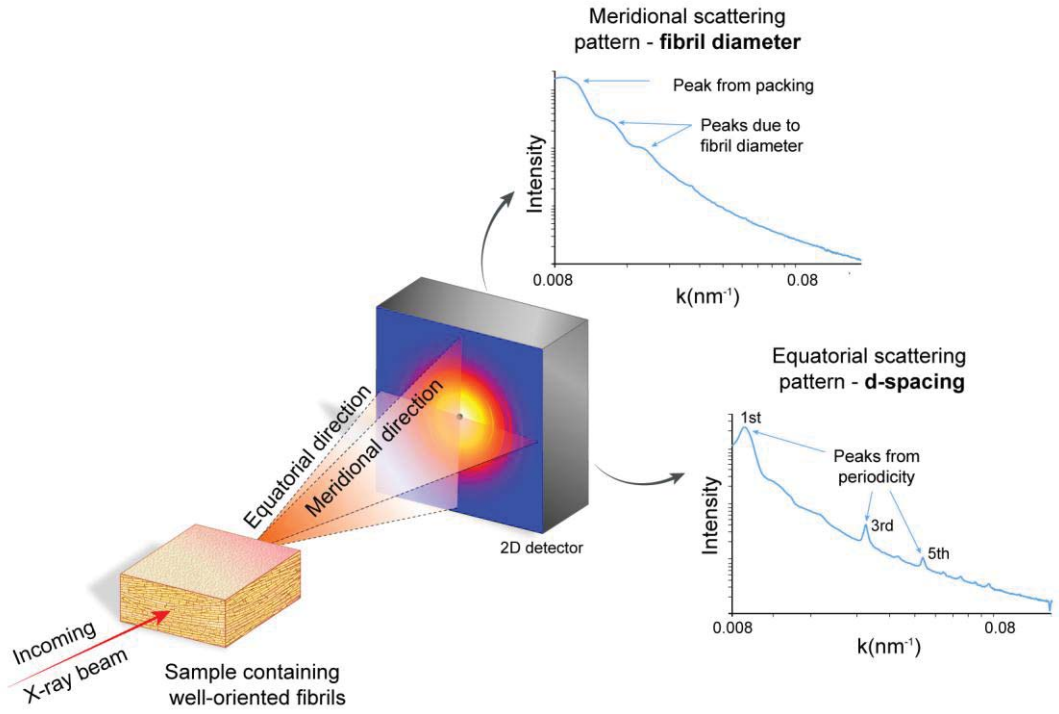

FIGURE 8: MERIDIONAL AND EQUATORIAL SCATTERING FROM A SAMPLE CONTAINING WELL-ORIENTATED COLLAGEN FIBRILS.

From the scattering pattern a scattering profile can be obtained by integrating about the beam centre. Scattering profiles can be used to obtain useful structural characteristics of a material such as particle size and particle shape. When investigating collagen structures within a sample, which are long cylindrical shapes, plotting the intensity as a function of k at different azimuthal angles will give different structural information, as demonstrated in figure 8. The average size of the fibril diameters of collagen in a sample can be determined by fitting data to a scattering profile that is plotted at 90° to the long axis of most of the collagen fibrils; this is in the equatorial direction in the set-up shown in figure 8. Secondly, by plotting the scattering profile at an azimuthal angle 90° to that, in the meridional direction if referring to figure 6, the size of the d-spacing along the collagen fibrils can be determined by fitting a Gaussian curve to the data. A third structural characteristic of collagen materials has been determined during SAXS studies for this project, and that is the orientation index (OI). OI is an index that has been developed as a measure of fibril alignment to compare the collagen fibril alignment in various materials(*74*). The determination of collagen diameter size, d-spacing and orientation index is discussed in more detail in the appropriate proceeding chapters.

Scanning and Transmission Electron Microscopy (SEM and TEM)

SEM and TEM involve using a focused beam of electrons to illuminate a sample and form a magnified image. Electron beams have a shorter wavelength compared with visual light; therefore a much higher resolution and magnification can be achieved when using an electron microscope over a light microscope. SEM involves scanning a samples surface with electrons to obtain information on the samples surface topography. In TEM, the electron beam is passed through the entire sample. Both methods are capable of producing high resolution images of samples to obtain valuable information on the samples composition and structure; however TEM is capable of achieving higher magnification and resolution than SEM. An advantage of SEM is that three dimensional images can be produced unlike TEM which produces a two dimensional image. Using SEM we were able to observe the structure of collagen fibre bundles and when using higher magnifications, the individual fibrils that make up fibre bundles (figure 9a and 9b). TEM was able to achieve a close image of the individual fibrils as well as fibril d-spacing and clearer fibril diameter sizes (figure 10a and 10b). TEM and SEM were used to visually study and compare collagen structures of both leather and ADM materials for this project. Below are some examples of the types of images achieved using SEM and TEM on bovine leather.

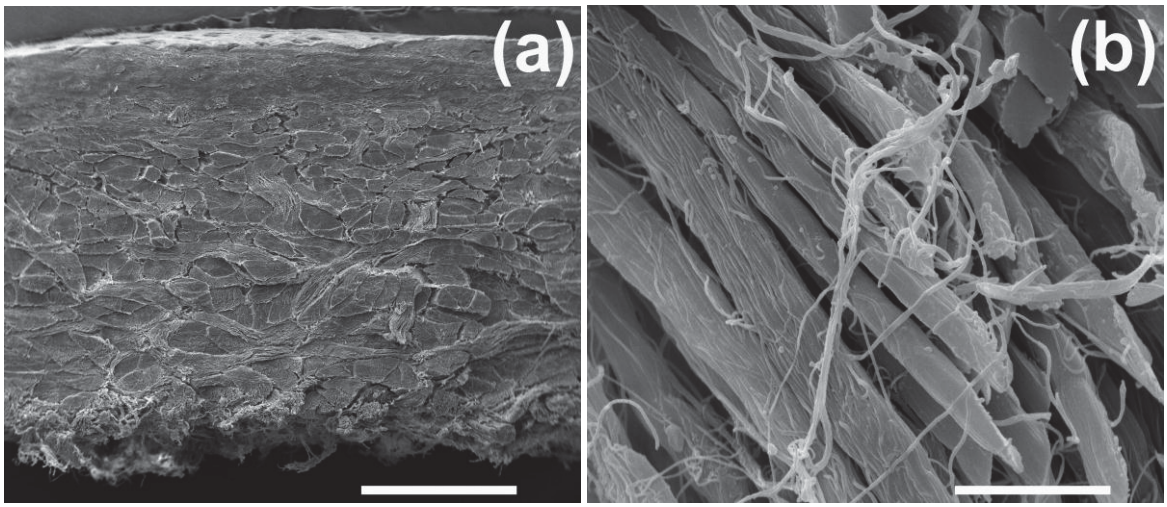

FIGURE 9: A) AN SEM IMAGE TAKEN OF THE ENTIRE CROSS-SECTIONAL STRUCTURE OF A BOVINE LEATHER SAMPLE, SHOWING THE COLLAGEN STRUCTURE. BUNDLE SIZE AND OVERALL STRUCTURE IS VISIBLE HOWEVER THE FIBRILS ARE TOO SMALL AT THIS MAGNIFICATION. SCALE BAR IS 1 MM. B) AN SEM TAKEN AT A MUCH HIGHER MAGNIFICATION OF BOVINE LEATHER, BOTH COLLAGEN FIBRIL AND BUNDLE STRUCTURES CAN BE SEEN. SCALE BAR IS 10 µM.

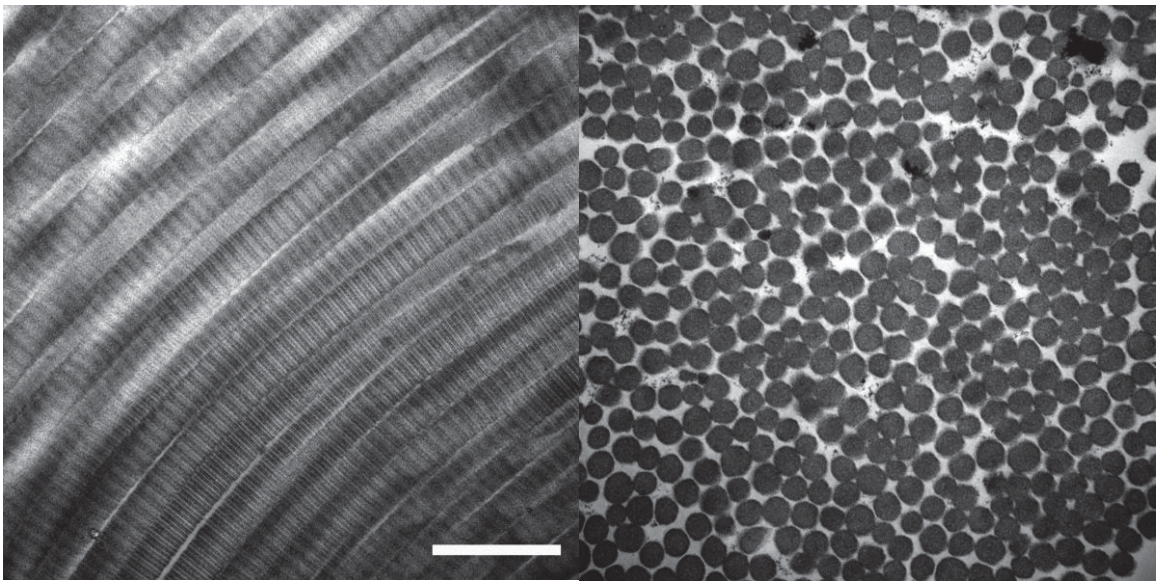

FIGURE 10: EXAMPLES OF IMAGES ACHIEVED USING TEM OF COLLAGEN WITHIN A LEATHER SAMPLE. THE FIGURE ON THE LEFT IS AN EXAMPLE OF AN IMAGE TAKEN END-ON TO THE FIBRILS, FROM WHICH THE FIBRIL DIAMETER CAN BE OBSERVED. THE FIGURE ON THE RIGHT SHOWS AN IMAGE TAKEN PERPENDICULAR TO THE LONG AXIS OF THE COLLAGEN FIBRILS, FROM WHICH D-SPACING CAN BE OBSERVED. SCALE BAR IS 500 NM.

For this project, the electron microscopy analyses were carried out at the Manawatu Microscopy Centre. The Manawatu Microscopy Centre, based at Massey University in Palmerston North, contains various microscopes including an SEM and TEM. When carrying out scanning electron microscopy on leather, the samples are sputter coated with gold before images are taken with an accelerating voltage of 20kV. To record the images, a FEI Quanta 200 instrument is used (FEI, Eindhoven, The Netherlands). For TEM, samples are micro-toned to produce very thin slices to allow the electron beam to pass through. After they are prepared for imaging, images are taken using a Philips CM10 TEM, with SIS Morada high-resolution digital imaging, or a FEI Tecnai G2 Biotwin TEM with a tomography unit. More information on the methodology used for the samples analysed during this project are given in the appropriate chapters.

Ultrasonic Imaging

Ultrasound has been used as a method to identify the presence of looseness in leather. As mentioned previously, the current method for identifying looseness in leather involves visual analysis and grading by a worker carrying out a pinch type test, which is not a quick or

accurate method. For this reason, ultrasound has been explored as a more effective method for looseness grading. The use of ultrasound to identify leather looseness is a new idea. Liu et al (2013) has used ultrasound to identify and evaluate leather hides for defects close to the surface, but not looseness, which is more of an internal structure defect.

Ultrasound is a form of energy generated by oscillating sound pressure waves at frequencies above the upper limit of the human ear (above 16 kHz). Ultrasound is used in a wide range of fields, one industrial use of ultrasound is for flaw detection in building materials, pipelines and structures(*75*). The frequency range typically used in ultrasonic non-destructive testing ranges from 100 kHz to 50MHz, depending on the material type, the resolution and depth required. Ultrasound behaves in a similar way to audible sounds, however has a much smaller wavelength and can therefore reflect off very small discontinuities in a material, making it a useful tool for non-destructive testing (NDT) and flaw detection in a number of materials.

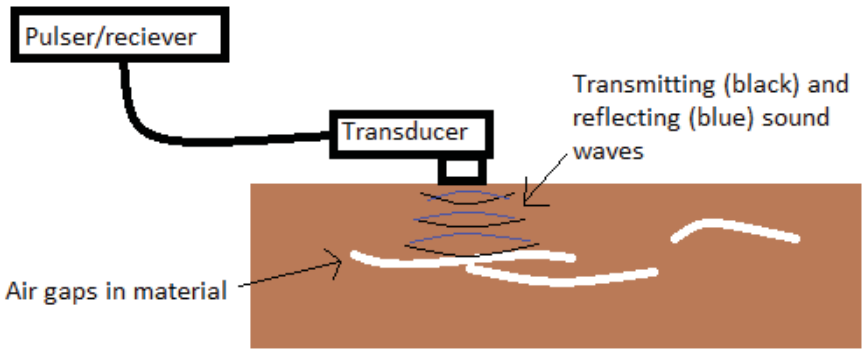

FIGURE 11: A SCHEMATIC DEMONSTRATING THE BASIC IDEA OF HOW ULTRASOUND CAN BE USED TO DETECT FLAWS, SUCH AS AIR GAPS, IN A MATERIAL FOR NON-DESTRUCTIVE TESTING.

Sound waves are transmitted from the transducer and travel through the material, which can be a solid, liquid or gas, at a specific velocity, wavelength and frequency. The sound waves will continue through the material until they encounter a change in material density or medium, indicating a flaw. When this occurs, some of the waves are reflected back through the material to the receiver/transducer to be interpreted by software to give information on the size and depth of the flaw.

Another use of ultrasound is for medical and veterinary imaging, also known as diagnostic sonography or ultrasonography. Ultrasound is used for a wide range of applications in the medical/veterinary field and can be used for imaging and real-time visual analysis of internal body structures ranging from internal organs, tendons, joints, muscles, vessels and skin.

For the analysis of leather, a skin scanner ultrasound presented the required range of frequencies and settings that could be adjusted for the use on leather, therefore a range of skin ultrasonic devices were investigated for purchase. The general features and set-up of a skin ultrasound device is discussed further below.

Ultrasound components and set-up

The general set up for a high frequency ultrasound system used to investigate skin consists of an ultrasound platform and transducers probes. The platform usually contains the pulser/receiver and preamplifiers, and can be directly plugged into a PC via the USB port for the display screen and further data analysis. Platforms are design to support a number of transducer probes with varying designs and frequencies, depending on their application. For skin ultrasound, the penetration depth required is not very high (to just under the skin), but the resolution desired is usually very high, in order to identify small features or discontinuities in the skin. Therefore, very high frequency ultrasound is usually sought after for skin applications, generally in the megahertz range.

1) Pulser/Receiver

The pulser/receiver is required to generate high voltage electrical pulses to drive the transducer. The pulser section of the device is responsible for generating these electrical pulses which are converted to ultrasonic pulses by the transducer in the system. The receiver part of the pulser/receiver is responsible for receiving the voltage signals back from the transducer (which have been converted back from ultrasonic signals to electric signals). The receiver amplifies the received signals to then be available for signal processing or as an output display.

2) Transducer

Transducers are devices that are designed to transfer power from one system to another in the same or different form. Ultrasonic transducers are used to convert electrical pulses from the pulser/receiver to mechanical vibrations (or sound), and convert the received sound signals back to electrical pulses again to be processed by a computer. The phenomenon

involving the conversion between electrical and mechanical energy forms is known as the piezoelectric effect and is carried out using piezoelectric or single crystal materials which are contained within a transducer. Transducers types and properties range widely and the selection of the transducer for a specific application is critical; it is important to consider specifications such as frequency, bandwidth, and the element diameter when selecting a transducer (*76*). The transducer used to collect data on the collagen structure in dermal tissues for this research is shown in figure 12 (Cortex Technology, Denmark)

There are different transducer set-ups that can be used in ultrasonic testing. The two most common are the pulse-echo technique and the through transmission technique. In pulse-echo mode, the transducer carries out both the sending and receiving of the sound waves. The ultrasound platform then measures the time of flight of the sound waves through a material and the amplitude of the received signal. Pulse-echo set-up can be more useful for high density material, material that is too thick for the signal to pass the entire way through, or for in-situ testing where it is not possible to place the receiver on the receiving side of the material being tested (i.e. in skin analysis on a patient). In through transmission mode, a transmitter sends ultrasound waves through a material and a separate receiver collects the resulting signals on the other side of the material, therefore two probes are required. Imperfections within the material can affect the amount of sound that transmits through the material, which is detected by the receiver and thus enables flaws or structures within a material to be identified. The technique used is based mainly on the properties of the material being tested and the desired outputs. Due to the high density properties of leather and ADM materials we used pulse-echo transducer set-up.

FIGURE 12: PHOTO OF THE TRANSDUCER PROBE USED FOR THE ANALYSIS ON LEATHER AND ADM MATERIALS. THIS TRANSDUCER WAS PURCHASED ALONG WITH THE DERMASCAN C USB DEVICE FROM CORTEX TECHNOLOGIES IN DENMARK.

The main components of a transducer probe include the active element, backing and wear plate:

The active element is the most important part of a transducer. It is responsible for both generating an electric field according to a mechanical deformation (direct effect), and generating a mechanical deformation or dimension change due to an electric field (inverse effect) in ultrasound applications (*76*). Active elements are piezoelectric materials that are either natural or synthetically made and can include various crystals, ceramics and polymers. Ceramics are most commonly used as they generally present better piezoelectric properties and can be more easily manufactured into various shapes and sizes(*77*). Some commonly used ceramics include lead zirconate titanate, lead titanate, and barium titanate (*78*). Over recent years, piezo-polymers and composites have also been introduced and are becoming more common as active elements in piezoelectric transducers. These polymers include PVDF and P(VDF-TrFE) (*79*). In order to achieve the desired wavelength in a transducer the active element should be cut to a thickness of ½ that wavelength(*77*) (*80*).

The wear plate sits in front of the active element to protect it from the environment. Since it acts as a protective material it must be durable and non-corrosive. In some cases, such as in

immersion transducers, the wear plate has an additional matching layer which also sits between active element and the external surface to which the transducer is in contact with (water, test object, etc.) (*80*). The matching layer is designed with acoustical impedance to allow the transmission of energy from the active element to the load or sample with the least possible loss of energy (*81*). The matching layer is designed with a thickness that is ¼ the of wavelength required in order to achieve the optimal impedance match. If a transducer is not designed with care and the thickness of the wear plate is slightly wrong when taking into account the wavelength, the sound waves will not be in phase. This would cause a disruption in the wave front and result in poor quality scans (*80*).

As the name suggests, the backing is located on the back end of the active element. It is designed to dampen and control the mechanical vibrations of the transducer to a desirable level (*81*). It does this by absorbing the energy which radiates from the back of the active element of the transducer. Matching the acoustic impedance of the backing material to the active element results in a good range of resolutions being accomplished by the transducer, but can potentially lower the signal amplitude (*80*). The backing material is needs to be dense and highly attenuative, with the most common material to use being a mixture of resin epoxy and tungsten powder (*81*).

3) Preamplifier

In order to achieve optimum signal acquisition, certain ultrasonic systems require the addition of a preamplifier unit to provide further broadband signal-to-noise enhancement. The addition of a preamplifier is almost always required for industrial applications involving flaw detection or thickness measurements of highly attenuative materials. It is also important to include a preamplifier in testing systems that require the amplification of low signal amplitude disruptions. If there is a significant length of cable required between the transducer unit and the display unit in the system, a preamplifier may be used to compensate for amplitude losses across the cable (*80*).

4) Data collection/ Image Display

An image display unit can be part of the platform or a separate computer. There are a number of formats to present the collected data in an ultrasound system. The most common

formats are the A-scan and B-scan displays. Each format presents the data differently, allowing the observer to view and analyse specific parameters. It is possible for some systems to display more than one (or all) formats simultaneously.

An A-scan profile presents the strength of the received signal as a function of time or position. This format is able to provide information on the signal amplitude and time of flight at a specific area on the test material and therefore can be used to give information on the size and position/depth of any discontinuities (*82*). An A-scan is one-dimensional, creating a line profile of reflection strength received from the surface through to the maximum penetration depth, at a specific point on the surface of the material, The maximum penetration depth is determined by the attenuation within the material and the technical set up and settings used. Reflection strength is determined by changes in density within the material. Changes in density represent flaws, gaps and discontinuities within a material internal structure.

A B-Scan profile is composed of a number of A-scan lines, to form a cross-sectional image. This provides a cross-sectional profile of a test material. Here, the time of flight of sound is plotted verse the linear position of the transducer on the material. This can therefore determine the approximate planar position and size of changes in density, representing flaws, as well as their depth in a material.

Dermascan C USB Device

A number of ultrasound options were explored when deciding on the most appropriate for the use on leather and ADM materials. The option that came out on top was the Dermascan C USB device, from Cortex Technologies in Denmark. The Dermascan device is a skin scanner, designed to visualise the layers of the skin and subcutaneous tissues. It is used to identifying skin damage, such as that caused by over exposure to the sun, and does this by identifying any density changes within skin. Normal tissue is homogenous in structure and therefore provides very little or no density change, generating little or no reflections in the Dermascan. When skin is damaged, the structure is changed and density differences can be detected. This also can be applied for identifying tumours within the structure of skin.

A Dermascan C USB was purchased for research, along with two compatible 2D probe heads from Cortex Technologies; one being a 20MHz probe, and the other a 50MHz. Both probes are capable of near real-time scanning, taking 6-8 frames per second. For skin, the 20MHz probe has an axial and lateral resolution of 60 x 150 μm respectively, with a

penetration depth of 14mm. The 50MHz has a higher resolution of 30 x 60 μm but only 3 mm penetration. Because of the short range of the 50 MHz probe, this wasn't as suitable to visualise the lower grain and corium regions in leather and therefore the 20MHz probe was used for most of the research carried out here. The probes required calibrating to determine the sound velocity in leather, and this in turn determined the axial resolution. Calibration for leather was made by comparing the actual thickness of leather (measured using a micrometre) to the thickness of the material when displayed in an ultrasound image on the Dermascan. Multiple calibration measurements were made and averaged to determine the sound velocity in leather using the 20 MHz probe (Table 1).

Table 1. Calibration values and sound velocities calculated to determine the sound velocity through leather for the 20 MHz probe.

Velocity air (m/s)	Thickness of leather (mm)	Width of leather in image (mm)	Velocity, leather (m/s)
1580	0.48	0.75	2468.75
	0.5	0.8	2528.00
	0.515	0.8	2454.37
	0.46	0.8	2747.83
	0.45	0.75	2633.33
	0.46	0.738	2534.87
		Average	**2561.19**
		St dev	**99.45**

The velocity in leather above was calculated from the equation:

$$Sound\ velocity\ in\ leather\ =\ Sound\ velocity\ in\ air \times \frac{Width\ of\ leather\ in\ image}{Thickness\ of\ leather}$$

The axial resolution was then determined from:

$$60\mu m\ \times \frac{1580 m/s}{2561 m/s} = 97\mu m$$

The lateral resolution is determined from the probe design and does not change. Therefore the resolution possible when scanning leather with the 20 MHz probe was 97 x 150 μm.

The Dermascan probes have an internal water chamber to reduce attenuation, which is contained using a disposable water barrier supplied by Cortex Technologies. The barrier is a designed plastic film material that allows ultrasound to pass though without affecting the

signal or image quality. The probes connect up to a platform which connects to PC with the Dermascan software installed for image display and analysis.

Data collection

Once the Dermascan was purchased and set-up, a custom gain profile was developed for the use on leather specifically. This custom profile was created with the purpose of detecting any change in collagen fibril structure within leather from the grain surface, through to below the grain-corium junction and into the corium layer of leather.

Klaus Ahlbech and Suzanne Holst Borre from Cortex Technologies assisted in the development of this custom profile while visiting Cortex Technologies headquarters in Aalborg, Denmark. All leather testing was carried out underwater to further reduce attenuation of the signal and optimise penetration depth and image quality. The partially processed leather, the wet-blue and pickle, were also scanned while submerged underwater.

Data analysis

A-scan and B-scan analysis can be recorded simultaneously using the Dermascan set-up, and both were used for leather and ADM analysis. A B-scan image is made up of 224 A-scans using the Dermascan software. Depth measurements, distances and thicknesses can be selected and determined on the Dermascan software A-scan analysis. The B-scan function provides more in-depth information such as ‘Intensity segmentation’. This is the calculation of an image area which falls within a specific intensity range. This range can be set by adjusting the intensity level settings in the program. The program is capable of automatically detecting material edges, or otherwise a specific area of interest can be manually selected for analysis. When an area of a B-scan image has been selected, information such as the total area, segmented area selected in mm^2, minimum and maximum distances in mm, the total intensity in %, and the intensity within the set range in %, are all automatically and instantly calculated by the software. This quick analysis of the recorded ultrasound intensity and area of a sample has proved to be a very useful tool in the analysis of fibril packing and density in leather samples. This work is further discussed in chapters 1 and 2.

Poisson’s Ratio of Materials

Poisson’s ratio, named after Simeon Poisson, offers a fundamental metric to compare the mechanical performance of materials when strained elastically. It is a negative ratio of the transverse to axial strain when a material is compressed or stretched in one direction. Materials such as glass, wood, metal, ceramics, polymers and tissues all behave very differently when under stress; Poisson’s ratio allows for universal numerical comparisons of how extensible or incompressible materials are(*83*). Poisson’s ratio of stable, isotropic materials cannot be less than -1 or greater than 0.5 due to the requirements of Young’s modulus. Most materials have a Poisson’s ratio between 0 and 0.5, where a completely incompressible material, where volume is maintained, has a Poisson’s ratio of 0.5.

Negative Poisson’s ratios below -1 are possible for auxetic materials, where the thickness of a material increases in the perpendicular direction to strain when strain is applied. Conversely, an auxetic material decreases in thickness or diameter when it is compressed. This behaviour is often due to unique molecular bonding in a material, and results in interesting mechanical properties such as fracture resistance and high energy absorption(*84*).

Anisotropic materials can have a Poisson’s ratio above 0.5. These materials decrease in thickness or diameter faster than the rate of elongation. In other words, the structure collapses and the total volume decrease when strain is applied. Previously, it has been shown that collagen based materials such as cartilage (*85*) ligaments (*86*) and tendon (*87*), are anisotropic and can exhibit high Poisson’s ratios. This is an unusual characteristic for most materials, and therefore this could play an important role in the mechanics of these tissues. While this was known to occur for some bulk collagen materials, the behaviour of the collagen fibrils within these materials when under strain had not been widely studied. It is wondered how the collagen fibrils themselves behave under strain, as this may help to understand the bulk mechanics of collagen tissues and materials.

Section A: Looseness in Leather

Chapter 1: Looseness in Bovine Leather: microstructural characterisation

Chapter 1 is published as an academic journal article in the Journal of Science Food and Agriculture:

- **H. C. Wells,** G. Holmes, R. G. Haverkamp, "Looseness in bovine leather: microstructural characterization" **(2015)** *J. Sci. Food Agric.* DOI:10.1002/jsfa.7392

ABSTRACT

A substantial proportion of bovine leather production may be of poor quality, with the leather suffering from a characteristic known as looseness. This defect results in a poor visual appearance and greatly reduced value. The structural mechanism of looseness is not well understood. Samples of loose and tight bovine leather are characterized using small angle X-ray scattering, ultrasonic imaging, and electron microscopy. The density of fibre packing and the orientation of the fibrils are analysed. Tensile strength is also measured. Loose leather is characterized by more highly aligned collagen fibrils. This results in a weaker connection between the layers. There is a looser packing of the fibres in loose leather than in tight leather, with more gaps between fibre bundles, particularly in a region in the lower grain. This region is visible with in-situ ultrasonic imaging. Loose leather has a higher tensile strength than tight leather. While a high degree of collagen fibril alignment is normally associated with strong leather, it has been shown that too much alignment results in loose leather. Understanding the physical basis of looseness is the first step in identifying looseness in hides and learning how to prevent looseness from developing during leather manufacture.

INTRODUCTION

To maximize the income from leather production it is paramount that the finished leather be of high quality. Leather is produced from hides and skins on a large scale, in a multibillion dollar industry. The raw products come from a wide range of animals, but the largest volume and value are associated with bovine leather(*88*). The main uses of bovine leather are in footwear, upholstery (including automotive) and apparel. While many properties of leather make it suitable for use in these applications, one important property in all of these uses is appearance. Surface features that give what is considered an undesirable appearance or that result in variation in appearance from one region to another reduce the value of a hide considerably. Looseness is one such feature that degrades leather quality.

Specifically, in the industry, “looseness” is a term applied to leather with an excessive tendency to exhibit wrinkles or creases in a finished product. Looseness describes a coarse (bad) “break”, which is defined in the standard (*89*) as “the pattern of wrinkles formed on the grain surface of upper leather when it is bent grain in to form a concave surface. . . A fine break, or a grain pattern which shows many fine wrinkles when it is bent . . . reflects favourably upon appearance and serviceability. A coarse break . . . where a few coarse wrinkles are formed on bending the grain to form a concave surface may indicate that the grain layer is separating from the corium or main stratum . . . Shoes made from fine-break leather are more attractive and tend to wear longer than shoes made from coarse-break leather.”

Typically looseness might result in the downgrading of 5–10% of bovine leather produced at a tannery, even after trimming(*6*). Looseness is prevalent in specific regions of the hide, especially the shoulders and flanks. Where this looseness stretches more than half-way up the side of the leather, it is deemed to be a reject. This represents a substantial loss in profits and a waste of processing capacity and resources. Currently, looseness cannot be detected until a hide is part processed. The test for looseness is simple: an operator folds a piece of leather with the grain side in to observe surface wrinkles. However, despite the potential loss of value to the industry through looseness, there is little understanding of the structure of loose leather and how that structure results in the features observed in the looseness test or in a loose product. This work attempts to fill this gap in understanding.

Not only bovine leather is susceptible to looseness: it is also observed in, for example, ovine and deer leather. However, only bovine leather is investigated in this study, in part because of the industry’s perception that looseness in ovine and deer leather may have very different

characteristics to looseness in bovine leather. Nonetheless, this work draws on existing published research on the structures of leather derived from a variety of species.

One of the few published studies on looseness, which combined microscopic observation and mechanical tests, found that in loose leather the grain layer tends to be separated into sheet-like structures and that there are larger gaps between the collagen fibres than in tight leather (*90*). The presence of sufficient elastin in the grain layer has been suggested as being necessary to prevent looseness (*91*). The effect of different fillers on break have also been investigated (*92-97*), as has the effect of different tanning agents (*92*).

Structural characterization of leather has recently been advanced with state-of-the-art synchrotron-based X-ray scattering techniques to give insights into collagen fibril arrangement and dimensions that relate to leather tear strength (*57*). A large variability in the collagen fibril alignment in the plane of leather has been documented between species and the alignment correlates strongly with leather tear strength (*25, 98*). Fibril diameter has been found to be weakly correlated with tear strength (*99*). Tests of the response of leather structure under stress have shown how different leathers response structurally to strain in different ways (*100*) and that the collagen fibrils are very resilient, with a high Poisson's ratio (*101*). These techniques are applied here to improve understanding of the structural differences between loose and tight leather, and are combined with electron microscopy and ultrasonic imaging techniques.

METHODS

Leather preparation

The hides used for measurements in this study were obtained part-processed from a production run of hides at a local tannery. The hides weighed around 35 kg and have been green fleshed and processed using a conventional recipe. This recipe is based on sodium sulfide, sodium hydrosulfide and lime to both depilate and open-up the structure to allow the removal on non-collagenous proteins in drums of 4 m diameter by 3.8 m wide, which are loaded with approximately 8500 kg of hides at a time. Rotational speed is kept at 0.0179 g during the liming stage and 0.0716 g during washing. Hides are taken from the processing drums after 8 h liming. The lime splitter operated at a splitting thickness of 3.5-4.0 mm. Hides were observed passing through the splitter, and hides selected at this stage which displayed more “draw” across the shoulder and flanks than others in the batch. The selected hides were returned to the Leather and Shoe Research Association (LASRA) for onward processing in the LASRA pilot tannery to leather using a conventional recipe for shoe leather production. The next day the horsed-up leather was sammed and set to achieve a moisture content of 650 g kg^{-1} and toggle dried at 40 °C on a tunnel drier until dry in all regions. The leathers were conditioned heavily with water on the flesh-side and held in this condition for 24 h. The next day moisture measurements were taken to ensure a moisture content of 140 – 160 g kg^{-1} in all areas prior to Molissa staking on settings of 4 and 5.

Looseness evaluation

Looseness was evaluated using the standard break test method (*89*), which involves folding the leather grain side in, and quantifying the wrinkles against a standard break scale. Two independent operators measured the break score and the results were averaged. From three hides of leather, samples were taken from five regions: the OSP, the lower axilla, the belly, the upper axilla and the neck. The looseness was evaluated and the samples were determined to be either loose or tight. Samples were considered tight if they gave a break of less than 3 and loose if they have a break of 5 or more. Those samples with a break between 3 and 5 were not evaluated.

Ultrasonic imaging

Ultrasonics images of the leather were recorded with a DermaScan C USB instrument (Cortex Technologies, Denmark). A 20 MHz 2D-scanning head was used to carry out scanning at 6-8 frames per second. The scanning head contains an internal water chamber to minimize attenuation of the acoustic signal. To further improve image quality, scanning was carried under water once the leather had been soaked in water for at least 24 h. The sound velocity in leather was calibrated from the time of signal reflection and found to be 2561 (σ = 99) m/s. The bandwidth is 0.75, which resulted in an axial resolution of 97 µm (60 µm at 1580 m/s). The lateral resolution is 150 µm, owing to the mechanical scanning of the transducer. The focal point sits at a depth of 13 mm from the ultrasonic transducer face, which allows for the distance from the transducer (through the water-filled chamber) to the barrier membrane and through the water film on the leather, such that the focal point falls approximately within the leather sample. The transducer gain level and gain profile were used to adjust the amplification of the signal. Setting the amplification correctly reduces attenuation, allowing for better signal penetration and image quality. The 20 MHz probe transmits ultrasound with a peak intensity of 0.19 W/mm^2. A custom gain profile was created for use on leather with a minimum intensity of 21 dB at the leather grain surface, increasing to a maximum intensity of 42 dB at the corium.

Scanning electron microscopy

Small cubes of sample were fixed for 8 h at room temperature in a modified Karnovsky's fixative, containing 30 g kg^{-1} glutaraldehyde, 20 g kg^{-1} formaldehyde in 0.1M phosphate buffer, pH 7.2. Three washes, each 10–15 min, were carried out in phosphate buffer (0.1M, pH 7.2) followed by dehydration in a graded ethanol series (250, 500, 750, 950, 1000 g kg^{-1}) for 10–15 min each. Samples were finally washed for 1 h in pure ethanol. Samples were critical-point dried in liquid CO_2 (CP fluid) and pure ethanol (intermediary), using the Polaron E3000 series II critical point drying apparatus. Samples were mounted and sputter-coated with gold (Baltec SCD 050 sputter coater) on to aluminium stubs and viewed in the FEI Quanta 200 Environmental Scanning Electron Microscope at an accelerating voltage of 20 kV.

Transmission electron microscopy

For transmission electron microscopy (TEM), samples were fixed with 20 g kg^{-1} formaldehyde and 30 g kg^{-1} glutaraldehyde in 0.1 M phosphate buffer (pH 7.2) for 2 h at room temperature. The samples were washed and then post fixed with 10g kg^{-1} OsO_4 in buffer for 1 h at room temperature. After three washings for 10 min, they were dehydrated using an acetone/water series (250, 500, 750, 950, 1000 g kg^{-1}) for 10–15 min each, followed by two changes of pure acetone for 1 h each. The leather samples were first embedded with an acetone resin (Procure 812 ProSciTech, Australia) mixture (50 : 50), being left on a stirrer overnight, and then the 50:50 mixture was replaced with pure resin and the samples left for another 8 h and stirred; this step was repeated twice. The samples were finally embedded in fresh pure resin at 60° C for 48 h.

Sections 1 µm thick were cut from trimmed resin blocks using a glass knife (Leica, Australia). They were heat-mounted onto a glass slide, stained with 5 g kg^{-1} toluidine blue for approximately 12 s and viewed under a light microscope to select areas of interest for TEM examination. Ultra-thin sections (100 nm thick) were cut using a diamond knife and ultramicrotome (Diatmone, Switzerland). They were stretched with chloroform and mounted on a copper grid using a Coat G pen (Diado Sangyo, Japan). The sections were stained with uranyl acetate in 50% ethanol for 4 min, washed with 500 g kg^{-1} ethanol and MilliQ water and then stained with lead citrate for another 4 min. Finally, they were again washed with MilliQ water. The specimens were examined with a FEI Tecnai G2 Biotwin Transmission Electron Microscope with a tomography unit.

Small angle X-ray scattering

Diffraction patterns were recorded on the Australian Synchrotron SAXS/WAXS beamline. The beamline has an undulator source and a cryo-cooled Si (III) double-crystal monochromator. It has an energy resolution of 10^{-4}, a beam size full width half maximum (FWHM) at the sample of 250 x 150 µm and a photon flux of approximately 2 x 10^{12} ph/s. Patterns were recorded with an X-ray energy of 11 keV and an exposure time of 1–2 s on a Pilatus 1M detector with an area of 981 x 1043 pixels. A sample-to-detector distance of 3371 mm and an active area of 170 x 170 mm were used. The energy is calibrated using the zinc K-edge from zinc foil at 9.659 keV and is maintained within 2 eV of the nominal energy.

Each sample was mounted on a remotely controlled sample plate that was placed in the path of the X-ray beam. Samples were analysed from grain to corium with spectra recorded at 0.2 mm increments. All samples were stored under the same humidity conditions. Data were processed using SAXS15ID software (*102*).

Orientation Index (OI) is used to measure the spread of orientation of the collagen fibrils. It is calculated from the azimuthal angle spread of the most intense Bragg's peak at around 0.058–0.060 $Å^{-1}$. OI is defined as (90° – OA)/90° where OA is the minimum azimuthal angle range, centered at maximum peak intensity, that contains 50% of the fibril scattering intensity. An OI value of 1 indicates that the fibrils are completely parallel to each other, while a value of 0 indicates orientation of the fibrils is completely isotropic.

Tear and tensile test

Tear strengths were determined using standard methods for double-edge tear testing (*103, 104*). Samples were cut and stored at 20 °C and 650 g kg^{-1} relative humidity for 24 h before the tear strength was measured using an Instron 4467. Thickness was measured using method BS EN ISO 2589:2002. Six measurements were taken on tight leather (3 parallel and 3 perpendicular to the line of the backbone) and six on loose leather.

RESULTS

Break and Looseness

An example of the break being demonstrated on a sample of loose and tight leather is shown in Fig. 1.1. The larger wrinkles are visible in the loose leather (with a break of 7), whereas tight leather (with a break of 1) exhibits smaller and finer wrinkles.

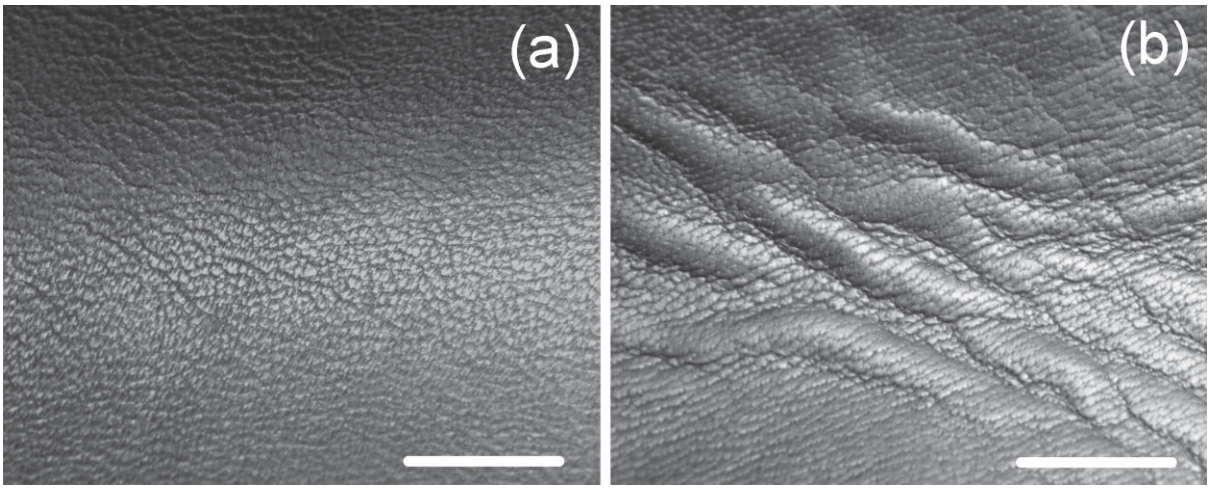

FIGURE 1.1: COMPARISON OF THE BREAK IN (A) TIGHT LEATHER WITH A BREAK OF 1 AND (B) LOOSE LEATHER WITH A BREAK OF 7. PHOTOS WERE TAKEN DURING THE BREAK TEST OF THE CONCAVE SURFACE OF THE GRAIN). SCALE BAR IS 2 MM.

Small Angle X-ray Scattering

SAXS analysis of cross sections shows differences between tight leather and loose leather (Fig. 1.2). The tight leather is characterized by a marked difference in OI between the corium and the grain, with a lower OI in the corium. The loose leather is characterized by a more uniform OI throughout most of the thickness, with a small drop in OI towards the bottom of the corium. The average OI for the loose leather, 0.61 (σ = 0.01), is higher than for the tight leather 0.43 (0.03) (t = 0.47, P < 0.001 for α = 0.05).

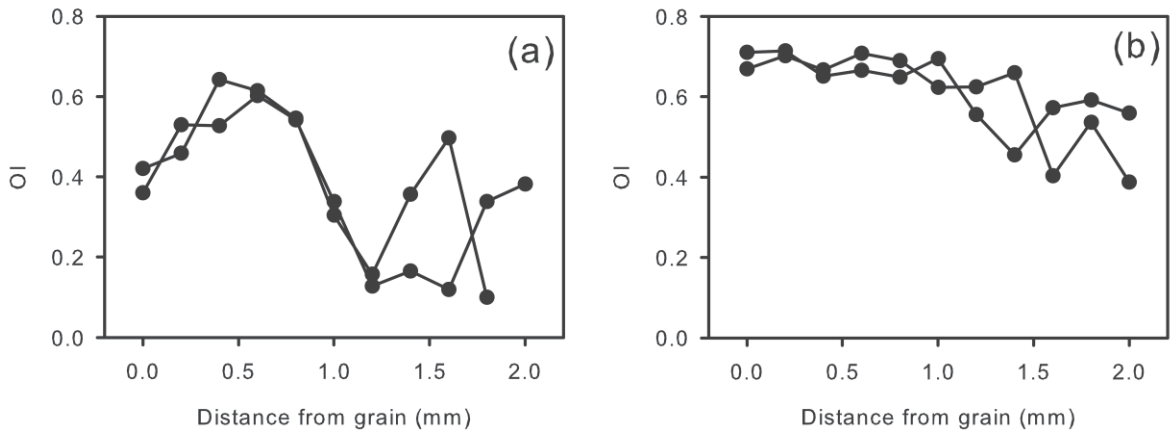

FIGURE 1.2: EXAMPLES OF ORIENTATION INDEX (OI) OF (A) TIGHT LEATHER AND (B) LOOSE LEATHER.

Ultrasonics

There are clear differences between the ultrasonic images of loose and tight leather (Fig. 1.3). In the loose leather, there is a band of reduced intensity below the top surface of the leather in the grain or grain-corium boundary region. This band suggests a less dense region with more space between the leather fibres. In the samples imaged here that space is filled with water but in dry leather the space would contain air. This region is not apparent in the tight leather, which clearly has a more dense structure in the grain or grain-corium boundary region.

The images demonstrate that there is a difference in the packing of the fibres in these leathers, with the loose leather having a more loosely packed structure. The difference is greatest in the middle of the grain layer: there is very little reflected ultrasonic signal in loose leather (the dark band), and an intense region of reflection the tight leather.

While the intention of this study was not a survey of the distribution of looseness in hides, because samples were taken from different positions on a number of hides some comment can be made on the distribution of looseness. The OSP, upper axilla tend to be tighter regions, while the lower axilla and belly are where the looseness is most strongly manifested. The neck region tends to be intermediate. In Fig. 1.3 the different regions displayed are identified with the looseness scores given.

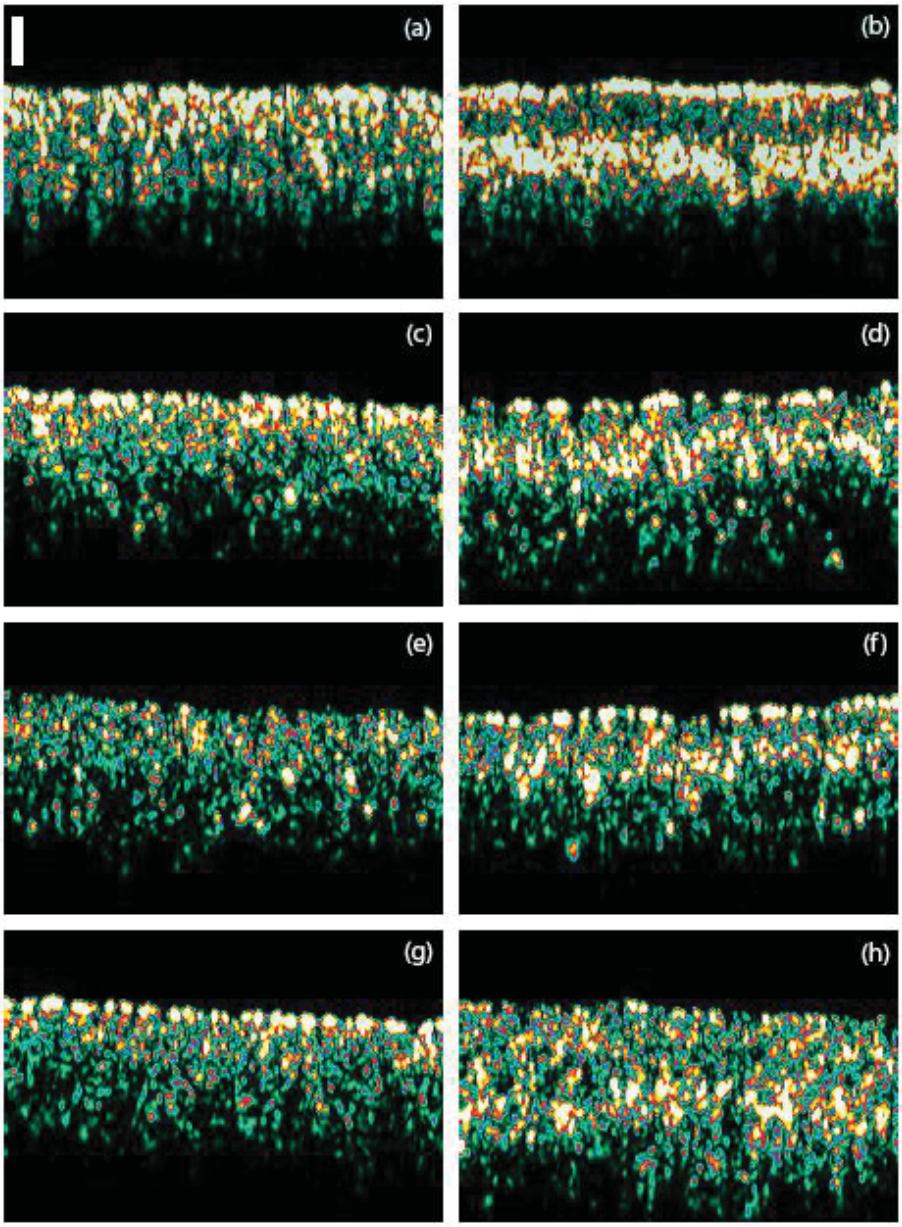

FIGURE 1.3: ULTRASONIC IMAGE OF (A, C, E, G) TIGHT LEATHER AND (B, D, F, H) LOOSE LEATHER (SCALE BAR 1 MM). THE GRAIN IS AT THE TOP OF EACH IMAGE AND THE IMAGE WAS TAKEN FROM THE GRAIN SIDE. SOME OF THE BOTTOM PART OF THE LEATHER (CORIUM) IS NOT VISIBLE AS THE ULTRASONIC SIGNAL IS GREATLY ATTENUATED AS IT PASSES THROUGH THE SAMPLE. POSITIONS OF THESE SAMPLES WITH THEIR LOOSENESS SCORES ARE: TIGHT – A (2) OSP, C (2) OSP, E (2) OSP, G (2.5) UPPER AXILLA; LOOSE – B (7) LOWER AXILLA, D (6) LOWER AXILLA, F (5) BELLY, H (6.5) LOWER AXILLA. SAMPLES A AND B ARE THE SAME AS THOSE DISPLAYED IN THE SAXS, SEM AND TEM FIGURES BELOW.

SEM

Scanning electron microscopy images of samples of tight and loose leather reveal that the tight leather appears to have a larger region with the characteristic grain structure than does the loose leather, with one representative image of each displayed in Fig. 1.4 a, b. Although the fibres of the upper grain region appear to be tightly packed in both the loose and tight leather, the loose leather also appears to have a region below the grain or in the lower part of the grain that contains cavities where the fibres are not densely packed together and this region is not apparent in the tight leather. The grain-corium region also differs between tight and loose leather in the closeness of the fibril bundle packing when viewed under higher magnification (Fig. 1.4 c, d), and of the collagen fibrils in some fibril bundles having looser packing in loose leather.

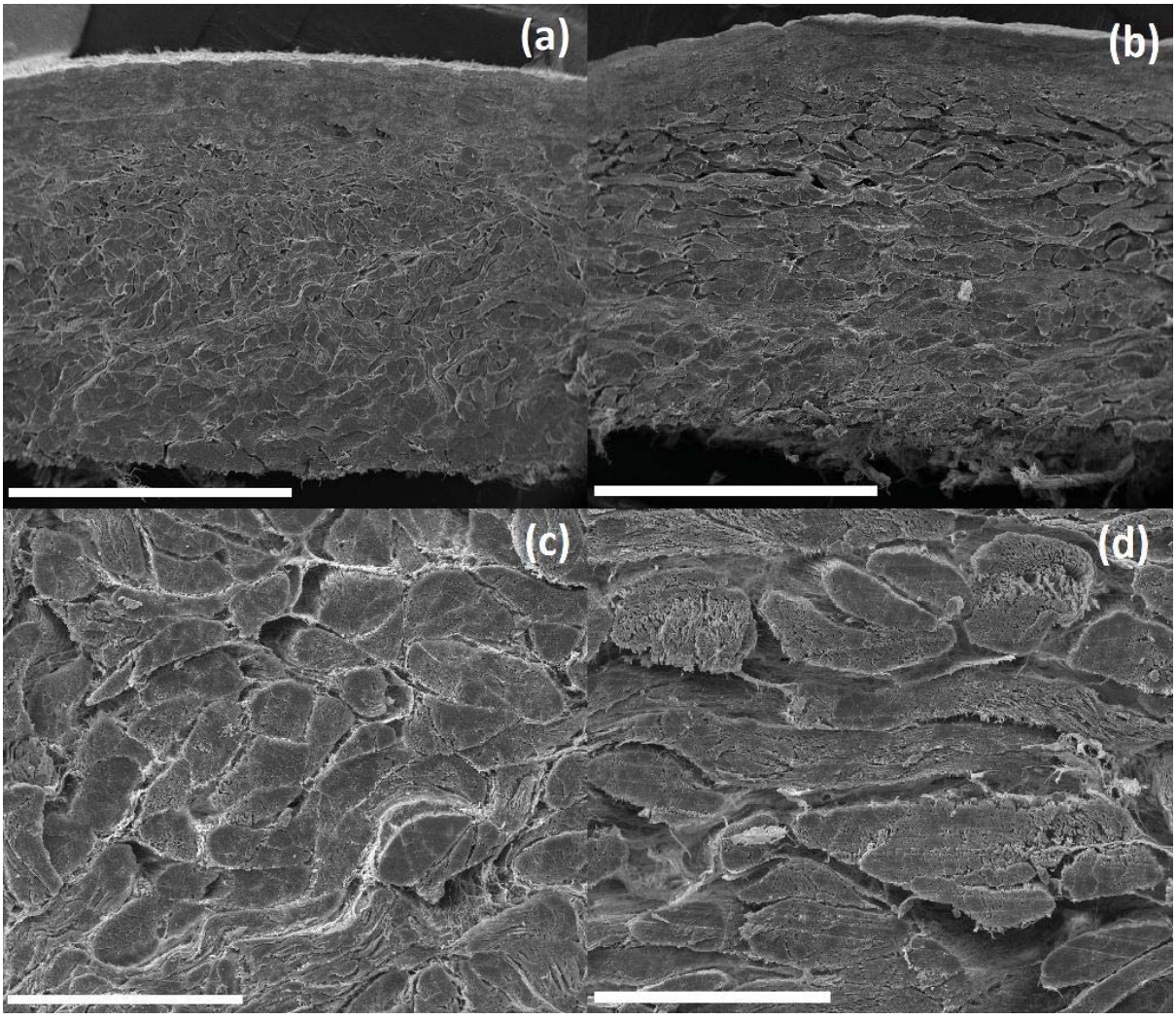

FIGURE 1.4: REPRESENTATIVE SEM IMAGES OF CROSS-SECTIONS OF (A, C) TIGHT AND (B, D) LOOSE LEATHER FROM THE GRAIN - CORIUM BOUNDARY REGION. SCALE BAR (A, B) IS 2 MM, (C, D) 300 µM.

TEM

There is significant variation within each leather type at the scale of TEM, which provides images at a magnification two orders of magnitude greater than shown in the SEM images. In both the corium and the grain, there appears to be larger separation between the fibre bundles in the loose leather than in the tight leather, which is visible in the representative images in Fig. 1.5.

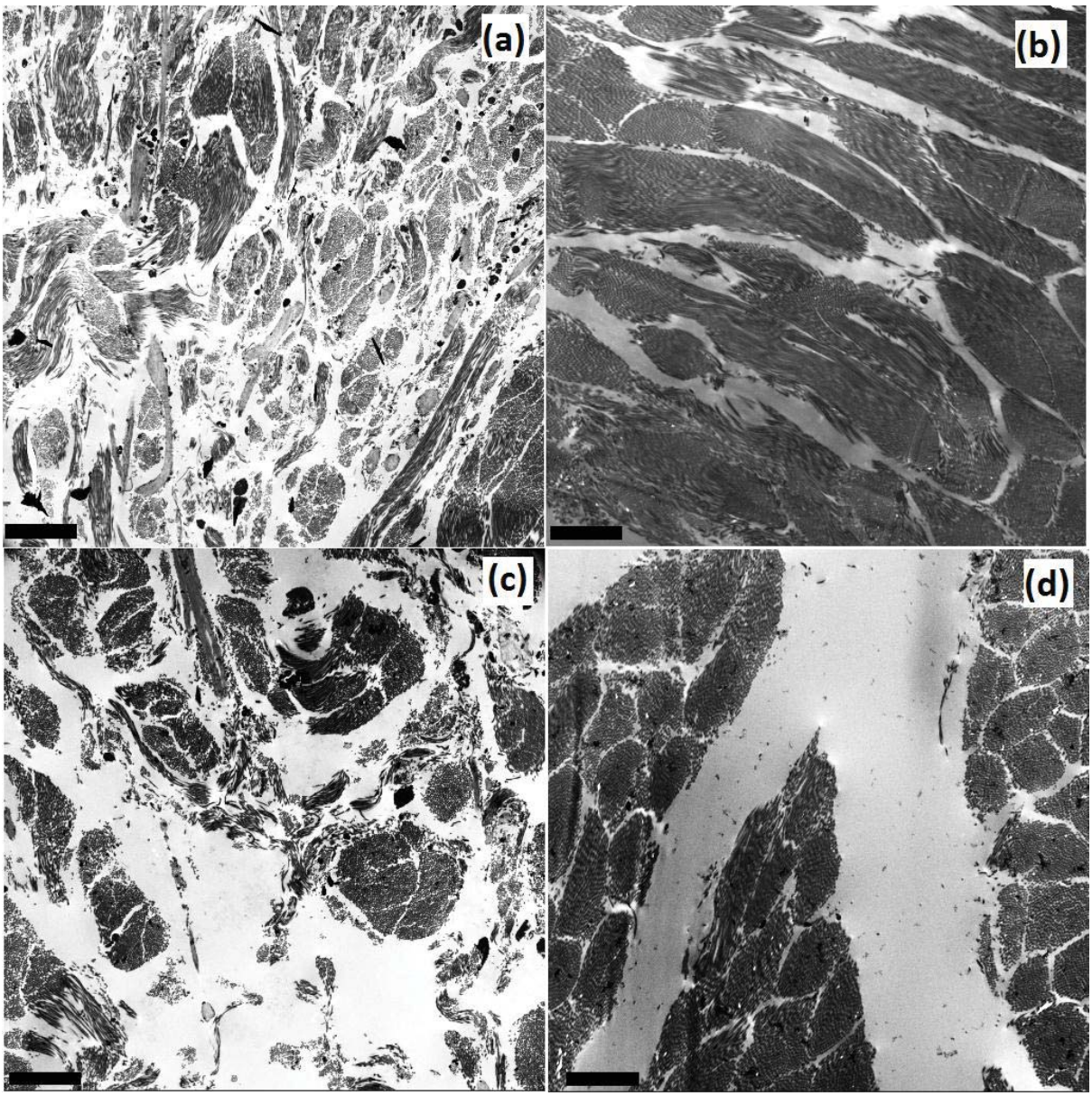

FIGURE 1.5: REPRESENTATIVE TEM IMAGES OF CROSS-SECTIONS THOUGH THE FIBRE BUNDLES OF (A, B) TIGHT LEATHER AND (C, D) LOOSE LEATHER. GRAIN (A, C) AND CORIUM (B, D). SCALE BAR IS 5 µM.

Tear and tensile strength

Loose leather is significantly stronger than tight leather, yielding a tear strength of 130 (σ = 61) N/mm as compared to 73 (σ = 10) N/mm (t = 16, P < 0.001 for α = 0.05).

DISCUSSION

The test for looseness is a measure of a physical manifestation of a structural property of leather. The undesirable characteristic that is manifested is the separation of the grain surface of the leather from the corium (or a separation within the grain). This results in a poor physical appearance. Looseness results from a structural deficiency in the leather, affecting the bonding of the layers either in the leather or in a specific layer or region in the leather. To date, specific detail on the structure that gives rise to this failure has not been available.

A weakness throughout the leather, where the leather fibre or collagen fibrils are able to separate, may be a consequence of a structure quite different to that responsible for a weakness in only one layer in the leather, for example in the grain or between grain and corium. We, therefore, investigated cross sections of leather with each of the structural characterization techniques. By taking the end members on the break scale, it is possible to characterize the structure of these materials and observe the relevant differences which may relate to looseness.

The combined evidence of ultrasonic imaging, electron microscopy and SAXS analysis shows that loose leather has a poorer connection between the “layers” due to less interweaving of the fibres between the layers and looser packing of the fibres and fibrils. The interweaving of these layers is clearly important for layer interconnectivity and its lack results in parts of the layers separating more easily. The looser packing of the collagen fibre bundles in the loose leather reflects that they are not as well held together as in the tight leather. “Looseness” is therefore a good descriptor not only for the external appearance of the leather, with the part of the grain coming loose from the rest of the leather, but also for the internal structure of the collagen fibres. This can be clearly seen in the ultrasonics images, with a region in the grain or grain-corium boundary showing more cavities, a state not unlike that seen below the dermis of age or sun-damaged skin (*105*).

The SEM images also reveal a large gap in the region in the grain or grain-corium boundary. The higher magnification SEM and the TEM provides confirming evidence at an even finer scale of differences between loose and tight leather. In loose leather, there is less close packing of the fibril bundles and less close packing in some of the fibril bundles of the collagen fibrils.

This technique is used for investigation of skin disease, for example in identification of tumours and inflammatory diseases(*106, 107*).

The OI profiles from SAXS of loose and tight leather are quite different, with fairly uniform highly oriented fibrils throughout the thickness of the loose leather but a lower and more varied orientation in the tight leather. OI profiles have previously be shown to differ between strong and weak leather and between different species (*100*), with strong, tight bovine leather typically showing a dip in OI in the central part of the leather, similar to the results shown here. It appears that a key feature of looseness is the absence of this central low OI region, and therefore the absence of the highly interlocked connection between layers in this region.

The higher tensile strength of loose leather might seem surprising, considering that this leather is thought to be defective leather of inferior quality. The separation of layers could be expected to weaken the material. However, an explanation can be provided that is consistent with the analytical results here and with previous work on strength in leather and other collagen materials (*98, 100, 108*). Fibril orientation is very important for strength: the collagen fibrils are strong along the length of the fibrils but do not have as much bonding strength between them. Therefore, strong leather results when fibrils are highly aligned in the plane of the leather (tensile testing is done in the plane of the leather, not across the thickness). However, when the fibrils are too highly aligned, the connection between the layers becomes compromised and loose leather results. Therefore, optimum bovine leather of sufficient strength requires the fibres to be aligned but not so aligned that the interconnecting layers are absent, resulting in looseness.

CONCLUSIONS

It has been shown that looseness is a structural defect that results from a poor connection within or between leather layers, particularly in the lower grain region or the grain-corium boundary. This is manifested as less closely packed collagen fibrils and is due to a highly

aligned collagen fibrils within the loose leather. Looseness can easily be identified in situ with ultrasonic imaging. The more loosely packed and weakly bonded grain of the loose leather, in comparison to tight leather, becomes separated during folding, resulting in the symptoms of poor break or looseness. Whether the incidence of looseness varies among different animals – for example, among animals of different breeds, sex, age or condition, or animals exposed to varying environmental factors – forms part of a separate study. Why such variations might lead to this skin structure would then be a useful avenue for investigation.

Chapter 2: Early Detection of Looseness in Bovine Hides using Ultrasonic Imaging

Chapter 2 is published as a journal article in the Journal of the American Leather Chemists Association:

- **Hannah C. Wells**, Geoff Holmes, Richard G. Haverkamp "Early Detection of Looseness in Bovine Hides using Ultrasonic Imaging" *J. Am. Leather Chem. Assoc.* **(2016)** 111 (3).

ABSTRACT

The processing of bovine hides to leather results in a significant proportion of defective leather known as loose leather. It has not previously been possible to recognize hides that may produce loose leather. Hides were processed through to leather with samples retained at the pickle, wet blue and leather stages with material that resulted in loose leather compared with that resulting in tight leather, using ultrasonic imaging. The loose precursor is characterized by a lower density of material in the mid grain layer. The looseness is quantified by amplitude differences in ultrasound line scans or cross-sectional area scans between loose leather and tight leather with 2-4 times the amount of low intensity area in loose leather at all three process stages. This enables detection of hides that will result in loose leather and may enable unsuitable hides to be diverted to other process streams to save substantial processing costs.

INTRODUCTION

Leather produced from bovine hides may exhibit a defect known as looseness (*109*). This defect is present in 5-10% of finished bovine leather and results in a greatly reduced value for the leather and therefore a loss of revenue to the industry. At present there is no way to identify unprocessed hides that may result in loose leather nor is it yet possible to predict which animals are likely to produce loose leather. Many unsuitable hides are therefore processed to leather and subsequently rejected or downgraded at the leather stage.

Looseness is a term used in the leather industry to describe an undesirable characteristic of leather with an excessive tendency to exhibit wrinkles or creases in a finished product. Looseness describes a coarse (bad) "break" as defined in the ASTM standard (*89*) "…where a few coarse wrinkles are formed on bending the grain to form a concave surface may indicate that the grain layer is separating from the corium or main stratum"

In loose leather the grain layer tends to be separated into sheet like structures and there are larger gaps between the collagen fibres than in tight leather (*90*). The presence of sufficient elastin in the grain layer has been suggested as being necessary to prevent looseness (*91*). It has been shown that looseness is a structural defect that results from a poor connection within or between layers particularly in the lower grain region or grain-corium boundary. This is manifested in less closely packed collagen fibrils and results from a high degree of alignment of collagen fibrils within the loose leather. The more loosely packed and weakly bonded grain of the loose leather, in comparison to tight leather, becomes separated during folding grain-in resulting in the symptoms of poor break or looseness(*109*).

Ultrasonic imaging has been shown to be able to clearly identify looseness in the leather with a layer of lower intensity of reflected signal in the grain (*109*). Ultrasonic images of looseness in leather look similar to that of aged or sun damaged skin which also shows a low intensity of reflected signal in the dermis (*105*). The technique can also be used for investigation of skin disease, for example in identification of tumors and inflammatory diseases (*106, 107*).

While looseness is defined for leather, it may be that the structural characteristics that result in looseness are present in the unprocessed hides and could be identified in the hides or in early stages of the tanning process. The looseness test, that of folding leather grain-in to observe the size of the creases, is not able to detect looseness precursors in unprocessed hides or early stages of leather processing. However, if looseness in leather results from structural characteristics of the hide, then it should be possible to identify these structural

characteristics by other means. Here we attempt to identify looseness prior to the leather stage using ultrasonic imaging.

METHODS

Sample selection

A range of hides were selected from the lime-splitting machine at Tasman Tanning Ltd (New Zealand) with the intention to collect some that might turn out to be loose and some that might be tight. There was no way to accurately determine which hides would turn out loose, however some that appeared to have more draw were chosen as being likely candidates. The selection that was hoped to contain some loose and some tight hides was subsequently processed in the LASRA pilot tannery as detailed below.

Leather preparation

The hide used for measurements in this study was obtained part-processed from a production run of hides at a local tannery. The hides weighed around 35 kg and have been green fleshed and processed using a conventional recipe. This recipe is based on sodium sulphide, sodium hydrosulphide and lime to both depilate and open-up the structure to allow the removal on non-collagenous proteins in drums of 4 m diameter by 3.8 m wide, which are loaded with approximately 8500 kg of hides at a time. The rotational speed provided a sample acceleration of 0.179 ms^{-2} during the liming stage and 0.716 ms^{-2} during washing. Hides are taken from the processing drums after 8 h liming. The lime splitter operated at a splitting thickness of 3.5-4.0 mm. Hides were observed passing through the splitter, and hides selected at this stage which displayed more “draw” across the shoulder and flanks than others in the batch. The selected hides were returned to LASRA for onward processing in the LASRA pilot tannery to leather using a conventional recipe for shoe leather production. The next day the horsed-up leather was sammed and set to achieve a moisture content of 65 % and toggle dried at 40 °C on a tunnel drier until dry in all regions. The leathers were conditioned heavily with water on the flesh-side and held in this condition for 24 h. The next day moisture measurements were taken to ensure a moisture content of 14 – 16 % in all areas prior to Molissa staking on settings of 4 and 5.

From the leather, samples showing looseness were taken from the shoulder region, just above the axilla, with tight samples cut from adjacent areas outside of the affected region. The results presented here are from only one hide. However, other leather samples were analysed which provided results consistent with those reported here.

Looseness evaluation

Looseness was evaluated using the standard break test method (*89*), which involves folding the leather grain side in, and quantifying the wrinkles. Samples were considered tight if they gave a break of 2 or less and loose if they had a break of 4 or more.

Ultrasonic imaging

Ultrasonic images of the leather were recorded with a Dermascan C USB instrument (Cortex Technologies, Denmark). A 20 MHz 2D-scanning head was used to carry out scanning at 6-8 frames per second over a distance of 12.1 mm in 224 steps. The scanning head contains an internal water chamber to minimize attenuation of the acoustic signal. To further improve image quality, scanning was carried out under water once the leather had been soaked in water for at least 24 h. The sound velocity in leather was calibrated from the time of signal reflection and found to be 2561 (σ = 99) m/s. The bandwidth is 0.75, which resulted in an axial resolution of 97 µm (60 µm at 1580 m/s). The lateral resolution is around 150 µm. The focal point sits at a depth of 13 mm from the ultrasonic transducer face, which allows for the distance from the transducer (through the water-filled chamber) to the barrier membrane and through the water film on the leather, such that the focal point falls approximately within the leather sample. The transducer gain level and gain profile were used to adjust the amplification of the signal. Setting the amplification correctly reduces attenuation, allowing for better signal penetration and image quality. The 20 MHz probe transmits ultrasound with a peak intensity of 0.19 W/mm^2. A custom gain profile was created for use on leather with a minimum intensity of 21 dB at the leather grain surface, increasing to a maximum intensity of 42 dB at the corium.

The ultrasonic data can be displayed in what is conventionally called an A-scan or a B-scan. An A-scan is a line scan that represents depth information from one point on the surface of

the leather; a B-scan is a two dimensional image that represents a cross-sectional area of leather (and is composed of a large number of A-scans, but displayed using colour for intensity).

Scanning electron microscopy

Small samples were fixed for 8 h at room temperature in a modified Karnovsky's fixative, containing 30 g kg^{-1} gluteraldehyde, 20 g kg^{-1} formaldehyde in phosphate buffer (0.1M, pH 7.2) then washed in phosphate buffer (0.1M, pH 7.2) followed by dehydration in a graded ethanol series. The samples were finally washed for 1 h in pure ethanol and critical-point dried in liquid CO_2 and pure ethanol (intermediary), using the Polaron E3000 series II critical point drying apparatus. The samples were mounted on to aluminium stubs and sputter-coated with gold (Baltec SCD 050 sputter coater) and viewed in the FEI Quanta 200 Environmental Scanning Electron Microscope (SEM) at an accelerating voltage of 20 kV.

RESULTS

Sample selection

A selection of samples of loose and tight leather were successfully made with materials from the pickle and wet blue stages for each of these retained for testing. The leather resulting from these had a break of 2 for the tight leather and 5 for the loose leather.

Ultrasonic images

The ultrasonic imaging of different stages during the processing of leather was able to clearly show differences between the loose and tight leather at each stage of the process (Fig. 2.1). The images display the intensity of the reflected ultrasonic signal. Reflection occurs at interfaces between areas of high and low density so that the signal can be a measure of the number of these interfaces. Therefore an area of very uniform (at the scale of the wavelength of the ultrasound) high density or very uniform low density should both show as black or

green on these images. However, leather is not uniform at the scale of the ultrasonic wavelength used so that regions of a high density of collagen fibres contain many interfaces and display as high intensity colour scale (white) while regions of low density show as black or green.

In the tight leather the grain is uniformly more dense than the corium and grades gradually to less dense material. In contrast, in loose leather the top surface of the grain looks dense (high intensity ultrasonic reflections) but there is a region about 0.5 mm below the top of the grain that is less dense (lower intensity ultrasonic reflections) followed by a denser region below this layer towards the corium. In the tight wet blue material there is a gradation of density from higher density towards the top of the grain. In the loose wet blue there is a more uniform density through the leather. In the tight pickle the hide has dense top grain surface with a gradation of decreasing density deeper into the hide, whereas in the loose pickle there is a low density layer at the grain surface with a more dense region about 0.5 mm below the grain.

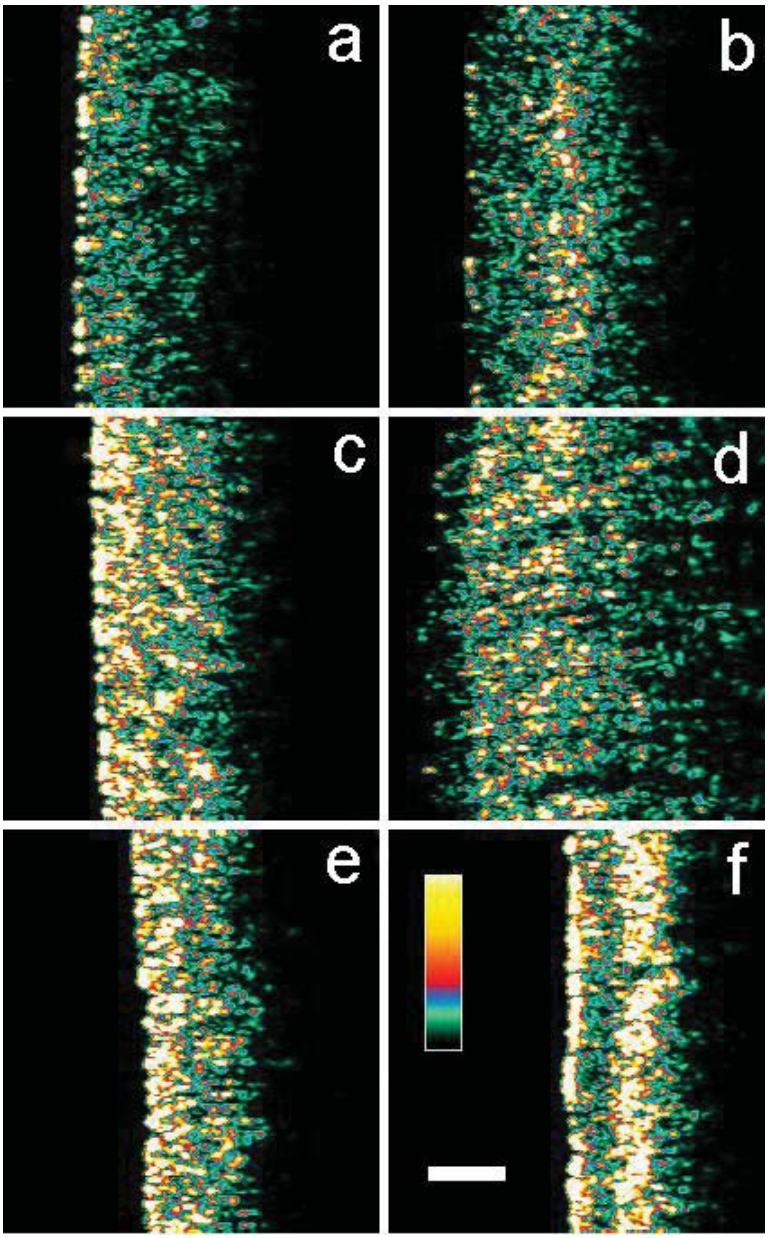

FIGURE 2.1: ULTRASONIC IMAGES (B-SCANS) OF A, TIGHT PICKLE, B, LOOSE PICKLE, C, TIGHT WET BLUE, D, LOOSE WET BLUE, E, TIGHT LEATHER, F, LOOSE LEATHER. THE GRAIN IS ON THE LEFT, CORIUM ON THE RIGHT. SCALE BAR IS 0.5 MM. THE COLOUR SCALE REPRESENTS SIGNAL INTENSITY FROM BLACK (MINIMUM INTENSITY) TO WHITE (MAXIMUM INTENSITY).

From the ultrasonic images it is possible to measure the proportion of the leather that consists of lower density regions. To do this, the “B-scan measure” software feature of the Dermascan was used. A region of interest was selected, and for this a rectangular band 0.378 mm thick was chosen containing the grain or the top part of the grain. The proportion of pixels that were in the intensity range 0-20 (where the total range is 0-255 so that 20

represents 7.8%), under the measurement conditions used for all the samples, was measured (Fig. 2.2).

The portion of the grain that gives low intensity ultrasonic reflections, representing regions of low density, can be quantified as a percentage of the total area selected. From these measurements the differences between tight and loose leather can be represented as a ratio of this low density region (Table 2). The loose leather contains 2–4 times the amount of low density area than the tight leather and this is at least as apparent in the pickle and wet blue stages of processing as it is in the leather. These differences are statistically significant.

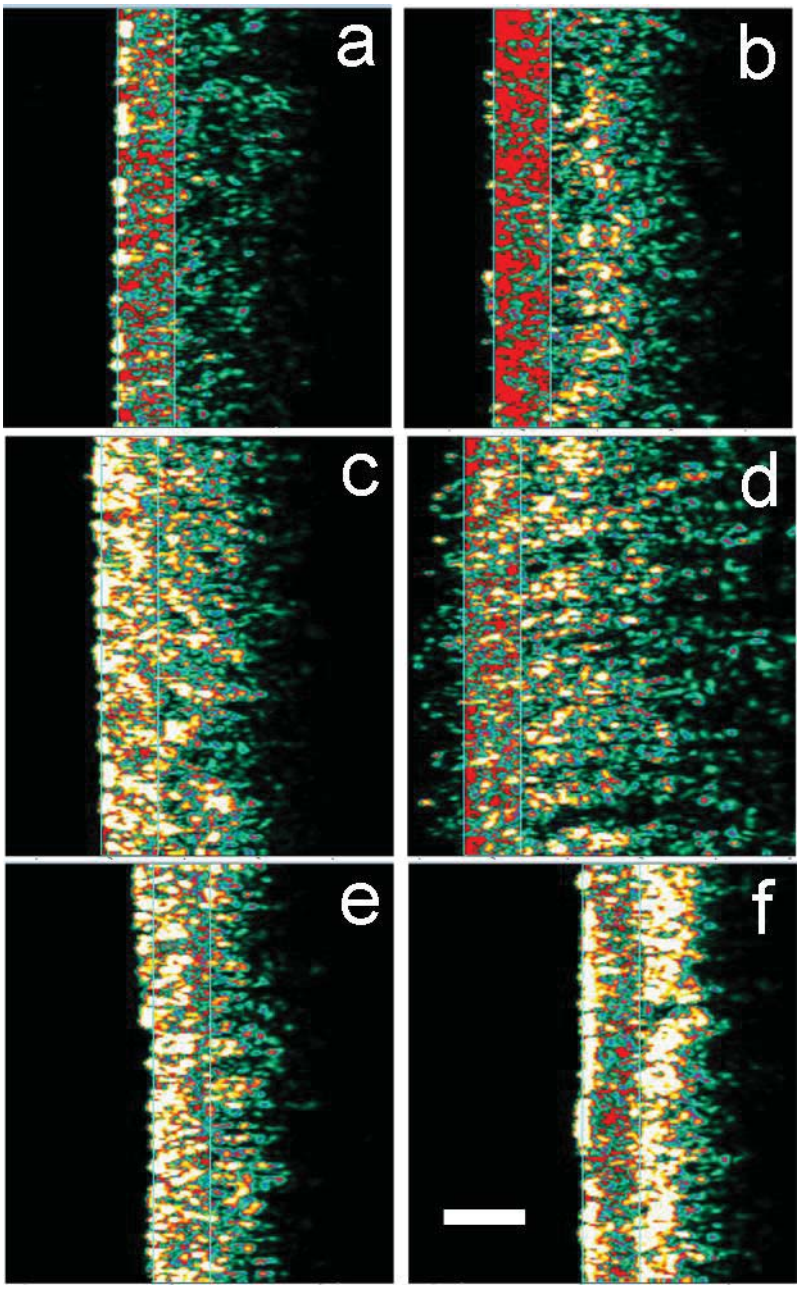

FIGURE 2.2: DISPLAY OF THE PORTION WITH INTENSITY BELOW 7.8% OF THE MAXIMUM INTENSITY OF REFLECTED ULTRASONIC SIGNAL (IN RED) FOR A SELECTED REGION 0.378 MM

WIDE (DEFINED BY THE WHITE LINE) AT THE GRAIN. A, TIGHT PICKLE, B, LOOSE PICKLE, C, TIGHT WET BLUE, D, LOOSE WET BLUE, E, TIGHT LEATHER, F, LOOSE LEATHER. THESE ARE THE SAME DATASETS AS IN FIGURE. 2.1.

Table 2. Percentage of the area in the selected region that has low intensity ultrasonic reflection (0-20 / 255). Averages are from the analysis of 8–13 images.

Sample type	Tight % area (σ)	Loose % area (σ)	Ratio loose/tight	t-test for difference t-stat, P
Pickle	20.6 (4.1)	38.0 (13)	1.8	-4.6, <0.0001
Wet blue	3.4 (1.0)	12.6 (2.2)	3.7	-12, <0.0001
Leather	5.3 (1.4)	9.8 (2.7)	1.9	-4.7, 0.0001

An alternative method of analysing the ultrasonic data is by using A-scans (single point depth scans). By averaging a series of A-scans to give an average composition of a volume of leather the differences between tight and loose leather are easily seen (Fig. 2.3) with a marked dip in the reflected ultrasonic intensity in the loose leather below the grain surface. The tight leather does not have a comparable drop in intensity in this region.

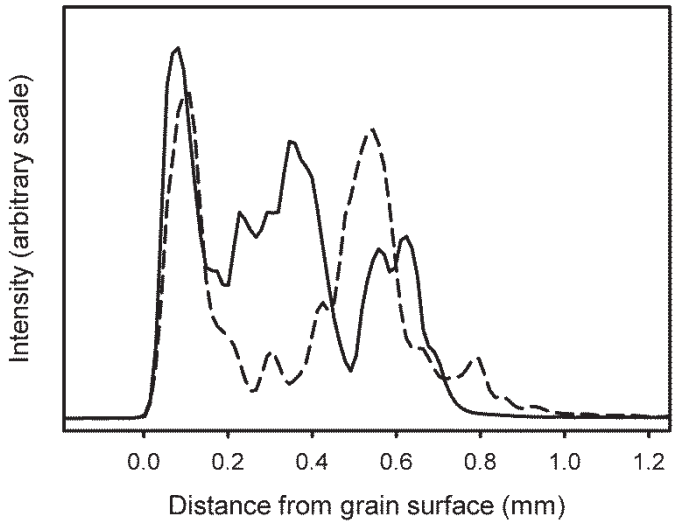

FIGURE 2.3: A-SCANS OF TIGHT (SOLID LINE) AND LOOSE (DASHED LINE) LEATHER. EACH PLOT IS AN AVERAGE OF 20 SCANS, REPRESENTING A TOTAL OF 1.0 MM MOVEMENT ACROSS

THE SURFACE OF THE LEATHER. THESE ARE TAKEN FROM RECORDINGS SIMILAR TO, BUT NOT IDENTICAL TO, THE IMAGES FROM FIGURE. 2.1 AND 2.2, E AND F.

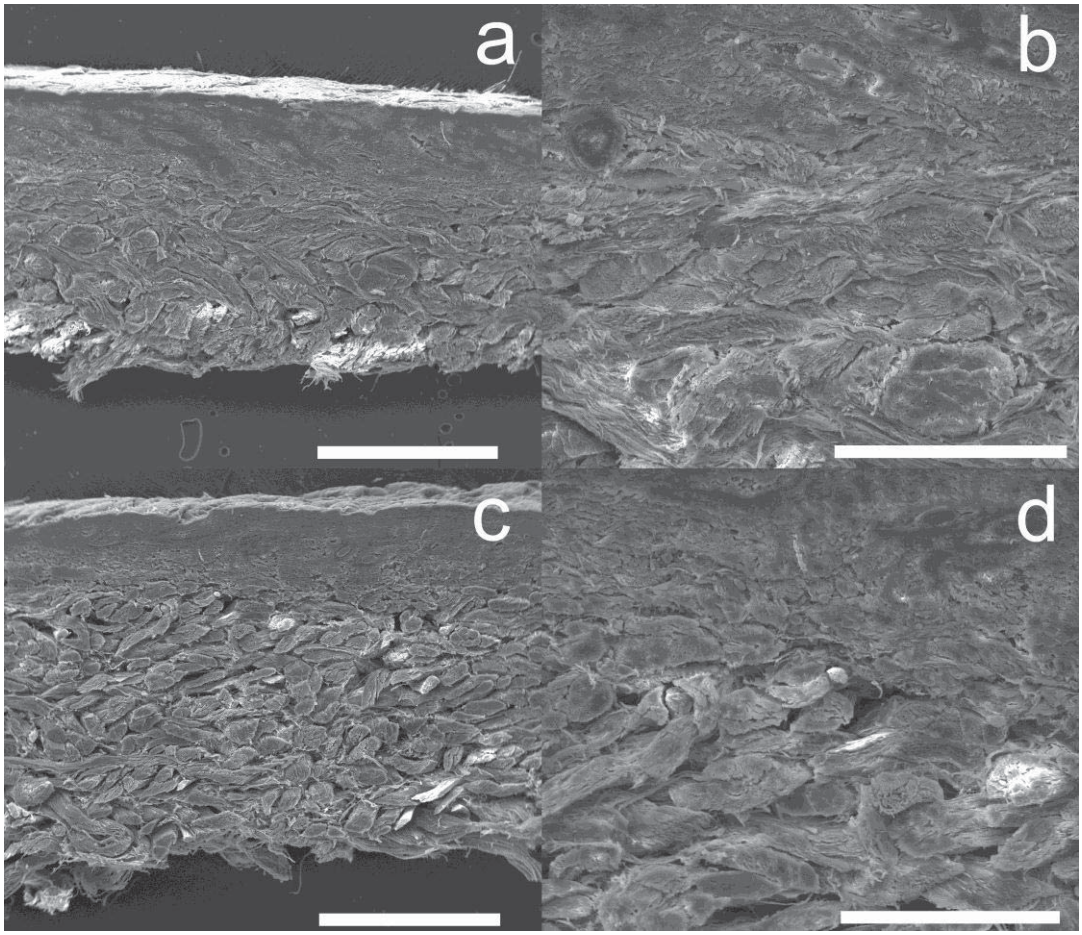

FIGURE 2.4: SEM IMAGES OF CROSS SECTIONS OF TIGHT (A, B) AND LOOSE (C, D) LEATHER. GRAIN IS AT THE TOP. THE ENLARGEMENTS (B, D) ARE NEAR THE GRAIN–CORIUM BOUNDARY. SCALE BAR (A, C) 1 MM, (B, D) 400 MM.

Scanning electron microscopy

SEM was used to confirm the loose and tight internal structure of the leather used in this work (Fig. 2.4). It is clear from these images that the tight leather has a compact structure in both the grain and corium including at the grain-corium boundary (Fig. 2.4 a, b) whereas the loose leather has fiber bundles that in the corium are not tightly packed together (Fig. 2.4 c, d).

DISCUSSION AND CONCLUSIONS

Looseness in leather is a structural defect that results from a poor connection within or between leather layers, particularly in the lower grain region or the grain-corium boundary. This is manifested as less closely packed collagen fibrils and is due to highly aligned collagen fibrils within the loose leather (*109*). The more loosely packed and weakly bonded grain of the loose leather, in comparison to tight leather, becomes separated during folding, resulting in the symptoms of poor break or looseness.

The ultrasonic imaging on hides and wet blue show that there are differences between loose and tight precursors present in these stages. These differences can be identified relatively easily even at the pickle stage. At the pickle stage the differences in structure between the loose and tight precursor hides is rather similar to the differences in the final leather with a low density region in the loose precursor about 0.3 mm below the grain surface. This indicates that looseness in leather is a direct result of the structure of the hide rather than being formed by some deficiency of processing. At the wet blue stage, which is an intermediate process stage between raw hide and leather there is still a distinctive difference between tight and loose precursors. However this difference is manifested not by a gap below the grain surface but by differences in the density distribution. The tight precursor wet blue shows a higher density at the grain surface with the density gradually decreasing with depth while the loose precursor shows a lower density at the grain surface and a fairly uniform density throughout the rest of the material. The wet blue is a stage where a lot of hides are traded and therefore identification of the propensity to looseness at this stage may also have commercial utility.

We have shown that this tendency of loose leather to have a region of lower density below the surface of the grain can be quantified by measuring the proportion of low density material from the ultrasonic images. What is perhaps surprising is that this feature is apparent even in the wet blue and pickle stages of the processed hide, with loose pickle and wet blue containing 2–6 times the amount of low density area than the tight pickle or wet blue, with these differences of the same order as in the leather. There is no published evidence that it is possible for a leather maker to identify looseness visually in the pickle or wet blue, but the features that lead to looseness, namely a less dense layer below the grain surface, which results from a high alignment of the collagen fibrils (*109*), are present in these stages.

From this investigation into looseness through the leather process it is clear that the tendency for looseness is an inherent property of the hide. At the pickle stage the density

profile through a hide follows a similar pattern to that in leather and the differences between tight and loose hides are preserved. In wet blue the hide is swollen so that the appearance of the ultrasound images is rather different to the pickle and leather, however the quantification of low density regions reveals a similar structural difference between loose and tight as in the other stages.

The underlying cause of this low density region has been shown previously to be at least partly attributable to the higher alignment of collagen fibrils in the grain region of loose leather, leading to poorer interlayer connections of the collagen fibre structure, and therefore a tendency to come apart in this region (*109*) even though this may result in greater strength in the leather (*74, 108-110*).

Ultrasonic imaging is a non-destructive technique so this method could be used for hide selection, with those hides that have inherent looseness being diverted to other lower value process streams. This could save around 5% of processing costs in a typical New Zealand tannery for bovine leather and probably similar amounts in other countries.

We have not investigated whether these tests could be conducted while the hide is still on the living animal, and this would be an interesting avenue for further investigation.

This work also does not answer the question of why some animals have hide that results in loose leather. This could be due, for example, to breed, sex, age, condition, or maybe even sun exposure. This is the subject of another study that is running in parallel to the work reported here.

Chapter 3: A Small Angle X-ray Scattering Study of the Structure and Development of Looseness in Bovine Hides and Leather

Chapter 3 has preliminary acceptance for publication in the Journal of the Science of Agriculture and Food.

- **H. C. Wells**, G. Holmes, J. U-Ser, W. Wei-Ru, N. Kirby, A. Hawley, S. Mudie, R. G. Haverkamp. “A Small Angle X-ray Scattering Study of the Structure and Development of Looseness in Bovine Hides and Leather” **(2016)** *J. Sci. Agri.Food.*

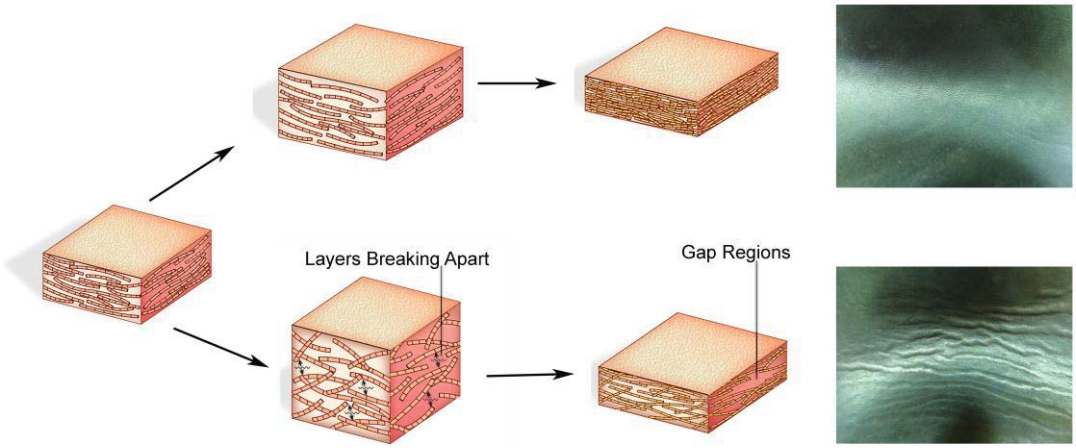

ABSTRACT

Some bovine hides produce poor quality leather, known as loose leather. The mechanism by which looseness develops and the structural characteristics of hides and intermediate processed stages that lead to loose leather are not well understood. Here, synchrotron-based small angle X-ray scattering (SAXS) is used to investigate the collagen fibril orientation at different stages of processing, from hide through to leather, that result in both tight and loose leathers. Tight leather of a relatively isotropic fibril density has a lower orientation index (OI) than loose leather of a more pronounced stratified fibril density; conversely, tight pickled hide and wet blue have a higher OI than loose pickled hide and wet blue. There is a greater increase in OI on processing from pickled hide to leather for loose material than for tight. The differences in OI are due largely to different hide thickness changes during processing. From fresh hide, there is a greater increase in hide thickness

prior to pickling for loose hide than tight, followed by a greater decrease at the leather stage. The collagen fibrils in loose leather and wet blue more readily orient under stress than do those in tight. Loose leather has a more pronounced layered structure than tight leather but this difference is not apparent from SAXS measurements of hide prior to the leather stage; it develops during processing. The greater swelling of the loose hide during processing disrupts the network structure and leads to a more highly layered collagen structure on shrinking at the final dry stage.

INTRODUCTION

"Looseness" is the term used in the leather industry for a defect that results in a greatly reduced value for leather. It causes wrinkles and creases in the finished product and may be present in 5–10% of finished bovine leather hides (*6*). The loss to the New Zealand bovine leather industry alone is estimated at $50 million per annum. The measure of looseness is known as the "break" and is defined in an ASTM standard (*89*) where a course break (high number) is a loose (poor quality) material. Looseness may also develop in leather produced from the skins of other animals.

Relatively recent research found that in loose leather, the grain layer tends to be separated into sheet-like structures and that there are larger gaps between the collagen fibers than in tight leather (*90*). A weak layer exists in the lower grain layer or at the grain–corium boundary, allowing the surface grain to partially detach and, therefore, wrinkle when bent inwards (towards the grain) (*109, 111*). "Tight leather" is the term applied to leather that does not have these deficiencies.

It is possible to use ultrasonic imaging to identify looseness in leather (*109*). The characteristic features in images of loose leather are also present in images of wet blue and pickled hide that subsequently develop into loose leather even though looseness is not apparent in these materials when subjected to the break test (*112*).

Small angle X-ray scattering (SAXS) studies of loose and tight leather support the idea that in loose leather the collagen fibrils are more layered, exhibiting a higher orientation index (OI) than in tight leather when the OI is measured with the X-rays edge-on to the leather (*109*). SAXS has been shown to be valuable in improving our understanding of the structure of leather and its relation to other physical properties such as tear strength and response to strain (*74, 110, 113, 114*). The overall goal of this work is to determine how looseness develops during the processing of bovine hides to leather. SAXS was used to monitor collagen fibril arrangement during various stages of processing, and for comparing hides that developed into loose and tight leathers. One specific aim was to ascertain whether looseness is an inherent property of a hide and, if not, to what extent it results from processing. Another aim was to investigate why looseness is not detectable in a break test during the early stages of processing and is obvious only at the final leather stage. This work also looked at how the collagen fibril structure of loose and tight leathers and partially processed hides responded to strain, using a similar approach to that in studies of other leather and collagen-based materials (Basil-Jones et al. 2012; Wells et al. 2015c) to address

the question: is there a difference in the behavior under strain that may partially explain separation of the grain?

METHODS

Sample selection

A range of hides was selected from the lime-splitting machine at a local tannery, Tasman Tanning Ltd (New Zealand), with the intention that some might become loose and some tight leathers. As mentioned above, it is not possible to accurately pre-determine whether a hide will develop looseness; however, some hides that appeared to have more draw were considered to be likely candidates and were included.

Leather preparation

At the time of selection, the hides were part-processed (from a production run). Each hide weighed c. 35 kg and had been green fleshed and processed using a conventional recipe. This recipe is based on sodium sulphide, sodium hydrosulphide and lime to both depilate and open-up the structure to allow the removal on non-collagenous proteins. Processing involved loading c. 8500 kg of hides at a time into drums of 4 m diameter by 3.8 m wide, which were rotated at 0.0179 g (units of radial acceleration) during the liming stage and 0.0716 g during washing. Hides were taken from the drums after 8 h of liming and returned to LASRA for onward processing in its pilot tannery to leather using a conventional recipe for shoe leather production. The next day, the horsed-up leather was sammed and sett to achieve a moisture content of 650 g kg^{-1} and toggle dried at 40 °C on a tunnel drier until dry in all regions. The leathers were conditioned heavily with water on the flesh side and held in this condition for 24 h. The next day, moisture was measured to ensure a moisture content of 140–160 g kg^{-1} in all areas prior to Molissa staking on settings of 4 and 5.

From the leather, samples showing looseness were taken from the shoulder region, just above the axilla, which is the region normally most prone to looseness, and tight samples were cut from areas adjacent to the affected region. The results presented here are from three hides processed through to leather.

Standard test of looseness.

Looseness was evaluated using the standard break test method (*89*), which involves folding the leather grain side in, and quantifying the wrinkles. Samples were considered tight if break was ≤ 2 and loose break was ≥4.

Thickness assessment

A sample's thickness was measured using calipers closed to a light pressure with minimal compression of the leather or hide. Because the range of samples prepared for SAXS did not include initial fresh hides and subsequent interpretation of the SAXS results revealed that the thickness changes from fresh hide stages are important, a separate batch of hides was processed from fresh through to leather with thickness recorded at each stage. In this separate batch, splitting did not occur so that data for each stage was derived from the full-thickness raw hide, whereas for the SAXS samples, splitting occurred post liming. One limitation of the "unsplit" hides was that the tanning chemicals might not have penetrated to the center of the hide's thickness.

SAXS measurement

To prepare the samples for SAXS, 1–2 mm thick strips of loose and tight leather, at the wet-blue and pickle stages, were cut. For the static tissue analyses, the samples were mounted edge-on to the incoming X-rays. Diffraction patterns were recorded every 0.2 mm, with the samples being analyzed from the grain to the corium. For the SAXS analyses of samples under strain, each 1–2 × 33 mm strip was mounted on a purpose-built frame attached to a linear motor, Linmot PS01 48 × 240/30 × 180-C (NTI AG, Switzerland) (see (*114*). Clamps fitted between the motor and a L6D OIML single-point load cell (Hangzhou Wanto Precision Technology Co., Zhejiang, China) held the samples. The samples were mounted without tension and stretched in 1 mm increments until the slack was taken up and tension was just registered by the load cell. This was the starting point for each analysis. An initial diffraction pattern was recorded, and the sample was stretched in 1 mm increments until it failed. After each extension the sample was allowed to stabilize for 1 min before the diffraction pattern was recorded.

Diffraction patterns were recorded on the SAXS/WAXS beam line at the Australian Synchrotron and the X-ray Nano-probe beamline at the National Synchrotron Radiation Research Centre (NSRRC) in Taiwan, which have similarly configured beamlines. The Australian beamline uses a high-intensity undulator source from which an X-ray energy of 12 keV was used. An energy resolution of 10^{-4} (e.g., 1×10^{-4} for 1 radiation) was used from a

cyro-cooled Si(III) double-crystal monochromator with a beam size of 250 × 80 μm (FWHM focused at the sample), and a total photon flux of about 2 × 10^{12} phs^{-1}. A Pilatus 1 M detector with an active area of 170 × 170 mm was used with a sample-to-detector distance of 3371 mm. The 23A SWAXS beamline of the Taiwan Light Source provides an energy range of 5–23 keV. A 12 keV beam was used for the leather samples, with an energy resolution (1.2–1.8) × 10^{-2} from a double-multilayer crystal monochromator for a flux of 2.8 × 10^{11} ph s^{-1}. With a beam size 0.25 mm dia. and a Pilatus 1 MF detector was used for data collection, with an exposure time of 1–2 s. Diffraction patterns for the unstrained and strained samples of pickle, wet-blue and dry (leather) were recorded on the Australian Synchrotron and diffraction patterns of a separate set of unstrained and strained samples of loose and control leather were recorded on the NSRRC SWAXS beamline. Representative examples of diffraction patterns of the leather samples are presented in Fig 3.1.

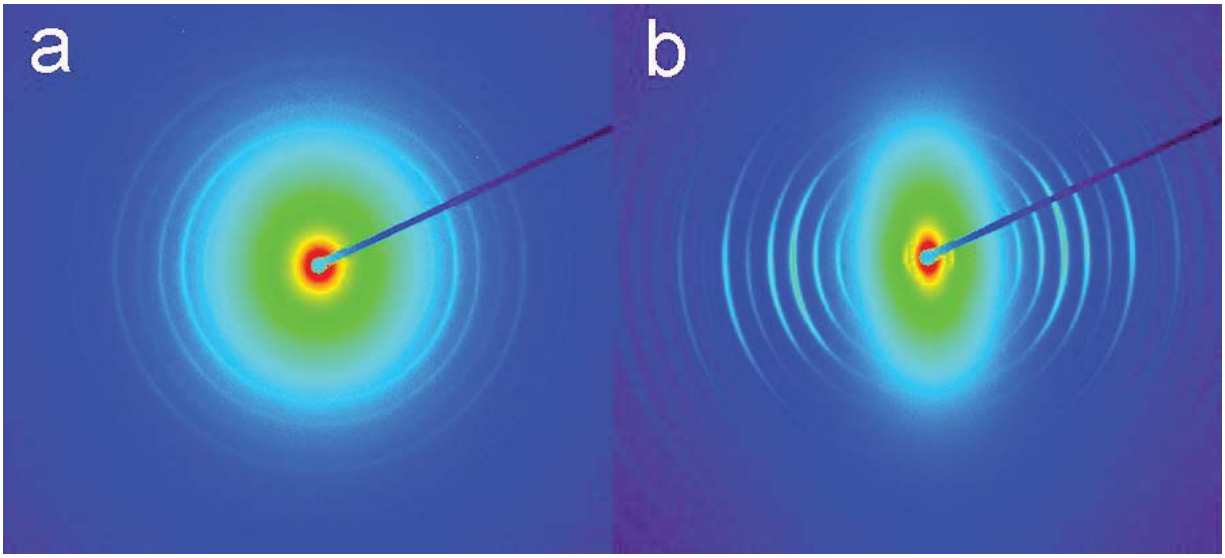

FIGURE 3.1: REPRESENTATIVE SCATTERING PATTERNS OF A) POORLY ALIGNED LEATHER WITH A LOW OI, B) LEATHER UNDER TENSION AND THEREFORE HIGHLY ALIGNED WITH A HIGH OI. 76X34 MM (300 X 300 DPI).

SAXS data were analysed using the SAXS15ID software. d-spacing of the collagen fibrils was found by integrating the intensity plots from the azimuthal range of 45° to 135°, fitting a Gaussian curve to the 6th order diffraction peak and determining the position of the centre of the curve. The orientation index (OI) is defined by

$$OI = \frac{90° - OA}{90°}$$

where OA (orientation angle) is the minimum azimuthal angle range centred around 180°, that contains 50% of the collagen fibrils, based on the method of Sacks for light scattering but converted to an index(*74*) using the spread in azimuthal angle of d-spacing diffraction peaks. The OI is a measure of spread of collagen fibril orientation in a sample, where an OI of 1 indicates the fibrils are parallel to each other and an OI of 0 indicates the fibrils are randomly oriented.

RESULTS

Sample selection

Sample selection was successful, with both loose and tight leather being included in testing, according to data from break testing of the samples at the leather stage (break = 2 for tight leather; break = 5 for loose leather).

Thickness

The hide thickness data (Table 3) revealed that as it passes from the pickled to the wet-blue stage, a hide swells, and that loose leather swelled more (132%) than did tight leather (42%). By contrasts, from the wet-blue to leather stage, a hide shrinks in thickness, more so for loose leather (20%) than for tight (5%).

Table 3. Thickness of materials at different process stages. Average of two hides each.

Process stage	Tight (OSP) Thickness (mm)	Loose (lower axilla) Thickness (mm)
Raw	4.10	2.40
Pickle	3.83	1.85
Wet blue	4.23	2.31
Wet leather	5.43	4.30

Dry leather	5.15	3.43

Orientation index through sample cross sections

Average collagen fibril OI for each sample type (Table 4) was derived from measurements along two or three cross sections of each sample type (Fig. 3.2). There is good consistency between the replicates. Leather had the highest OI (fibrils were the most highly oriented) while wet blue had the lowest OI, with pickled hide with an OI just a little higher than the wet blue. Loose leather had an average OI higher than tight leather and this was especially evident in the central and corium regions. However, the same OI relationship between tight and loose material was not apparent in the wet blue and pickled hide; rather, the opposite relationship was observed. The cross sections revealed a region of very low OI in the corium for loose wet blue, in contrast to loose leather, and the loose pickled hide had a lower OI than the tight pickled hide across much of the thickness.

Table 4. Average OI measured edge-on at different stages, n = 18-41 ($P < 0.003$ for $\alpha = 0.05$ in all comparisons between loose and tight).

Average OI	Pickle	Wet blue	Leather
Loose	0.31	0.30	0.61
Tight	0.45	0.38	0.54

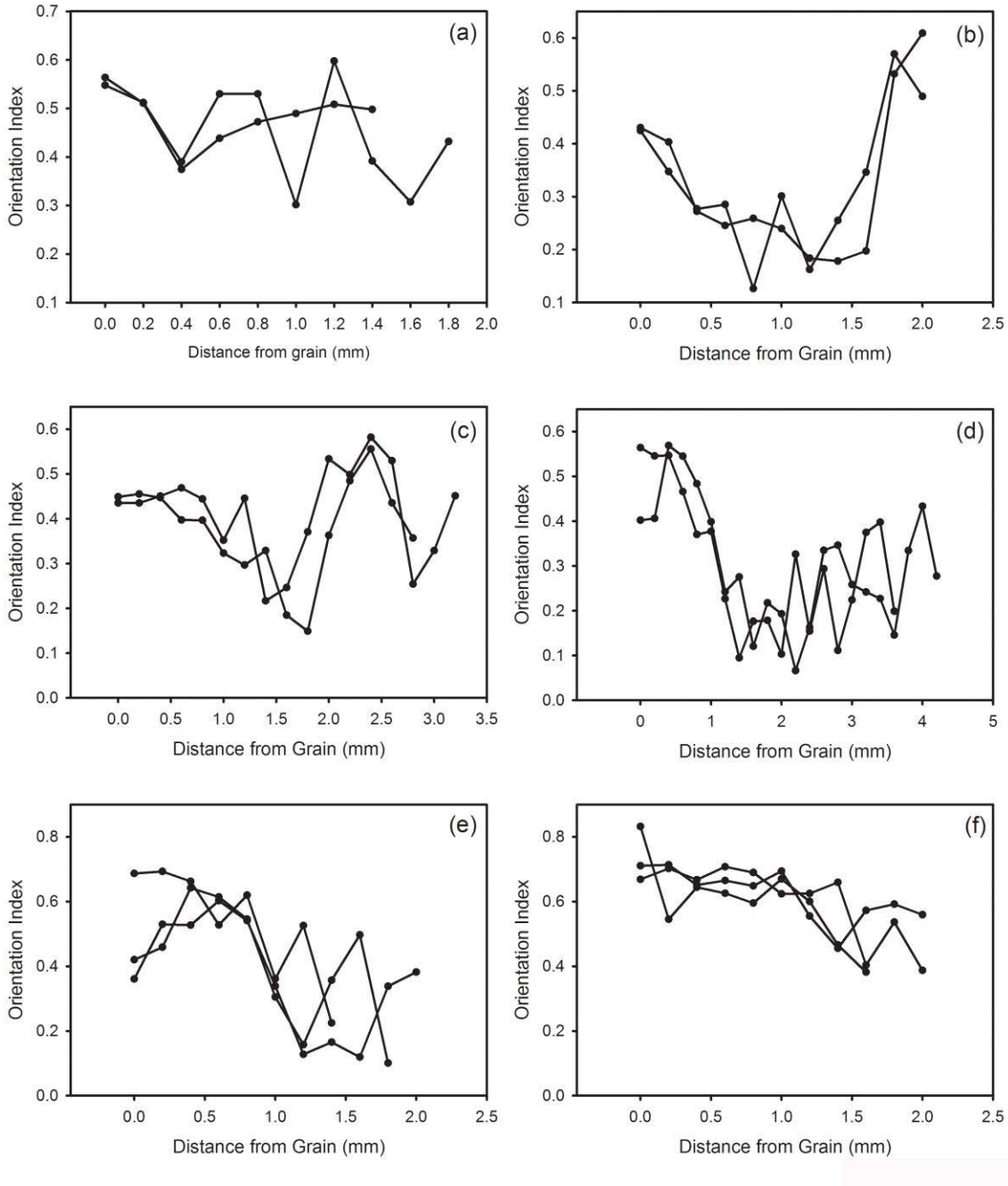

FIGURE 3.2: SAXS OI DATA FROM CROSS SECTIONS OF LOOSE AND TIGHT HIDE AND LEATHERS. A) TIGHT PICKLED HIDE; B) LOOSE PICKLED HIDE; C) TIGHT WET BLUE; D) LOOSE WET BLUE; E) TIGHT LEATHER; F) LOOSE LEATHER. THE TWO LINES IN EACH PLOT REPRESENT DUPLICATE MEASUREMENTS (AT DIFFERENT POSITIONS).

d-spacing through sample cross section

From the plots of data for collagen fibril d-spacing through cross sections (Fig. 3.3), it is apparent that d-spacing decreased as hides went from the pickled to wet-blue stages and decreased further to leather. The loose pickled hide had a significantly lower d-spacing than

did tight pickle. There was no large variation in d-spacing with depth through the samples and d-spacing and OI were not correlated.

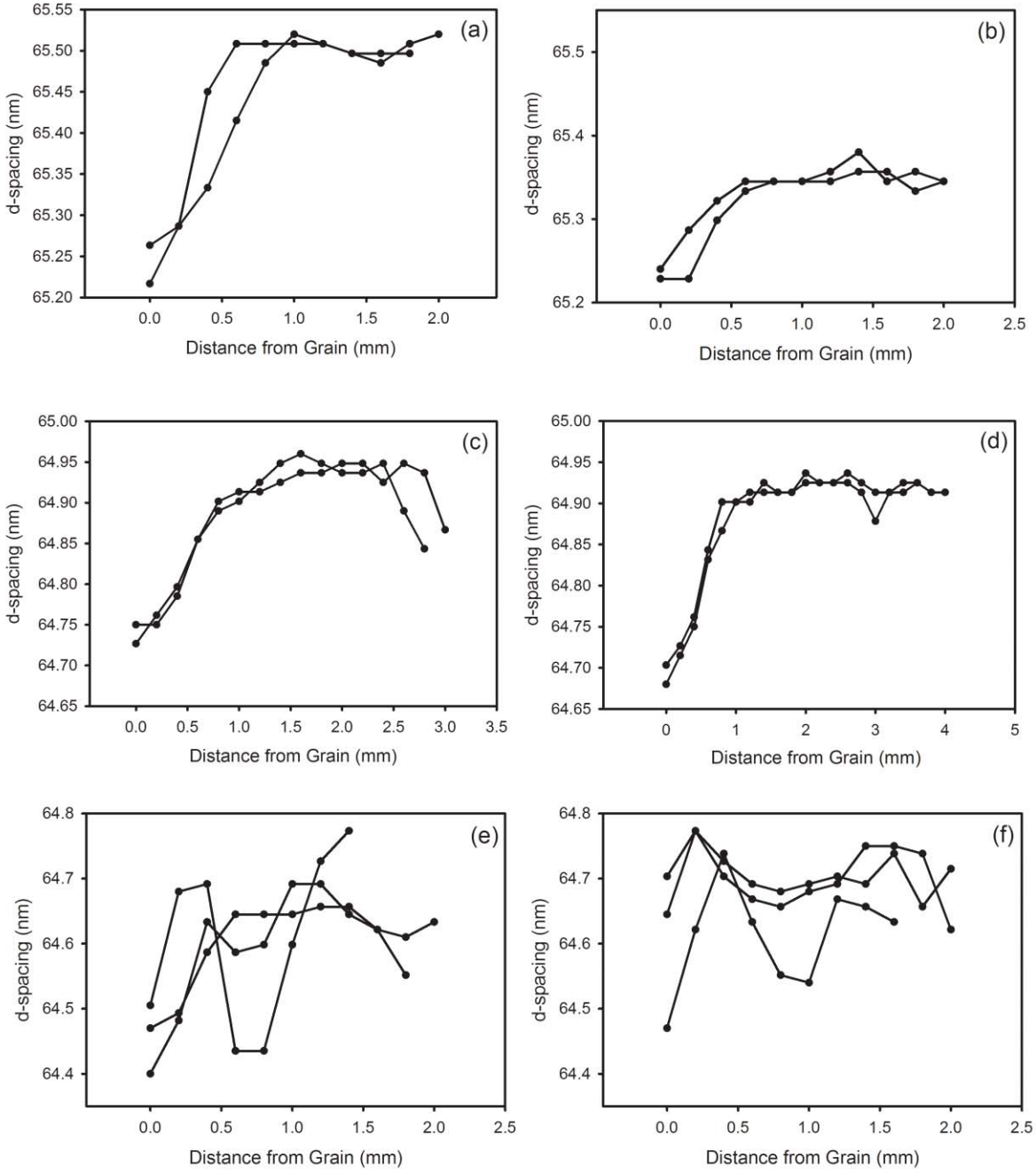

FIGURE 3.3: D-SPACING MEASURED EDGE-ON THROUGH CROSS SECTIONS OF A) TIGHT PICKLED HIDE; B) LOOSE PICKLED HIDE; C) TIGHT WET BLUE; D) LOOSE WET BLUE; E) TIGHT LEATHER; F) LOOSE LEATHER. THE TWO LINES IN EACH PLOT REPRESENT DUPLICATE MEASUREMENTS AT DIFFERENT POSITIONS.

Changes in OI and d-spacing with strain.

The OI and d-spacing were determined for strained samples with the X-rays edge-on (Fig. 3.4) and with the X-rays normal to the surface (Fig. 3.5). Edge-on measurements indicate the

degree of fibril layering while the normal-to-the-surface data give a measure of the "weft/weave" nature of the fibrils as viewed looking down on a flat surface.

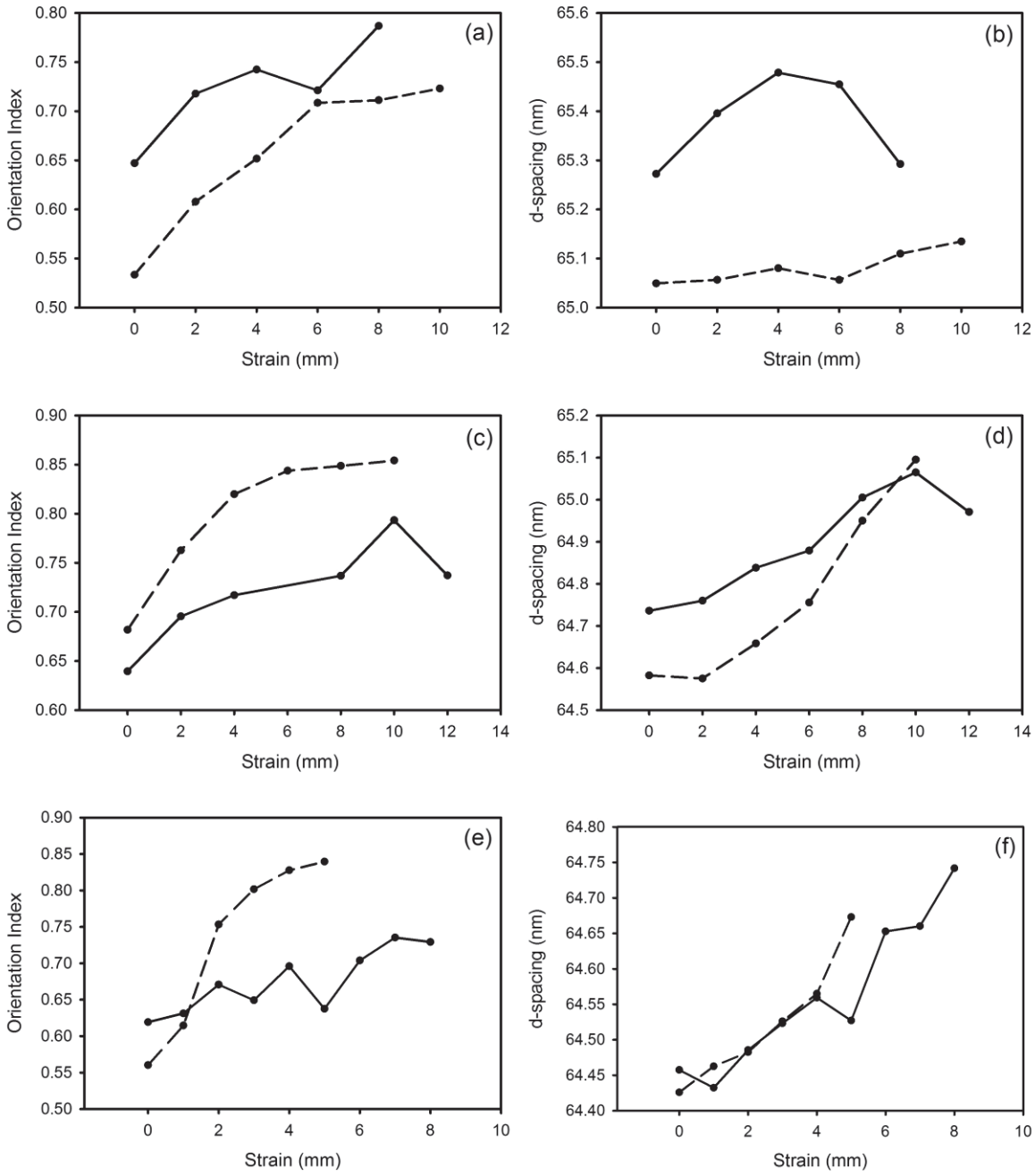

FIGURE 3.4: OI AND D-SPACING MEASURED EDGE-ON DURING STRAIN (AVERAGE VALUES). SOLID LINES: TIGHT MATERIALS, DASHED LINES: LOOSE. A, B) PICKLED HIDE; C, D) WET BLUE; E, F) LEATHER. THE TWO LINES IN EACH PLOT REPRESENT DUPLICATE MEASUREMENTS AT DIFFERENT POSITIONS.

Measured edge-on, the fibrils of the loose wet blue and leather oriented more readily than those of tight materials on stretching (Fig. 3.4); measurements normal to the surface did not

exhibit this pattern (Fig. 3.5). This difference shows that in loose leather and wet blue, the collagen formed into parallel layers on stretching more than it did in tight leather. However, pickled hide did not behave this way.

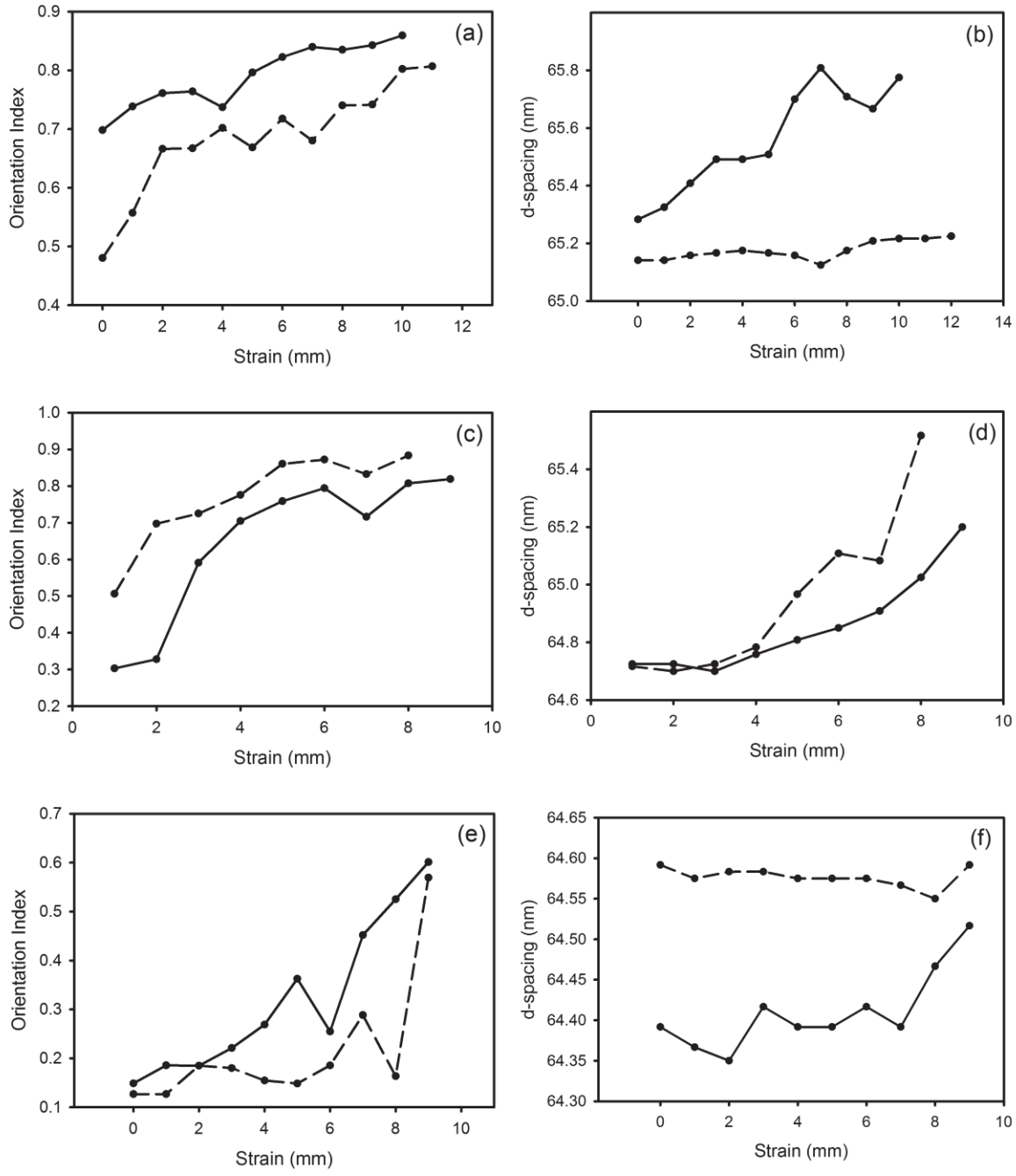

FIGURE 3.5: OI AND D-SPACING MEASURED NORMAL TO THE SURFACE DURING STRAIN. SOLID LINES: TIGHT MATERIALS, DASHED LINES: LOOSE. A, B) PICKLED HIDE; C, D) WET BLUE; E, F) LEATHER. THE TWO LINES IN EACH PLOT REPRESENT DUPLICATE MEASUREMENTS AT DIFFERENT POSITIONS.

Measured normal to the surface, the OI changes on stretching of loose and tight materials were similar. Pickled hide and wet blue underwent a large change in OI and became highly

oriented (0.8–0.9) while leather, which also underwent a large change in OI, reached an OI of only c. 0.7, having started from a lower initial value.

The d-spacing changes in leather were similar for tight and loose leathers measured edge-on, but the changes were greater in tight than loose leather in normal measurements. For wet blue measured both edge-on and normal, the d-spacing changed less in tight than in loose, but this was reversed in all the data for pickled leather. Since d-spacing changes indicate the stress experienced by individual collagen fibrils in a leather, acting as an internal stress or strain gauge (*101, 115*), the d-spacing data suggest that individual fibrils undergo greater strain in tight compared to loose in leather examined in the weft/weave dimension and in pickled hide examined in any dimension. Only in wet blue did fibrils of loose samples undergo increased strain compared to tight samples (in any dimension).

DISCUSSION

The goal of this work is to further our understanding of the structural basis of looseness in bovine leather and how it develops as hides are processed from raw hide to leather. Using this knowledge, it might be possible to develop processing strategies that minimize the likelihood of looseness developing.

The degree of collagen fibril orientation changed as hides were processed to leather, and the thinnest material, leather, had the highest OI, measured with the X-rays edge-on. This has been described previously (*116*) and can be modeled by considering a sample of leather containing a fiber that expands uniformly in thickness (from original thickness T_1 to new thickness T_2), and its θ_1 from the base changes to a new angle θ_2, depending on the change in thickness (eqn. 1):

$$\theta_2 = \tan^{-1}\left(\frac{T_2}{T_1}\tan\theta_1\right) \qquad (1)$$

Where θ is the angle of fibrils relative to the base. From equation 1, the change in OI can be calculated since OI is related to orientation angle, OA, by the relationship (2):

$$OI = \frac{90 - OA}{90} \qquad (2)$$

The change in OI resulting from a change in thickness (where OI_2 is for T_2 and OI_1 is for T_1) is obtained by substituting OA for θ_1 in eqn 1 to give eqn 3:

$$OI_2 = \tan^{-1}\left(\frac{T_2}{T_1}\tan\left[90\left(1-OI_1\right)\right]\right) \qquad (3)$$

While the loose pickled hide and loose wet blue had a lower OI than the tight material at the same stages, leather had a higher OI in the loose leather because of the greater change in thickness it underwent compared to tight leather. This change, when corrected for eqn 3, does not account well for the higher OI of the final dry (Table 5). Therefore, some other mechanism is acting to increase the fibril OI between the wet-blue and the dry stages.

Table 5. OI corrected for changes in thickness and dryness.

Process stage	Thickness (mm)	OI as measured	OI, thickness corrected* (relative to pickled hide OI)
Tight:			
Pickled hide	3.83	0.45	0.45
Wet blue	4.23	0.38	0.41
Dry leather	5.15	0.54	0.63
Loose:			
Pickled hide	1.85	0.31	0.31
Wet blue	2.31	0.30	0.36
Dry leather	3.43	0.61	0.77

* “Thickness corrected” means what the OI would be had thickness not changed.

One possible additional contributor to the changes in fibril orientation could be the cross linking between collagen fibrils. It is believed that collagen cross links are responsible for mechanically coupling fibrils to restrict fibril sliding (*117*) and collagen cross links can affect fibril orientation in some collagen-based materials (Kayed et al. 2015). However, the overall effect of cross linking on collagen fibril structure has been shown to be only minor (*22*) and so changes in cross linking are not significant enough to alone explain the structural difference seen between loose and tight hides and leathers in this investigation.

The change in thickness during processing between loose and tight materials can explain both the development of looseness and some of the OI differences. When a hide swells “too much”, the connections between (virtual) layers of collagen fibrils in the hide are broken by the physical expansion (Figure 3.6). From pickled hide to wet blue, swelling was found to greater in loose material (132%) than in tight leather (42%). This greater swelling in the hides that went on to develop looseness would be associated with a much greater destruction of the inter-layer connections. It may be that there are also differences in swelling between loose and tight with liming, but that was not measured here. The second consequence of the greater swelling – the lower OIs observed in loose pickled hide and wet blue compared to OIs of comparable tight material – reflects the fact that as hide swells, the collagen fibrils become increasingly tilted out of the plane of the leather.

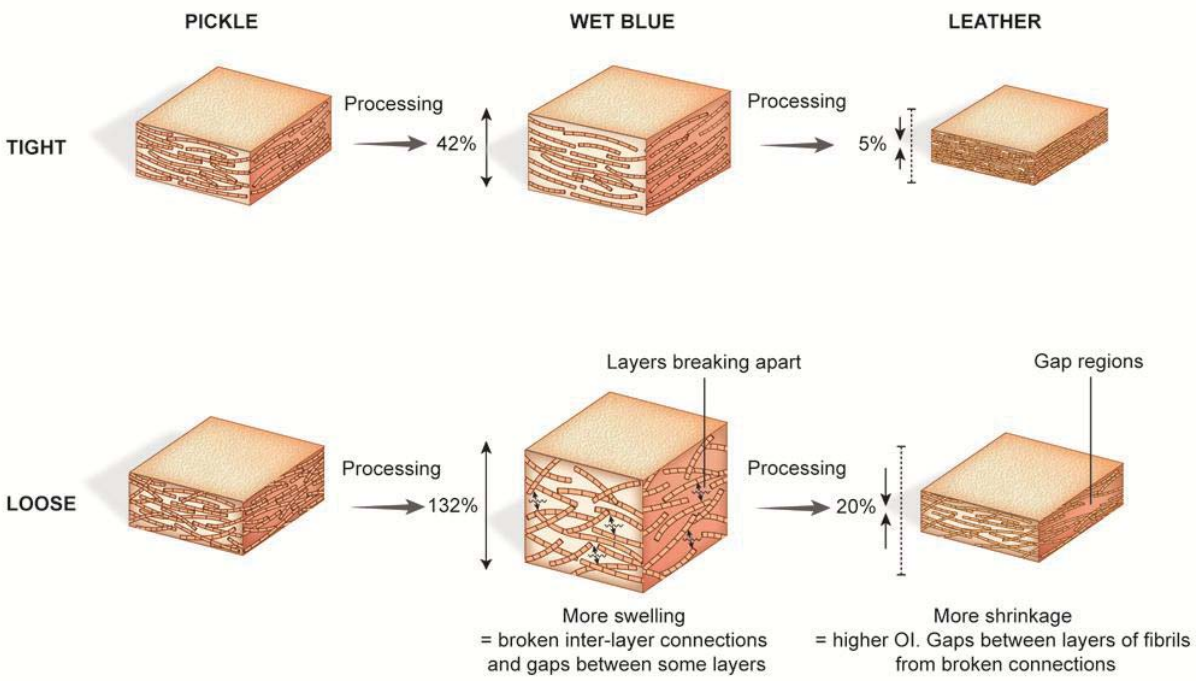

FIGURE 3.6: ILLUSTRATION OF THE DIFFERENT BEHAVIOUR OF LOOSE AND TIGHT LEATHERS DURING PROCESSING.

Once these inter-layer connections have been broken, during further processing of the hide to leather, the hide shrinks and these layers are compressed back together. From wet-blue to leather, the hide shrank more for loose leather (20%) than for tight leather (5%). The high OIs at the leather stage indicate that the collagen was well oriented in these layers, and there was little connection between the layers in the loose leather (Figure 3.6). (In tight leather, the connections might be in the form of some fibrils traversing the layers or branching of some fibrils.) The lack of connection between the layers in loose material results in a weakness between the layers, which permits the layers to slide over each other,

particularly near the lower part of the grain. Once the grain layer detaches from the corium, it bunches up as it is bent inward on the grain side. This disconnection in the lower grain region for loose leather is apparent in ultrasound imaging (*109, 112*).

These findings raise the question of why hides prone to looseness swell more than those that yield tight leather. Two possibilities are that either loose hides have a pre-existing weakness between layers so that there is less resistance to swelling (i.e. swelling is a result of looseness) or that some other factor, such as a different affinity to water, perhaps as a function of a different fat content, results in greater swelling and therefore looseness (i.e. swelling is a cause of looseness).

A third possibility is that elasticity and shrinkage in the grain differ from those in the corium, and that the differential shrinkage produces looseness. If the expansion and contraction was in area (i.e. laterally) and was markedly different between these regions, it might force these two layers to become disconnected, regardless of how well they were initially bonded to each other. While here, only changes in hide thickness were measured, and were found to be greater in the material that became loose, it is plausible that the lateral expansion, and therefore grain–corium shear forces, would also be greater in material that becomes loose. However, this is not necessarily consistent with the SAXS OI data. Lateral expansion would be expected to increase OI while an expansion in thickness would decrease the OI. As discussed above, the OI changes during processing can be largely attributed to thickness changes, and the fractional change in thickness (up to 132%) is much greater than the fractional change in area (not measured in this study but believed to be typically c. 2%). The hypothesis of lateral shear causing looseness does not appear to be supported by the SAXS analysis during strain of these materials.

The response of the processed hides to strain revealed some information on the structure of these materials and the differences between material that develops into loose and tight leathers. In pickled hide, the fibrils in loose material oriented with strain more readily than did those in tight when measured with X-rays normal to the surface (but not measured with X-rays edge-on to the hide). For the pickled hide, the d-spacing of tight material changed much more than that of loose material when measured both edge-on and normal to the surface. This behavior suggests that the tight pickled hide has a more constrained fibril network, with stress developing on the fibrils but no movement resulting in reorientation; in loose material, the network does not appear to be as constrained. This further suggests that the loose pickled hide did not initially have or had already lost some of its connecting network structure and was, therefore, destined to produce loose leather. Alternatively, it could be that in loose

material (which was more swollen with water), the strain was taken up by water being squeezed out rather than much movement of fibers.

In wet blue, loose material reoriented under strain more readily than tight material, again suggesting that the fibrils of it had less network-like arrangement and so were less constrained (because the network had been damaged by swelling). However, the greater d-spacing changes of loose wet blue with increasing strain, measured both edge-on and normal to the surface, compared to tight wet blue suggests that the collagen fibrils in loose material experienced more stress for a given strain. This observation supports the idea that swelling breaks the connections between layers; it is not consistent with pre-existing weak connections between the layers causing swelling. The extra d-spacing increase shows that extra force was required to break the inter-layer connections.

In the leather, the loose leather reoriented more readily under strain than did tight leather, and the d-spacing changes were similar for the two types of leather when measured edge-on, and larger for tight leather when measured normal to the surface. This suggests that a collagen fibril network is more constrained in tight leather than in loose leather, hence individual layers of collagen fibrils are freer to move or separate in the loose leather.

The interpretation of the observed behaviors of the materials under increasing strain, in terms of the structural differences between loose and tight leather, is consistent with the analyses of samples not under strain.

If looseness develops during processing from the excessive swelling of some hides, it may be possible to alter processing strategies for these hides (if they could be identified at the raw hide stage) to inhibit the swelling. This might then prevent the development of looseness.

The material with more highly oriented fibrils that eventually exhibits looseness has been shown elsewhere to in fact be stronger in the standard tear test (*109*). This strength is, therefore, clearly not dependent on bonding or on a network structure between the layers but rather on the number of collagen fibrils in the plane of the leather. This relationship is similar to that found in studies of a large number of ovine and bovine leather samples (*74*) and a range of different animal leathers (*110*). However, tear strength is only one consideration in leather value; looseness degrades appearance and perhaps also serviceability, and therefore also devalues leather.

Chapter 4: Stabilising Chromium from Leather Waste in Biochar

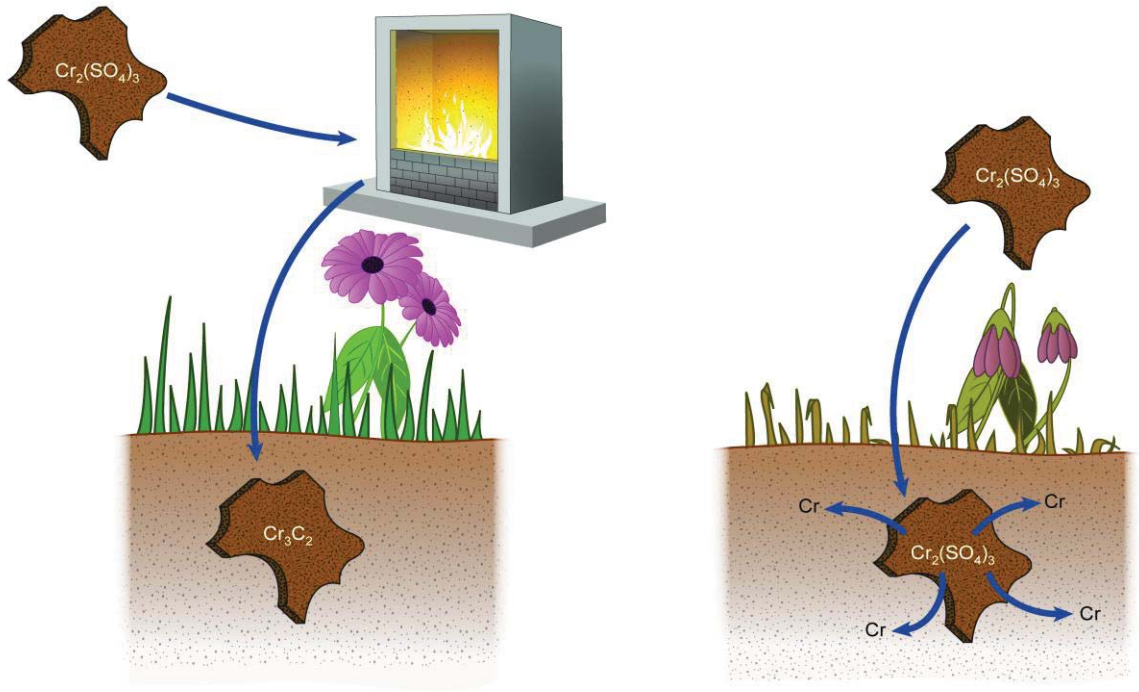

Chapter 4 was published as an academic journal article in the Journal ACS Sustainable Chemistry and Engineering:

- **Wells, H. C.**; Sizeland, K. H.; Edmonds, R. L.; Aitkenhead. W.; Kappen, P.; Glover, C.; Johannessen, B.; Haverkamp, R. G. (**2014**). "Stabilizing Chromium from Leather Waste in Biochar." *ACS Sustainable Chem. Eng.* **2**: 1864-1870.

ABSTRACT

Disposal of chrome-tanned leather waste provides an environmental challenge, with land-based methods risking leaching of chromium into the environment. We investigate the production of biochar from leather as an alternative means to dispose of leather waste. Chrome-tanned leather is heated at 500–1000 °C in an environment excluding oxygen to form biochar. The char is leached in 1 M HCl for 15 hr and the leachate analysed for Cr to confirm that Cr does not leach from char formed at or above 600 °C. The char is analysed by XAS for chemical state and structure. XANES analysis shows that the leather and biochar contain Cr as a mixture of Cr sulphate and Cr carbide, with the proportion of Cr as carbide

increasing from 0% for fresh leather to 88% for char formed at 1000 °C. Modelling of the EXAFS spectra show the atomic near-range structure is consistent with that of chromium carbide for the high-temperature samples. Biochar produced from chrome leather waste contains highly dispersed chromium present as a stable, carbide-like structure (provided sufficiently high temperatures are used). This material, rather than being an environmental problem, may be used for soil remediation and carbon sequestration.

INTRODUCTION

Most leather is produced from skins and hides by tanning with chromium salts. Leather is used in upholstery (car and home), shoes and clothing but at the end of the life of these goods, the leather needs to be disposed of in an environmentally benign manner. Leather manufacture and production of goods from leather also produces leather scrap which requires disposal. Annual global leather production is about 6.8 million tonnes (*88*), around 80% of which contains Cr.

The main concern in the disposal of leather is the leaching from leather of Cr. Soluble Cr in a hexavalent oxidation state is considered to be undesirable in the environment (*118, 119*) and sites where Cr(VI) is present can require remediation (*120*).

Current and proposed leather disposal methods include: extraction of Cr before disposal (*121-123*); disposal to wetlands for vegetation to absorb the Cr (*124*); production of other reconstituted structural materials to bind the Cr in new products (*125, 126*); and heating leather in an oxidizing environment to create a residue with soluble Cr (*127, 128*). Cr contained in or on particulates from the burning of coal and biomass (in the presence of oxygen) can produce Cr(VI) (*129*). Therefore, it is possible that burning leather may also generate Cr (VI), which is undesirable.

We have proposed that the production of biochar, carbonized organic matter, from waste leather may be a better alternative to other disposal methods (*130*). Biochar is produced by heating organic matter in an oxygen deficient environment. The application of leather biochar is a way of sequestering carbon, thereby reducing the amount of carbon that may have otherwise become atmospheric CO_2. Biochar also has the demonstrated benefit of improving agricultural soil productivity (*131*). Carbonized leather has previously been considered as a disposal option, with the suggestion of producing an activated carbon product for filtration applications(*132-134*).

Ideally, a leather biochar product could be produced that does not leach Cr. Exposing leather that has been “heat stabilised” in a non-oxidising environment to leaching indicates that the material has a low solubility of Cr. Specifically, when leather was stabilised at 350 °C or higher in a CO_2 environment, no soluble Cr is detected over a wide pH range in contrast to untreated, chrome-tanned leather (*132*). It is also important that the Cr is resistant to oxidation, since both Cr oxidation and reduction between the Cr(III) and Cr(VI) couple (*135*) can occur in soils, depending on the nature and condition of the soils, and other factors that

control the redox environment. This has led to interest in the analysis of soils for the type of Cr contamination present (*136, 137*).

The chemical nature of Cr in leather has been characterised: Cr sulphate is used during tanning, and Cr bonds to the leather's collagen (*138, 139*) and is well dispersed. However, the form of Cr present in biochar is unknown, as are its stability and dispersion. In an earlier study of the leaching of leather after heat treatment in a non-oxidising environment, the chemical state of the Cr was not determined, despite some interest in doing so (*132*).

The purpose of the work reported here is to investigate the speciation and structure of the Cr in biochar produced from chrome-tanned leather as a function of the heating conditions. We wish to confirm the earlier reports of decreased solubility of Cr from leather heated in a non-oxidising environment and determine that the samples we are studying for Cr speciation do in fact exhibit low Cr solubility. Developing an understanding of the nature of entrapment of Cr in leather biochar may enable us to predict the likely stability of the Cr in the char in the longer term. For the determination of the chemical speciation and structure of Cr, we use X-ray Absorption Spectroscopy (XAS) which is known to exhibit obvious spectral differences for different oxidation states and chemical environments.

EXPERIMENTAL

Leather

Standard, commercial chrome-tanned bovine leather was used for all experiments. Raw hides were stripped of hair and limed by treating them with a mixture of sodium sulphide, sodium hydrosulphide and lime, then bated by treatment with a pancreatic trypsin, followed by tanning with basic Cr sulphate, then retanning with a mix of syntans and vegetable tannins, followed finally by fat liquoring with a blend of sulphated natural fats.

Pyrolysis process

The biochar was produced from leather by pyrolysis. Two pyrolysis reactors were used: a larger unit with no purge gas for the lower-temperature samples (up to 600 °C) and a smaller unit with the sample held under argon for higher-temperature samples (600–1000 °C).

For the larger, lower-temperature reactor, 100 g of leather was placed in a 1 L high-temperature 304 grade stainless-steel reactor. The reactor lid was sealed with a thin layer of potters' clay and the reactor flushed with 5 volumes of nitrogen (99.999% pure). The lid contains a non-return valve. The reactor was placed in a furnace and heated from ambient to the desired temperature over 1 hr, held for 1 hr at temperature and cooled to 100°C over 3 hr before being opened. No control over the atmosphere in the reactor vessel was attempted other than the provision of the non-return valve (which resulted in a partial vacuum inside the vessel after cooling).

For the smaller, higher-temperature reactor, 4 g of leather was placed in a 25-ml 304 grade stainless-steel reactor through which a continuous flow of 0.2 L/min argon was passed. The furnace was heated from ambient to the desired temperature and held for 1 hr before being rapidly cooled to below 100°C, at which point the sample was removed; Ar flow was maintained continuously. Three high temperatures were tested, with the following heating and cooling times: heated to 1000°C over 60 min, held for 60 min, cooled 25 min; heated to 800°C over 35 min, held for 60 min, cooled 20 min; heated to 600°C over 50 min, held for 60 min, cooled 5 min. A visual inspection suggested that there was no direct transfer of corrosion product from the stainless steel to the leather char.

Total Chromium Content of Leather and Char

The Cr content of the char and leather samples was measured using a standard industry test method (*140*). The leather or char is first ashed in air. The residue is then treated with an oxidising acid (perchloric acid-sulphuric acid mix) to convert the Cr to hexavalent Cr. The hexavalent Cr is then reduced back to trivalent Cr using iodine in excess and the excess iodine is back titrated with potassium thiosulfate.

Leaching of Chromium

Leachable chromium was measured with duplicate samples of char (5 g) leached in 100 mL of 1 M HCl while shaken for 15 hours at room temperature. The char material produced was finely ground prior to leaching. The Cr content of the aqueous HCl leachate was then

assessed in duplicate with a Varian 220 SpectrAA using a standard industry test method (*141*).

XAS Measurements

X-ray absorption spectra were recorded on the XAS beam line at the Australian Synchrotron, Victoria, Australia. Cr K edge absorption spectra were recorded in transmission mode using a set of flow-through ion chambers supplied with He. The energy was controlled using a fixed exit Si (111) double crystal monochromator. The beam was conditioned using a collimating mirror (Si) and a toroidal focussing mirror (Rh coated). Higher harmonics were rejected using these two mirrors and a flat harmonic rejection mirror (SiO_2). For XAS scans, energy steps of 0.25 eV were employed in the XANES region using 1 s count per step whilst a step size of 0.035 $Å^{-1}$ was used in the EXAFS region to 14 $Å^{-1}$ with count times up of 6 s per step. The energy resolution was about 1 eV, and the photon flux was in the range 10^{11} to 10^{12} photons s^{-1}. The X-ray beam was about 1.5 x 0.4 mm^2 at the sample. The energy scale was calibrated by simultaneously measuring a Cr foil placed between two downstream ion chambers. Samples were packed in 1 mm thick poly(methyl methacrylate) sample holders. Reference standards were Cr_2O_3 (Prolab), $Cr_2(SO_4)_3.xH_2O$ (BDH), $Cr_2(SO_4)_3.xH_2O$ (Chromosal B, Lanxess), $Cr(CO)_6$ (BDH), Cr_3C_2 (Aldrich), and $Cr(O_2C_5H_7)_3$ (Aldrich) all diluted with BN (Aldrich). Data processing was performed with ATHENA (*142*) and VIPER (*143*).

RESULTS AND DISCUSSION

Biochar Formation

Heating leather under a stream of Ar in the small reactor, or in a larger closed vessel with a pressure release valve, resulted in well-formed char that retained the general shape of the leather feedstock, albeit at a smaller size. Weight loss (from ambient moisture) increased with heating temperature, with 62% weight loss being recorded at 300 °C, 73% at 600 °C, 76% at 800 °C and 79% at 1000 °C. In the small reactor there was a hint of green colour (perhaps Cr_2O_3) on the edge of some char that had formed near the outlet of the reactor

suggesting that there was some ingress of oxygen near the outlet. These parts of the sample were not used in the analysis.

Leachable Cr

We found that a small amount of Cr can be leached from leather that has not been heat treated (Table 6), as has been reported previously (*132*). After heating of the leather, the leachability of Cr diminishes. At 600 °C where the leather is clearly char very little leaching of Cr could be detected (Table 6). In an earlier leaching study it was found that at 350 °C the Cr was no longer able to be leached from the heated leather (*132*). We have therefore sought to understand why Cr has much lower solubility from the charred leather.

Table 6. Initial chromium content and leachable chromium of leather and of biochar samples produced under various heat treatments.

Sample	Initial % Cr (SD)	Leachable Cr, as % of initial Cr
Leather	0.99 (0.01)	4.67
300 °C*	2.60 (0.02)	3.50
600 °C*	7.39 (0.04)	0.31
600 °C†	11.8 (0.8)	0.08
800 °C†	12.5 (0.1)	0.06
1000 °C†	15.4 (0.1)	0.03

*Larger reaction vessel. †Finely ground, from small reaction vessel.

XANES

X-ray absorption near edge structure (XANES) is a spectroscopic technique that is element specific and is local bonding sensitive. The technique requires irradiating a sample of interest with X-rays across a range of energy that includes an absorption edge. An inspection of the features of the spectrum provides information on the bonding of the element of interest. XANES is most often used in a comparative study between spectra of know standards and unknown samples.

Beam damage

Alteration to the state of Cr is possible in an intense, focused X-ray beam. The likelihood of this was investigated by doing multiple scans on the same spot of a representative sample and observing differences in the XANES spectra (total collection time up to 2 hrs). From these measurements it was determined that beam damage is negligible under the conditions that the samples are measured.

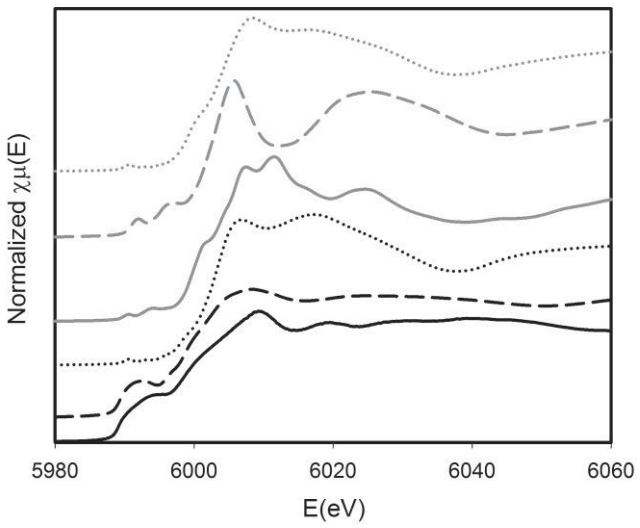

FIGURE 4.1: XAS OF STANDARDS. CR METAL (——), CR_3C_2 (— —), $CR(O_2C_5H_7)_3$ (▪▪▪), CR_2O_3 (——), $CRCO_6$ (— —), $CR_2(SO_4)_3$ (▪▪▪).

XANES of Reference Compounds

In the range of reference compounds for which XAS spectra were collected, it is apparent that there are strong differences in all parts of the spectra including the pre-edge region, the

edge energy and the post-edge region (Figure 4.1). We were unable to analyze any Cr(VI) compounds; however, reference spectra are available in the literature (*136, 144, 145*) and always show a strong signature pre-edge feature and a large edge shift.

XANES Edge Position and Cr Oxidation State

The energy position of the absorption edge is very sensitive to the oxidation state of the Cr atom that is excited(*144, 146*). The Cr in Cr_3C_2 is seen to have an effective oxidation state similar to that of Cr metal (Figure 1), and the charge on the Cr in Cr_3C_2 is calculated to be +0.33 (*1*). We are confident that there is no Cr(VI) in any of the samples because Cr(VI) has a distinct and sharp pre-edge feature at around 5993.0 eV (*144, 145*). The feature arises from non-local dipole transitions in Cr(VI) compounds, which are tetrahedrally coordinated (*147-149*)). None of the samples showed this pre-edge feature.

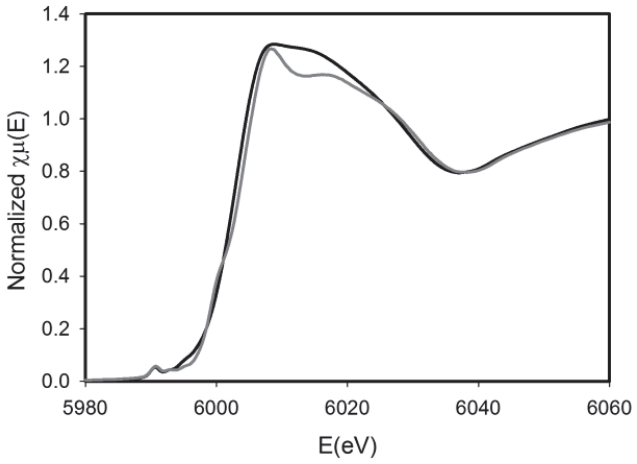

FIGURE 4.2: XANES OF DRY LEATHER (▬▬) AND $CR_2(SO_4)_3.xH_2O$ (▬▬).

XANES of Leather

The XANES spectrum of dried chrome leather is very similar to that of $Cr_2(SO_4)_3.xH_2O$ (Figure 4.2). This is the salt that is used in chrome tanning, so clearly some structural

aspects of this salt are retained in the tanned leather. Detailed studies on this subject have been reported previously (*138, 139*).

XANES of Biochar

With heating, changes in leather's XANES spectra are observed from 600 °C, with significant differences with each 200 °C increase to the experimental maximum (Figure 4.3). The spectrum of the sample heated to 600 °C in the larger vessel appears to be equivalent to that of a sample heated to a lower temperature in the small scale vessel. With heating, a pre-edge peak of 5993.4 eV appears and it increases in intensity after higher temperature treatment. The pre-edge peak that forms in the samples at 600 °C and 800 °C is in the same position as the peak from the Cr_3C_2 standard but is sharper and is not a good match to the shape of the Cr carbide pre-edge peak (or that of any of the standards) and may reflect a different structure to any of the standards. After treatment at 1000 °C, this peak broadens and begins to look more like the Cr carbide pre-edge feature.

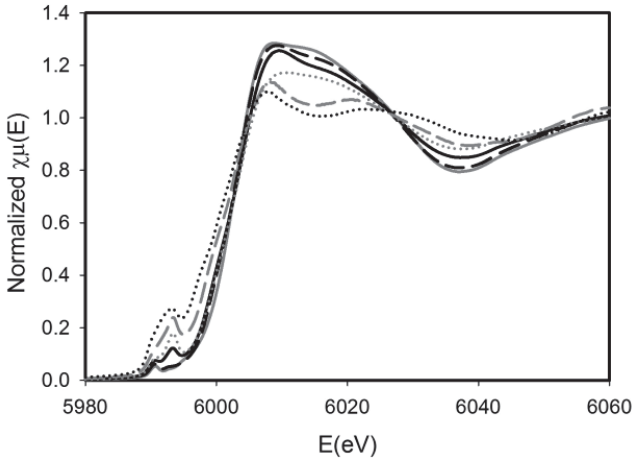

FIGURE 4.3: XANES OF LEATHER AND LEATHER BIOCHAR HEATED TO DIFFERENT TEMPERATURES. LEATHER STANDARD (——); HEATED IN THE LARGE VESSEL: 500°C (— —), 600°C (——); HEATED IN THE SMALL VESSEL: 600°C (····), 800°C (— —), 1000°C (▪▪▪▪).

A shift in the absorption edge to a lower energy after heating becomes apparent from 800 °C, with a shift of 0.8 eV, and with a further shift apparent at 1000 °C, yielding a total shift of 1.5 eV from the dry leather or chromium sulphate spectrum. The shape of the post-edge spectrum changes consistently with heating.

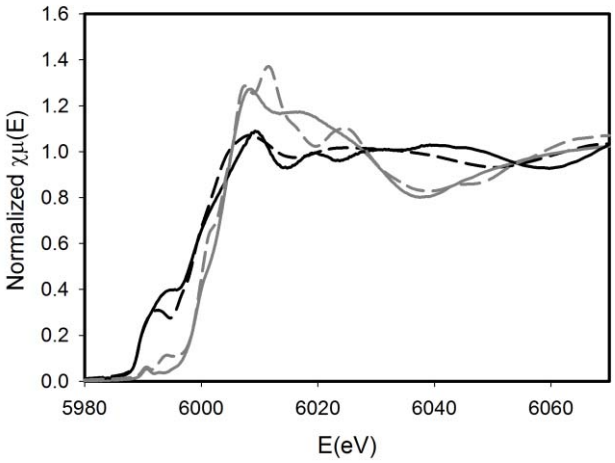

FIGURE 4.4: XANES OF STANDARDS TESTED FOR LINEAR COMBINATION FIT. $CR_2(SO_4)_3$ (——), CR_3C_2 (— —), CR METAL (——), CR_2O_3 (— —).

XANES Linear Fits for Biochar

Using the Athena software (*142*), linear combination fitting to normalized χμ(E) and to $k^3\chi(k)$ were performed. Unconstrained linear combination fitting was attempted using the spectra for Cr_2 $(SO_4)_3.xH_2O$, Cr metal, Cr_2O_3 and Cr_3C_2 (Figure 4.4). Dry leather is substituted as a proxy for the Cr_2 $(SO_4)_3.xH_2O$ spectrum since $Cr_2(SO_4)_3.xH_2O$ is the tanning agent used in chrome tanned leather and the Cr is well dispersed in leather and therefore gave a better XAS at high k than the ground pure compound mixed with BN. The dry leather better reflects the highly dispersed nature of the Cr. The fit range used was 40 eV below to 70 eV above E_0. Best fits were obtained using only two components, dry leather (or $Cr_2(SO_4)_3.xH_2O$) and Cr_3C_2 (Figure 4.5). With an unconstrained fit also containing an initial component of Cr metal or Cr_2O_3, these components do not contribute to the fit. As the treatment temperature increases, the amount of carbide increases. The calculated proportions of carbide and Cr sulfate (represented as the dry leather spectrum) are listed in Table 7. Fitting to the $k^3\chi(k)$ spectra gives similar proportions of Cr_3C_2 and $Cr_2(SO_4)_3.xH_2O$, as does fitting to the energy spectra.

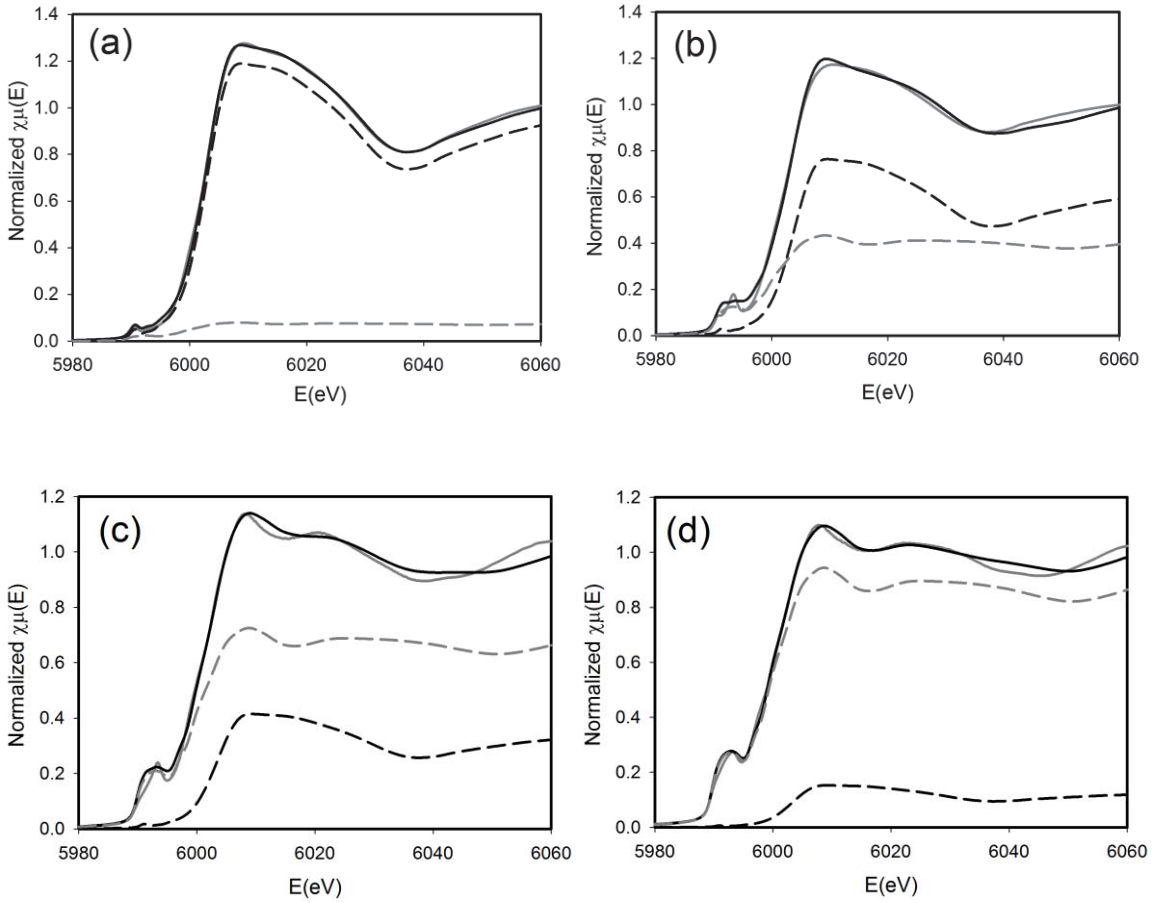

FIGURE 4.5: XANES LINEAR COMBINATION FIT OF BIOCHAR PREPARED AT A) 500°C; B) 600°C; C) 800°C; D) 1000°C. Cr_3C_2 (— —), DRY LEATHER (▬ ▬), DATA (——), FIT (▬▬).

Chromium Carbide Formation

Thermodynamic considerations suggest that under high carbon activity and low oxygen activity (as in char formation), Cr metal or Cr carbide may form (*150, 151*). This occurs at *log* P_{O2} (in bar) below about -16, with the carbides formed at *log* a_C (carbon activity) above about -2.8 (Cr metal forms at lower a_C) (*150*). In contrast, during oxy-fuel combustion of coal, Cr(III) in the form of Cr silicate and iron chromite are the dominant species (*152, 153*). We do not know exactly what conditions prevail in the char formation in our reaction vessels; however, we expect P_{O2} to be low and a_C to be high, and therefore it is not surprising that Cr carbide is found in the samples.

Table 7. Chemical components of linear combination fitting to the XAS energy spectrum. Uncertainty in mol% Cr in $Cr_2(SO_4)_3.xH_2O$ and Cr_3C_2 is around ± 5 %.

	$Cr_2(SO_4)_3.xH_2O$ (mol % Cr)	Cr_3C_2 (mol % Cr)	R factor ($\times 10^{-4}$), χ^2
Biochar 500°C*	93	7	1.7, 0.027
Biochar 600°C*	77	23	3.4, 0.051
Biochar 600°C	59	41	5.6, 0.081
Biochar 800°C	35	65	5.8, 0.081
Biochar 1000°C	12	88	2.2, 0.031

*Larger reaction vessel.

Fine atmospheric particulates containing Cr, supposed to be from natural and industrial sources, have been found to contain both Cr^0 and Cr carbide using XANES (*154*), which demonstrates that Cr carbides are not uncommon in the environment.

It has been reported that carbothermal reduction by pitch of various transition metal oxides, including Cr oxide, forms carbides (*155*). In a N_2 atmosphere or an ammonia atmosphere, nitrides may also be formed for most of the metal oxides studied in that report, with the exception of Cr, which did not form nitrides, only carbide (*155*). These studies indicate that leather biochar is likely to contain Cr carbide, and not Cr nitride, even if the biochar is formed in the presence of nitrogen. The XANES shows that the Cr changes from the initial, dispersed Cr sulfate to some possibly intermediate compound (which may be a form of carbide) to form a Cr carbide at 1000 °C not dissimilar to Cr_3C_2.

EXAFS of biochar for Structural Information

Information about the structural environment of the Cr in the leather biochar is obtained from an analysis of the EXAFS range of the data acquired. Data were processed using Viper (*143*), and a Hanning window applied to the Fourier transforms. Theoretical *ab initio* EXAFS spectra for pairs of atoms were calculated using FEFF6L (*156*), with crystal structures from the ATOMS database (Centre for Advanced Radiation Sources, University of Chicago). Modelling in k space of the experimental spectra (from selected regions of the Fourier transform) using combinations of EXAFS spectra for these atom pairs was then performed

with Viper (*143*). To validate the modelling of the EXAFS data, we used the spectrum of Cr_2O_3, which is a crystalline material with a relatively simpler structure than Cr_3C_2. The resultant bond lengths are consistent with the crystallographic structure, validating the EXAFS data and fitting and enabling the analysis of the more complex biochar, which XANES has shown to contain a mixture of Cr_3C_2 and other components.

Chromium Carbide

To interpret the EXAFS of the biochar, it is helpful to refer to the literature on EXAFS of Cr carbide. A detailed study of the electronic structure of Cr carbides (*1*) notes that crystalline Cr_3C_2 belongs to the space group *pnma*, with lattice parameters a = 5.485 Å, b = 2.789 Å and c = 11.474 Å. Common phases that may form in Cr-based coatings include Cr_3C_2, Cr_7C_3 and $Cr_{23}C_6$. Based on the enthalpies of formation, Cr_3C_2 is the most stable of the Cr carbide phases, followed by Cr_7C_3, with $Cr_{23}C_6$ and Cr_3C equal third (*1*). The bonding is described as a combination of metallic, ionic and covalent, in character with a strong proportion of metallic character (e.g. metallicity for Cr_3C_2 is estimated at 15%, and is higher for the other Cr carbides). The charge on Cr of Cr_3C_2 is calculated to be $Cr^{+0.33}$ (*1*). Bond lengths in these compounds (*1*) and in Cr_3C_2 and Cr doped diamond-like carbon (DLC) films obtained from EXAFS (*2*) are detailed in Table 8. The bond distances measured in the leather biochar are therefore similar to those reported for Cr carbide reported in the literature and to one crystalline compound measured here.

Table 8. Bond lengths in Cr carbide compounds reported from EXAFS in (*1*) (*2*).

Compound	Radial distribution peak Cr–C (Å)	Radial distribution peak Cr–Cr (Å)	Source
Cr_3C	2.12	2.58	Li et al., 2011
Cr_3C_2	2.11	2.63	Li et al., 2011
Cr_7C_3	2.14	2.58	Li et al., 2011
$Cr_{23}C_6$	2.10	2.56	Li et al., 2011
Cr_3C_2	2.2	2.7	Singh et al., 2006
Cr–DLC	2.17–2.25	2.75–2.79	Singh et al., 2006

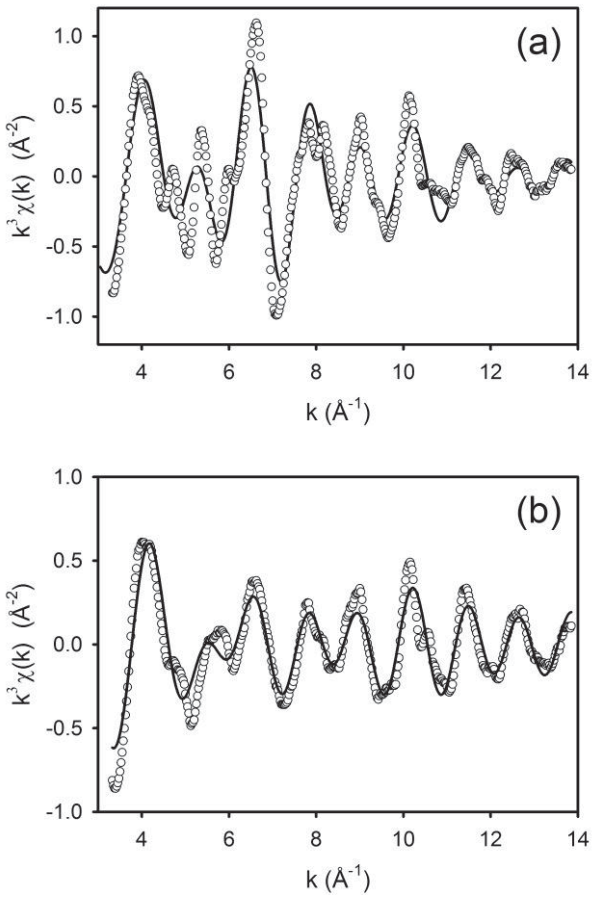

FIGURE 4.6: EXAFS OF BIOCHAR PRODUCED AT A) 800 °C; B) 1000 °C. CIRCLES $K^2X(K)$, SOLID LINE FITTED MODEL.

EXAFS of Biochar

There are numerous different atom–atom scattering path lengths in Cr carbide, some of which are quite similar in size. Therefore, the EXAFS spectra of the biochar prepared at 800 °C and 1000 °C are fitted with one grouped Cr-C atom pair sets and two grouped Cr-Cr atom pair sets, representing similar atom–atom distances in each group (Figure 4.6). From the fits, we obtain the bond distances shown in Table 9. These are like those listed in Table 8. The char formed at 600 °C is too complex a mixture to enable reliable modelling of the EXAFS spectrum. This EXAFS analysis supports the XANES interpretation and confirms that Cr carbide is formed at higher temperatures.

Table 9. Bond lengths obtained from the modelling of Fourier transform of EXAFS spectra of leather biochar. Six scattering paths were combined for Cr-C, 12 paths for Cr-Cr in total (in two groups).

Sample	Cr-C (Å), coordination number	Cr-Cr (Å), coordination number	Cr-Cr (Å), coordination number
Biochar 800 °C	2.07, 3.6	2.58, 0.7	2.94, 3.0
Biochar 1000 °C	2.05, 1.7	2.70, 4.3	2.92, 1.8

Stability in the Soil Environment

While we have found that using acid to produce biochar leachate does not remove Cr from the biochar, we have not performed long-term stability tests of the material in soil environments. These would be desirable to ensure the safety of the material for use in agricultural settings. As noted above, oxidation or reduction of some Cr compounds can occur in soils, depending on redox environment of the soil (*135*). However, Cr carbide is a very stable material, and is resistant to oxidation or reduction (*157*). The charcoal or biochar matrix within which the Cr is contained is also known to be very stable in soils (*158*). The addition of charcoal to soil enhances the agricultural productivity of the soil, for example in

the traditional terra preta soils from South America (*159*) but also in more recent studies of soil productivity (*131*).

CONCLUSIONS

We have shown that there may be an environmental benefit in making biochar from chrome-tanned leather waste. The char does not release Cr with acid leaching, unlike untreated leather. We have also shown that the Cr becomes chemically reduced by a carbothermic reaction on charring at high temperatures forming Cr carbide. Cr carbide is an inherently stable compound and its stability is further enhanced by being highly dispersed in a stable carbon medium. Biochar has the added benefits of enhancing agricultural production from soil and providing long-term sequestration of carbon from the environment. This strategy may turn a large-scale, potentially troublesome waste into an economic resource.

Section B: Structural Characteristics of Collagen within Biomaterials in Relation to Strength.

Chapter 5: Collagen Fibril Diameter and Leather Strength

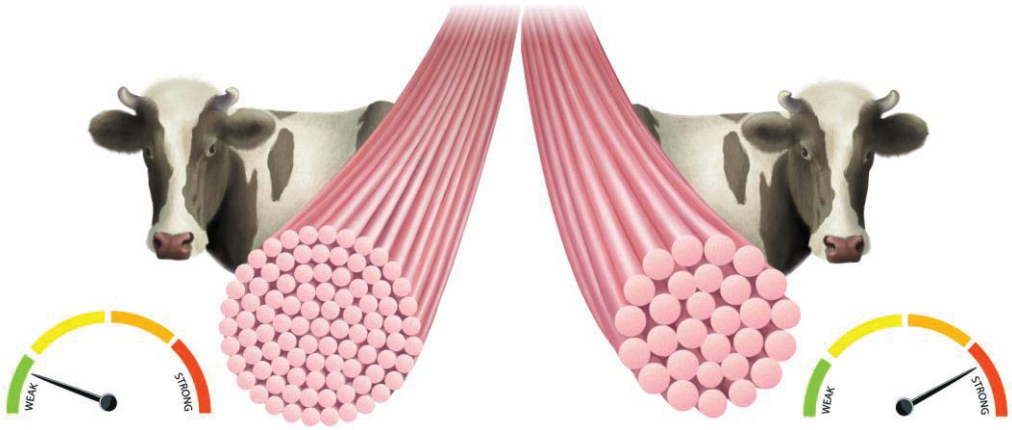

Chapter 5 has been published as an academic journal article in the Journal of Agriculture and Food Chemistry:

- **Wells, H. C.**; R. L.; Kirby, N.; Hawley, A.; Mudie, S. T.; Haverkamp, R. G. (**2013**). "Collagen Fibril Diameter and Leather Strength." *J. Agric. Food Chem.* **61** (47), 11524-11531.

ABSTRACT

The main structural component of leather and skin is collagen I in the form of strong fibrils. Strength is an important property of leather and the way in which collagen contributes to the strength is not fully understood. Synchrotron-based small angle X-ray scattering (SAXS) is used to measure the collagen fibril diameter of leather from a range of animals, including sheep and cattle, that had a range of tear strengths. SAXS data were fitted to a cylinder model. Collagen fibril diameter and tear strength were found to be correlated in bovine leather (r^2 = 0.59, P = 0.009), with stronger leather having thicker fibrils. There was no correlation between orientation index, i.e. fibril alignment, and fibril diameter for this dataset. Ovine leather showed no correlation between tear strength and fibril diameter. Neither was

there a correlation across a selection of other animal leathers. The findings presented here suggest that there may be a different structural motif in skin compared with tendon, particularly ovine skin or leather, in which the diameter of the individual fibrils contributes less to strength than does fibril alignment.

INTRODUCTION

The fundamental structural motifs that result in strong leather and skin are complex and not yet fully understood. For many high-value commercial applications, strong leather is necessary. The skins from some animals such as cattle, kangaroo and goat generally produce strong leather, while other animals including sheep produce weaker leather(*98*). In order to develop methods to increase the strength of leather, especially that produced from the inherently weaker animal skins, it is necessary to understand the skin and leather structures that are characteristic of high strength material.

The main structural component of leather is type I collagen and this is primarily responsible for skin and leather strength(*160*). Of the many factors contributing to the strength of natural skin and finished leather, the three most important have been proposed to be: the type and nature of cross-linking between the collagen fibrils; the orientation of the collagen fibrils; and the fibril diameter. Skin and leather also contain keratins, type III collagen and elastin, and these may contribute to strength to a lesser degree.

Natural cross-linking of collagen is present in living skin and is also achieved in processed leather using chromium, tannins or gluteraldehyde. Cross-linking would be expected to mechanically couple the collagen fibrils and therefore increase their ability to transmit force(*17, 18, 117, 161-163*) and also increase toughness by absorbing energy through enthalpic changes(*164, 165*). While some researchers found that the tensile elastic modulus of tendon is reduced when the content of the natural cross-linking component glycosaminoglycan (GAG) is lowered(*166*), others have found no altered mechanical properties in tendon from the removal of GAGs(*167, 168*). However, with synthetic cross-linking of bovine pericardium by gluteraldehyde the material becomes stronger than untreated tissue(*169, 170*), suggesting that cross-links are important for strength.

It has been widely reported that when fibrils are more highly aligned in the plane of the leather, the material is stronger than otherwise(*25, 98*). The way in which collagen fibril alignment would increase strength in collagen tissues has been accurately modeled in two dimensions(*171, 172*). It has been shown that in two dimensions this model accurately predicts observed behavior with fibrils which are more highly aligned in the plane of the leather resulting in stronger material(*25, 98*). However one study has shown that, when tear strength is used as a measure of strength, in the third dimension, the model does not give a complete picture as less alignment could be preferable for stronger material(*98*).

These two factors that affect material strength, collagen fibril orientation and cross-linking, have been shown to be interdependent since cross-linking influences fibril alignment(*173*).

The contribution of collagen fibril diameter to strength is the subject of the work presented here. Fibril diameter varies with strength, with several studies finding larger diameter collagen fibrils present in stronger tissue. In human aortic valves, the collagen fibril diameter depends on whether the fibrils are from regions of high stress or low stress: larger diameter fibrils (in areas of lower fibril density) result from high stress, suggesting that these larger diameter fibrils provide increased strength(*174*). Similarly for mouse tendon, fibril diameters increase with loading(*175*). In rats, those that exercised were active and lean, and had larger diameter collagen fibrils with a bimodal diameter distribution, compared to inactive obese rats. The mechanism proposed for this observation is the extra mechanical load placed on the tendons on the exercising rats (due to their higher activity levels) stimulated fibril thickening(*176*).

The size distribution of the fibril diameter may also change with age. Fetal tissue has been found to have a unimodal distribution with smaller collagen fibril diameters, whereas older tissue has larger fibrils and may have a unimodal or bimodal size distribution depending on the tissue type and animal(*177*). Growth of collagen in tissue culture has found that larger fibril diameters are associated with a rise in strength(*178*). It has been proposed that at small strain the smaller diameter fibrils prevent creep while at high strain, the larger diameter fibrils provide higher tensile strength(*177, 179*). These ideas have been further developed with the concept of the total absorbed energy providing tendon resilience and resistance to rupture(*179*).
In studies of equine digital flexor tendons, fibril diameter decreases with exercise, suggesting weakening of tendon with exercise (i.e. fatter fibril is stronger). Unusually, the fibril diameter in these tendons decreases with age, but this is associated with the decrease in strength(*180, 181*).

Collagen fibril diameter has been measured with a range of techniques, each having advantages and limitations. Transmission electron microscopy (TEM) has been used to determine fibril diameters(*182-184*). However, this requires that a large number of individual fibrils be measured(*182*) and the diameters obtained from the analysis depend on the processing methods and the type of fixation used in sample preparation(*185*); the results of TEM analysis need to be interpreted with caution. Atomic force microscopy (AFM) is another microscopic method used for fibril diameter analysis(*186, 187*). It also requires a large number of measurements to test for statistical significance but, unlike TEM, the environment

is relatively easy to control and it does not require any fixing or chemical processing of the sample.

In this study, fibril diameter was measured using small angle X-ray scattering (SAXS). This method has been used to measure collagen fibril diameters in tendon (*188*). The key advantage of SAXS is that it gives a size distribution for a large number of fibrils (the whole analysis volume) with one measurement. This enables robust statistical analyses and minimizes the sampling error and experimenter bias that may be present with techniques such as TEM and AFM. Like in AFM, the samples require no fixing or specific chemical processing prior to analysis, and some degree of environmental control may be possible.

There is a general consensus that larger fibril diameters result in stronger tendon and other tissue. Our purpose in this study is to investigate whether collagen fibril diameter is associated with strength in leather produced from bovine and ovine skins and to see if such a relationship might be generalized to other animals.

METHODS

Ovine pelts were from 5-month-old, early season lambs of breeds with "black face" lambs, which may include Suffolk, South Suffolk and Dorset Down. The bovine hides were from 2–3 year old cattle of a variety of breeds.

Skins were processed to produce leather by the following procedure. After mechanical removal of adhering fat and flesh, conventional lime sulfide paint, comprising 140 g/L sodium sulfide, 50 g/L hydrated lime and 23 g/L pre-gelled starch thickener, was applied to the flesh side of the skin at 400 g/m². The skin was incubated at 20 °C for 16 h and the keratinaceous material manually removed. The skin was then washed to remove the lime, and the pH lowered to 8 with ammonium sulfate, followed by the addition of 0.1% (w/v) Tanzyme (a commercial bate enzyme). After 75 min at 35 °C, the treated skin was washed and then pickled (20% w/v sodium chloride and 2% w/v sulfuric acid). Pickled pelts were degreased (4% nonionic surfactant; Tetrapol LTN, Shamrock, New Zealand) at 35 °C for 90 min then washed. The skins were neutralized in 8% NaCl, 1% disodium phthalate solution (40% active; Feliderm DP, Clariant, UK) and 1% formic acid for 10 min. The running solution was then made up to 5% chrome sulphate (Chromosal B, Lanxess, Germany) and processed for 30 min followed by 0.6% magnesium oxide addition, based on the weight of the skins, to fix the chrome, and processed overnight at 40 °C. These wet-blue pelts were neutralized in 1% sodium formate and 0.15% sodium bicarbonate for 1 h then washed followed by retanning

with 2% synthetic retanning agent (Tanicor PW, Clariant, Germany) and 3% vegetable tanning (mimosa; Tanac, Brazil). Next, 6% mixed fat liquors were added and the leathers, which were then maintained at 50 °C for 45 min, followed by fixing with 0.5% formic acid for 30 min, and finally by washing in cold water.

In addition, a single leather sample from each of crocodile, deer, elephant, goat, horse, pig, possum, seal and water buffalo were similarly processed.

Thickness normalized tear strengths were measured for all samples using standard methods(*103*). Samples were cut from the leather at the official sampling position (OSP)(*189*) except for the “other animals” where the leather was taken from near the center line. The samples were then conditioned at a constant temperature and humidity (20 °C and 65% relative humidity) for 24 h, and then tested on an Instron 4467. Two groups were selected from the ovine leather with one group consisting of low strength material and one group of high strength material. The range of samples with strengths in between were not analyzed further.

For scanning electron microscopy (SEM), samples were sputter coated with gold and imaged using a 20 kV accelerating voltage. Images were recorded on a FEI Quanta 200 (FEI, Eindhoven, The Netherlands).

Samples were prepared for SAXS analysis by cutting strips of leather of 1 x 30 mm. To record the scattering patterns, each sample was mounted in the X-ray beam either with the face of the leather normal the incoming X-rays or with the edge facing the X-ray beam. For the edge-on analyses, measurements were made every 0.25 mm, with the samples analyzed from the grain to the corium. For when the beam was directed normal to the surface of the leather, samples were cut parallel to the surface, producing a grain sample and a corium sample(*57*). Diffraction patterns were recorded on the Australian Synchrotron SAXS/WAXS beamline, using a high-intensity undulator source. Energy resolution of 10^{-4} was obtained from a cryo-cooled Si(111) double-crystal monochromator and the beam size (FWHM focused at the sample) was 250 x 80 μm, with a total photon flux of about 2 x 10^{12} ph/s. Diffraction patterns were recorded with an X-ray energy of 8 keV using a Pilatus 1M detector with an active area of 170 x 170 mm and a sample-to-detector distance of 3371 mm. Exposure time for the diffraction patterns was 1 second and initial data processing was carried out using the SAXS15ID software(*102*).

Fibril diameters were calculated from the SAXS data using the Irena software package(*190*) running within Igor Pro. The data were fitted at the wave vector, Q, in the range of 0.01 – 0.04 $Å^{-1}$ and at an azimuthal angle which was 90° to the long axis of most of the collagen fibrils. This angle was selected by determining the average orientation of the collagen fibrils from the azimuthal angle for the maximum intensity of the D-spacing diffraction peaks. The "cylinderAR" shape model with an arbitrary aspect ratio of 30 was used for all fitting. We did not attempt to individually optimize this aspect ratio and the unbranched length of collagen fibrils may in practice have a length that exceeds an aspect ratio of 30.

The orientation index, OI, is defined as (90° – OA)/90°, where OA is the minimum azimuthal angle range, centered at 180°, that contains 50% of the microfibrils(*57, 191*). An OI of 1 represents perfect alignment, while an OI of 0 represents perfect isotropy. We calculated the OI from the spread in azimuthal angle of the D-spacing peak at 0.059–0.060 $Å^{-1}$. Each OI value presented here represents the average of 14–36 measurements of one sample.

RESULTS

SEM

Scanning electron microscopy images of ovine and bovine leather (Figure 5.1) show collagen fibrils aligned and organized into fibril bundles (of around 5 – 10 μm diameter).

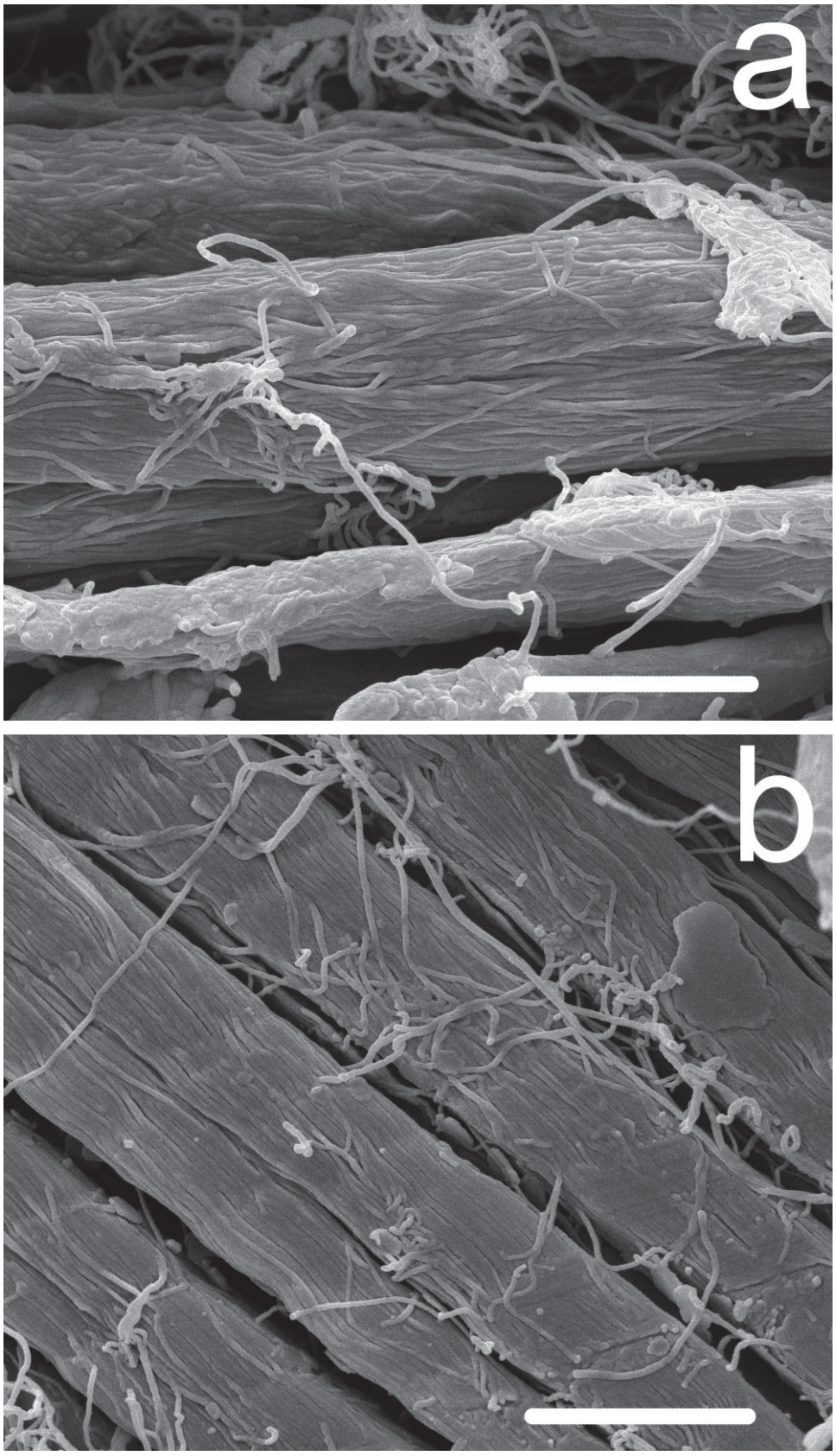

FIGURE 5.1: SEM IMAGES OF A) BOVINE AND B) OVINE LEATHER, WITH THE ALIGNED COLLAGEN FIBRILS VISIBLE AND ORGANIZED IN BUNDLES.

SAXS patterns

The well-defined rings that were observed are due to diffraction from the D-banding structure of the collagen fibrils and are most noticeable at high Q (Figure 5.2). Each ring can be seen to be of variable intensity around the azimuthal angle. This variation in intensity is due the alignment of the fibrils. The scattering at low Q, in the center of the pattern, provides the information from which the fibril diameter is determined. The diffraction from the D-banding and the scattering due to the fibril diameter are oriented at right angles to each other because the D-banding occurs along the length of a fibril and the diameter is at right angles to the length of the fibril. This can be seen to some extent in the raw diffraction images (Figure 5.2) with the central region elongated vertically and the d-banding diffraction bands aligned horizontally. Therefore it is possible to partially separate these two components of the scattering pattern by using integrated scattering intensity versus Q information from azimuthal segments at right angles to each other (Figure 5.3). With the fibril diameter measurements, an azimuthal segment that was at right angles to the maximum D-banding diffraction peaks was therefore used so that there is minimal interference to the scattering due to fibril diameter by low order d-band diffraction.

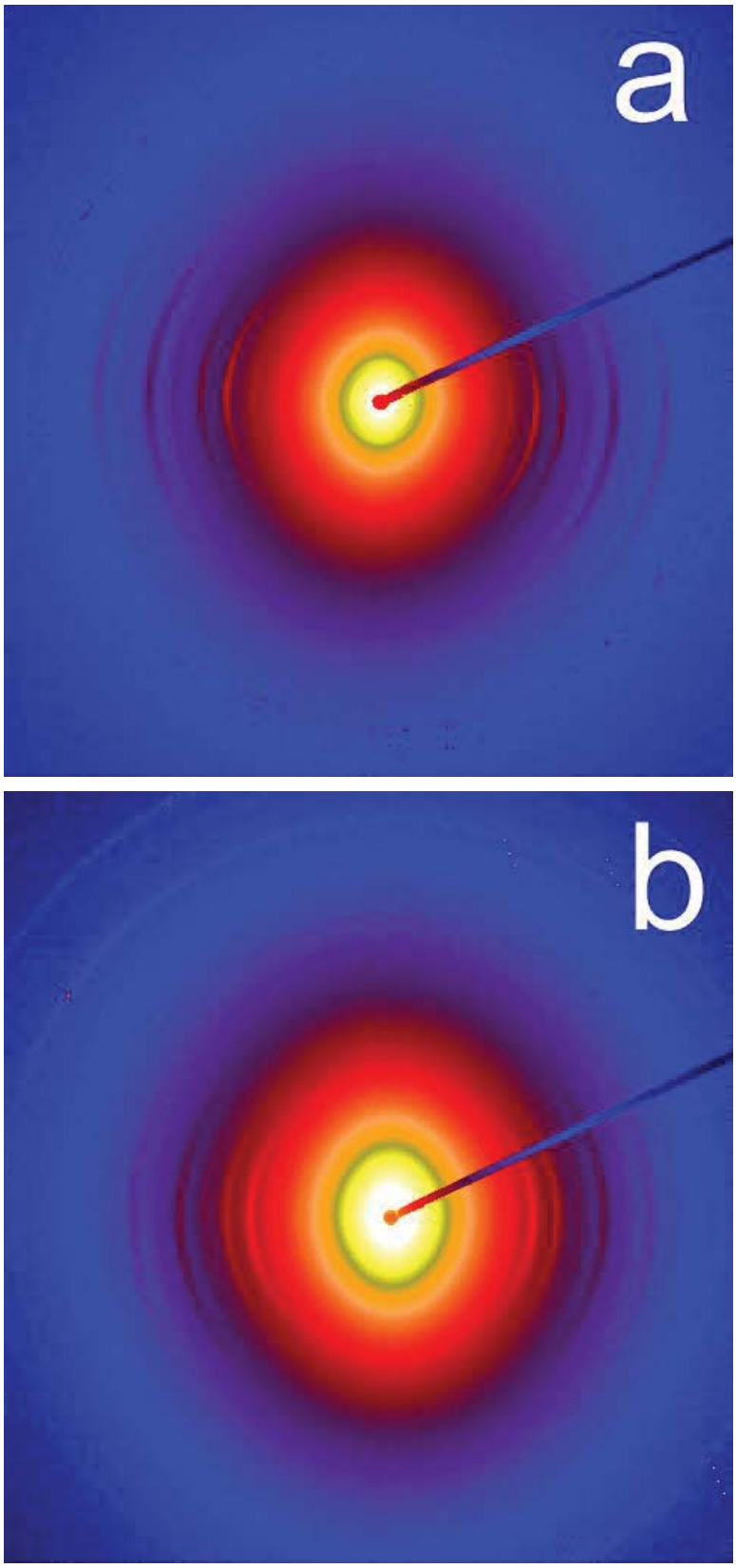

FIGURE 5.2: SAXS PATTERNS FOR A) OVINE AND B) BOVINE LEATHER, SHOWING THE REGION OF THE PATTERNS SELECTED FOR FIBRIL DIAMETER ANALYSIS.

Fibril diameter measurement

A good fit is achieved using the cylinder mode with an aspect ratio of 30 for both the bovine and ovine data. The ovine and the bovine samples produce scattering profiles that are qualitatively different with a straighter profile for bovine than for ovine. The average diameter (with standard deviation) of collagen fibrils for ovine leather was 61.5 (48) nm and for bovine leather 59.8 (21) nm, and these are statistically different (t = 4.6, P < 0.0001).

Fibril diameter and strength.

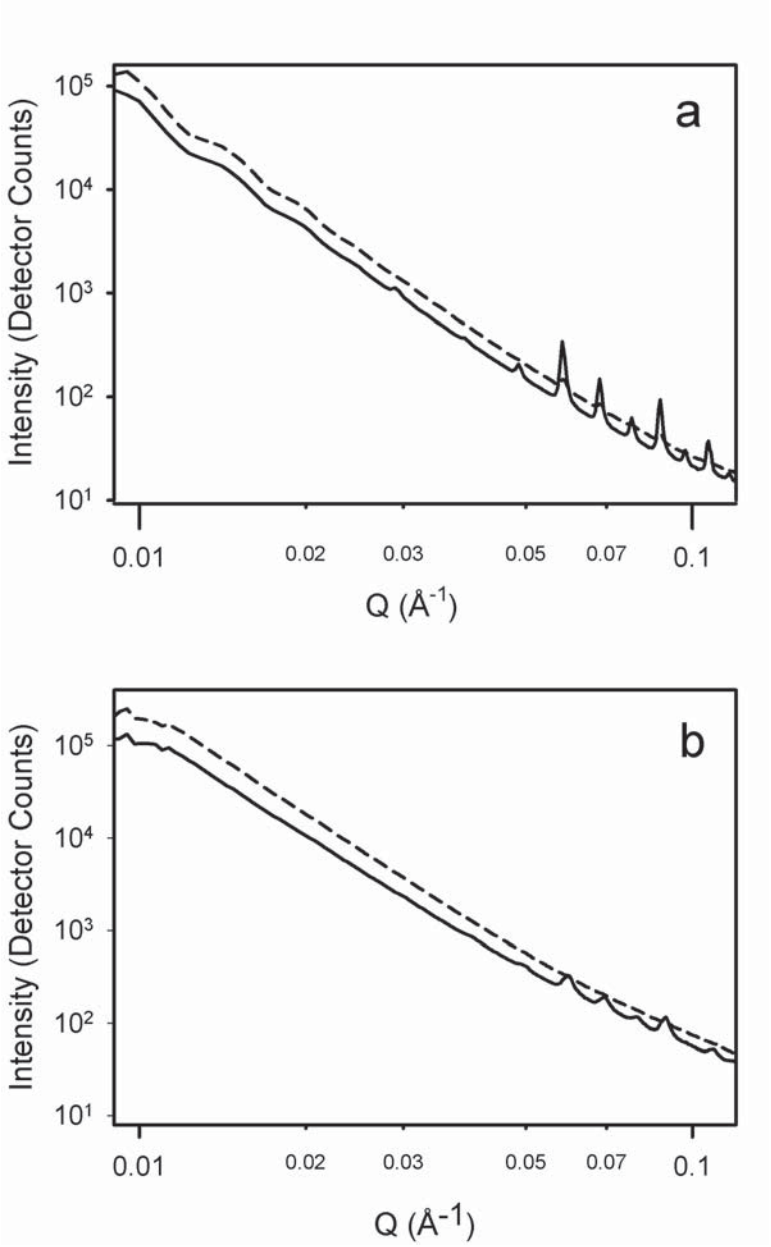

FIGURE 5.3: SAXS PROFILES OF EXAMPLES OF A) OVINE LEATHER; AND B) BOVINE LEATHER. THE PROFILE AT TWO AZIMUTHAL ANGLE RANGES ARE SHOWN WITH THE SOLID LINES AT THE

AZIMUTHAL ANGLE RANGE WHERE THE D-SPACING DIFFRACTION PEAKS ARE MAXIMUM (TYPICALLY A RANGE Ψ = –30 TO 30°) AND THE DASHED LINES AT RIGHT ANGLES TO THIS, TYPICALLY Ψ = 60 TO 120°. THE DATA SHOWN IN THE DASHED LINES REPRESENT THAT USED FOR THE FIBRIL DIAMETER ANALYSIS.

The measured fibril diameters are plotted against strength for three datasets: ovine leather (Figure 5.4a), bovine leather (Figure 5.4b) and leather of "other animals" which includes crocodile, deer, elephant, goat, horse, pig, possum, seal and water buffalo (Figure 5.4c). There is no correlation between strength and fibril diameter for the leather from sheep or the "other animals". However, for bovine leather, there is a statistically significant correlation between fibril diameter and strength with stronger leather containing thicker fibrils (r^2 = 0.59, P = 0.009).

Fibril diameter and OI

A strong correlation between leather strength and fibril orientation (OI) has been reported (*25, 98*) therefore we wished to see whether fibril diameter is correlated with OI. Plots of fibril diameter versus OI for ovine and bovine leather (Figure 5.5) show no correlation between these two structural aspects of leather.

DISCUSSION

Fibril diameter

The average diameter (with standard deviation) of collagen fibrils found here for ovine leather of 61.5 (48) nm and for bovine leather of 59.8 (21) nm are similar to those found in other studies. Fibril diameters reported for sheep included 65 nm diameter(*192*) (skin, measured using TEM), 73 (20) nm (spine ligament, SAXS) and 69 (14) nm (spine ligament, TEM)(*188*).

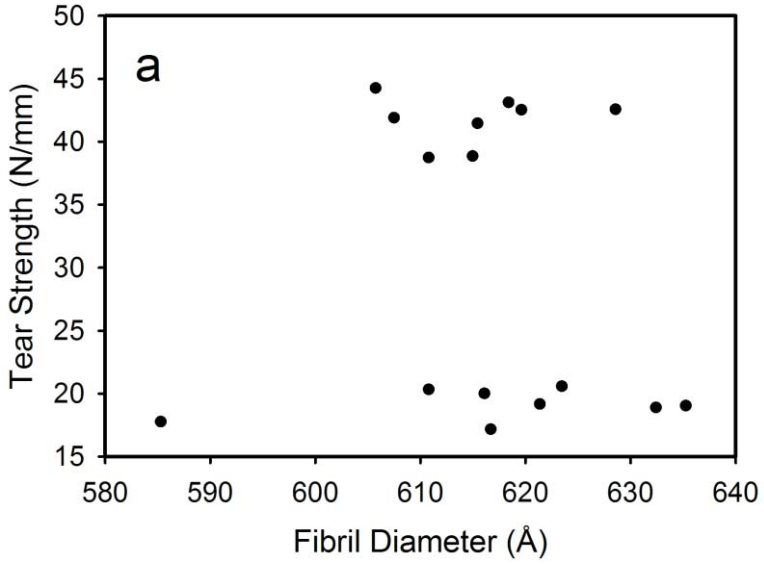
a
Tear Strength (N/mm)
50
45
40
35
30
25
20
15
580
590
600
610
620
630
640
Fibril Diameter (Å)

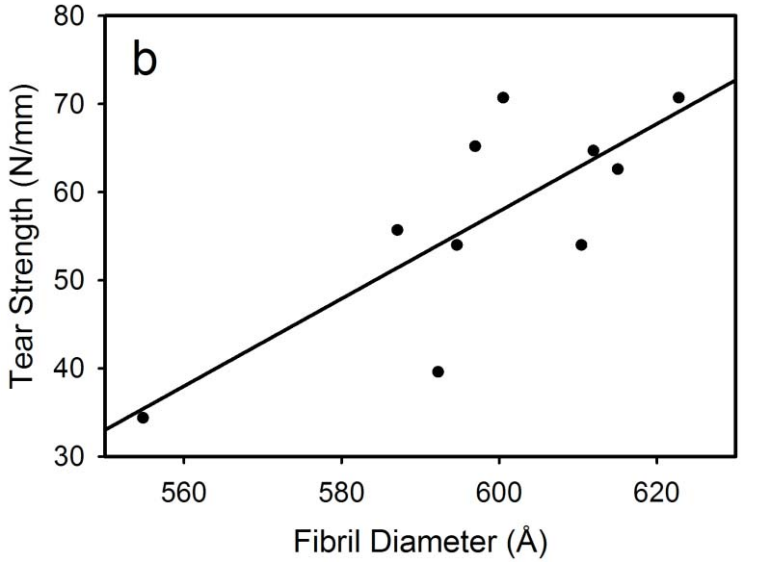
b
Tear Strength (N/mm)
80
70
60
50
40
30
560
580
600
620
Fibril Diameter (Å)

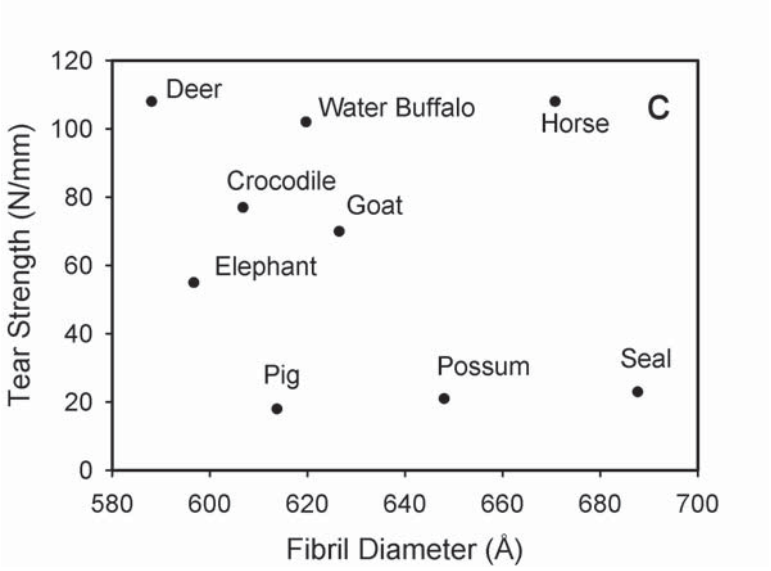

FIGURE 5.4: COLLAGEN FIBRIL DIAMETER VERSUS TEAR STRENGTH FOR A) OVINE LEATHER; B) BOVINE LEATHER; C) A RANGE OF OTHER ANIMALS. BOVINE R^2 = 0.59, P = 0.009 (FOR SLOPE); OVINE R^2 = 0.0077, P = 0.75 (FOR SLOPE); OTHER ANIMALS R^2 = 0.080, P = 0.46 (FOR SLOPE). EACH POINT IS THE AVERAGE VALUE FROM 12–20 DIFFRACTION PATTERNS.

Collagen fibrils produced *in vitro* from cow skin, measured with TEM, were found to have a diameter of 67 nm(*193*). These studies also reported that collagen fibrils from sheep have a slightly larger diameter than those from cattle, which is consistent with our findings.

However, other reports give quite different values for fibril diameters in skin and tendon: 202–204 nm in diameter (ovine tendon, TEM) (*184*) and 142–163nm in diameter (bovine skin, TEM)(*194*). As mentioned in the Introduction, diameters determined by TEM can vary greatly depending on the sample preparation procedures and fixation method (*185*).

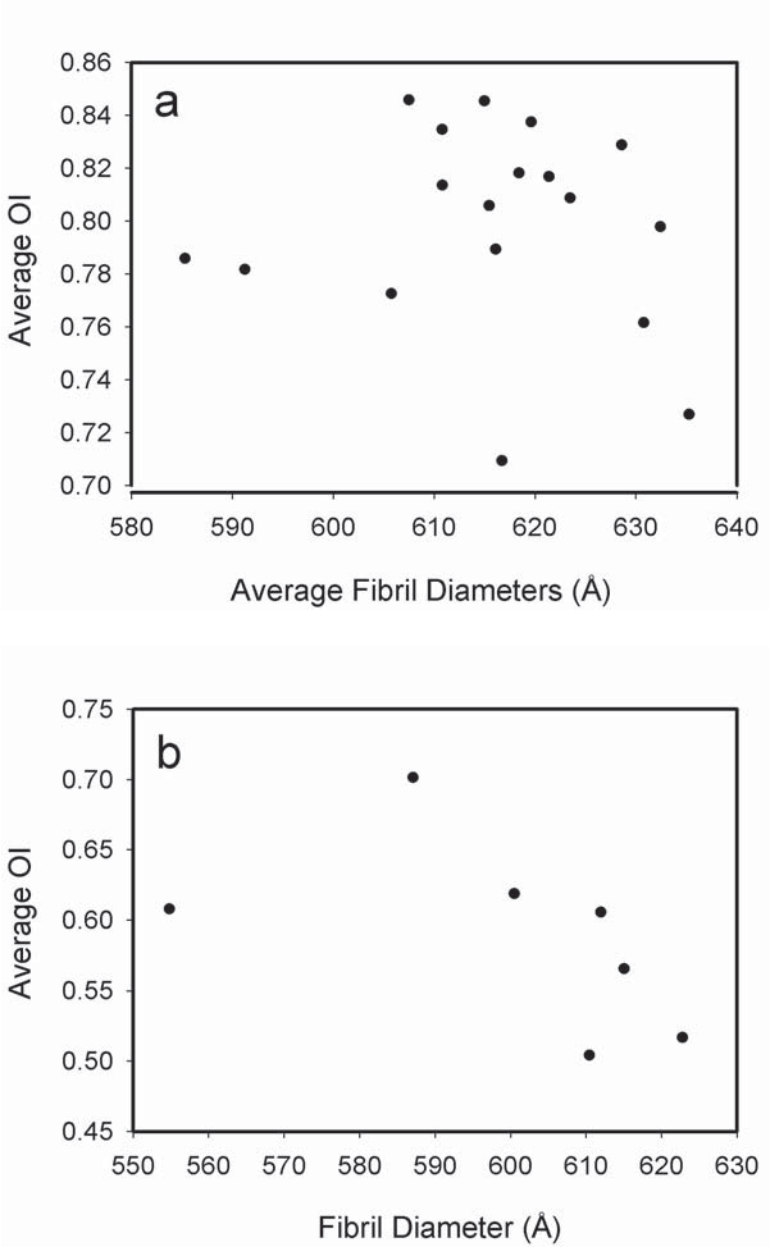

FIGURE 5.5: ORIENTATION INDEX VERSUS FIBRIL DIAMETER FOR A) OVINE AND B) BOVINE LEATHER, SHOWING A LACK OF CORRELATION BETWEEN THESE PROPERTIES. OVINE R^2 = 0.011, P = 0.6747 (FOR SLOPE); BOVINE R^2 = 0.28, P = 0.22 (FOR SLOPE).

We find that in some parts of the cross sections (not shown) of some samples, particularly the ovine leather, there is a bimodal distribution of fibril diameter. In these cases, we took the modal size (which was the larger fibril diameter). The details of fibril diameter distribution through the cross sections and in different species are complex and could benefit from further study and analysis, particularly in light of the reported importance of a non-uniform fibril size on strength in tendons(*177, 179*).

Fibril diameter and strength

For bovine leather, collagen fibril diameter was correlated with strength (Figure 4b), and the correlation was statistically significant (P = 0.009). This provides robust and quantitative support of previous studies that relate fibril diameter to strength in a variety of tissues using various methods used to measure fibril diameter and inferring strength. For example, human aortic valves that, like skin, are composed largely of collagen I, show increased fibril diameter when they have been exposed to high stress(*174*). In several studies of tendon, which also consists largely of collagen I, mechanical loading, which is presumed to result in increased strength, is found to lead to larger diameter collagen fibrils(*175, 176*). The mechanism that results in larger fibril diameters providing higher strength has been proposed: tendons with larger diameter fibrils have a greater ability to absorb energy and thus are more resilient and resistant to rupture(*179*).

By contrast, no correlation was found between fibril diameter and tear strength in ovine leather. It is known that the ovine leather has a less oriented structure than bovine leather (and much less than tendon) and this contributes to its lower strength(*25, 100*). The lower OI suggests that any increase in alignment can have a significant effect on strength. This is in contrast to the more aligned structure of bovine leather, suggesting that OI as a determinant of strength is dominant in ovine leather. The difference in the spread of age of the ovine and bovine animals, as discussed later, could perhaps have contributed to these differences. Other factors that may contribute and which were not explicitly considered in this study are the breed, the condition of the animal and variations in processing conditions.

Comparison with tendon

One of the important differences between skin and tendon in the arrangement of collagen is that the collagen fibrils are less aligned in skin than in tendon. The very strong relationship between fibril alignment and strength in skin, if extended to tendon, could to a large extent explain the high strength of tendon. In this study, the different degree of alignment between collagen in tendon and leather suggests that small increases in alignment in skin have significant consequences for strength, but are less important in the already highly aligned tendon. Therefore, for tendon, where changes in fibril alignment are not significant, the effect of fibril diameter on strength becomes dominant. In contrast, for skin and leather, the fibril

alignment is much less than that in tendon; and changes in alignment, such as those found between different skins dominate and changes in fibril diameter have less significance.

Inter-species comparisons

While we see that there is a correlation with fibril diameter within the bovine group of samples, and there is not a correlation within ovine, we can also see that the relationship between fibril diameter and strength does not extend to inter-species comparison (Figures 5.4a,b,c). Bovine leather is stronger yet ovine leather has the thicker fibrils. The strength differences have previously been shown to relate to fibril orientation, which is different in the two animals(*25*). The lack of correlation between fibril diameter and strength across species leads us to conclude that fibril diameter comparisons are valid only within a species and not between species.

Age

The age of the animal may also contribute to the skin strength, as it has been shown previously that tendon strength and collagen fibril diameter increases with age (*175, 177, 179*); this may also apply to leather produced from skin. However, we did not explicitly factor age into the experimental design. The ovine leather was from young animals (5 months old) in a narrow age range (a few days) and the bovine leather was from older animals (2–3 years old) of a slighter broader age range of 1 year. It is possible that the broader age range of animals supplying the bovine leather was a factor in the variation in observed strength and the correlation with fibril diameter. It may therefore have contributed to the lack of correlation between fibril diameter and strength in ovine leather in contrast to the correlation observed for bovine leather. However, this is purely speculation and the effect of age on fibril diameter and tear strength merits further investigation.

Cross-linking

Cross-linking in tendon and pericardium has been shown to affect structure(*173*) and probably influence strength (*166, 169, 170*) although this is not universally agreed(*167, 168*). Therefore, the amount or nature of cross-linking could influence strength in leather. Because this cross-linking is between fibrils, fibril diameter might influence the amount and effect of

the cross-linking and therefore the effect of cross-linking on strength. We did not explicitly consider variations in cross-linking in our experimental design.

Other factors affecting fibril diameter

It might be expected that genetic and environmental factors may also contribute to fibril diameter such as the breed of the animal and the condition of the animal (the amount of fat(*176*), type of feed, level of exercise).

Orientation index and fibril diameter

It had previously been reported that there is a strong correlation between leather strength and fibril orientation. (*25, 98*) It was therefore necessary to test whether the observed correlation between fibril diameter and strength for bovine leather was merely due to a correlation of fibril diameter with OI rather than a causal relationship between diameter and strength. We found that these two properties are not interdependent, with no correlation found between the OI and fibril diameter for bovine leather (Figure 5.5b). Therefore, we cannot dismiss the correlation we have observed between fibril diameter and strength in bovine leather as being simply a cross correlation with OI.

Bundle size

Collagen fibrils form into bundles of several tens or hundreds (Figure 5.1). It would be interesting to see if there was a relationship between fibril bundle size and strength. Just as a highly braided, multi-strand rope has high strength compared with a loose collection of fibers, well-defined and thick fibril bundles, held together with covalent cross links or multiple hydrogen bonds or hydrophobic interactions, could have increased strength. We did not collect data to sufficiently low Q to be able to confidently determine fibril bundle sizes, but we are pursuing this with future studies.

Packing density

It has been suggested that fibril volume fraction could be a determinant for tissue strength(*195, 196*). Two factors that may influence this are fibril diameter and fibril size

distribution. It has been claimed that larger fibril diameters enable higher packing densities(*195*) with one experimental observation on age series for mouse tendon weakly supporting this(*196*). However geometric considerations indicate that the opposite should be true(*197*) with the packing of circles in a circle resulting in a general increase in packing density as the number of circles is increased (equivalent to smaller fibril cross sections in a bundle). Fibril size alone leading to denser packing does not therefore provide an explanation for the experimental observations reported here. However, if the collagen fibrils are not of uniform diameter then increased packing density is possible and therefore the volume fraction of collagen in a bundle increases(*195, 196*) and this could be expected to influence strength. We have not investigated fibril packing density or different size distributions in detail but the techniques reported here can be applied to study this further and form part of the ongoing research program.

CONCLUSIONS

We studied the relationship between tear strength and fibril diameter in ovine and bovine leather and leathers of a range of other animals. We found that there is a correlation between strength and fibril diameter in the bovine leather. For ovine leather, however, we did not find a correlation of fibril diameter with strength. In bovine leather, the collagen fibrils are more aligned than in ovine skin, while tendon contains even more highly aligned fibrils. We conclude that where the tissue contains highly aligned fibrils, the fibril diameter becomes a significant determinant of strength. In tissues where the fibrils are not well aligned, the influence of fibril alignment on strength is greater than that of fibril diameter. Therefore in leather and skin, larger fibrils may lead to stronger material, but for weaker leathers, fibril diameter is secondary to fibril alignment for strength. An inter-species assessment showed that it is not possible to make inferences on strength from inter-specific comparisons of fibril diameter. Tissues composed of collagen have complex structures with many different aspects of the structure contributing to the mechanical properties. We have shown how one aspect of this structure may contribute in some types of leather and that these principles may be extended to other tissue types.

Chapter 6: Poisson's Ratio of Collagen Fibrils Measured by Small Angle X-ray Scattering

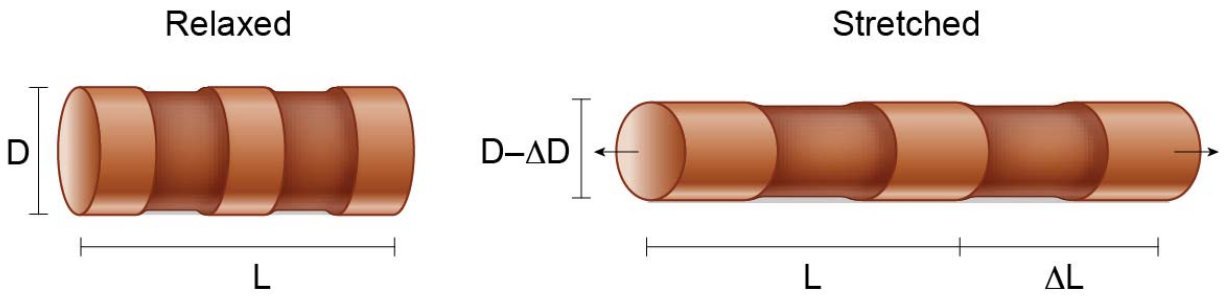

$$\frac{\Delta L/L}{\frac{\pi}{4}\left(\frac{\Delta D}{D}\right)^2} > 0.5$$

Chapter 6 has been published as an academic journal article in the Journal of Applied Physics:

- **H. C. Wells**, K. H. Sizeland, H. R. Kayed, N. Kirby, A. Hawley, S. T. Mudie, R. G. Haverkamp, "Poisson's Ratio of Collagen Fibrils Measured by Small Angle X-ray Scattering of Strained Bovine Pericardium" **(2015)** *J. Appl. Phys.* **117** (4), 044701.

ABSTRACT

Type I collagen is the main structural component of skin, tendons, and skin products, such as leather. Understanding the mechanical performance of collagen fibrils is important for understanding the mechanical performance of the tissues that they make up, while the mechanical properties of bulk tissue are well characterized, less is known about the mechanical behaviour of individual collagen fibrils. In this study, bovine pericardium is subjected to strain while small angle X-ray scattering (SAXS) patterns are recorded using synchrotron radiation. The change in d-spacing, which is a measure of fibril extension, and the change in fibril diameter are determined from SAXS. The tissue is strained 0.25 (25%) with a corresponding strain in the collagen fibrils of 0.045 observed. The ratio of collagen fibril width contraction to length extension, or the Poisson's ratio, is 2.1 ± 0.7 for a tissue strain from 0 to 0.25. This Poisson's ratio indicates that the volume of individual collagen fibrils decreases with increasing strain, which is quite unlike most engineering materials. This high Poisson's ratio of individual fibrils may con- tribute to high Poisson's ratio observed for tissues, contributing to some of the remarkable properties of collagen-based materials.

INTRODUCTION

Type I collagen is a key structural material in animals. It is the main structural component of skin and tendons. Type I collagen is also important in products made from animal skin, or related tissues, such as leather and extracellular matrix scaffolds for surgical applications(*198, 199*). Type II collagen has a fairly similar fibril structure to type I collagen, although with more branching and cross-linking, and is the main structural component of tissues, such as cartilage, therefore parallels may be drawn between type I and type II collagens. The mechanical properties of collagen-based materials are central to the natural and industrial uses of these materials and have been studied in a variety of tissues.

The bulk mechanical properties of tissues have been well characterised, including measurements of Poisson's ratio. Poisson's ratio, v, is the ratio of transverse strain ∆W/W (where W is width of a cube or bar) to longitudinal strain ∆L/L (where L is the length of a cube or bar) in the loading direction:

$$v = -\frac{(\Delta W/W)}{\Delta L/L}$$

For isotropic materials, v > 0.5 is excluded on theoretical grounds however, fibrillar collagen is anisotropic. When v > 0.5 for a material under tension, the volume decreases as the tissue is strained. A wide range of values of v have been measured for type I and II collagen materials in compression and tension, with many of these giving v > 0.5. These include tendon under compression(*200*) with v = 0.8, spinal dura mater under uniaxial tension v = 0.5–1.6 depending on the direction of the tissue section taken(*201*), bovine articular cartilage in compression(*202, 203*) v = 0.15–0.20 and 0.16 measured by microindentation,(*204*) and human patellar cartilage measured in tension(*85*) v = 0.6–1.9. The Poisson's ratio in tendon fascicles has been shown to increase with stress(*86*) up to v = 4 and in articular cartilage up to v = 1.2 with increasing strain.(*205*)

While the mechanical properties of tissue have been well characterized, the mechanical properties of individual collagen fibrils that constitute the tissue are less well known. Collagen fibril diameter has been shown to have some influence on tissue strength.(*99, 177*) In addition, proteoglycan connections between collagen fibrils in tendon subjected to tensile stress have been suggested as contributing to the strength of the tissue.(*165, 206*) Examination of individual collagen fibrils in rat tail tendon with atomic force microscopy can

yield an estimate of the Poisson's ratio measured in compression in a transverse direction.(*207, 208*)

Modelling of the crimp present in many collagen tissues, such a tendon and ligament or helical structure of the fibrils, has suggested that these features could explain much of the high Poisson's ratio of the tissue composed of collagen.(*87*) It has also been suggested that in tendon, the strain may be taken up by sliding of fibrils within the tendon rather than by extension of the collagen fibrils.(*209*) In leather, where there is very little crimp, the reorientation of fibrils may be an important mechanism for absorbing strain.(*19, 114*) Here, the behaviour of individual fibrils of collagen I as strain is applied is studied using small angle X-ray scattering (SAXS) to simultaneously measure the fibril length extension and fibril diameter contraction. Bovine pericardium is used as a model material for this work because it is elastic and strong and has application in medical devices.(*108*)

MATERIALS AND METHODS

Fresh bull (Charolais Cross) pericardium samples were obtained from John Shannon, Wairapara, New Zealand, within 2 h of slaughter. The tissue was cut into rectangles ca. 50mm × 6 mm, with the long axis aligning with the long axis of the heart. The pericardium was washed for 24 h in a 1% octylphenol ethylene oxide condensate (Triton X-100, Sigma), 0.02% EDTA solution made up in phosphate buffered saline (PBS) (Lorne Laboratories Ltd).(*210*) The samples were stored in PBS. SAXS diffraction patterns were recorded at room temperature while the pericardium was wet.

For transmission electron microscopy (TEM), samples were fixed with 2% formaldehyde and 3% gluteraldehyde in phosphate buffer, post fixed with 1% OsO4 and dehydrated using an acetone/water series. The sections were stained with uranyl acetate and then with lead citrate and examined with a Philips CM10 TEM (Philips, Eindhoven, The Netherlands). These show the collagen fibrils with the d-banding visible (Fig. 6.1).

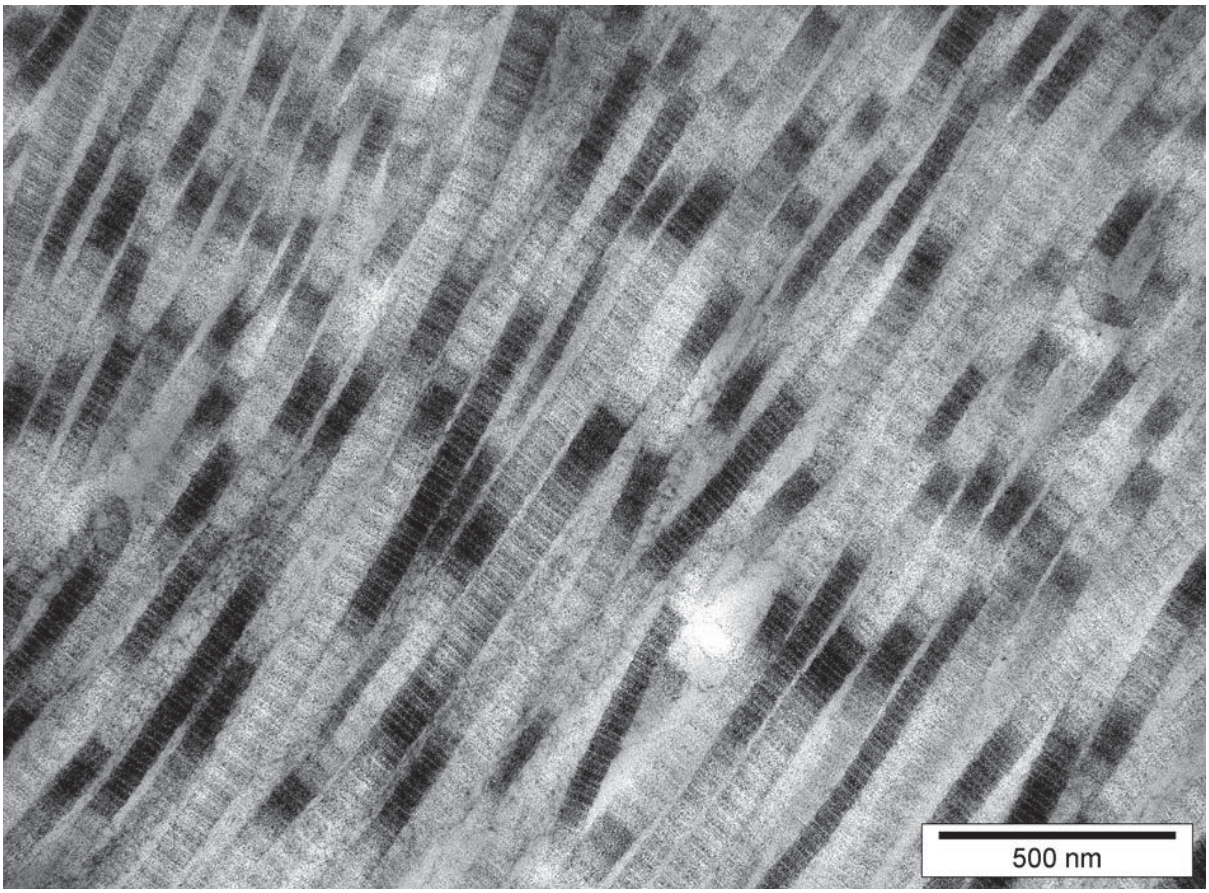

FIGURE 6.1: TRANSMISSION ELECTRON MICROSCOPY OF PERICARDIUM.

A stretching apparatus was built as described previously.(*114*) A linear motor, Linmot PS01 48 × 240/30 × 180-C (NTI AG, Switzerland), was mounted on a purpose-built frame. Clamps to hold the pericardium were fitted between the linear motor and a L6D OIML single-point loadcell (Hangzhou Wanto Precision Technology Co., Zhejiang, China). The pericardium was mounted horizontally without tension. The sample (30mm between jaws) was stretched in 1mm increments to take up the slack until a force was just registered by the loadcell, then backed off so that it was not under tension. Diffraction patterns were collected in a 0.5mm grid of eight points. The sample was stretched in 1mm increments and maintained for 1min at each extension to stabilize before SAXS patterns, the extension and the force information were recorded. This process was repeated until the sample failed, with the interval between strain increments around 8–13 min.

The diffraction patterns were recorded on the Australian Synchrotron SAXS/WAXS beamline which uses a high intensity undulator source. An X-ray energy of 12 keV was used with energy resolution of 10^{-4} (e.g., 1×10^{-4} for 1 radiation) from a cryo-cooled Si(111) double-crystal monochromator with a beam size (FWHM focused at the sample) of 250×80 μm, and a total photon flux of about 2×10^{12} ph s^{-1}. A Pilatus 1M detector with an active area of 170×170mm and a sample-to-detector distance of 3371mm was used. Exposure time was 1 s and data processing was carried out using the SAXS15ID software.(*102*) Each data point presented is the average from of a minimum of eight diffraction patterns recorded on a grid of positions on the sample.

Fibril diameters were calculated from the SAXS data using the Irena software package(*190*) running within Igor Pro. The data were fitted at the wave vector Q, in the range of 0.01–0.04$Å^{-1}$ and at an azimuthal angle which was 90° to the long axis of most of the collagen fibrils. This angle was selected by determining the average orientation of the collagen fibrils from the azimuthal angle for the maximum intensity of the d-spacing diffraction peaks. The “cylinder AR” shape model with an arbitrary aspect ratio of 30 was used for all fitting. We did not attempt to individually optimize this aspect ratio and the unbranched length of collagen fibrils may in practice have a length that exceeds an aspect ratio of 30.

The d-spacing was determined from the position of the centre of a Gaussian curve fitted to the 9th order diffraction peak taken from the integrated intensity plots from the azimuthal range from 45° to 135°. The orientation index (OI) is defined by

$$OI = (90° - OA)/90° \qquad (1)$$

where OA (orientation angle) is the minimum azimuthal angle range that contains 50% of the fibrils, based on the method of Sacks for light scattering(*191*) but converted to an index,(*74*) using the spread in azimuthal angle of one or more d-spacing diffraction peaks. The OI is used to give a measure of the spread of fibril orientation (an OI of 1 indicates the fibrils are parallel to each other; 0 indicates the fibrils are randomly oriented).

RESULTS AND DISCUSSION

The integrated intensity plots show well-defined peaks corresponding to the collagen d-period (Fig. 6.2). The odd numbered peaks have a much higher intensity than the even numbered peaks, a characteristic attributed to a fully hydrated sample.(*211*) At right angles to the direction of alignment, the d-peaks are not as apparent, and the scattering results from the fibril diameter distribution. The diffraction that is no longer present at an azimuthal angle rotated by 90° is due to the d-banding, while the broader features that remain or enhanced are due to the fibril diameter or fibrillar spacing. The stress-strain curve recorded from the in-situ stretching is shown in Fig. 6.3. The maximum strain obtained before rupture was 25%. The time dependency of the stress-strain curve was not considered as it has been found not to affect elastic properties(*201*) and the time between each data point was approximately constant.

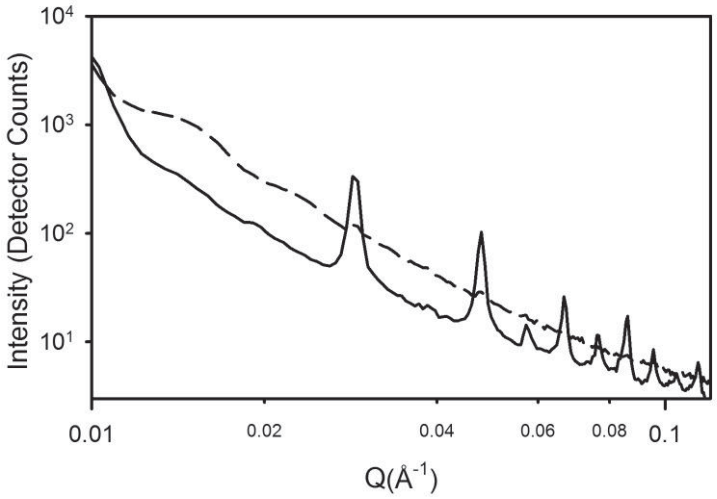

FIGURE 6.2: REPRESENTATIVE INTEGRATED SCATTERING PATTERN OF PERICARDIUM. SOLID LINE – AT AN AZIMUTHAL ANGLE SEGMENT CENTRED 90°, WHICH IS USED FOR ASSESSING D-SPACING, DASHED LINE – AT AN AZIMUTHAL ANGLE SEGMENT CENTRED ON 0°, WHICH IS USED FOR FIBRIL DIAMETER.

There are two stages in the structural changes at the collagen fibril level we observe. In the first stage (up to a strain, fractional change in length, of about 0.09), we observe is a decrease in collagen fibril diameter with a small increase in d-spacing and a large increase in OI. During this stage, the strain is taken up by reorientation of the fibrils. Pericardium has a marked crimp so that a portion of the observed OI can be due to crimp. It is trivial to show that the shape of the curve from which the OI is derived, if the crimp takes a sinusoidal shape, should have the form

$$I = A \sin(\phi) \cos(\phi) \qquad (2)$$

where I is the diffraction peak intensity, ϕ is the azimuthal angle, and A is the magnitude of the crimp. It has been shown elsewhere that, during biaxial strain crimp is maintained, (*212*) therefore we believe the change in OI is largely due to fibril reorientation rather than straightening of crimp.

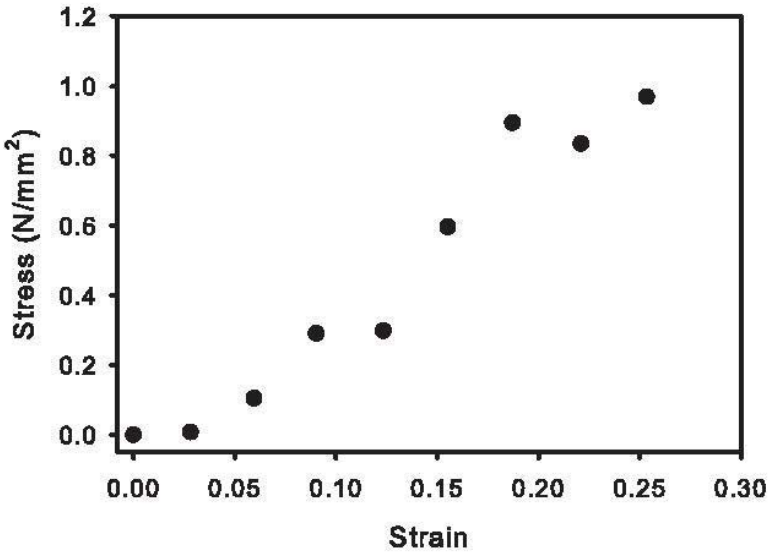

FIGURE 6.3: STRESS-STRAIN CURVE MEASURED ON PERICARDIUM DURING IN-SITU SAXS MEASUREMENTS.

During the second stage of strain, there is no significant change in the OI but the d-spacing increases markedly (fibril length) and the fibril diameter decreases (Fig. 6.4). The d-spacing can be thought of as an internal strain gauge for the collagen fibrils with an increase in d-spacing, indicating an increase in stress on the fibril. At a tissue strain above 0.15, the fibrils continue to stretch but there is a decrease in fibril diameter plateaus. From the unstrained state to the maximum strain state, the d-spacing increases from 66.13 nm to 69.12 nm, a

change of 2.99 nm or 4.5%. The OI increases from 0.53 to 0.75 (at a strain of 0.09) and then is stable at around 0.80 at higher strain values (Fig. 6.4). Fibril diameter decreases from 62.1 nm for the unstretched collagen to 55.4 nm at the maximum strain experienced (Fig. 6.4), a decrease in 6.7 nm or 10.8%. At first, while the fibril diameter changes, there is little change in d-spacing, then at higher strain, as the fibril diameter decreases, the d-spacing increases.

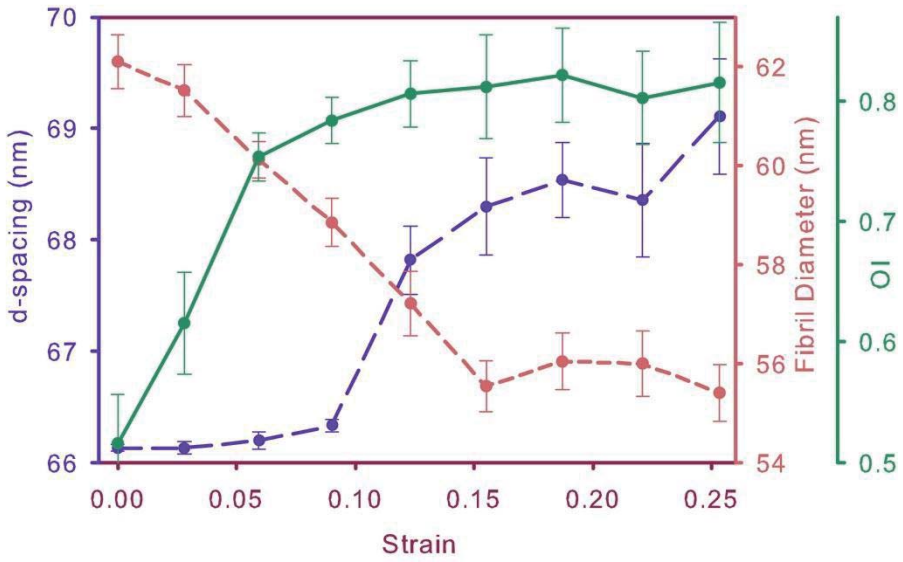

FIGURE 6.4: D-SPACING (LONG DASH, BLUE), FIBRIL DIAMETER (SHORT DASH, RED) AND OI (SOLID, GREEN) CHANGES WITH INCREASING STRAIN. LINES ARE A GUIDE FOR THE EYE ONLY.

During this second stage of strain, the change in d-spacing strain (fibril strain) is about 30% of the whole tissue strain. This shows that the strain in the tissue is taken up partly by the strain in the collagen fibrils, as has been observed with light scattering(*212*) and partly by the tissue strain being transferred to inter-fibrillar sliding or rearrangement of the fibrils. By contrast, in weak ovine leather (data taken from published work(*114*)), our calculations of fibril strain versus leather strain give 10% d-spacing strain to whole tissue strain for leather. The collagen fibrils in leather are less aligned than in pericardium, allowing more possibility for realignment. For rat tail tendon, this ratio is 40% for the second (linear) region of the strain curve,(*213*) perhaps reflecting the high alignment of collagen in tendon.

From the d-spacing change and fibril diameter change, we calculate the Poisson's ratio. Since v is defined for a cube, we correct the ratio by $\sqrt{\pi}/2$ to account for the approximately cylindrical shape of the collagen fibril (in order to retain the property that a Poisson's ratio of 0.5 represents a material in which the volume does not change with strain). So that the equivalent Poisson's ratio, v', can be calculated for a rod with diameter D by

$$v' = -\frac{\sqrt{\pi}/2(\frac{\Delta D}{D})}{\Delta L/L} \qquad (3)$$

For collagen in bovine pericardium, at low strain, the Poisson's ratio appears to have a very high value (15–27), but for strain above 0.09, the Poisson's ratio is in the range 2.1 – 2.8. For the total strain (from 0 to 0.25), the change in d-spacing and diameter gives v' = 2.1 ± 0.7 (these values of v' can be calculated from Fig. 6.4). The v' > 0.5 could be due to tighter packing within the fibril under strain, which may include compression of hydrogen bonding in the fibril, microfibril, or tropocollagen. The extension of the fibrils with increasing strain has previously been ascribed largely to the sliding of the tropocollagen within the fibrils, resulting in an increase in the gap region, rather than to the extension of the tropocollagen molecules that constitute the fibrils.(*214*) We note that the stress-strain curve does not show a marked foot region, it does not exhibit a low Young's modulus at low strain, which suggests that an entropic straightening of the fibrils may not be a major factor in the strain of the material.

We can know, because of the evidence provided by the OI, that this Poisson's ratio we measure must be due largely to stretching of the fibrils and not to changes in crimp. A straightening of crimp must result in an increase in OI (as can be derived from the relationship represented by (1)), and there was no large increase in OI after the first 0.05 strain and therefore there must be no change in crimp above 0.05 strain.

Using data from a recently published atomic force microscope study on tendon,(*215*) we calculate v'=1.9 (tendon was stretched by 15%), similar to the value we find from our measurements.

CONCLUSION

While it has previously been shown that bulk materials based on collagen may have v>0.5, we have provided experimental evidence that the collagen fibrils also may have v' >0.5. Therefore, this property of collagen fibrils may contribute to the bulk properties of the tissue.

Previously, it has been proposed that much of the high Poisson's ratio of tendon and cartilage is due to the volume loss from fluid exudation (*216*) although specific attempts to measure this have not always shown water to be exuded (*205, 217*). We now demonstrate that there could be a contribution to the high Poisson's ratio of the tissue from the high Poisson's ratio of the collagen fibrils. This does not exclude the possibility that water is exuded from the fibrils.

Chapter 7: Collagen Fibril Structure and Strength in Acellular Dermal Matrix Materials of Bovine, Porcine and Human Origin

The work presented in Chapter 7 was supported by TEI Biosciences who provided samples and the motivation for the work. The work was initially presented as a client report to TEI Biosciences, and later turned into an academic journal article, published in the journal ACS Biomaterials Science and Engineering:

- **H. C. Wells**, K. H. Sizeland, N. Kirby, A. Hawley, S. Mudie, R. G. Haverkamp "Collagen Fibril Structure and Strength in Acellular Dermal Matrix Materials of Bovine, Porcine and Human Origin" **(2015)** *ACS Biomat. Sci. Eng.* 1 (10), 1026-1038.

ABSTRACT

Strength is an important characteristic of acellular dermal matrix (ADM) materials used for surgical scaffolds. Strength depends on the material's structure, which may vary with the source from which the product is produced, including species and animal age. Here, variations in the physical properties and structures of ADM materials from three species are investigated: bovine (fetal and neonatal), porcine and human materials. Thickness normalized, the bovine materials have a similar strength (tear strength of 75–124 N/m) to the human material (79 N/m), and these are both stronger than the porcine material (43 N/m). Thickness-normalized tensile strengths were similar among all species (18–34 N/mm^2 for bovine although higher in fetal material, 18 N/mm^2 for human and 21 N/mm^2 for porcine). Structure is investigated with synchrotron-based small angle X-ray scattering (SAXS) for collagen fibril orientation index (OI) and scanning electron microscopy (SEM). SEM reveals a more open structure in bovine ADM than in the porcine and human material. A correlation is found between OI and thickness-normalized tear strength in neonatal bovine material measured with the X-rays edge-on to the sample, but this relationship does not extend across species. The collagen fibril arrangement, viewed perpendicular to the surface, varies between species, with the human material having a unimodal distribution and rather isotropic (OI 0.08), the porcine being strongly bimodal and rather highly oriented (OI 0.61), the neonatal bovine between these two extremes with a bimodal distribution tending towards isotropic (OI 0.14–0.21) and the fetal bovine material being bimodal and less isotropic than neonatal (OI 0.24). The OI varies less through the thickness of the porcine and human materials than through the bovine materials. The similarities and differences in structure may inform the suitability of these materials for particular surgical applications.

INTRODUCTION

Scaffold materials are required when a tissue is being reinforced or replaced in a number of reconstructive surgical procedures. These materials must meet a range of requirements such as: be immunologically compatible with the body, be readily incorporated into living tissue, have sufficient strength to perform the task and have appropriate elastic properties. These scaffold materials may be synthesized from a variety of materials(*218*) or produced by decellurization of native materials. Extracellular matrix materials (ECM) derived from a wide variety of tissues have been successfully used a scaffolds(*219*). ECM materials derived from dermal tissues are commercially available and are produced from a variety of species including porcine, bovine and human dermal tissue. The physical properties of materials manufactured from different source materials differ, yet there is an incomplete understanding of these differences and the structural characteristics that lead to the differences in strength.

The mechanical properties of collagen tissue materials are due in part to the highly fibrillar nature of type I collagen(*101, 220*) and the tissue's ability to respond to imposed stresses(*221*). Factors that have been considered as contributing to the strength of collagenous tissue materials include the structure of the collagen (d-spacing, collagen type), the nature of the cross-linking between collagen, collagen fibril diameter and collagen orientation. The fibril arrangement can be described in terms of orientation direction and spread. Collagen orientation (quantified as orientation index, OI) has been investigated in the cornea(*222*), heart valve tissue(*223*), pericardium(*69, 108*), bladder tissue(*224*), skin(*225*), aorta(*226*), ovine forestomach derived scaffold materials(*227*) and leather made from animal skins(*113*). The arrangement of collagen fibrils in most tissues is anisotropic due to the non-uniform requirements for mechanical performance. It has been shown that leather's tear strength is correlated with collagen fibril orientation as measured by SAXS with the X-ray beam edge-on to the sample. Specifically, when the collagen fibrils are arranged in parallel or almost-parallel sheets (i.e. have a high OI), the leather is stronger(*25, 98*), although OI is also affected by the swelling of the material(*116*). This relationship was observed in a large sample of ovine and bovine skins, including bovine pericardium(*108*), and across seven species of mammals over a large range of strength (factor of five). The relationship between OI and strength has been explained as being due to the high strength of the collagen fibrils in their longitudinal axis when suitably arranged to resist the tearing process(*98*).

D-spacing in collagen varies with animal age(*228, 229*), animal species(*98*) and tissue type(*230*), and the tissue's chemical treatment including water and fat content(*229, 231-234*). However, there does not appear to be a relationship between d-spacing and the strength of leather(*25, 98*) or rat tail tendon(*235*).

Collagen fibril diameter may be correlated with strength in some materials. For example: in human aortic valves, regions of high stress may contain larger-diameter fibrils(*174*); in mouse tendon, fibril diameter increases with loading(*175*); and in bovine leather, higher strength material has larger fibril diameters(*99*). Fibril diameter may also increase with age(*177*).

Here, we investigate the structure of acellular dermal matrix (ADM) materials, how it differs between bovine, porcine and human materials, and how it changes with age in bovine materials. We attempt to develop an understanding of how ADM structure influences the physical properties of the materials.

EXPERIMENTAL

Source Material

Commercial ADM materials included Strattice Firm porcine ADM (LifeCell Corporation, US), Alloderm human ADM (LifeCell Corporation, US) and a range of SurgiMend bovine ADM (TEI Biosciences, US), including bovine third trimester fetal ADM and neonatal ADM (animals less than 5 months old) with thicknesses of approximately 1.7, 2.0, 3.0 and 4.0 mm. The Strattice and Alloderm materials were already hydrated whereas the SurgiMend materials required hydrating with distilled water prior to SAXS analysis or tensile testing.

Synchrotron SAXS

Diffraction patterns were recorded on the Australian Synchrotron SAXS/WAXS beamline, using a high-intensity undulator source. Energy resolution of 10^{-4} was obtained from a cryo-cooled Si(111) double-crystal monochromator and the beam size (FWHM focused at the sample) was 250 x 80 μm, with a total photon flux of about 2 x 10^{12} ph.s^{-1}. All diffraction patterns were recorded with an X-ray energy of 12 keV using a Pilatus 1M detector with an

active area of 170 x 170 mm and a sample-to-detector distance of 3371 mm. Exposure time for diffraction patterns was 1–5 s and initial data processing was carried out using Scatterbrain software(*102*).

SAXS analysis was carried out in two directions through the samples. The X-ray beam was either passed through the flat surface of the sample normal to the surface (here referred to as normal) or edge-on to the sample (here referred to as edge-on or cross sections) (Fig. 7.1). For the edge-on measurements, because it is known that structure varies through the thickness of a sample, structure was analyzed at intervals of typically 0.15 mm through the whole thickness of each sample.

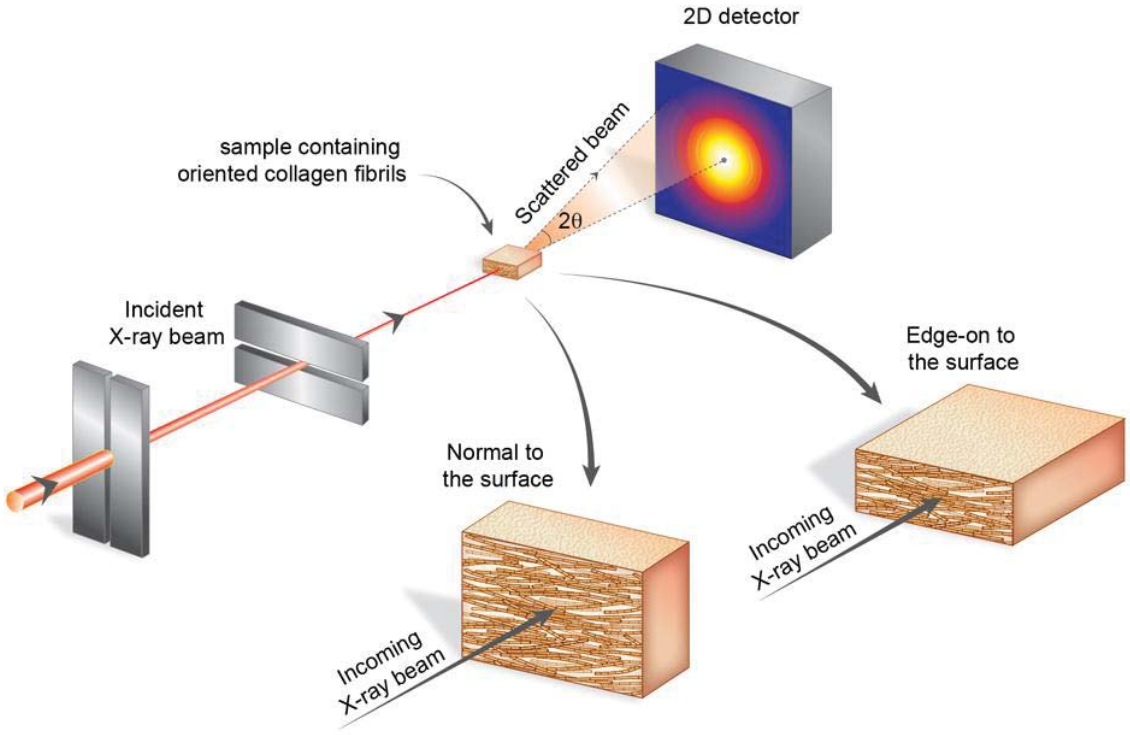

FIGURE 7.1: EXPERIMENTAL SETUP FOR SAXS ANALYSIS.

Fibril Diameter

Fibril diameters were calculated from the SAXS data using the Irena software package(*190*) running within Igor Pro. The data were fitted at the wave vector, Q, in the range of 0.01 – 0.04 $Å^{-1}$ and at an azimuthal angle which was 92.5° (over a 5° segment) to the long axis of

most of the collagen fibrils. This azimuthal angle of the long axis of the collagen fibrils was determined as the position for the maximum intensity with azimuthal angle of the d-spacing diffraction peaks. The “cylinderAR” shape model with an arbitrary aspect ratio of 30 was used for all fitting. We did not attempt to individually optimize this aspect ratio and the unbranched length of collagen fibrils may in practice exceed an aspect ratio of 30.

d-spacing

The d-spacing was determined from the position of the centre of a Gaussian curve fitted to the 5th order diffraction peak taken from the integrated intensity from the azimuthal range from 45º to 135º.

Orientation Index

The OI is a quantification of the spread of microfibril orientation, with 1 indicating parallel microfibrils and 0 indicating randomly oriented microfibrils. OI is defined as (90° – OA)/90°, where OA, the orientation angle, is the minimum azimuthal angle range that contains 50% of the microfibrils(*191*) converted to an index(*25*), using the spread in azimuthal angle of one or more D-spacing diffraction peaks. The peak area is measured, above a fitted baseline, at each azimuthal angle.

In many of the diffraction patterns, particularly those measured with the X-ray beam perpendicular to the surface, two peaks were observed in the plot of intensity verses azimuthal angle. In such patterns, an OA calculated using the minimum angle centered on one of these peaks is large and depends on the spacing between the two peaks, therefore not reflecting accurately the isotropy of the collagen fibrils. So, an alternative method to measure the OA was used: the intensities of 5º intervals of azimuthal angle were ranked and sufficient of these were summed to give 50% of the total intensity over a 180º range, where the total angle covered by the summed intervals becomes the OA. When there is only one peak in the intensity verses azimuthal angle plot, this method gives the same OA as when the OA is calculated by summing the area starting at the centre of the peak(*25*). Another way of describing this is that the OA for one peak is equivalent to 0.675 of the standard deviation of a Gaussian (if the peak were approximately Gaussian in shape). When there are two peaks, the standard method of finding a combined standard deviation from two Gaussians to obtain a single OI value would not give a good measure of anisotropy since it depends on the separation of the two Gaussians. A more useful way would be to combine the two

Gaussians after shifting them so that they are superimposed. This is effectively what the method used here achieves in a numerical way that is not reliant on Gaussian distributions.

Mechanical Testing

Tear strength(*103*) and tensile strength(*236*) were measured using standard methods on an Instron device. Two samples were tested for each of tear strength and tensile strength, with the samples taken orthogonally, and the values averaged.

Electron Microscopy

Samples of ADM materials were cut into small cube-shaped pieces and fixed for over 8 hr at room temperature in Modified Karnovsky's fixative containing 3% glutaraldehyde and 2% formaldehyde in 0.1 M phosphate buffer (pH 7.2). The samples were then washed three times for 10–15 minutes in phosphate buffer (0.1 M, pH 7.2) before being dehydrated in a graded series of ethanol washes (25%, 50%, 75%, 95%, 100%), each dehydration stage being 10–15 minutes long, followed by a final 100% ethanol wash for 1 hour. Samples were critical-point (CP) dried using the Polaron E3000 series II critical point drying apparatus with liquid CO_2 as the CP fluid and 100% ethanol as the intermediary fluid. They were then mounted on to aluminum stubs and sputter coated with gold using the Baltec SCD 050 sputter coater. The samples were viewed in the FEI Quanta 200 Environmental Scanning Electron Microscope at an accelerating voltage of 20kV.

RESULTS

Tear test

Tear tests were performed in two orthogonal directions for each sample, one test in each direction. The results of these tests have been averaged and are listed in Table 10. The nature of the tearing, once tearing starts, is similar for all the samples.

The neonatal bovine ADM materials are the strongest on an absolute scale, followed by the human, the fetal bovine and then the porcine material. On a thickness-normalized scale, the fetal bovine material is the strongest followed by the thicker neonatal bovine materials, with the thinner neonatal bovine having a lower strength in the same range as the human ADM. The lowest strength material on a thickness-normalized basis is the porcine ADM. This may

be a partial explanation for the higher intraoperative device failures observed for the porcine cohort in study of porcine and bovine matrix for abdominal wall reconstruction(*199*).

Table 10. Tear test results for ADM materials.

Sample	Thickness (mm)	Force at rupture (N)	σ (for force at rupture, N)	Thickness-normalized force at rupture (N/mm)
Bovine Fetal	0.98	76.1	9.0	78.0
Bovine Neonatal 1.7	1.67	127.0	0.6	76.0
Bovine Neonatal 2.0	2.01	172.0	11.7	85.6
Bovine Neonatal 3.0	3.02	227.0	22.8	75.1
Bovine Neonatal 4.0	3.98	494.3	0.4	124.2
Porcine	1.69	73.0	7.9	43.2
Human	1.01	79.5	5.9	79.0

Tensile test

Tensile tests were performed in two orthogonal directions for each sample, one test in each direction and the averages are listed in Table 11. In the bovine samples, strength increases with thickness, however, the fetal material was the strongest on a thickness-normalized basis. Although not presented here, a large number of measurements have been made by others on these materials which confirms that the bovine fetal material typically has a higher cross section-normalized tensile strength than bovine neonatal material(*237*).

Table 11. Tensile test results for ADM materials.

Sample	Thickness* (mm)	Average Force at rupture (N)	σ (for force at rupture, N)	Cross section normalized force at rupture (N/mm^2)
Bovine Fetal	0.97	381†		39.3†

Bovine Neonatal 1.7	1.76	415	111	23.8
Bovine Neonatal 2.0	2.01	451	147	22.4
Bovine Neonatal 3.0	3.04	561	6	18.5
Bovine Neonatal 4.0	4.06	>963‡		>23.7‡
Porcine	1.57	328	7	21.0
Human	1.11	201	120	17.7

*Some of the thicknesses vary a little from the values in Table 10 but represent the thickness as measured on the cut samples used in each of these tests. †Only one test, but see text. ‡Sample was not taken to failure.

Extensibility

Extensibility can be approximated as the strain at a force of 10 N/mm^2 on a sample cross section (which is similar to an inverse of elastic modulus over the complete extension range but not thickness normalized). The test results show that the 1.7, 2.0 and 3.0 mm bovine neonatal and human materials are the most extensible while the porcine and 4.0 mm neonatal bovine are the least extensible at this level of force (Table 12).

Table 12. Strain (approximate) of different sample types.

Sample	**Strain at 10 N/mm^2 stress**
Bovine Neonatal 1.7	0.48
Bovine Neonatal 2.0	0.54
Bovine Neonatal 3.0	0.47
Bovine Neonatal 4.0	0.30
Porcine	0.31
Human	0.45

Small angle X-ray scattering

The SAXS diffraction patterns (Fig. 7.2) can be analysed in different ways to get structural information on the collagen. The patterns provide information on the structure of the fibrils (d-spacing and fibril diameter) and on the arrangement of these fibrils (OI).

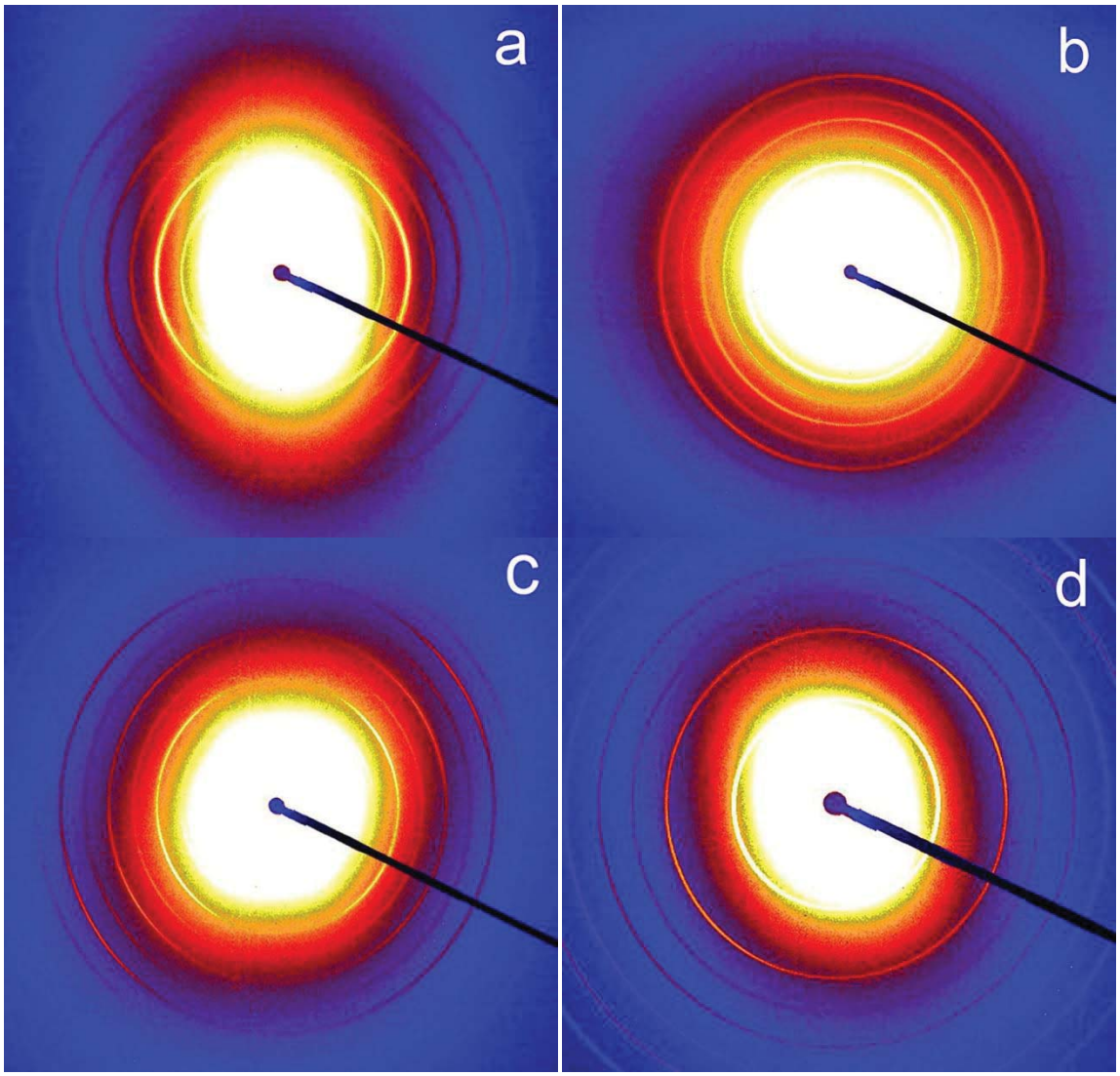

FIGURE 7.2: EXAMPLES OF SCATTERING PATTERNS TAKEN WITH THE X-RAY BEAM EDGE-ON TO THE SAMPLES: A) FETAL BOVINE; B) 3 MM THICK NEONATAL BOVINE; C) PORCINE; D) HUMAN ADM MATERIALS.

Collagen fibril orientation index (OI)

Collagen fibril orientation was measured with the X-ray beam edge-on to the ADM materials and perpendicular to the face of the ADM. The OI measured for each material is listed in Tables 13 and 14.

Table 13. Orientation index for collagen from SAXS measured with the X-ray beam edge-on.

Sample	OI (X-rays edge-on)	σ	Number of measurements
Bovine Fetal	0.43	0.08	24
Bovine Neonatal 1.7	0.27	0.06	22
Bovine Neonatal 2.0	0.32	0.13	22
Bovine Neonatal 3.0	0.31	0.11	25
Bovine Neonatal 4.0	0.45	0.15	29
Porcine	0.40	0.05	29
Human	0.23	0.08	24

A pairwise multiple comparison of the edge-on measurements (Dunn Method) gave significant differences ($P < 0.05$) between human and both the bovine and porcine ADM materials; between porcine with both human and bovine materials; and between fetal bovine and neonatal bovine. No significant difference in OI was seen when comparing neonatal bovine with either porcine or human.

Table 14. Orientation index for collagen from SAXS measured with the X-ray beam perpendicular to the surface.

Sample	OI (X-rays perpendicular)	σ	Number of measurements
Bovine Fetal	0.24	0.04	18
Bovine Neonatal 1.7	0.21	0.06	9
Bovine Neonatal 2.0	0.20	0.07	9
Bovine Neonatal 3.0	0.14	0.03	9
Bovine Neonatal 4.0	0.19	0.05	9
Porcine	0.61	0.05	9
Human	0.08	0.06	9

A pairwise multiple comparison of the flat-on measurements (Dunn Method) gave significant differences ($P < 0.05$) between human and the porcine ADM materials; porcine and both the bovine and human.

Detail of fibril orientation

The OI presented for each of the materials is calculated from plots of diffraction intensity for the 5th or 6th d-spacing diffraction peak (Figs 7.3, 7.4 & 7.5), however, the calculation reduces complex information to just one number. More detail of the collagen fibril orientation and the differences between different sample types can be obtained from plots of diffraction intensity (for any of the d-spacing diffraction peaks) with azimuthal angle. An analysis of the three-dimensional structure requires at least two diffraction patterns normal to each other. Plots are provided for diffraction intensity verses azimuthal angle with the X-rays edge-on (Figs 7.3 & 7.4) and perpendicular (Fig. 7.5) to the plane of the ADM material.

Fibril orientation (X-rays edge-on)

The distribution of orientation of the collagen fibrils in the dermal ECM materials is apparent from the diffraction intensity verses azimuthal angle plots. Single plots at just one point in a section of the ADM are shown in Figure 7.3. The way the diffraction intensity varies with

azimuthal angle gives an indication of how the collagen fibrils are arranged. Where there is only one peak (within a 180º range) and the curve approaches the baseline, there is only one preferred direction of orientation and the spread of fibril direction is around this angle. Examples of this are the edge-on measurements for fetal bovine ADM material (Fig. 7.3a) and to a lesser extent edge-on measurements for neonatal bovine ADM (Fig. 7.3b) and human ADM materials (Fig. 7.3d). Where there are two peaks in this plot, there are two preferred directions of orientation of the collagen fibrils, as seen in the porcine ADM with X-rays edge-on (Fig. 7.3c). When the curve remains considerably above the baseline, the collagen fibril distribution is tending towards isotropic.

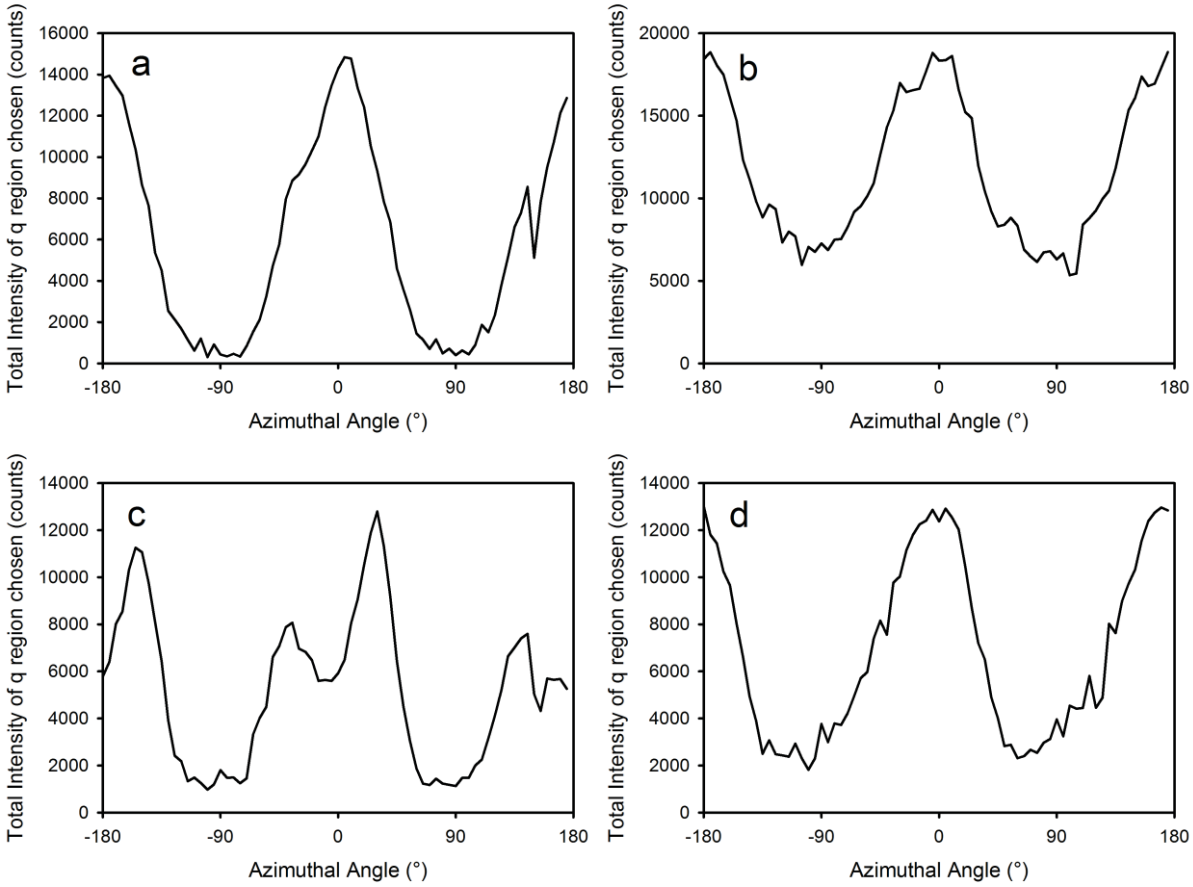

FIGURE 7.3: VARIATION IN INTENSITY OF THE 5TH DIFFRACTION PEAK WITH AZIMUTHAL ANGLE (MEASURED WITH THE X-RAY BEAM EDGE-ON TO THE SURFACE) TO ILLUSTRATE THE NATURE OF THE FIBRIL ORIENTATION: A) FETAL BOVINE ADM MATERIAL; B) 3 MM THICK NEONATAL BOVINE; C) PORCINE; D) HUMAN. THESE PLOTS CORRESPOND WITH THE DIFFRACTION PATTERNS IN FIG. 39.

Fibril orientation sections (X-rays edge-on)

The distribution of orientation of the collagen fibrils and the variation of fibril orientation through the thickness of the ECM materials can be shown with plots of diffraction peak intensity verses azimuthal angle at points at different positions on a cross section of the material representing different depths (Fig. 7.4). These are essentially compilations of plots such as in Fig. 7.3 but with just a -90° to 90° range for simplicity. There is some variation in the fibril arrangement with depth. The bovine, especially fetal, and human materials tend to be a little more highly oriented with increasing depth. The porcine is highly oriented throughout the thickness although the direction of orientation changes with depth.

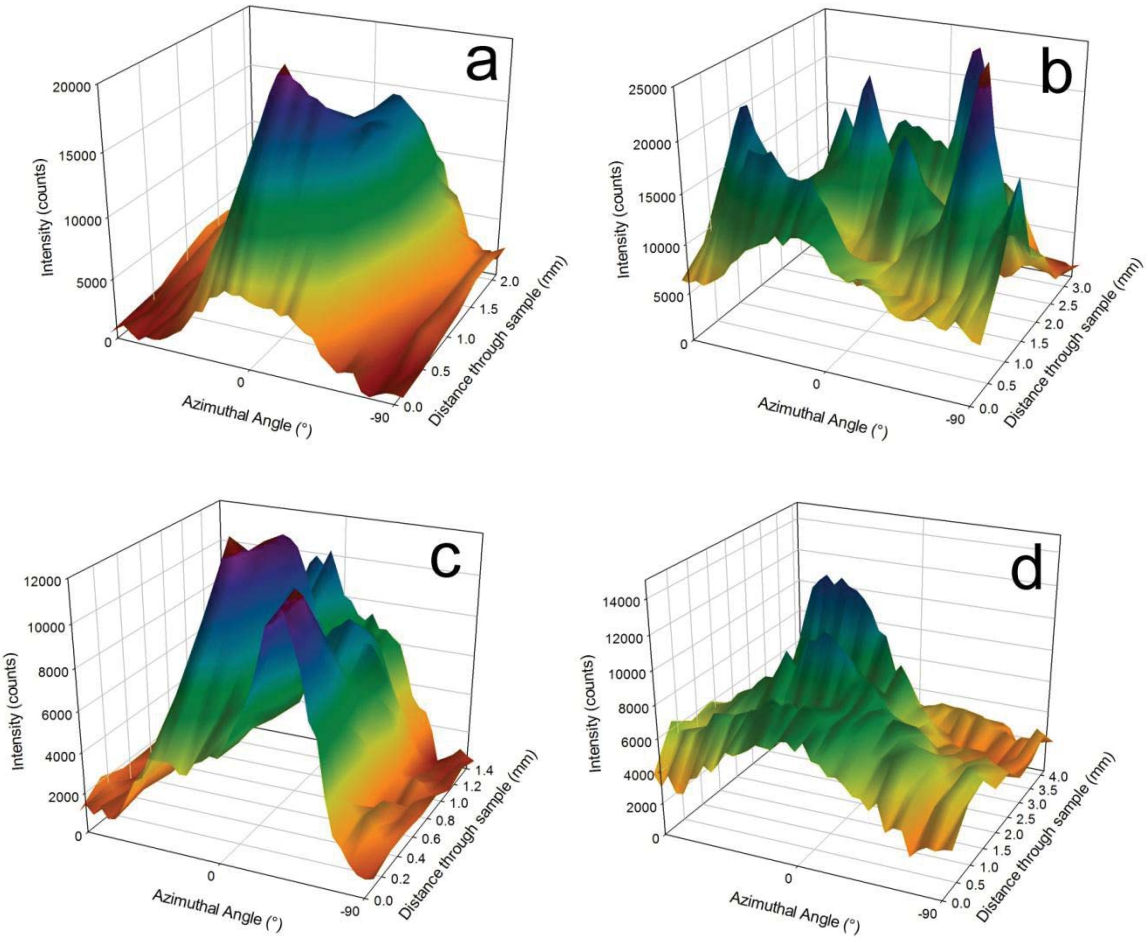

FIGURE 7.4: VARIATION IN INTENSITY OF THE 5TH DIFFRACTION PEAK WITH AZIMUTHAL ANGLE (MEASURED WITH THE X-RAY BEAM EDGE-ON TO THE SURFACE) AND DISTANCE THROUGH THE SAMPLE (EQUIVALENT TO A SERIES OF PLOTS OF THE TYPE IN FIG. 3) TO ILLUSTRATE THE NATURE OF THE FIBRIL ORIENTATION THROUGH THE SAMPLE THICKNESS: A) FETAL BOVINE ADM MATERIAL; B) 3 MM THICK NEONATAL BOVINE; C) PORCINE; D) HUMAN. THESE PLOTS ARE JUST FOR 90° EITHER SIDE OF THE ORIGIN TO SIMPLIFY THE IMAGES BECAUSE THE INFORMATION IS DUPLICATED IN THE REGION FOR 90 TO 180° AND -90 TO -180°.

Fibril orientation (X-rays normal)

Measurements with the X-ray beam perpendicular to the surface reveal differences in fibril orientation between sample types (Fig. 7.5). When the curve remains a long way above the baseline this indicates a tendency towards an isotropic distribution of the collagen fibrils, The fetal bovine ADM material has two well defined peaks of similar intensity (Fig. 7.5a), as does the neonatal bovine (Fig. 7.5b) although with greater spread and both remaining well above the baseline. The porcine material also has two peaks (Fig. 7.5c), but these are more separate than those of the bovine material (roughly 90º to each other), with one direction dominant, and the curve approaches close to the baseline, showing that the material is far from isotropic. The plots of the human ADM material (Fig. 7.5d) reveal that the fibrils barely exhibit a preferred orientation and are not bimodally distributed.

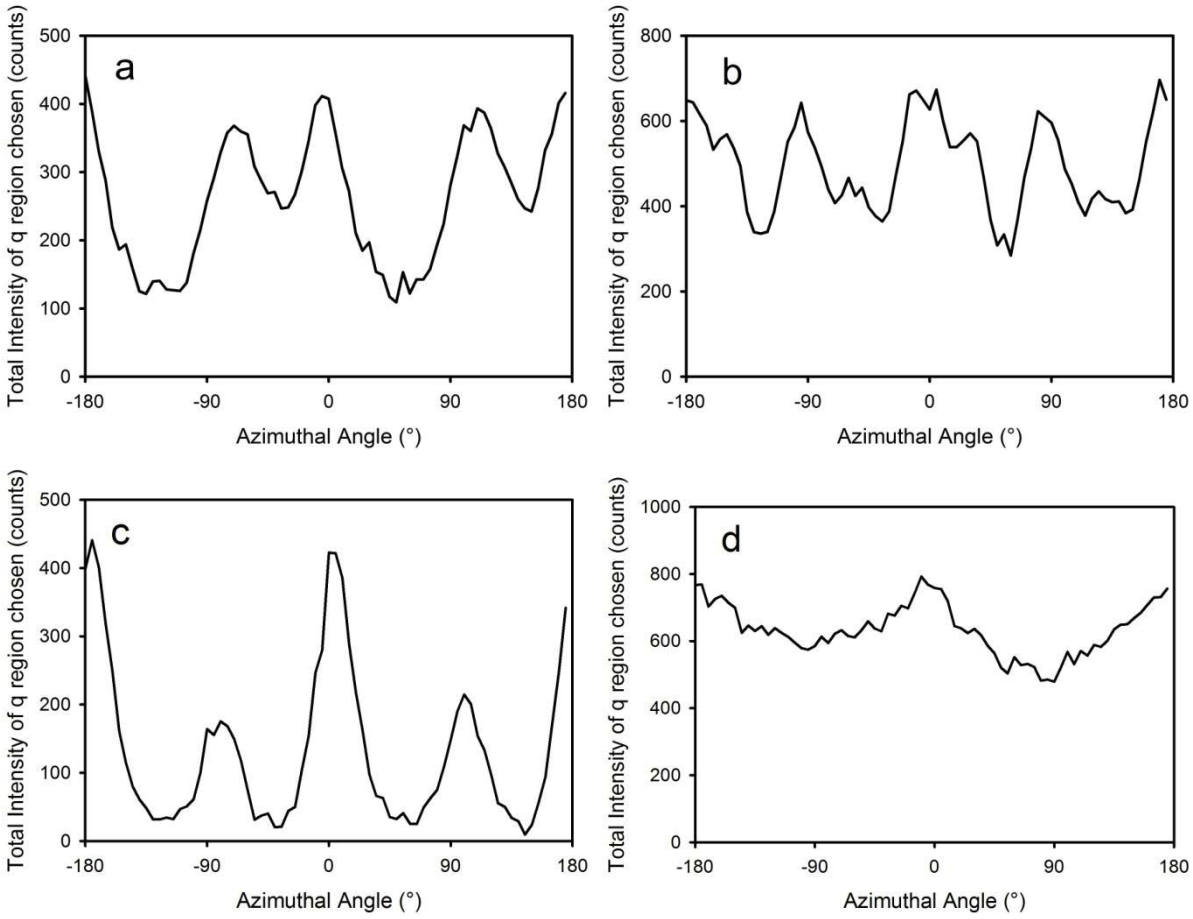

FIGURE 7.5: VARIATION IN INTENSITY OF THE 5TH DIFFRACTION PEAK WITH AZIMUTHAL ANGLE (MEASURED WITH THE X-RAY BEAM PERPENDICULAR TO THE SURFACE) TO ILLUSTRATE THE NATURE OF FIBRIL ORIENTATION: A) FETAL BOVINE ADM MATERIAL; B) 3 MM THICK NEONATAL BOVINE; C) PORCINE; D) HUMAN.

OI cross sections of ADM

The cross sections through the thickness of the ADM materials (Fig. 7.6) show a variation in OI through the thickness of the bovine materials which, unsurprisingly, is similar to that observed in bovine leather(*114*). The fetal bovine material (Fig. 7.6a) is similar to the neonatal material (Fig. 7.6b–e). In the porcine (Fig. 7.6f) and human (Fig. 7.6g) materials, OI varies less through the samples.

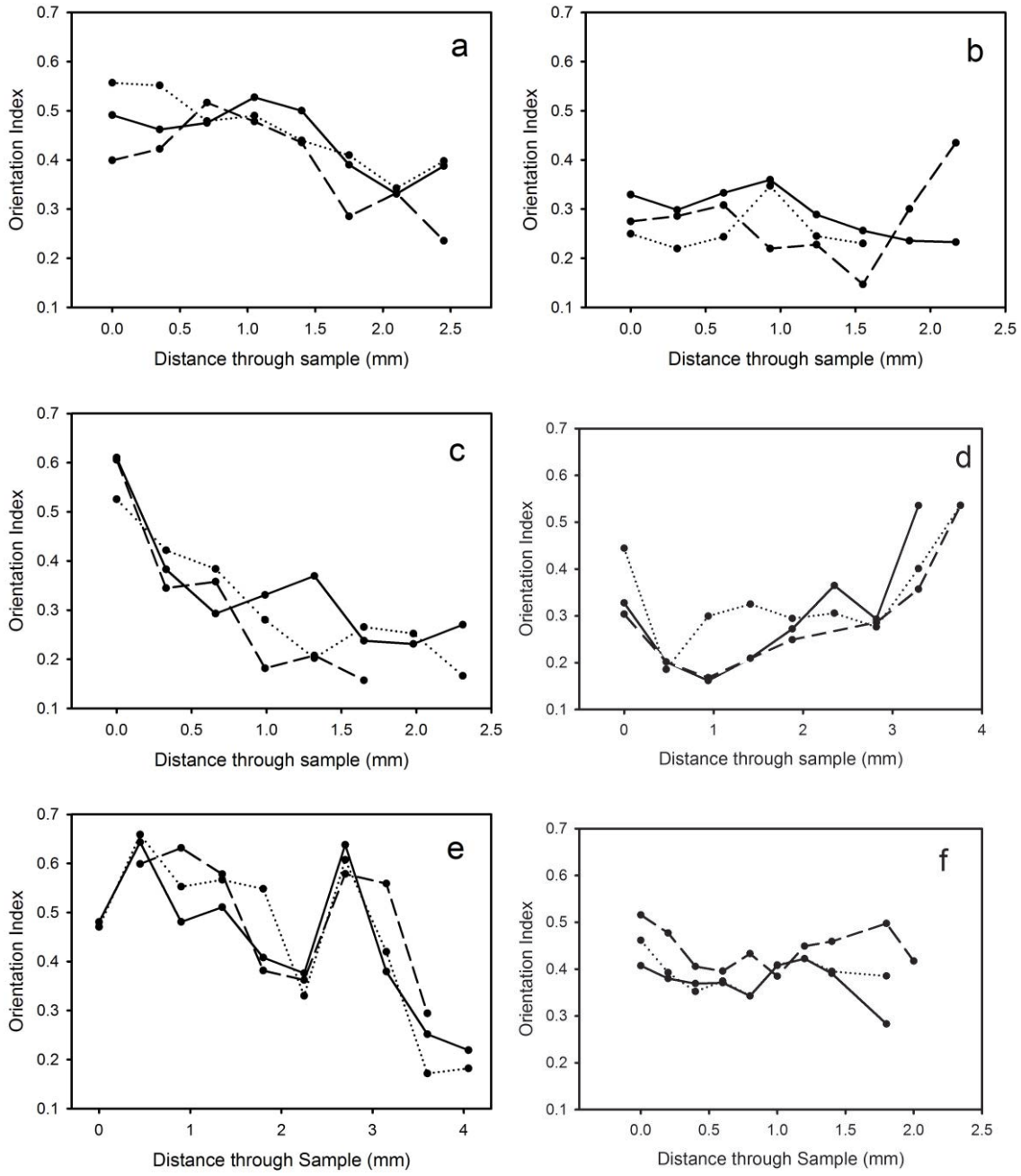

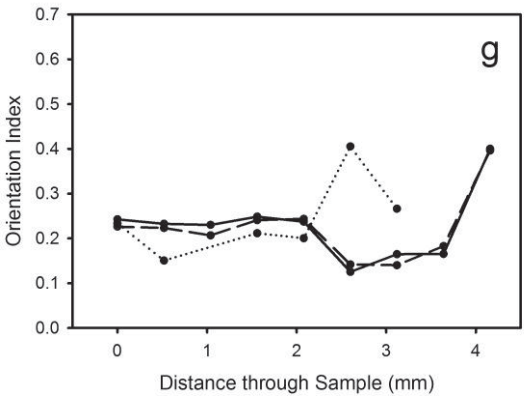

FIGURE 7.6: VARIATION IN OI THROUGH THE THICKNESS OF THE MATERIALS: A) FETAL BOVINE ADM MATERIAL; B) 1.7 MM THICK NEONATAL BOVINE; C) 2 MM THICK NEONATAL BOVINE; D) 3 MM THICK NEONATAL BOVINE; E) 4 MM THICK NEONATAL BOVINE; F) PORCINE; G) HUMAN.

Fibril diameter

Average collagen fibril diameters for each of the sample types calculated from X-ray edge-on measurements are listed in Table 15. A pairwise multiple comparison (Dunn Method) gave significant differences ($P < 0.05$) between porcine and both the human and bovine as well as between human and both the porcine and bovine (except neonatal 3.0). The fetal bovine is not statistically different from the neonatal bovine.

Fetal collagen (rat tail tendon) has been reported to have smaller fibril diameters than collagen from mature animals(*177*) but we do not observe a difference in collagen fibril diameter between fetal and neonatal bovine ADM materials.

Table 15. Average diameter of collagen fibrils from SAXS analysis.

Sample	Fibril diameter (nm)	Variance σ	Number of measurements
Bovine Fetal	58.6	1.3	28
Bovine Neonatal 1.7	58.3	1.7	26
Bovine Neonatal 2.0	60.8	1.9	26
Bovine Neonatal 3.0	57.1	2.5	29
Bovine Neonatal 4.0	56.0	8.2	32
Porcine	61.1	2.1	28
Human	55.2	2.7	30

d-spacing

Average d-spacing for the collagen fibrils for each of the sample types is listed in Table 16. A pairwise multiple comparison (Dunn Method) gave significant differences ($P < 0.05$) between human and both the bovine and porcine; porcine and the bovine (except 4.0 mm); porcine and human; but not between fetal bovine and the neonatal bovine.

Table 16. Average d-spacing for collagen from SAXS analysis (on hydrated materials).

Sample	d-spacing	Number of Measurements
Bovine Fetal	64.00	24
Bovine Neonatal 1.7	64.13	22
Bovine Neonatal 2.0	63.95	23
Bovine Neonatal 3.0	64.01	25
Bovine Neonatal 4.0	64.23	29
Porcine	64.20	28
Human	64.60	25

d-spacing cross sections of ADM

The d-spacing variation through the cross sections is similar for all samples except for the 4 mm neonatal bovine material (Fig. 7.7). The variation between sections is greater for the human, porcine and 4 mm neonatal bovine than for the thinner bovine samples.

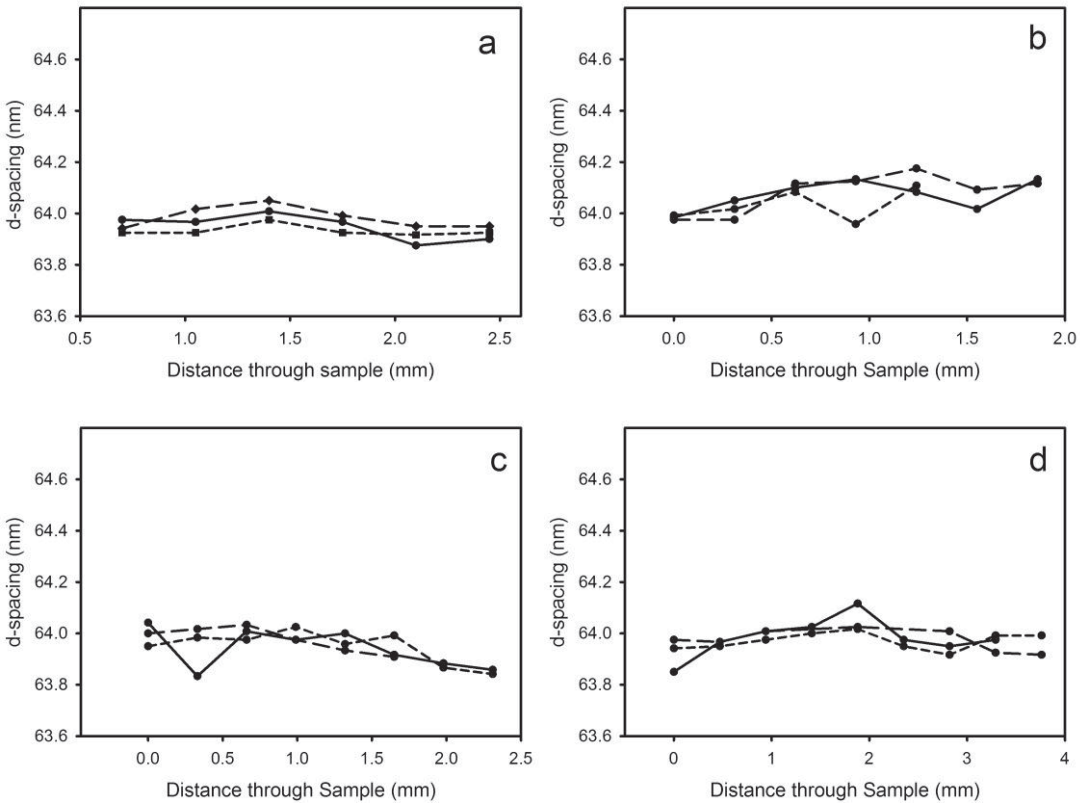

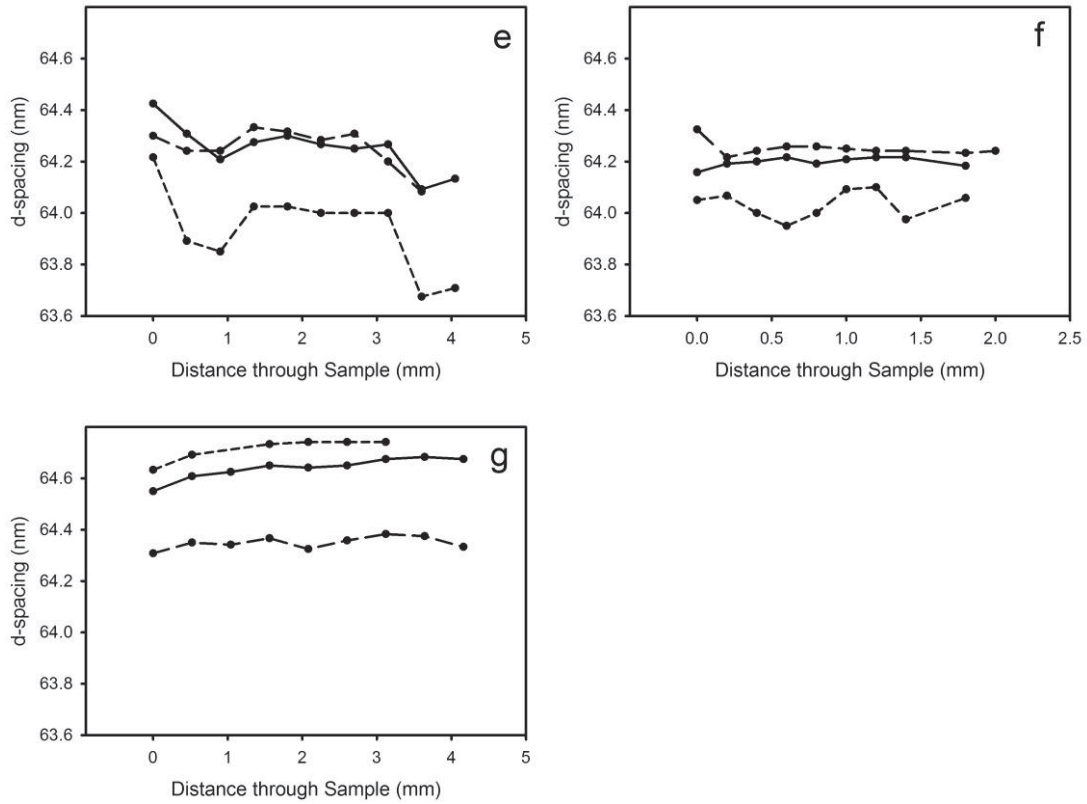

FIGURE 7.7: VARIATION IN D-SPACING THROUGH THE THICKNESS OF ADM MATERIALS: A) FETAL BOVINE; B) 1.7 MM THICK NEONATAL BOVINE; C) 2 MM THICK NEONATAL BOVINE; D) 3 MM THICK NEONATAL BOVINE; E) 4 MM THICK NEONATAL BOVINE; F) PORCINE; G) HUMAN.

Correlation of OI and strength

Based on measurements with the X-ray beam edge-on to the sample, a statistically significant correlation was found only between OI and tear strength (Fig. 7.8 left); tensile strength is not significantly correlated with OI (Fig. 7.8 right). These findings are consistent with observations for leather(*25*).

For the OI verses tear strength and OI verses tensile strength measured with the X-ray beam perpendicular to the samples there is no statistically significant correlation (Fig. 7.9).

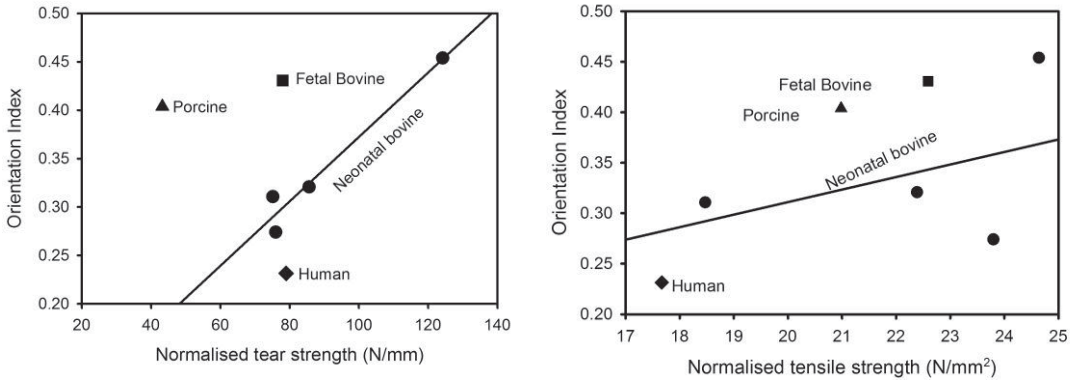

FIGURE 7.8: TEAR (LEFT) AND TENSILE (RIGHT) STRENGTH AND OI FOR ADM MATERIALS MEASURED WITH THE X-RAY BEAM EDGE-ON TO THE SAMPLES. LINE FOR LINEAR CORRELATION FOR JUST THE NEONATAL BOVINE ADM OF VARYING THICKNESS (TEAR R^2 = 0.97, P = 0.002 FOR A = 0.05; TENSILE R^2 = 0.44, P = 0.22 FOR A = 0.05).

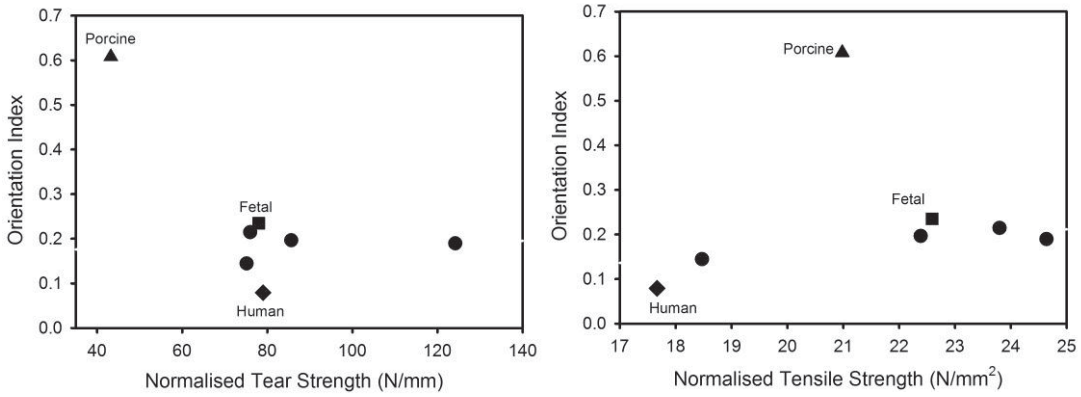

FIGURE 7.9: TEAR (LEFT) AND TENSILE (RIGHT) STRENGTH AND OI FOR ADM MATERIALS MEASURED WITH THE X-RAY BEAM PERPENDICULAR TO THE SAMPLES. UNMARKED POINTS ARE BOVINE NEONATAL ADM.

Fibril diameter and strength

Fibril diameter has been shown to correlated with tear strength in bovine leather(*99*). In collagen grown in tissue culture, larger fibril diameters are associated with higher strength(*178*). However, in the bovine neonatal material we analyzed here, there is no statistically significant correlation between fibril diameter and strength (Fig. 7.10). There is also no correlation in the material of the other species investigated (Fig. 7.10).

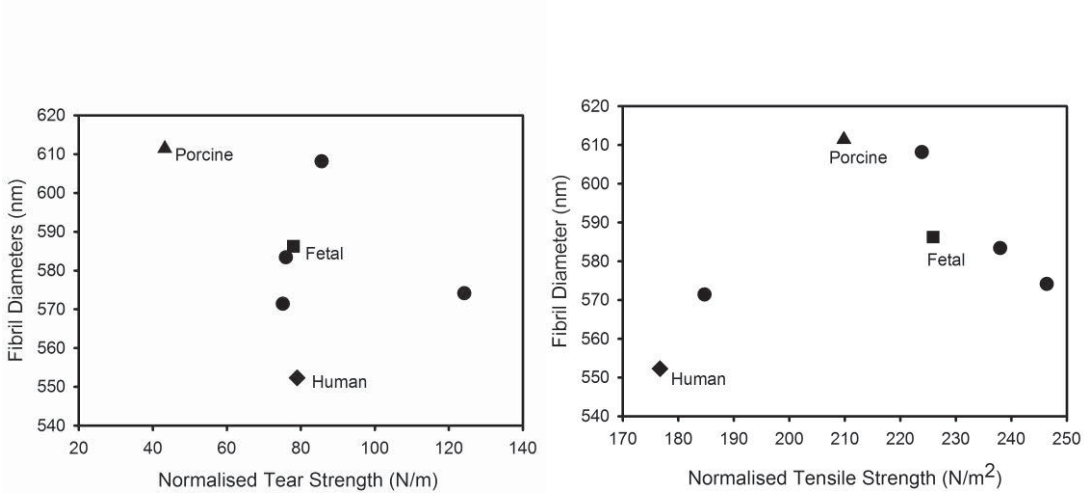

FIGURE 7.10: TEAR STRENGTH AND FIBRIL DIAMETER. UNMARKED POINTS ARE BOVINE NEONATAL ADM.

SEM images

The SEM images show structural differences between the bovine, porcine and human ADM (Figs 7.11 & 7.12). The bovine material has a more open structure than the porcine and human material, which have a much finer texture.

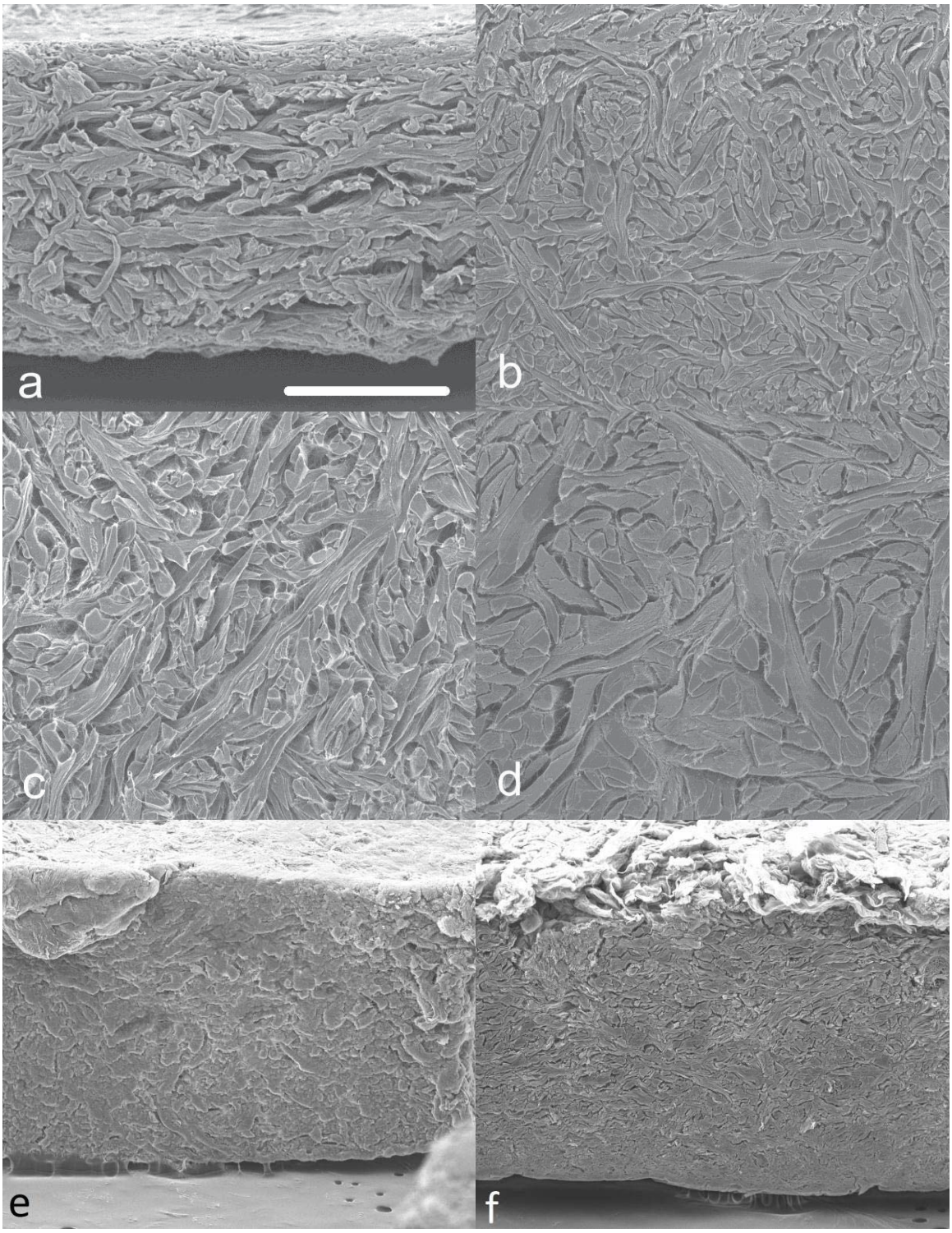

FIGURE 7.11: SCANNING ELECTRON MICROSCOPY IMAGES THROUGH THE THICKNESS OF THE ADM MATERIALS: A) FETAL BOVINE; B) NEONATAL BOVINE 2 MM THICK; C) NEONATAL BOVINE 3 MM THICK; D) NEONATAL BOVINE 4 MM THICK; E) PORCINE; F) HUMAN. ALL AT THE SAME MAGNIFICATION; BAR IS 500 MM.

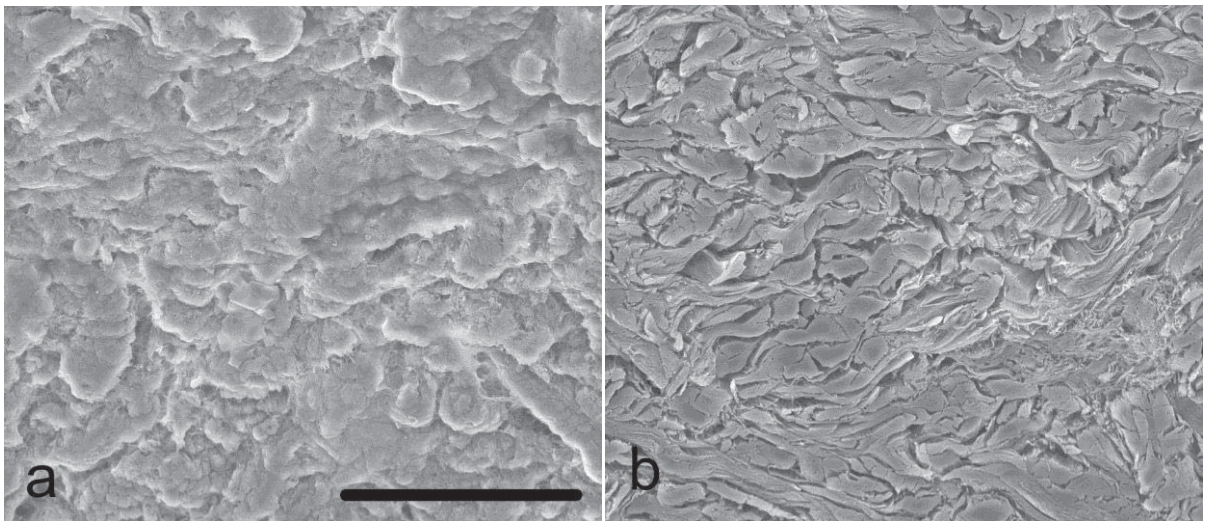

FIGURE 7.12: SCANNING ELECTRON MICROSCOPY IMAGES AT HIGHER MAGNIFICATION THROUGH THE THICKNESS OF THE ADM MATERIALS: A) PORCINE; B) HUMAN. BOTH AT THE SAME MAGNIFICATION; BAR IS 200 MM.

DISCUSSION

Strength from structure

Collagen structure, as determined by SAXS, is related to the tear strength of the materials. The tear strength differences among bovine pericardium materials are correlated with differences in the collagen fibril orientation index of those materials (Fig. 7.8a). In stronger samples, the fibrils are oriented in a planar manner parallel to the surface of the material (Fig. 7.13b); in weaker materials, fibrils are less oriented in the planar direction (Fig. 7.13a). Orientation direction, as measured with the X-ray beam perpendicular to the plane of the sheets of ADM (Fig. 7.14), does not however have a strong relationship to strength. This has also been seen in leather produced from bovine hides(*25*). However, in the ADM materials here, although this relationship was evident in the bovine materials, fibril orientation is not correlated with strength across species. Therefore, while tear strength might be predictable for given OI in bovine materials, this OI will not be associated with the same strength in porcine or human ADM materials. In contrast, studies on leather of seven mammals found a good correlation between OI measured edge-on and strength (although no correlation was found for alligator leather)(*25, 98*). However, we are not able to confirm whether such an OI–strength relationship holds within a selection of porcine or human ADM materials because we did not analyze a range of samples from the two relevant species.

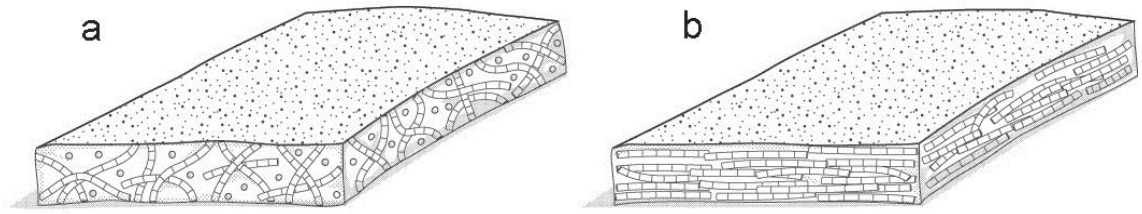

FIGURE 7.13: ILLUSTRATION OF THE DIFFERENCE BETWEEN ADM MATERIAL THAT IS: A) POORLY ORIENTED WHEN MEASURED WITH THE X-RAY BEAM EDGE-ON; B) HIGHLY ORIENTED WHEN MEASURED WITH THE X-RAY BEAM EDGE-ON.

Model for strength

The relationship between fibril direction and strength has been modeled previously and it can be shown that the strength is due to the sum of the vector components of the fibrils that lie in the direction of force (*98, 108, 172*). A model orientation index is derived which we will call OI′ to distinguish it from the experimentally measured OI (Eqn. 1).

$$\mathrm{OI}' = \frac{\int_0^{2\pi}\int_0^{\pi/2} \cos^4\theta\, F(\theta,\phi)\, d\theta\, d\phi}{\int_0^{2\pi}\int_0^{\pi/2} F(\theta,\phi)\, d\theta\, d\phi} \qquad (1)$$

Where $F(\theta,\phi)$ is the angular distribution function where θ and ϕ are fibril angles orthogonal to each other. We have previously applied this model to collagen orientation in leather produced from the skins of a selection of mammals where it was found to be valid across a wide range of strength(*98*) and also in collagen in bovine pericardium(*108*). Other factors which prevent notch growth during tearing are also important(*221*).

Distribution of fibril orientation with X-rays normal

The collagen fibril distribution, as measured with the X-rays normal to the surface, perhaps may influence the properties of the materials in service. Although there is no correlation between tear strength and fibril orientation measured with X-rays normal to the surface (Fig. 8b), as also seen with leather(*25*), elastic properties may vary with fibril direction when the ADM is not isotropic in this dimension. The materials from the different species have different distributions for fibril orientation. A material with an isotropic distribution might be expected to

have uniform mechanical properties in all directions (e.g. human and bovine ADM material) whereas one that has a strong unimodal distribution might be expected to behave quite differently in the direction of the orientation compared with a direction at right angles to the orientation. With a bimodal distribution (e.g. as in porcine or fetal bovine ADM materials), the properties would be expected to be more complex but differ in different directions. Other researchers have found that the elastic properties of fetal bovine material are significantly different parallel to the spine (stronger) compared to those perpendicular to the spine (weaker but more elastic)(*237*). These differences in mechanical properties with direction, if identified for each piece of the material, perhaps could be used to advantage in the selection of materials in specific surgical cases. A detailed study of directional mechanical properties was not part of this study.

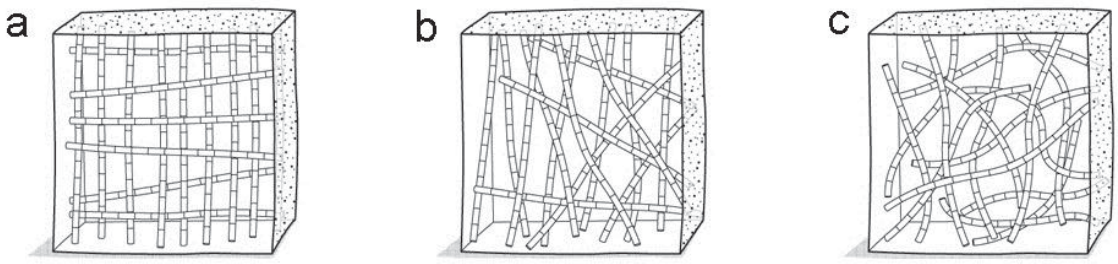

FIGURE 7.14: ILLUSTRATION OF THE DIFFERENCE BETWEEN ADM MATERIAL THAT IS: A) HIGHLY ORIENTED IN TWO ORTHOGONAL DIRECTIONS WHEN MEASURED WITH THE X-RAY BEAM PERPENDICULAR TO THE SAMPLE FACE, SUCH AS IN PORCINE MATERIAL; B) PARTLY ORIENTED WHEN MEASURED WITH THE X-RAY BEAM PERPENDICULAR TO THE SAMPLE FACE, SUCH AS IN BOVINE MATERIAL; C) LARGELY ISOTROPIC WHEN MEASURED WITH THE X-RAY BEAM PERPENDICULAR TO THE SAMPLE FACE, SUCH AS IN HUMAN MATERIAL.

d-spacing and fibril diameter

While there are differences between species for both d-spacing and fibril diameter, these differences do not appear to be correlated with strength or elasticity. It is known that d-spacing decreases with dehydration[19, 21-24] however for these measurements the samples were fully hydrated to reflect the state they would be used in surgical application.

Tight or open structure

The SEM cross sections show that there are differences in the structure of the different materials. The bovine materials have the most open structure, with porosity between the

fibers, whereas the human and porcine materials are tighter and more compact. At higher magnification, the human ADM looks slightly similar to the bovine material but with a finer texture with some minor porosity between the fibers visible. It may be that a more open structure helps with the integration of the ADM material in vivo(*238*), but further, detailed investigation is required.

Variation through material thickness

Both the OI (Figs 7.4 & 7.6) and d-spacing (Fig. 7.7) vary through the thickness of the ADM materials. In the porcine and human ADM material, OI varies less with thickness than do the bovine materials. For other bovine dermal materials, this variation has been well documented(*114*); however, the same information is not available for porcine and human ADM. The human material investigated here may, in fact, not reflect a full-thickness dermal material; if so, any measured variation with thickness would be less than for full-thickness material. The d-spacing variation through each cross section is similar for all samples.

Strength

The tear test provides a measure of the toughness of the ADM material and the results are a useful indicator of the in-service stresses and where failure by tearing or bursting is most likely to occur. The neonatal bovine ADM materials are the strongest of the material types in the tear test on an absolute scale, followed by the human, the fetal bovine and then the porcine material. The thickness of a surgical scaffold material is also important, partially for aesthetic reasons, and a thin but strong material may be desirable. Therefore, thickness-normalized strength is also a useful measure of the relative merits of different materials. On a thickness-normalized scale, the fetal bovine material is the strongest and its fibers are the most oriented, which perhaps is a general feature of fetal materials (and note that younger bovine pericardium was found to be stronger than older(*108*)). The thicker neonatal bovine materials have the next greatest strength, with the thinner neonatal bovine having a lower strength. The strength of these bovine materials is correlated with the OI measured edge-on (Fig. 8) as it does in bovine and other leathers(*19*). In the same strength range as the thinner bovine is the human ADM material, and the lowest strength material on a thickness-normalized basis is the porcine ADM. The strength of the human and porcine ADM material is consistent with the correlation of OI and strength in the bovine materials, so other factors are clearly also important for strength.

These materials derived from different species have largely similar properties and similar structures. There are some differences in strength and in thickness-normalized strength that may provide a preference for one of these materials over others in certain surgical applications. There are also differences in the porosity of the materials, which could be further investigated, quantified and related to differences in the integration of the scaffold materials in vivo.

CONCLUSIONS

The study of strength and structure of a range of ADM materials has revealed insights into the differences between the materials and the relationship between the structure and some of the physical properties. Bovine ADM material is similar in strength to or a little stronger than human ADM and is significantly stronger than porcine ADM. There is a wide variation in strength in bovine ADM materials and that variation is due to differences in collagen fibril orientation, with stronger materials having a more layered fibril structure. The human ADM material and the thinner (1.7, 2.0 and 3.0 mm) neonatal bovine materials are the most extensible (extensibility to 10 N/mm^2) while the porcine, fetal bovine and 4.0 mm neonatal bovine are the least extensible at this force. Bovine ADM materials have a more open structure than human or porcine ADM and we speculate (however without evidence) that this open structure might help with the integration of the ADM in vivo. The "weft/weave" structures of bovine, porcine and human ADM differ. The human material is the most isotropic, followed by bovine, while the porcine is the most anisotropic; these variations may affect the properties of the material in service, although this has not been studied in depth here. It has been shown that there are many similarities in the structures in the different materials but also some subtle differences which affect physical properties and it may be that the differences in porosity are also important and are worth also investigating.

Overall Conclusions

This research aimed to reveal the properties and behaviour of the collagen matrix that is the structural foundation of a range of biomaterials. These biomaterials include heart pericardium and dermal tissues, as well as the materials produced from dermal tissues including leather and acellular dermal matrix (ADM) materials.

It has been revealed that looseness, a collagen structure defect that occurs in leather, occurs as a result of poor connections existing between the layers of collagen fibrils in the grain-corium boundary region in leather. A range of analytical techniques were used to study and compare the collagen structure in loose and tight (control) leather including small angle X-ray scattering (SAXS), electron microscopy and ultrasonic imaging. SAXS revealed that these poor connections result when collagen fibrils are too highly aligned. The ultrasonic imaging was able to identify differences in structure between loose and tight leather, with a region of low intensity being visible below the grain boundary in loose leather, due to the existence of gaps in the collagen structure.

Following on from this, it was discovered that it is possible to use ultrasonic imaging to detect the presence of looseness not only in leather, but also earlier in processing, in partially processed hides. In pickle and wet-blue hides, looseness can be seen as a low density region below the grain surface, much like that seen in leather. Using ultrasonic imaging as a method to detect looseness earlier in the production of leather would allow tanners to select out and divert defective hides to an alternative processing line earlier in processing, saving a significant amount in processing costs.

SAXS was used to investigate the collagen fibril structure in loose and tight hides more closely from the pickled hide stage of processing through to leather. It was revealed that loose leather undergoes a greater change in fibril orientation, when looking perpendicular to the leather surface, during processing from pickled hide through to wet-blue which is linked with an excessive amount of material swelling. When a material swells too much, there is a large change in fibril orientation in the material and the collagen fibrils become less aligned. The excessive swelling and change in fibril arrangement causes the connections between fibril layers to weaken, forming gaps in the collagen structure. When the hide shrinks back down during processing to leather, these gaps and weak connections remain and result in looseness. This discovery of collagen fibril behaviour during the processing stages from pickled hide through to leather has led to a greater understanding of the structural motif of looseness and its causes. This is a significant step towards determining what processing

changes can be made to minimise looseness in leather, and improve the quality of leather produced being in tanneries here in New Zealand and around the world.

Another issue investigated relating to leather production and looseness was the methods of disposing of chrome tanned leather, and ways to minimize chromium leaching into the environment. Leather that is too badly affected by defects such as looseness is often unusable, and is sent straight to waste. This leather, as well as leather in old and used products, should be disposed of in a manner that has little or no environmental impact. Most of our defective and used leather is currently disposed of into landfill, however this is causing an environmental concern due to the chromium from the leather leaching out as the leather biodegrades. It has been determined that heating leather to temperatures above 600°C in the absence of oxygen forms a biochar where the chromium is contained in a stable and highly dispersed carbide-like structure. The stability of this structure makes chromium significantly less available to form the toxic hexavalent form. Therefore instead of being an environmental risk in our landfills, chrome tanned leather, when transformed into a biochar, presents a soil product that is a safe and stable and can be used for soil remediation and carbon sequestration.

In addition to the work focused on leather, a range of collagen based materials have been studied to uncover correlations between collagen fibril structure in a material, and bulk strength. The characteristics of the individual fibrils themselves were studied including fibril diameter, fibril d-spacing and fibril orientation, and were related to properties such as the overall tear and tensile strengths in a range of biomaterials. For these studies, the primary analytical technique used was synchrotron based small angle X-ray scattering (SAXS). Electron microscopy was also used to analyse collagen structure.

The relationship between collagen fibril diameter and strength was studied in leather from a range of species, including bovine and ovine. It was already well known that fibril orientation can affected the strength of a material; however the effect of fibril diameter on material strength had not yet been studied. There was a small correlation between fibril diameter and strength in bovine leather, where thicker fibrils resulted in stronger leather. However this correlation did not appear true for the other species. Therefore it can be said that collagen fibril diameter has a much lesser effect on strength than the orientation of fibrils within a material.

Following on from the analysis on collagen fibril diameter and material strength, we extended our research to look at changes in fibril diameter, fibril extension and fibril orientation when applying strain to a collagen material. In this study, bovine heart pericardium was used as the collagen material. To compare the behaviour of collagen to the likes of other engineering

materials the Poisson Ratio of the fibrils was calculated and found to be 2.1 ± 0.7; a surprisingly high value. This suggests that collagen fibrils decrease in volume when subjected to strain. In addition to this, it was found that there are two distinct stages of collagen behaviour during increased strain. Initially, when strain is first applied, the stress is taking up by the re-orientation of the fibrils within the material and there is very little change in fibril extension or diameter. When higher strain is applied and the fibrils have straightened somewhat, the stress begins to transfer to the fibrils themselves, causing them to elongate and the diameter to decrease. These features of the collagen fibril could help explain the behaviour of bulk collagen materials, and could be useful to understand and utilise in various industrial applications.

After already looking at the collagen materials leather and pericardium, research on collagen structure and strength was extended to include acellular dermal matrix (ADM) materials of bovine, porcine and human origin. Structural differences between the three types of ADM materials were revealed, and it was found that each slightly differs in physical properties. Bovine ADM was the strongest material, followed closely by human ADM, with porcine being significantly weaker than the other two. The variation in strength appears to be influenced by the orientation and arrangement of collagen fibrils in the materials, with a more layered fibril structure resulting in a stronger bulk material. Human ADM was highly isotropic in fibril arrangement and the porcine ADM was largely anisotropic, with the bovine ADM being somewhere in the middle of the two. Variations in porosity were seen between the different types of ADM, with bovine being more porous. The similarities and variations uncovered in this study could help medical professionals select the most suitable ADM material for particular surgical applications, leading to more successful surgeries taking place.

References

1. Li, Y. F.; Gao, Y. M.; Xiao, B.; Min, T.; Yang, Y.; Ma, S. Q.; Yi, D. W., The electronic, mechanical properties and theoretical hardness of chromium carbides by first-principles calculations. *Journal of Alloys and Compounds* **2011,** *509*, 5242-5249.
2. Singh, V.; Palshin, V.; Tittsworth, R. C.; Meletis, E. I., Local structure of composite Cr-containing diamond-like carbon thin films. *Carbon* **2006,** *44*, 1280-1286.
3. Lodish, H. B., A; Zipursky, S.L; et al., Section 22.3 Collagen: The Fibrous Proteins of the Matrix. In *Molecular Cell Biology. 4th Edition*, 4th Edition ed.; W. H. Freeman: New York, 2000.
4. Rome *World Statistical compendium for raw hides and skins, leather and leather footwear 1990-2011*; Commodities and Trade Division FAO: United Nations, 2012.
5. UNIDO *Future Trends in the World Leather and Leather Products Industry and Trade*; UNIDO: Vienna, 2010; p 120
6. Thiele, C., Tasman Tanneries, Personal communication. In Wanganui, New Zealand, 2014.
7. Fratzl, P., *Collagen: Structure and mechanics*. SpringerScience+Business Media: New York, 2008; Vol. Collagen: Structure and mechanics.
8. Baer, E.; Cassidy, J. J.; Hiltner, A., Hierarchical structure of collagen composite systems: lessons from biology. *Pure & Applied Chemistry* **1991,** *63*, 961-973.
9. Brodsky, B.; Ramshaw, J. A. M., The Collagen Triple-Helix Structure. *Matrix Biology* **1997,** *15*, 545-554.
10. Diamant, J.; Keller, A.; Baer, E.; Litt, M.; Arridge, R. G. C., Collagen; ultrastructure and its relation to mechanical properties as a function of ageing. *Proc. R. Soc. Lond. B* **1972,** *180*, 293-315.
11. Williams, B. R.; Gelman, R. A.; Poppke, D. C.; Piez, K. A., Collagen Fibril Formation. *The Journal of Biological Chemistry* **1978,** *253*, 6578-6585.
12. Gautieri, A.; Vesentini, S.; Redaelli, A.; Buehler, M. J., Hierarchical Structure and Nanomechanics of Collagen Microfibrils from the Atomistic Scale Up. *Nano Lett.* **2011,** *11*, 757-766.
13. Shoulders, M. D.; Raines, R. T., Collagen Structure and Stability. In *Annual Review of Biochemistry*, 2009; Vol. 78, pp 929-958.
14. Svensson, Rene B.; Mulder, H.; Kovanen, V.; Magnusson, S P., Fracture Mechanics of Collagen Fibrils: Influence of Natural Cross-Links. *Biophysical Journal* **2013,** *104*, 2476-2484.
15. Scott, J. E., Elasticity in extracellular matrix 'shape modules' of tendon, cartilage, etc. A sliding proteoglycan-filament model. *Journal of Physiology-London* **2003,** *553*, 335-343.
16. Liao, J.; Vesely, I., Skewness angle of interfibrillar proteoglycans increases with applied load on mitral valve chordae tendineae. *J. Biomech.* **2007,** *40*, 390-398.
17. Puxkandl, R.; Zizak, I.; Paris, O.; Keckes, J.; Tesch, W.; Bernstorff, S.; Purslow, P.; Fratzl, P., Viscoelastic properties of collagen: synchrotron radiation investigations and structural model. *Phil. Trans. Roy. Soc.* **2002,** *357*, 191-197.
18. Cranford, S. W.; Buehler, M. J., Critical cross-linking to mechanically couple polyelectrolytes and flexible molecules. *Soft Matter* **2013,** *9*, 1076-1090.
19. Sizeland, K. H.; Basil-Jones, M. M.; Edmonds, R. L.; Cooper, S. M.; Kirby, N.; Hawley, A.; Haverkamp, R. G., Collagen Orientation and Leather Strength for Selected Mammals. *Journal of Agricultural and Food Chemistry* **2013,** *61*, 887-892.
20. Cheung, D. T.; Nimni, M. E., Mechanism of Crosslinking of Proteins by Glutaraldehyde 2. Reaction with Monomeric and Polymeric Collagen. *Connect. Tiss. Res.* **1982,** *10*, 201-216.
21. Cheung, D. T.; Perelman, N.; Ko, E. C.; Nimni, M. E., Mechanism of crosslinking of proteins by glutaraldehyde. 3. Reaction with collagen in tissues. *Connect. Tiss. Res.* **1985,** *13*, 109-115.
22. Kayed, H. R.; Sizeland, K. H.; Kirby, N.; Hawley, A.; Mudie, S. T.; Haverkamp, R. G., Collagen Cross Linking and Fibril Alignment in Pericardium. *RSC Adv.* **2015,** *5*, 3611-3618
23. Buehler, M. J., Nature designs tough collagen: Explaining the nanostructure of collagen fibrils. *Proceedings of the National Academy of Sciences* **2006,** *103*, 12285-12290.
24. Menon, G. K., New insights into skin structure: scratching the surface. *Advanced Drug Delivery Reviews* **2002,** *54*, s3-s17.
25. Basil-Jones, M. M.; Edmonds, R. L.; Cooper, S. M.; Haverkamp, R. G., Collagen fibril orientation in ovine and bovine leather affects strength: A small angle X-ray scattering (SAXS) study. *J. Agric. Food Chem.* **2011,** *59*, 9972-9979.
26. Kelly, K., Imputrescible Corium: The Production and Structure of pre-1900 Bookbinding Leather. *Technology and Structure of Records Materials* **2004**, 2-13.
27. Daniels, R., Back to Basics: Raw material and Preservation. *World Leather* **2002**, 52-77.

28. Pistori, H.; Paraguassu, W. A.; Martins, P. S.; Conti, M. P.; Pereira, M. A.; Jacinto, M. A., Defect Detection in Raw Hide and Wet Blue Leather. *CNPQ* **2006**, 1-6.
29. Mann, B. R.; McMillan, M. M.; Ltd, B. C., The Chemistry of the Leather Industry. *V-Animal products-C-Leather* **DNK**, 1-17.
30. Covington, A. D., Modern tanning chemistry. *Chem.Soc. Rev.* **1997,** *26*, 111-126.
31. Jupp, P. The Tanning Process.
32. Roma The leather production process.
33. Liu, C. L., N.P.; Lee, J.; Cooke, P.H., Microscopic Observations of Leather Looseness and its Effects on Mechanical Properties. *JALCA* **2009,** *104*, 230-236.
34. Looseness in Leather. (30/04),
35. Kasturi, V.; Mukhopadhyay, S. C., Planar Interdigital Sensors Based Looseness Estimation of Leather. *Sensing Technology* **2008,** *1*, 462-466.
36. Gamboa-Bobadilla, G. M., Implant Breast Reconstruction Using Acellular Dermal Matrix. *Annals of Plastic Surgery* **2006,** *56*, 22-25.
37. Patton Jr, J. H.; Berry, S.; Kralovich, K. A., Use of human acellular dermal matrix in complex and contaminated abdominal wall reconstructions. *The American Journal of Surgery* **2007,** *193*, 360-363.
38. Jin, J.; Rosen, M. J.; Blatnik, J.; McGee, M. F.; Williams, C. P.; Marks, J.; Ponsky, J., Use of Acellular Dermal Matrix for Complicated Ventral Hernia Repair: Does Technique Affect Outcomes? *Journal of the American College of Surgeons* **2007,** *205*, 654-660.
39. Wainwright, D. J., Use of an acellular allograft dermal matrix (AlloDerm) in the management of full-thickness burns. *Burns* **1995,** *21*, 243-248.
40. Thomas W. Gilbert, T. L. S., Stephen F. Badylak, Decellularization of tissues and organs. *J. Biomaterials* **2006,** *27*, 3675-3683.
41. Peter M. Crapo, T. W. G., Stephen F. Badylak, An overview of tissue and whole organ decellularization process. *J. Biomaterials* **2011,** *32*, 3233-3243.
42. Hoganson, D. M.; O'Doherty, E. M.; Owens, G. E.; Harilal, D. O.; Goldman, S. M.; Bowley, C. M.; Neville, C. M.; Kronengold, R. T.; Vacanti, J. P., The retention of extracellular matrix proteins and angiogenic and mitogenic cytokines in a decellularized porcine dermis. *Biomaterials* **2010,** *31*, 6730-6737.
43. Bin Yang, Y. Z., Liuhua Zhou, Zeyu Sun, Junhua Zheng, Yun Chen, and Yutian Dai, Development of a Porcine Bladder Acellular Matrix with Well-Preserved Extracellular Bioactive Factors for Tissue Engineering. *Tissue Engineering Part C: Methods.* **2010,** *16*, 1201-1211.
44. Brown, B. N.; Freund, J. M.; Han, L.; Rubin, J. P.; Reing, J. E.; Jeffries, E. M.; Wolf, M. T.; Tottey, S.; Barnes, C. A.; Ratner, B. D.; Badylak, S. F., Comparison of three methods for the derivation of a biologic scaffold composed of adipose tissue extracellular matrix. *Tissue engineering. Part C, Methods* **2011,** *17*, 411-21.
45. Prasertsung, I.; Kanokpanont, S.; Bunaprasert, T.; Thanakit, V.; Damrongsakkul, S., Development of acellular dermis from porcine skin using periodic pressurized technique. *Journal of Biomedical Materials Research Part B: Applied Biomaterials* **2008,** *85B*, 210-219.
46. Hoerstrup, S. P. W., B., European Heart Journal: Biological Heart Valves. *European Society of Cardiology* **2015,** *36*, 325-332.
47. Carpentier, A., From valvular xenograft to valvular bioprosthesis (1965-1977). *Medical instrumentation* **1977,** *11*, 98-101.
48. Khor, E., Methods for the treatment of collagenous tissue for bioprostheses. *Biomaterials* **1997,** *18*, 95-105.
49. Gray, H., *Anatomy of the Human Body*. Bartleby: New York, 2000; Vol. 20.
50. P. Singhal, A. L., J. Butany, Bioprosthetic Heart Valves: Impact of Implantation on Biomaterials. *ISRN Biomaterials* **2013**, 14.
51. Vesely, I., The evolution of bioprosthetic heart valve design and its impact on durability. *Cardiovascular Pathology* **2003,** *12*, 277-286.
52. Schoen, F. J.; Tsao, J. W.; Levy, R. J., Calcification of bovine pericardium used in cardiac valve bioprostheses: Implications for the mechanisms of bioprosthetic tissue mineralization. *American Journal of Pathology* **1986,** *123*, 134-145.
53. Joyce, E. M.; Liao, J.; Schoen, F. J.; Mayer, J. E.; Sacks, M. S., Functional collagen fiber architecture of the pulmonary heart valve cusp. *Ann. Thorac. Surg.* **2009,** *87*, 1240-1249.
54. Golomb, G.; Schoen, F. J.; Smith, M. S.; Linden, J.; Dixon, M.; Levy, R. J., The role of glutaraldehyde-induced cross-links in calcification of bovine pericardium used in cardiac valve bioprostheses. *American Journal of Pathology* **1987,** *127*, 122-130.

55. Bonhoeffer, P.; Boudjemline, Y.; Saliba, Z.; Hausse, A. O.; Aggoun, Y.; Bonnet, D.; Sidi, D.; Kachaner, J., Transcatheter Implantation of a Bovine Valve in Pulmonary Position: A Lamb Study. *Circulation* **2000,** *102*, 813-816.
56. Mazilu, D.; Li, M.; Kocaturk, O.; Horvath, K. A., Self-Expanding Stent and Delivery System for Aortic Valve Replacement. *Journal of Medical Devices* **2012,** *6*, 0410061-9.
57. Basil-Jones, M. M.; Edmonds, R. L.; Allsop, T. F.; Cooper, S. M.; Holmes, G.; Norris, G. E.; Cookson, D. J.; Kirby, N.; Haverkamp, R. G., Leather structure determination by small angle X-ray scattering (SAXS): Cross sections of ovine and bovine leather. *J. Agric. Food Chem.* **2010,** *58*, 5286-5291.
58. Basil-Jones, M. M.; Haverkamp, R. G. In *Fibrilar collagen structure determination of cross-sections of ovine leather using Small Angle X-ray Scattering (SAXS)*, Pacifichem 2010, Honolulu, HI, 15-20 Dec 2010, 2010; Honolulu, HI, 2010.
59. Basil-Jones, M. M.; Edmonds, R. L.; Cooper, S. M.; Kirby, N.; Hawley, A.; Haverkamp, R. G., Collagen Fibril Orientation and Tear Strength across Ovine Skins. *J. Agric. Food Chem.* **2013,** *61*, 12327-12332.
60. Fratzl, P.; Groschner, M.; Vogl, G.; Plenk Jr., H.; Eschberger, J.; Fratzl-Zelman, N.; Koller, K.; Klaushofer, K., Mineral crystals in calcified tissues: A comparative study by SAXS. **1992,** *7*, 329-334.
61. Fratzl, P.; Fratzl-Zelman, N.; Klaushofer, K., Collagen packing and mineralization: an x-ray scattering inverstigation of turkey leg tendon. *Biophysical Journal* **1993,** *64*, 260-266.
62. Masic, A.; Bertinetti, L.; Schuetz, R.; Galvis, L.; Timofeeva, N.; Dunlop, J. W. C.; Seto, J.; Hartmann, M. A.; Fratzl, P., Observations of Multiscale, Stress-Induced Changes of Collagen Orientation in Tendon by Polarized Raman Spectroscopy. *Biomacromolecules* **2011,** *12*, 3989-3996.
63. Moger, C. J.; Barrett, R.; Bleuet, P.; Bradley, D. A.; Ellis, R. E.; Green, E. M.; Knapp, K. M.; Muthuvelu, P.; Winlove, C. P., Regional variations of collagen orientation in normal and diseased articular cartilage and subchondral bone determined using small angle X-ray scattering (SAXS). *OsteoArth. Cartilage* **2007,** *15*, 682-687.
64. Zizak, I.; Paris, O.; Roschger, P.; Bernstorff, S.; Amenitsch, H.; Klaushofer, K.; Fratzl, P., Investigation of bone and cartilage by synchrotron scanning-SAXS and -WAXD with micrometer spatial resolution. *Journal of Applied Crystallography* **2000,** *33*, 820-823.
65. Zizak, I.; Roschger, P.; Paris, O.; Misof, B. M.; Berzlanovich, A.; Bernstorff, S.; Amenitsch, H.; Klaushofer, K.; Fratzl, P., Characteristics of mineral particles in the human bone/cartilage interface. *Journal of Structural Biology* **2003,** *141*, 208-217.
66. Gupta, H. S.; Seto, J.; Wagermaier, W.; Zaslansky, P.; Boesecke, P.; Fratzl, P., Cooperative deformation of mineral and collagen in bone at the nanoscale. *Proceedings of the National Academy of Sciences* **2006,** *103*, 17741-17746.
67. Fratzl, P.; Fratzl-Zelman, N.; Klaushofer, K.; Vogl, G.; Koller, K., Nucleation and growth of mineral crystals in bone studied by small-angle X-ray scattering. *Calcif Tissue Int* **1991,** *48*, 407-413.
68. Rinnerthaler, S.; Roschger, P.; Jakob, H. F.; Nader, A.; Klaushofer, K.; Fratzl, P., Scanning small angle X-ray scattering analysis of human bone sections. **1999,** *64*, 422-429.
69. Liao, J.; Yang, L.; Grashow, J.; Sacks, M. S., Molecular orientation of collagen in intact planar connective tissues under biaxial stretch. *Acta Biomater.* **2005,** *1*, 45-54.
70. Bourges, J. Y.; Rojo Pérez, F. J.; Garcia Paez, J.; Atienza Riera, J. M.; Alvarez, L.; Guinea Tortuero, G. V., Relationship between fibre orientation and tensile strength of natural collagen membranes for heart valve leaflets. **2011**.
71. Zhang, L.; Biasci, J.; Plan, B. In *ESRF Thermal absorbers: temperature, stress and material criteria*, 2nd International Workshop on Mechanical Engineering Design of Synchrotron Radiation Equipment and Instrumentation (MEDS102), Argonne, Illinois, USA, 2002; Argonne, Illinois, USA, 2002.
72. Doniach, H. W. a. S., *Synchrotron Radiation Research*. Plenum Press: New York, 1980.
73. Guinier, A. F., A., *Small-Angle Scattering of X-rays*. Wiley: New York, 1955.
74. Basil-Jones, M. M.; Edmonds, R. L.; Cooper, S. M.; Haverkamp, R. G., Collagen fibril orientation in ovine and bovine leather affects strength: A small angle x-ray scattering (SAXS) study. *J. Agric. Food Chem.* **2011,** *59*, 9972-9979.
75. Sanabria, S. J. H., U.; Neuenschwander, J.; Niemz, P.; Sennhauser, U.; Thomen, H.; Wenker, J.L., Modeling and prediction of density distribution and microstructure in particleboards from acoustic properties by correlation of non-contact high-resolution pulsed air-coupled ultrasound and X-ray images. *Ultrasonics* **2013,** *53*, 157-170.
76. Liping, S. H. I. X., W.E.I.; Yanbo, W.E.I., Comparative Analysis on Piezoelectric Effect and Electromagnetc Effect for the Further Study of Multi-piezoelectric Effect. *International Conference on Measurement, Information and Control (MIC)* **2012,** *12*, 907-911.

77. Sodano, H. A.; Inman, D. J.; Park, G., Comparison of piezoelectric energy harvesting devices for recharging batteries. *Journal of Intelligent Material Systems and Structures* **2005,** *16*, 799-807.
78. Wang, J. All About Piezoelectric Materials.
79. Brown, L. F., The Effects of Material Selection for Backing and Wear Protection/Quarter-Wave Matching of Piezoelectric Polymer Ultrasound Transducers. *Ultrasonics Symposium* **2000,** *5*, 1029-1032.
80. Olympus, Ultrasonic Transducer Technical Notes: Basic Ultrasonic Principles. In NDT, O., Ed. Olympus NDT: USA, 2011; pp 41-49.
81. Brook, M. V., *Ultrasonic Inspection Technology Development and Search Unit Design: Examples of Pratical Applications*. Wiley: 2012.
82. Bond, L. J., Course Material: Ultrasound, Data Presentation. In *Introduction to Ultrasonic Testing*, Centre, N. E. R., Ed. Iowa State University: Iowa State, USA, 2012.
83. Greaves, G. N.; Greer, A. L.; Lakes, R. S.; Rouxel, T., Poisson's ratio and modern materials. *Nat Mater* **2011,** *10*, 823-837.
84. Rothenburg, L.; Ai. Berlin, A. I.; Bathurst, R. J., Microstructure of isotropic materials with negative Poisson's ratio. *Nature* **1991,** *354*, 470-472.
85. Elliott, D. M.; Narmoneva, D. A.; Setton, L. A., Direct measurement of the Poisson's ratio of human patella cartilage in tension. *J. Biomech. Eng.-T. ASME* **2002,** *124*, 223-228.
86. Reese, S. P.; Weiss, J. A., Tendon Fascicles Exhibit a Linear Correlation Between Poisson's Ratio and Force During Uniaxial Stress Relaxation. *Journal of Biomechanical Engineering-Transactions of the Asme* **2013,** *135*.
87. Reese, S. P.; Maas, S. A.; Weiss, J. A., Micromechanical models of helical superstructures in ligament and tendon fibers predict large Poisson's ratios. *Journal of Biomechanics* **2010,** *43*, 1394-1400.
88. Commodities and Trade Division, F. A. O., United Nations *World statistical compendium for raw hides and skins, leather and leather footwear 1990-2011*; Rome, 2012.
89. ASTM, D2941-13, Standard test method for measuring break pattern of leather (break scale). In ASTM International, West Conshohocken, PA., 2013; Vol. ASTM D2941-13.
90. Liu, C. K.; Latona, N. P.; Lee, J.; Cooke, P. H., Microscopic observations of leather looseness and its effects on mechanical properties. *J. Am. Leather Chem. Assoc.* **2009,** *104*, 230-236.
91. Xu, B. B.; Li, C. X.; Wang, R. R.; Zhang, C. X.; Peng, B. Y., The Impact of Proteases on Elastin in Leather Manufacture. *J. Soc. Leather Technolog. Chem.* **2012,** *96*, 100-105.
92. Musa, A. E.; Madhan, B.; Madhulatha, W.; Sadulla, S.; Gasmelseed, G. A., Henna extract: Can it be an alternative retanning agent? *J. Am. Leather Chem. Assoc.* **2008,** *103*, 188-193.
93. Taylor, M. M.; Marmer, W. N.; Brown, E. M., Effect of fillers prepared from enzymatically modified proteins on mechanical properties of leather. *J. Am. Leather Chem. Assoc.* **2008,** *103*, 128-137.
94. Taylor, M. M.; Lee, J.; Bumanlag, L. P.; Cooke, P. H.; Brown, E. M.; Balada, E. H., Treatment of low-quality hides with fillers produced from sustainable resources: Effect on properties of leather. *J. Am. Leather Chem. Assoc.* **2009,** *104*, 324-334.
95. Balada, E. H.; Taylor, M. M.; Brown, E. M.; Liu, C. K.; Cot, J., Whey protein isolate: A potential filler for the leather industry. *J. Am. Leather Chem. Assoc.* **2009,** *104*, 122-130.
96. Taylor, M. M.; Medina, M. B.; Lee, J.; Bumanlag, L. P.; Latona, N. P.; Brown, E. M.; Liu, C. K., Treatment of hides with tara-modified protein products. *J. Am. Leather Chem. Assoc.* **2013,** *108*, 438-444.
97. Taylor, M. M.; Lee, J.; Bumanlag, L. P.; Brown, E. M.; Hernàndez Balada, E., Use Of high molecular weight biopolymers to improve the properties of chrome-free leather. *J. Am. Leather Chem. Assoc.* **2011,** *106*, 353-359.
98. Sizeland, K. H.; Basil-Jones, M. M.; Edmonds, R. L.; Cooper, S. M.; Kirby, N.; Hawley, A.; Haverkamp, R. G., Collagen alignment and leather strength for selected mammals. *J. Agric. Food Chem.* **2013,** *61*, 887-892.
99. Wells, H. C.; Edmonds, R. L.; Kirby, N.; Hawley, A.; Mudie, S. T.; Haverkamp, R. G., Collagen fibril diameter and leather strength. *J. Agric. Food Chem.* **2013,** *61*, 11524-11531.
100. Basil-Jones, M. M.; Edmonds, R. L.; Norris, G. E.; Haverkamp, R. G., Collagen fibril alignment and deformation during tensile strain of leather: A SAXS study. *J. Agric. Food Chem.* **2012,** *60*, 1201-1208.
101. Wells, H. C.; Sizeland, K. H.; Kayed, H. R.; Kirby, N.; Hawley, A.; Mudie, S. T.; Haverkamp, R. G., Poisson's ratio of collagen fibrils measured by SAXS of strained bovine pericardium. *J. Appl. Phys.* **2015,** *117*, 044701.

102. Cookson, D.; Kirby, N.; Knott, R.; Lee, M.; Schultz, D., Strategies for data collection and calibration with a pinhole-geometry SAXS instrument on a synchrotron beamline. *J. Synchrotron Radiat.* **2006,** *13*, 440-444.
103. Williams, J., IULTCS (IUP) test methods - Measurement of tear load-double edge tear. *J. Soc. Leather Tech. Ch.* **2000,** *84*, 327-329.
104. IULTCS, Leather - Physical and mechanical tests - Determination of tear load - Part 2: Double edge tear. In ISO: Switzerland, 2002; Vol. BS EN ISO 3377-2:2002(E).
105. Crisan, D.; Lupsor, M.; Boca, A.; Crisan, M.; Badea, R., Ultrasonographic assessment of skin structure according to age. *Indian J Dermatol. Venerol. Leprol.* **2012,** *78*, 519.
106. Koenig, K.; Speicher, M.; Koehler, M. J.; Scharenberg, R.; Kaatz, M., Clinical application of multiphoton tomography in combination with high-frequency ultrasound for evaluation of skin diseases. *J. Biophotonics* **2010,** *3*, 759-773.
107. Jasaitiene, D.; Valiukeviciene, S.; Linkeviciute, G.; Raisutis, R.; Jasiuniene, E.; Kazys, R., Principles of high-frequency ultrasonography for investigation of skin pathology. *J. Eur. Acad. Dermatol.* **2011,** *25*, 375-382.
108. Sizeland, K. H.; Wells, H. C.; Higgins, J. J.; Cunanan, C. M.; Kirby, N.; Hawley, A.; Haverkamp, R. G., Age dependant differences in collagen fibril orientation of glutaraldehyde fixed bovine pericardium. *BioMed Res. Int.* **2014,** *2014*, 189197.
109. Wells, H. C.; Holmes, G.; Haverkamp, R. G., Looseness in bovine leather: microstructural characterization. *J. Sci. Food Agric.* **2015**, DOI: 10.1002/jsfa.7392.
110. Sizeland, K. H.; Basil-Jones, M. M.; Edmonds, R. L.; Cooper, S. M.; Kirby, N.; Hawley, A.; Haverkamp, R. G., Collagen Orientation and Leather Strength for Selected Mammals. *J. Agric. Food Chem.* **2013,** *61*, 887-892.
111. Voets, J.; von Behr, D., Floater leathers require a loose grain. *Leather International* 1 January, 2005.
112. Wells, H. C.; Holmes, G.; Haverkamp, R. G., Early Detection of Looseness in Bovine Hides using Ultrasonic Imaging. *J. Am. Leather Chem. As.* **2015,** *111*.
113. Basil-Jones, M. M.; Edmonds, R. L.; Allsop, T. F.; Cooper, S. M.; Holmes, G.; Norris, G. E.; Cookson, D. J.; Kirby, N.; Haverkamp, R. G., Leather structure determination by small-angle X-ray scattering (SAXS): Cross sections of ovine and bovine leather. *J. Agric. Food Chem.* **2010,** *58*, 5286-5291.
114. Basil-Jones, M. M.; Edmonds, R. L.; Norris, G. E.; Haverkamp, R. G., Collagen fibril alignment and deformation during tensile strain of leather: A small-angle X-ray scattering study. *J. Agric. Food Chem.* **2012,** *60*, 1201-1208.
115. Haverkamp, R. G., The Australian Synchrotron-a powerful tool for chemical research available to New Zealand scientists. *Chem. N. Z.* **2013,** *77*, 12-17.
116. Sizeland, K. H.; Edmonds, R. L.; Basil -Jones, M. M.; Kirby, N.; Hawley, A.; Mudie, S.; Haverkamp, R. G., Changes to collagen structure during leather processing. *J. Agric. Food Chem.* **2015,** *63*, 2499-2505.
117. Picu, R. C., Mechanics of random fiber networks-a review. *Soft Matter* **2011,** *7*, 6768-6785.
118. Gao, Y.; Xia, J., Chromium Contamination Accident in China: Viewing Environment Policy of China. *Environmental Science & Technology* **2011,** *45*, 8605-8606.
119. Izbicki, J. A.; Bullen, T. D.; Martin, P.; Schroth, B., Delta Chromium-53/52 isotopic composition of native and contaminated groundwater, Mojave Desert, USA. *Applied Geochemistry* **2012,** *27*, 841-853.
120. James, B. R., The challenge of remediating chromium-contaminated soil. *Environmental Science & Technology* **1996,** *30*, A248-A251.
121. Heidemann, E., Disposal and recycling of chrome-tanned materials. *Journal of the American Leather Chemists Association* **1991,** *86*, 331-333.
122. Cabeza, L. F.; Taylor, M. M.; DiMaio, G. L.; Brown, E. M.; Mermer, W. N.; Carrio, R.; Celma, P. J.; Cot, J., Processing of leather waste: pilot scale studies on chrome shavings. Isolation of potentially valuable protein products and chromium. *Waste Management* **1998,** *18*, 211-218.
123. Beltran-Prieto, J. C.; Veloz-Rodriguez, R.; Perez-Perez, M. C.; Navarrete-Bolanos, J. L.; Vazquez-Nava, E.; Jimenez-Islas, H.; Botello-Alvarez, J. E., Chromium recovery from solid leather waste by chemical treatment and optimisation by response surface methodology. *Chemistry and Ecology* **2012,** *28*, 89-102.
124. Dotro, G.; Castro, S.; Tujchneider, O.; Piovano, N.; Paris, M.; Faggi, A.; Palazolo, P.; Larsen, D.; Fitch, M., Performance of pilot-scale constructed wetlands for secondary treatment of chromium-bearing tannery wastewaters. *Journal of Hazardous Materials* **2012,** *239*, 142-151.

125. Ashokkumar, M.; Thanikaivelan, P.; Krishnaraj, K.; Chandrasekaran, B., Transforming Chromium Containing Collagen Wastes Into Flexible Composite Sheets Using Cellulose Derivatives: Structural, Thermal, and Mechanical Investigations. *Polymer Composites* **2011,** *32*, 1009-1017.
126. Przepiorkowska, A.; Chronska, K.; Zaborski, M., Chrome-tanned leather shavings as a filler of butadiene-acrylonitrile rubber. *Journal of Hazardous Materials* **2007,** *141*, 252-257.
127. Erdem, M., Chromium recovery from chrome shaving generated in tanning process. *Journal of Hazardous Materials* **2006,** *129*, 143-146.
128. Tahiri, S.; Albizane, A.; Messaoudi, A.; Azzi, M.; Bennazha, J.; Younssi, S. A.; Bouhria, M., Thermal behaviour of chrome shavings and of sludges recovered after digestion of tanned solid wastes with calcium hydroxide. *Waste Management* **2007,** *27*, 89-95.
129. Stam, A. F.; Meij, R.; Winkel, H. T.; van Eijk, R. J.; Huggins, F. E.; Brem, G., Chromium Speciation in Coal and Biomass Co-Combustion Products. *Environmental Science & Technology* **2011,** *45*, 2450-2456.
130. Aitkenhead, W.; Edmonds, R. L., Biochar: A possibility for solid waste disposal. *Leather International* **2013,** *215*, 28-30.
131. Chan, K. Y.; Van Zwieten, L.; Meszaros, I.; Downie, A.; Joseph, S., Agronomic values of greenwaste biochar as a soil amendment. *Australian Journal of Soil Research* **2007,** *45*, 629-634.
132. Erdem, M.; Ozverdi, A., Leaching behavior of chromium in chrome shaving generated in tanning process and its stabilization. *Journal of Hazardous Materials* **2008,** *156*, 51-55.
133. Oliveira, L. C. A.; Guerreiro, M. C.; Goncalves, M.; Oliveira, D. Q. L.; Costa, L. C. M., Preparation of activated carbon from leather waste: A new material containing small particle of chromium oxide. *Materials Letters* **2008,** *62*, 3710-3712.
134. Sekaran, G.; Shanmugasundaram, K. A.; Mariappan, M., Characterization and utilisation of buffing dust generated by the leather industry. *Journal of Hazardous Materials* **1998,** *63*, 53-68.
135. Brose, D. A.; James, B. R., Oxidation-Reduction Transformations of Chromium in Aerobic Soils and the Role of Electron-Shuttling Quinones. *Environmental Science & Technology* **2010,** *44*, 9438-9444.
136. Kappen, P.; Welter, E.; Beck, P. H.; McNamara, J. M.; Moroney, K. A.; Roe, G. M.; Read, A.; Pigram, P. J., Time-resolved XANES speciation studies of chromium on soils during simulated contamination. *Talanta* **2008,** *75*, 1284-1292.
137. Martin, R. R.; Naftel, S. J.; Sham, T. K.; Hart, B.; Powell, M. A., XANES of chromium in sludges used as soil ameliorants. *Canadian Journal of Chemistry-Revue Canadienne De Chimie* **2003,** *81*, 193-196.
138. Covington, A. D.; Lampard, G. S.; Menders, O.; Chadwick, A. V.; Rafeletos, G.; O'Brien, P., Extanded X-ray absorption fine structure sudies of the role of chromium in leather tanning. *Polyhedron* **2001,** *20*, 461-466.
139. Reich, T.; Rossberg, A.; Hennig, C.; Reich, G., Characterization of chromium complexes in chrome tannins, leather, and gelatin using extended X-ray absorption fine structure (EXAFS) spectroscopy. *Journal of the American Leather Chemists Association* **2001,** *96*, 133-147.
140. ISO, Leather -- Chemical determination of chromic oxide content -- Part 1: Quantification by titration. In 2007; Vol. ISO 5398-1:2007 (IULTCS/IUC 8-1).
141. ISO, Leather -- Chemical determination of chromic oxide content -- Part 3: Quantification by atomic absorption spectrometry. **2007,** *ISO 5398-3:2007 (IULTCS/IUC 8-3)*.
142. Ravel, B.; Newville, M., *ATHENA*, *ARTEMIS*, *HEPHAESTUS*: Data Analysis for X-ray Absorption Spectroscopy using *IFEFFIT*. *J. Synchrotron Radiat.* **2005,** *12*, 537-541.
143. Klementev, K. V., Extraction of the fine structure from x-ray absorption spectra. *Journal of Physics D-Applied Physics* **2001,** *34*, 209-217.
144. Pantelouris, A.; Modrow, H.; Pantelouris, M.; Hormes, J.; Reinen, D., The influence of coordination geometry and valency on the K-edge absorption near edge spectra of selected chromium compounds. *Chemical Physics* **2004,** *300*, 13-22.
145. Gardea-Torresday, J. L.; Tiemann, K. J.; Armendariz, V.; Bess-Oberto, L.; Chianelli, R. R.; Rios, J.; Parsons, J. G.; Gamez, G., Characterization of Cr(VI) binding and reduction to Cr(III) by the agricultural byproducts of Avena monida (Oat) biomass. *Journal of Hazardous Materials* **2000,** *80*, 175-188.
146. Farges, F., Chromium speciation in oxide-type compounds: application to minerals, gems, aqueous solutions and silicate glasses. *Physics and Chemistry of Minerals* **2009,** *36*, 463-481.
147. de Groot, F.; Vanko, G.; Glatzel, P., The 1s x-ray absorption pre-edge structures in transition metal oxides. *Journal of Physics-Condensed Matter* **2009,** *21*.

148. Frommer, J.; Nachtegaal, M.; Czekaj, I.; Weng, T. C.; Kretzschmar, R., X-ray Absorption and Emission Spectroscopy of Cr-III (Hydr)Oxides: Analysis of the K-Pre-Edge Region. *Journal of Physical Chemistry A* **2009,** *113*, 12171-12178.
149. Yamamoto, T., Assignment of pre-edge peaks in K-edge x-ray absorption spectra of 3d transition metal compounds: electric dipole or quadrupole? *X-Ray Spectrometry* **2008,** *37*, 572-584.
150. Chu, W. F.; Rahmel, A., The conversion of chromium-oxide to chromium carbide. *Oxidation of Metals* **1981,** *15*, 331-337.
151. Grabke, H. J.; Krajak, R.; Paz, J. C. N., On the mechanism of catastrophic carburization - metal dusting. *Corrosion Science* **1993,** *35*, 1141-1150.
152. Jiao, F.; Wijaya, N.; Zhang, L.; Ninomiya, Y.; Hocking, R., Synchrotron-Based XANES Speciation of Chromium in the Oxy-Fuel Fly Ash Collected from Lab-Scale Drop-Tube Furnace. *Environmental Science & Technology* **2011,** *45*, 6640-6646.
153. Chen, J.; Jiao, F.; Zhang, L.; Yao, H.; Ninomiya, Y., Use of Synchrotron XANES and Cr-Doped Coal to Further Confirm the Vaporization of Organically Bound Cr and the Formation of Chromium(VI) During Coal Oxy-Fuel Combustion. *Environmental Science & Technology* **2012,** *46*, 3567-3573.
154. Werner, M. L.; Nico, P. S.; Marcus, M. A.; Anastasio, C., Use of micro-XANES to speciate chromium in airborne fine particles in the Sacramento Valley. *Environmental Science & Technology* **2007,** *41*, 4919-4924.
155. Eick, B. M.; Youngblood, J. P., Carbothermal reduction of metal-oxide powders by synthetic pitch to carbide and nitride ceramics. *Journal of Materials Science* **2009,** *44*, 1159-1171.
156. Rehr, J. J.; Deleon, J. M.; Zabinsky, S. I.; Albers, R. C., Theoretical X-ray absorption fine-structure standards. *J. Am. Chem. Soc.* **1991,** *113*, 5135-5140.
157. Sen, S.; Ozdemir, O.; Demirkiran, A. S.; Sen, U., Oxidation Kinetics of Chromium Carbide Coating Produced on AISI 1040 Steel by Thermo-Reactive Deposition Method During High Temperature in Air. In *Materials and Manufacturing Technologies Xiv*, Yigit, F.; Hashmi, M. S. J., Eds. 2012; Vol. 445, pp 649-654.
158. Schmidt, M. W. I.; Torn, M. S.; Abiven, S.; Dittmar, T.; Guggenberger, G.; Janssens, I. A.; Kleber, M.; Kogel-Knabner, I.; Lehmann, J.; Manning, D. A. C.; Nannipieri, P.; Rasse, D. P.; Weiner, S.; Trumbore, S. E., Persistence of soil organic matter as an ecosystem property. *Nature* **2011,** *478*, 49-56.
159. Glaser, B.; Haumaier, L.; Guggenberger, G.; Zech, W., The 'Terra Preta' phenomenon: a model for sustainable agriculture in the humid tropics. *Naturwissenschaften* **2001,** *88*, 37-41.
160. Oxlund, H.; Andreassen, T. T., The roles of hyaluronic-acid, collagen and elastin in the mechanical-properties of connective tissues. *J. Anat.* **1980,** *131*, 611-620.
161. Chan, Y.; Cox, G. M.; Haverkamp, R. G.; Hill, J. M., Mechanical model for a collagen fibril pair in extracellular matrix. *Eur. Biophys. J.* **2009,** *38*, 487-493.
162. Fessel, G.; Snedeker, J. G., Equivalent stiffness after glycosaminoglycan depletion in tendon - an ultra-structural finite element model and corresponding experiments. *J. Theor. Biol.* **2011,** *268*, 77-83.
163. Redaelli, A.; Vesentini, S.; Soncini, M.; Vena, P.; Mantero, S.; Montevecchi, F. M., Possible role of decorin glycosaminoglycans in fibril to fibril force transfer in relative mature tendons - a computational study from molecular to microstructural level. *J. Biomech.* **2003,** *36*, 1555-1569.
164. Haverkamp, R. G.; Marshall, A. T.; Williams, M. A. K., Entropic and enthalpic contributions to the chair-boat conformational transformation in dextran under single molecule stretching. *J. Phys. Chem. B* **2007,** *111*, 13653-13657.
165. Haverkamp, R. G.; Williams, M. A. K.; Scott, J. E., Stretching single molecules of connetive tissue glycans to characterize their shape-maintaining elasticity. *Biomacromolecules* **2005,** *6*, 1816-1818.
166. Rigozzi, S.; Stemmer, A.; Muller, R.; Snedeker, J. G., Mechanical response of individual collagen fibrils in loaded tendon as measured by atomic force microscopy. *J. Structural Biol.* **2011,** *176*, 9-15.
167. Fessel, G.; Snedeker, J. G., Evidence against proteoglycan mediated collagen fibril load transmission and dynamic viscoelasticity in tendon. *Matrix Biol.* **2009,** *28*, 503-510.
168. Svensson, R. B.; Hassenkam, T.; Hansen, P.; Kjaer, M.; Magnusson, S. P., Tensile Force Transmission in Human Patellar Tendon Fascicles Is Not Mediated by Glycosaminoglycans. *Connect. Tiss. Res.* **2011,** *52*, 415-421.
169. Reece, I. J.; Vannoort, R.; Martin, T. R. P.; Black, M. M., The physical-properties of bovine pericardium - a study of the effects of stretching during chemical treatment in glutaraldehyde. *Ann. Thorac. Surg.* **1982,** *33*, 480-485.

170. Langdon, S. E.; Chernecky, R.; Pereira, C. A.; Abdulla, D.; Lee, J. M., Biaxial mechanical/structural effects of equibiaxial strain during crosslinking of bovine pericardial xenograft materials. *Biomaterials* **1999,** *20*, 137-153.
171. Kronick, P. L.; Sacks, M. S., Quantification of vertical-fiber defect in cattle hide by small-angle light-scattering. *Connect. Tissue Res.* **1991,** *27*, 1-13.
172. Bigi, A.; Ripamonti, A.; Roveri, N.; Jeronimidis, G.; Purslow, P. P., Collagen orientation by X-Ray pole figures and mechanical-properties of media carotid wall. *J. Mater. Sci.* **1981,** *16*, 2557-2562.
173. Kayed, H. R.; Sizeland, K. H.; Kirby, N.; Hawley, A.; Mudie, S.; Haverkamp, R. G. In *Cross-Linking Collagen affects Fibril Orientation.*, Australian Synchrotron User Meeting, Melbourne, November 21–22, 2013.
174. Balguid, A.; Driessen, N. J.; Mol, A.; Schmitz, J. P. J.; Verheyen, F.; Bouten, C. V. C.; Baaijens, F. P. T., Stress related collagen ultrastructure in human aortic valves - implications for tissue engineering. *J. Biomech.* **2008,** *41*, 2612-2617.
175. Michna, H., Morphometric analysis of loading-induced changes in collagen-fibril populations in young tendons. *Cell Tissue Res.* **1984,** *236*, 465-470.
176. Biancalana, A.; Veloso, L. A.; Gomes, L., Obesity Affects Collagen Fibril Diameter and Mechanical Properties of Tendons in Zucker Rats. *Connect. Tissue Res.* **2010,** *51*, 171-178.
177. Parry, D. A. D.; Barnes, G. R. G.; Craig, A. S., Comparison of size distribution of collagen fibrils in connective tissues as a function of age and a possible relation between fibril size distribution and mechanical-properties. *P. Roy. Soc. B-Biol. Sci.* **1978,** *203*, 305-321.
178. Herchenhan, A.; Bayer, M. L.; Svensson, R. B.; Magnusson, S. P.; Kjaer, M., In vitro tendon tissue development from human fibroblasts demonstrates collagen fibril diameter growth associated with a rise in mechanical strength. *Dev. Dynam.* **2013,** *242*, 2-8.
179. Goh, K. L.; Holmes, D. F.; Lu, Y.; Purslow, P. P.; Kadler, K. E.; Bechet, D.; Wess, T. J., Bimodal collagen fibril diameter distributions direct age-related variations in tendon resilience and resistance to rupture. *J. Appl. Physiol.* **2012,** *113*, 878-888.
180. PattersonKane, J. C.; Wilson, A. M.; Firth, E. C.; Parry, D. A. D.; Goodship, A. E., Comparison of collagen fibril populations in the superficial digital flexor tendons of exercised and nonexercised thoroughbreds. *Equine Vet. J.* **1997,** *29*, 121-125.
181. Cherdchutham, W.; Becker, C. K.; Spek, E. R.; Voorhout, W. F.; van Weeren, P. R., Effects of exercise on the diameter of collagen fibrils in the central core and periphery of the superficial digital flexor tendon in foals. *Am. J. Vet. Res.* **2001,** *62*, 1563-1570.
182. Hashimoto, M.; Tay, F. R.; Ohno, H.; Sano, H.; Kaga, M.; Yiu, C.; Kumagai, H.; Kudou, Y.; Kubota, M.; Oguchi, H., SEM and TEM analysis of water degradation of human dentinal collagen. *J. Biomed. Mater. Res. B* **2003,** *66B*, 287-298.
183. Frank, C.; Bray, D.; Rademaker, A.; Chrusch, C.; Sabiston, P.; Bodie, D.; Rangayyan, R., Electron-microscopic quantification of collagen fibril diameters in the rabbit medial collateral ligament - a baseline for comparison. *Connect. Tissue Res.* **1989,** *19*, 11-25.
184. Rumian, A. P.; Wallace, A. L.; Birch, H. L., Tendons and ligaments are anatomically distinct but overlap in molecular and morphological features - A comparative study in an ovine model. *J. Orthopaed. Res.* **2007,** *25*, 458-464.
185. Akhtar, S., Effect of processing methods for transmission electron microscopy on corneal collagen fibrils diameter and spacing. *Microsc. Res. Techniq.* **2012,** *75*, 1420-1424.
186. Jastrzebska, M.; Mroz, I.; Barwinski, B.; Zalewska-Rejdak, J.; Turek, A.; Cwalina, B., Supramolecular structure of human aortic valve and pericardial xenograft material: atomic force microscopy study. *J. Mater. Sci.-Mater. M.* **2008,** *19*, 249-256.
187. Deb Choudhury, S.; Haverkamp, R. G.; DasGupta, S.; Norris, G. E., Effect of oxazolidine E on collagen fibril formation and stabilization of the collagen matrix. *J. Agric. Food Chem.* **2007,** *55*, 6813-6822.
188. Goh, K. L.; Hiller, J.; Haston, J. L.; Holmes, D. F.; Kadler, K. E.; Murdoch, A.; Meakin, J. R.; Wess, T. J., Analysis of collagen fibril diameter distribution in connective tissues using small-angle X-ray scattering. *Biochim. Biophys. Acta* **2005,** *1722*, 183-188.
189. Williams, J., IULTCS (IUP) test methods - Sampling. *J. Soc. Leather Tech. Ch.* **2000,** *84*, 303-309.
190. Ilavsky, J.; Jemian, P. R., Irena: tool suite for modeling and analysis of small-angle scattering. *J. Appl. Crystallogr.* **2009,** *42*, 347-353.
191. Sacks, M. S.; Smith, D. B.; Hiester, E. D., A small angle light scattering device for planar connective tissue microstructural analysis. *Ann. Biomed. Eng.* **1997,** *25*, 678-689.

192. Flint, M. H.; Craig, A. S.; Reilly, H. C.; Gillard, G. C.; Parry, D. A. D., Collagen fibril diameters and glycosaminoglycan content of skins - indexes of tissue maturity and function. *Connect. Tissue Res.* **1984,** *13*, 69-81.
193. Kuc, I. M.; Scott, P. G., Increased diameters of collagen fibrils precipitated in vitro in the presence of decorin from various connective tissues. *Connect. Tissue Res.* **1997,** *36*, 287-296.
194. Kobayashi, A.; Takehana, K.; Eerdunchaolu; Iwasa, K.; Abe, M.; Yamaguchi, M., Morphometric analysis of collagen: a comparative study in cow and pig skins. *Anat. Histol. Embryol.* **1999,** *28*, 235-238.
195. Parry, D. A. D., The Molecular and Fibrillar Structure of Collagen and its Relationship to the Mechanical-Properties of Connective-Tissue. *Biophys.Chem.* **1988,** *29*, 195-209.
196. Goh, K. L.; Holmes, D. F.; Lu, H. Y.; Richardson, S.; Kadler, K. E.; Purslow, P. P.; Wess, T. J., Ageing changes in the tensile properties of tendons: Influence of collagen fibril volume fraction. *J. Biomech. Eng.-T ASME* **2008,** *130*.
197. Fodor, F., The densest packing of 19 congruent circles in a circle. *Geometriae Dedicata* **1999,** *74*, 139-145.
198. Floden, E. W.; Malak, S. F. F.; Basil-Jones, M. M.; Negron, L.; Fisher, J. N.; Lun, S.; Dempsey, S. G.; Haverkamp, R. G.; Ward, B. R.; May, B. C. H., Biophysical characterization of ovine forestomach extracellular matrix biomaterials. *J. Biomed. Mater. Res., Part B* **2011,** *96B*, 67-75.
199. Clemens, M. W.; Selber, J. C.; Liu, J.; Adelman, D. M.; Baumann, D. P.; Garvey, P. B.; Butler, C. E., Bovine versus Porcine Acellular Dermal Matrix for Complex Abdominal Wall Reconstruction. *Plastic Reconstruc. Surg.* **2013,** *131*, 71-79.
200. Cheng, V. W. T.; Screen, H. R. C., The micro-structural strain response of tendon. *J. Mat. Sci.* **2007,** *42*, 8957-8965.
201. Persson, C.; Evans, S.; Marsh, R.; Summers, J. L.; Hall, R. M., Poisson's Ratio and Strain Rate Dependency of the Constitutive Behavior of Spinal Dura Mater. *Ann. Biomed. Eng.* **2010,** *38*, 975-983.
202. Jurvelin, J. S.; Buschmann, M. D.; Hunziker, E. B., Optical and mechanical determination of Poisson's ratio of adult bovine humeral articular cartilage. *J. Biomech.* **1997,** *30*, 235-241.
203. Kiviranta, P.; Rieppo, J.; Korhonen, R. K.; Julkunen, P.; Toyras, J.; Jurvelin, J. S., Collagen network primarily controls Poisson's ratio of bovine articular cartilage in compression. *Journal of Orthopaedic Research* **2006,** *24*, 690-699.
204. Miller, G. J.; Morgan, E. F., Use of microindentation to characterize the mechanical properties of articular cartilage: comparison of biphasic material properties across length scales. *Osteoarthr. Cartilage* **2010,** *18*, 1051-1057.
205. Edelsten, L.; Jeffrey, J. E.; Burgin, L. V.; Aspden, R. M., Viscoelastic deformation of articular cartilage during impact loading. *Soft Matter* **2010,** *6*, 5206-5212.
206. Cribb, A. M.; Scott, J. E., Tendon response to tensile-stress - an ultrastructural investigation of collagen - proteoglycan interactions in stressed tendon. *J. Anat.* **1995,** *187*, 423-428.
207. Wenger, M. P. E.; Mesquida, P., Longitudinal variations in the Poisson's ratio of collagen fibrils. *Appl. Phys. Lett.* **2011,** *98*.
208. Minary-Jolandan, M.; Yu, M.-F., Nanomechanical Heterogeneity in the Gap and Overlap Regions of Type I Collagen Fibrils with Implications for Bone Heterogeneity. *Biomacromolecules* **2009,** *10*, 2565-2570.
209. Screen, H. R. C.; Bader, D. L.; Lee, D. A.; Shelton, J. C., Local strain measurement within tendon. *Strain* **2004,** *40*, 157-163.
210. Yang, M.; Chen, C. Z.; Wang, X. N.; Zhu, Y. B.; Gu, Y. J., Favorable Effects of the Detergent and Enzyme Extraction Method for Preparing Decellularized Bovine Pericardium Scaffold for Tissue Engineered Heart Valves. *J. Biomed. Mat. Res. B* **2009,** *91B*, 354-361.
211. Stinson, R. H.; Sweeny, P. R., Skin collagen has an unusual D-spacing. *Biochim. Biophys. Acta* **1980,** *621*, 158-161.
212. Sacks, M. S., Incorporation of Experimentally-Derived Fiber Orientation into a Structural Constitutive Model for Planar Collagenous Tissues. *Journal of Biomechanical Engineering* **2003,** *125*, 280-287.
213. Fratzl, P.; Misof, K.; Zizak, I.; Rapp, G.; Amenitsch, H.; Bernstorff, S., Fibrillar Structure and Mechanical Properties of Collagen. *Journal of Structural Biology* **1998,** *122*, 119-122.
214. Sasaki, N.; Odajima, S., Elongation mechanism of collagen fibrils and force-strain relations of tendon at each level of structural hierarchy. *Journal of Biomechanics* **1996,** *29*, 1131-1136.
215. Rigozzi, S.; Muller, R.; Stemmer, A.; Snedeker, J. G., Tendon glycosaminoglycan proteoglycan sidechains promote collagen fibril sliding-AFM observations at the nanoscale. *J. Biomech.* **2013,** *46*, 813-818.

216. Adeeb, S.; Ali, A.; Shrive, N.; Frank, C.; Smith, D., Modelling the behaviour of ligaments: A technical note. *Computer Methods in Biomechanics and Biomedical Engineering* **2004,** *7*, 33-42.
217. Helmer, K. G.; Nair, G.; Cannella, M.; Grigg, P., Water movement in tendon in response to a repeated static tensile load using one-dimensional magnetic resonance imaging. *Journal of Biomechanical Engineering-Transactions of the Asme* **2006,** *128*, 733-741.
218. Lutolf, M. P.; Hubbell, J. A., Synthetic biomaterials as instructive extracellular microenvironments for morphogenesis in tissue engineering. *Nature Biotechnol.* **2005,** *23*, 47-55.
219. Badylak, S. F.; Freytes, D. O.; Gilbert, T. W., Extracellular matrix as a biological scaffold material: Structure and function. *Acta Biomater.* **2009,** *5*, 1-13.
220. Meyers, M. A.; McKittrick, J.; Chen, P. Y., Structural biological materials: Critical mechanics-materials connections. *Science* **2013,** *339*, 773-779.
221. Yang, W.; Sherman, V. R.; Gludovatz, B.; Schaible, E.; Stewart, P.; Ritchie, R. O.; Meyers, M. A., On the tear resistance of skin. *Nat. Comm.* **2015,** *6*.
222. Boote, C.; Kamma-Lorger, C. S.; Hayes, S.; Harris, J.; Burghammer, M.; Hiller, J.; Terrill, N. J.; Meek, K. M., Quantification of collagen organization in the peripheral human cornea at micron-scale resolution. *Biophys. J.* **2011,** *101*, 33-42.
223. Sellaro, T. L.; Hildebrand, D.; Lu, Q. J.; Vyavahare, N.; Scott, M.; Sacks, M. S., Effects of collagen fiber orientation on the response of biologically derived soft tissue biomaterials to cyclic loading. *J. Biomed. Mater. Res. B* **2007,** *80A*, 194-205.
224. Gilbert, T. W.; Wognum, S.; Joyce, E. M.; Freytes, D. O.; Sacks, M. S.; Badylak, S. F., Collagen fiber alignment and biaxial mechanical behavior of porcine urinary bladder derived extracellular matrix. *Biomaterials* **2008,** *29*, 4775-4782.
225. Purslow, P. P.; Wess, T. J.; Hukins, D. W. L., Collagen orientation and molecular spacing during creep and stress-relaxation in soft connective tissues. *J. Exp. Biol.* **1998,** *201*, 135-142.
226. Gasser, T. C., An irreversible constitutive model for fibrous soft biological tissue: A 3-D microfiber approach with demonstrative application to abdominal aortic aneurysms. *Acta Biomater.* **2011,** *7*, 2457-2466.
227. Floden, E. W.; Malak, S.; Basil-Jones, M. M.; Negron, L.; Fisher, J. N.; Byrne, M.; Lun, S.; Dempsey, S. G.; Haverkamp, R. G.; Anderson, I.; Ward, B. R.; May, B. C. H., Biophysical characterization of ovine forestomach extracellular matrix biomaterials. *J. Biomed. Mat. Res. B* **2010,** *96B*, 67-75.
228. James, V. J.; McConnell, J. F.; Capel, M., The D-spacing of collagen from mitral heart-valves changes with aging, but not with collagen type-III content. *Biochim. Biophys. Acta* **1991,** *1078*, 19-22.
229. Scott, J. E.; Orford, C. R.; Hughes, E. W., Proteoglycan-collagen arrangements in developing rat tail tendon - an electron-microscopical and biochemical investigation. *Biochem. J.* **1981,** *195*, 573-584.
230. Fang, M.; Goldstein, E. L.; Turner, A. S.; Les, C. M.; Bradford, G. O.; Fisher, G. J.; Welch, K. B.; Rothman, E. D.; Banaszak Holl, M. M., Type I collagen D-spacing in fibril bundles of dermis, tendon, and bone: Bridging between nano- and micro-level tissue hierachy. *ACS Nano* **2012,** *6*, 9503-9514.
231. Ripamonti, A.; Roveri, N.; Braga, D.; Hulmes, D. J. S.; Miller, A.; Timmins, P. A., Effects of pH and ionic-strength on the structure of collagen fibrils. *Biopolymers* **1980,** *19*, 965-975.
232. Sizeland, K. H.; Wells, H. C.; Norris, G. E.; Edmonds, R. L.; Kirby, N.; Hawley, A.; Mudie, S.; Haverkamp, R. G., Collagen D-spacing and the effect of fat liquor addition. *J. Am. Leather Chem. Assoc.* **2015,** *110*, 66-71.
233. Wess, T. J.; Orgel, J. P., Changes in collagen structure: drying, dehydrothermal treatment and relation to long term deterioration. *Thermochim. Acta* **2000,** *365*, 119-128.
234. Masic, A.; Bertinetti, L.; Schuetz, R.; Chang, S.-W.; Metzger, T. H.; Buehler, M. J.; Fratzl, P., Osmotic pressure induced tensile forces in tendon collagen. *Nat. Comm.* **2015,** *65942*.
235. Gonzalez, A. D.; Gallant, M. A.; Burr, D. B.; Wallace, J. M., Multiscale analysis of morphology and mechanics in tail tendon from the ZDSD rat model of type 2 diabetes. *J. Biomech.* **2014,** *47*, 681-686.
236. Williams, J., IULTCS (IUP) test methods - Measurement of tensile strength and percentage elongation. *J. Soc. Leather Tech. Ch.* **2000,** *84*, 317-321.
237. Russakovsky, V., TEI Biosciences, Personal communication. In 2015.
238. Wolf, K.; Alexander, S.; Schacht, V.; Coussens, L. M.; von Andrian, U. H.; van Rheenen, J.; Deryugina, E.; Friedl, P., Collagen-based cell migration models in vitro and in vivo. *Sem. Cell Dev. Biol.* **2009,** *20*, 931-941.

Appendix One –Conference Abstracts, Posters and Symposiums

Listed below is the work presented at conferences from 2013 – 2015, in the form of either a poster or symposium.

1) **Poster presented at the 12th International Conference on Frontiers of Polymers and Advanced Materials, Auckland, December 8-13, 2013.**

Hannah C. Wells[1], Katie H. Sizeland[1], Richard L. Edmonds[2], Nigel Kirby[3], Adrian Hawley[3], Stephen Mudie[3], Richard G. Haverkamp[1]

[1] School of Engineering and Advanced Technology, Massey University, Private Bag 11222, Palmerston North, New Zealand 4442

[2]New Zealand Leather and Shoe Research Association, Palmerston North, New Zealand.

[3]Australian Synchrotron, Victoria, Melbourne, Australia

ABSTRACT

Collagen Fibril Diameter and Leather Strength

The main structural component of leather (and of skin and tendons) is collagen. The strength of leather is an important property that determines the possible uses of the leather and has a big impact on the value of the leather. Collagen forms fibrils which may be arranged in bundles. It has previously been reported that tendons composed of bundles of collagen fibrils with larger diameter fibrils are believed to be stronger. However, exercise has been shown to reduce the fibril diameter in tendons of horses and mice. We have used synchrotron based small angle X-ray scattering, combined with scanning electron microscopy and atomic force microscopy, to measure the fibril diameter in ovine and bovine leather and compared this with the measured strength of these materials. Early results indicate that stronger leather may be composed of thinner collagen fibrils. These results may cast a new light on the understanding of the strength of collagen based tissues and require a reinterpretation of previous experimental reports.

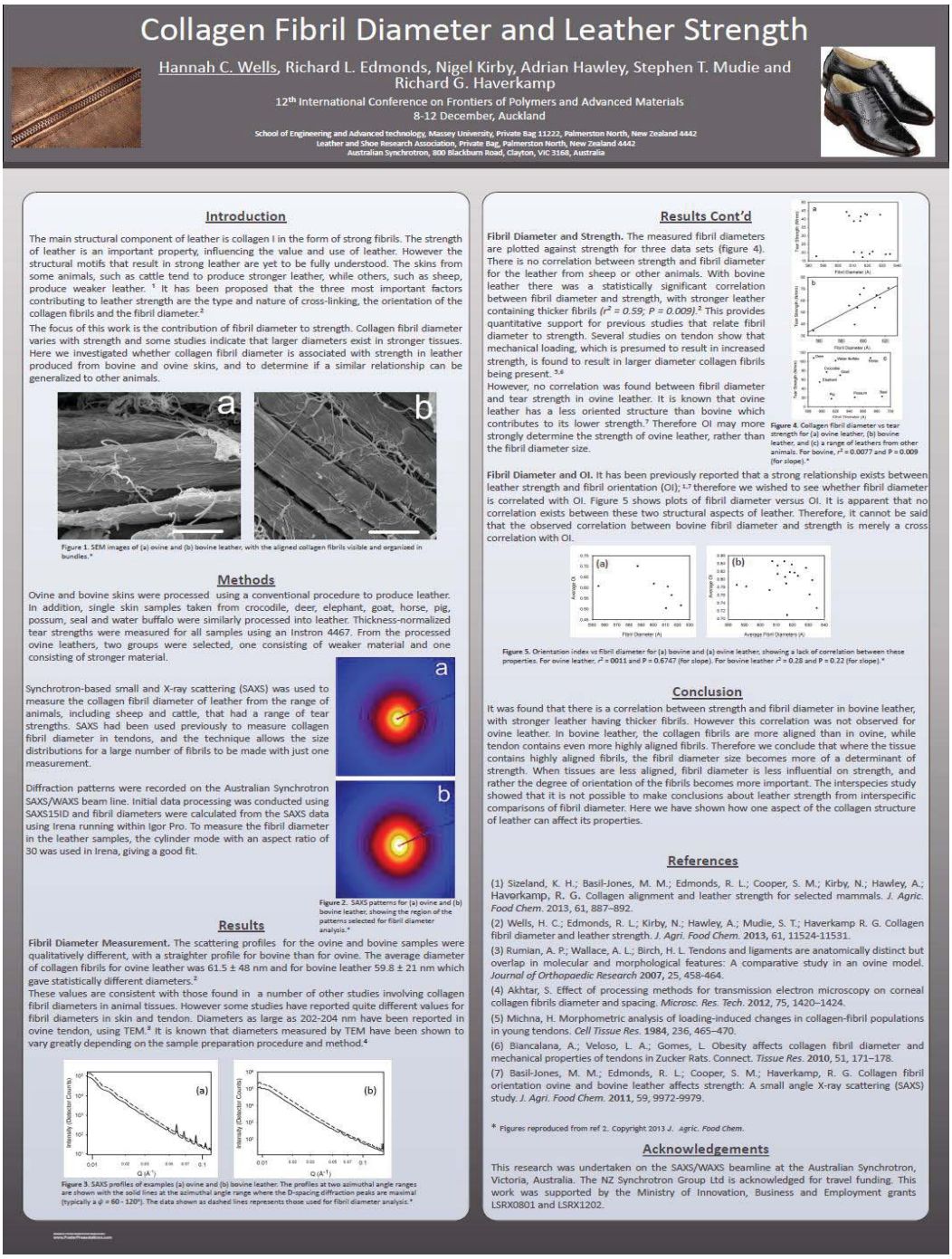

2) Symposium Presented at the 65th Annual Leather and Shoe Research Association Conference, Wellington, New Zealand, 13th August 2014.

Katie H. Sizeland[1], Hannah C. Wells[1], Gill E. Norris[2], Richard L. Edmonds[3], & Richard G. Haverkamp[1].

[1] *School of Engineering and Advanced Technology, Massey University, Private Bag 11222, Palmerston North, New Zealand 4442*

[2]*Institute of Fundamental Sciences, Massey University, Palmerston North, New Zealand*

[3] *New Zealand Leather and Shoe Research Association, Palmerston North, New Zealand*

ABSTRACT

Collagen D-spacing Modification by Fat Liquor Addition

Collagen is the main structural component of skin, both in an unprocessed state and as leather following chemical and mechanical processing. Leather is a remarkable biomaterial that exhibits strength, flexibility and, durability. Leather is processed skin consisting mostly of collagen and it is produced on a large scale for shoes, clothing and upholstery, with high strength being a primary requirement for high-value applications.

During the processing of skins and hides to leather, efforts are made to optimize the strength, flexibility and feel of leather. Adding penetrating oils, a process known as fat liquoring, is likely to improve both the flexibility and the texture of leather by lubricating the fibers to prevent adhesion between them. Little is known, however, about the effect of fat liquor on the molecular structure of the collagen fibrils. We have investigated the structural changes of collagen within leather upon addition of varying amounts of fat liquor. We have shown that as we increased the amount of fat liquor, the D-spacing of the collagen fibrils increased, and that this could be due to the lanolin component of the fat liquor. This shows that fat liquor does more than just lubricate the fibers in leather; it actually alters the structure of the collagen fibrils. Alternative mechanisms for this increase in D-spacing have been discussed, including an increase in the gap region or an increase in the length of the tropocollagen triple helix.

3) Symposium presented at SLTC 117th Annual Conference 26th April 2014, Northampton, UK.

Hannah C. Wells[1], Katie H. Sizeland[1], Richard L. Edmonds[2], William Aitkenhead[2], Peter Kappen[3], Chris Glover[3], Bernt Johannessen[3], Richard G. Haverkamp[1]

[1] School of Engineering and Advanced Technology, Massey University, New Zealand

[2]Leather and Shoe Research Association, Palmerston North, New Zealand

[3]Australian Synchrotron, Melbourne, Victoria, Australia

ABSTRACT

Biochar from Leather - the Fate of Chromium

Chrome-tanned leather waste, both post-consumer and tanning industry scrap, must be disposed of in an acceptable manner. There are environmental concerns around the chromium content of leather waste and the possibility of chromium leaching into the environment. We investigated the production of biochar from leather, the leaching characteristics of this char and the chemical form of Cr in the char. Chrome tanned leather was heated in an oxygen deficient environment at temperatures ranging from 500–1000 °C to form a char. The char was leached in 1 M HCl and the leachate analysed for Cr content. The char was analysed by synchrotron based Cr K edge X-ray absorption spectroscopy for the chemical state of the Cr. It is found that Cr does not leach from the biochar. The Cr is present in the high temperature char as highly dispersed Cr carbide, an insoluble and very stable material. Biochar made from leather waste may be beneficial to the environment as both a soil enhancer and for long term carbon sequestration.

4) Poster presented at the 1st MBE (Matrix Biology Europe) conference (XXIVth FECTS meeting), 21 - 24 June 2014, Rotterdam

---

Hannah C. Wells[1], Katie H. Sizeland[1], Richard L. Edmonds[2], Nigel Kirby[3], Adrian Hawley[3], Stephen Mudie[3], Richard G. Haverkamp[1].

[1] School of Engineering and Advanced Technology, Massey University, New Zealand

[2]Leather and Shoe Research Association, Palmerston North, New Zealand

[3]Australian Synchrotron, Melbourne, Victoria, Australia

ABSTRACT

Poisson Ratio of Collagen Fibrils

The main structural component of skin and tendons is type I collagen. These tissues are elastic and deform reversibly under stress. The mechanical properties of individual collagen fibrils contribute to the mechanical properties of the tissues which they comprise. We have used synchrotron based small angle X-ray scattering to investigate the deformation of collagen fibrils during stress in pericardium. Fibril diameter is calculated from the scattering pattern and fibril elongation is calculated from the diffraction peaks resulting from the d-spacing. As collagen fibrils are stretched their density increases. We are able to determine the poisson ratio for collagen fibrils. This knowledge may be incorporated into models of the macrolevel behaviour of tissues.

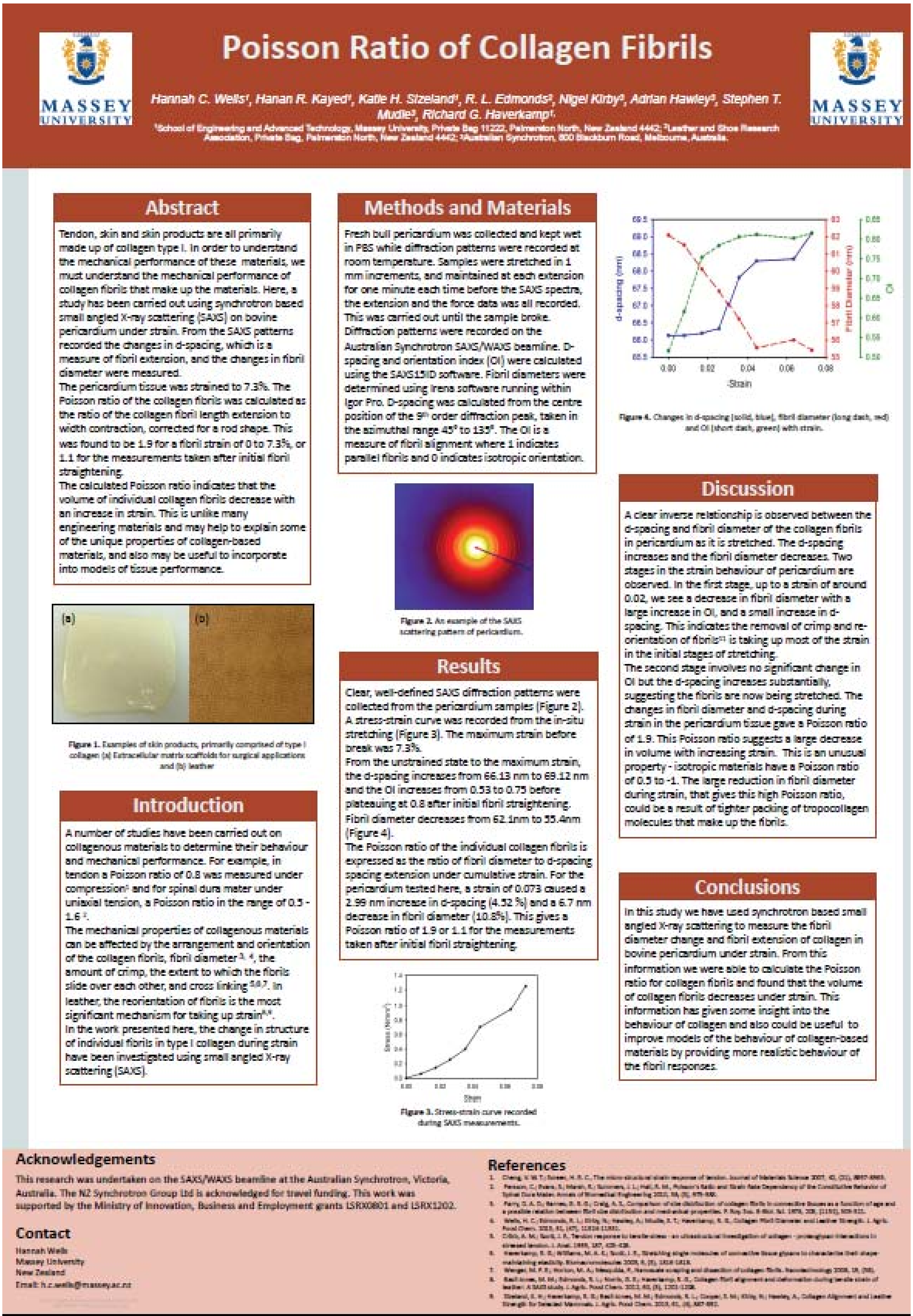

5) Symposium presented at the 1st MBE (Matrix Biology Europe) conference (XXIVth FECTS meeting), 21 - 24 June 2014, Rotterdam

Richard G. Haverkamp[1], Katie H. Sizeland[1], Hannah C. Wells[1], Hanan Kayed[1], Richard L. Edmonds[2], Nigel Kirby[3], Adrian Hawley[3], Stephen Mudie[3],.

[1] School of Engineering and Advanced Technology, Massey University, New Zealand

[2]Leather and Shoe Research Association, Palmerston North, New Zealand

[3]Australian Synchrotron, Melbourne, Victoria, Australia

ABSTRACT

Orientation of Collagen Fibrils in Tissue

Collagen (Type I) is the main structural component of skin and other animal tissues. We have investigated aspects to the structural basis of leather and pericardium using synchrotron based small angle X-ray scattering. We obtained quantitative measurements of fibril orientation, fibril size, and details of the structure (D-spacing) of individual fibrils. We measured tissues both in a relaxed state and under tension. Under tension, the extension of fibrils can also be measured. When tissues are stretched the fibrils first align in the direction of stress and then individual fibrils begin to stretch. We found that strength for leather and pericardium is a function of collagen fibril alignment. When fibrils are aligned in the plane of the tissue the material is stronger. These studies provide an insight into the structural basis of strength in tissues and the behaviour of these materials under stress.

6) Poster presented at the Fourth International Conference on Multifunctional, Hybrid and Nanomaterials, 9-13th March 2015, Sitges, Spain.

Hannah C. Wells[1], Katie H. Sizeland[1], Hanan R. Kayed[1], Nigel Kirby[2], Adrian Hawley[2], Stephen T. Mudie[2], Richard G. Haverkamp[1]

[1] School of Engineering and Advanced Technology, Massey University, New Zealand

[2]Leather and Shoe Research Association, Palmerston North, New Zealand

ABSTRACT

Poisson Ratio of Collagen Fibrils Measured by SAXS

Tendon, skin and skin products are primarily composed of the fibrous protein, type I collagen. Collagen provides strength and stability in biological tissues and therefore the mechanical properties of collagen are important in understanding the overall behaviour of the tissues. While the bulk tissues themselves have been well characterized, little is known about the mechanical properties of the individual collagen fibrils.

To determine the behaviour of collagen fibrils we have carried out an investigation using SAXS on bovine pericardium under stress. From the SAXS diffraction patterns the fibril diameter is calculated, the fibril elongation is calculated from the diffraction peaks that result from the collagen d-spacing.

The tissue is strained 25% with a corresponding strain in the collagen fibrils of 0.045 observed. There are two stages in the collagen fibril structure that we observe while increasing strain. The first stage, at low strain, we observe a decrease in fibril diameter, a small increase in d-spacing and a large increase in OI. This suggests the strain is taken up by the reorientation and removal of crimp in the fibrils. The second stage involves a small change in OI but the d-spacing increases significantly and the fibril diameter decreases. This indicates there is an increase in stress on each of the individual fibrils. We are able to determine the Poisson ratio for collagen fibrils from the changes in fibril diameter and d-spacing observed. The Poisson ratio, corrected for a rod shape, can be calculated using:

$$v' = -\frac{\sqrt{\pi}/2(\frac{\Delta D}{D})}{\Delta L/L}$$

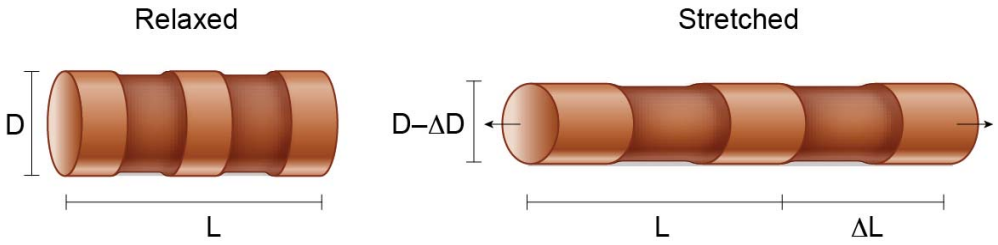

A Poisson's ratio of 2.1±0.7 was determined for a tissue strain from 0 to 0.25. This indicates the volume of the individual collagen fibrils decrease with an increasing strain which is an unusual observation for most engineering materials. This knowledge may help to explain some of the remarkable properties of collagen-based biomaterials.

Poisson Ratio of Collagen Fibrils Measured by SAXS

Hannah C. Wells[1], Katie H. Sizeland[1], Hanan R. Kayed[1], Nigel Kirby[2], Adrian Hawley[2], Stephen T. Mudie[2], Richard G. Haverkamp[1]

[1]School of Engineering and Advanced Technology, Massey University, Private Bag 11222, Palmerston North, New Zealand 4442; [2]Australian Synchrotron, 800 Blackburn Road, Melbourne, Australia.

Fourth International Conference on Multifunctional, Hybrid and Nanomaterials
9-13th March 2015, Sitges, Spain

Introduction

Type I collagen is the main structural protein of tendon, skin and skin products, providing strength and stability in these biological tissues. The mechanical properties of collagen-based tissues are fundamental to their natural and industrial uses. While the bulk materials have been widely studied, the mechanical properties of the individual collagen fibers that make up these materials have not.

Here we look at the Poisson ratio (ν) of collagen fibrils to characterize the collagen fibril structure and performance in tissue during tension. Previous studies on the bulk tissues have given Poisson ratio values greater than 0.5, indicating the volume of the tissue decreases as it is strained.

We have determined the behavior of collagen fibrils when stress is applied using synchrotron based small angle X-ray scattering (SAXS). Bovine pericardium was used as a collagen source, which was strained up to 25% during data collection.

Methods

SAXS Analysis

Bull pericardium was used as the collagen source for analysis using SAXS. The pericardium was kept fresh in PBS buffer while diffraction patterns were recorded on the SAXS/WAXS beam line at the Australian Synchrotron. The samples were stretched in 1 mm increments and were maintained at each position for one minute before SAXS spectra, the extension and the force were recorded. This was repeated for each sample, until the sample broke.

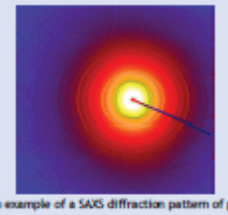

Figure 1. An example of a SAXS diffraction pattern of pericardium

From the recorded diffraction patterns, the d-spacing and orientation index (OI) were determined using saxs15ID software, and the fibril diameters were determined using Irena software running with Igor Pro. The d-spacing is a measure of fibril extension, the OI is a measure of fibril alignment in the bulk material.

Calculating Poisson's Ratio

The Poisson's ratio, ν, is the ratio of transverse strain to longitudinal strain in the loading direction and is calculated from the equation:

$$\nu = \frac{\left(\frac{\Delta W}{W}\right)}{\Delta L / L}$$

Where W is the width of a cube or bar, and L is the length of a cube or bar.

The Poisson ratio for collagen fibrils can be expressed as the ratio of fibril diameter to d-spacing extension under cumulative strain. Since ν is defined for a cube, we corrected the ratio by $\sqrt{\pi}/2$. Therefore, the equation for the Poisson ratio of collagen fibrils becomes:

$$\nu' = \frac{\sqrt{\pi}/2\left(\frac{\Delta D}{D}\right)}{\Delta L / L}$$

Where D is the fibril diameter and L is the d-spacing or fibril extension.

Collagen Structure During Tension

The tissue was strained up to 25%. We observed two stages in the structural changes at the collagen fibril level during strain.

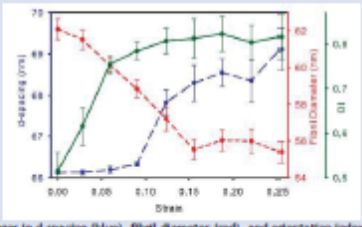

Figure 2. Changes in d-spacing (blue), fibril diameter (red), and orientation index (OI) of the collagen fibrils in pericardium as strain is increased. Figure from Wells et al. (2015) J. Appl. Phys. 117, 044701.

In the first stage (up to strain of 0.09), we notice a decrease in the collagen fibril diameter with a small increase in d-spacing and a large increase in OI. During this phase of strain, most of the strain is taken up by the reorientation of the individual fibrils within the tissue.

The second stage of strain (above 0.09) there is little change in OI, however the d-spacing begins to increase and the fibril diameter decreases. This indicates the stress is now mostly on the individual collagen fibrils. At a strain above 0.15, the fibrils continue to stretch however the change in fibril diameter plateaus.

Poisson's Ratio

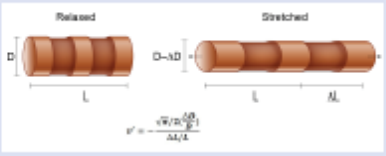

From an unstrained state to maximum strain before rupture, the d-spacing with the fibrils increased 4.5%. The fibril diameter decreased 10.8%. From the changes in d-spacing and fibril diameter, the Poisson's ratio was calculated to be 2.1±0.7 when the tissue is strained up to 25%.

The high Poisson's ratio (>0.5) indicates a volume decrease in the fibrils as the tissue is strained. This could help to explain some of the unique properties of collagen based materials. The high Poisson ration could be explained by tighter packing within the fibril under strain, where there could be compression of hydrogen bonding within the fibril, micro fibril or tropocollagen.

Conclusion

Synchrotron based SAXS has been a useful tool for characterizing the structure of individual collagen fibrils within pericardium tissue, as strain is applied to the tissue. From the SAXS diffraction patterns, the collagen d-spacing (or fibril extension), fibril diameter and orientation of the fibrils were determined and used to calculate the Poisson's ratio of collagen of 2.1 ± 0.7.

Previous studies on collagen based bulk materials have given $\nu > 0.5$ and here we have provided experimental evidence that the individual collagen fibrils may also have $\nu' > 0.5$. This suggests that this property of collagen fibrils may contribute to the bulk properties of tissues.

Acknowledgements

This research was carried out on the SAXS/WAXS beamline at the Australian Synchrotron, Victoria, Australia. The NZ Synchrotron Group Ltd is acknowledged for travel funding. This work was supported by the Ministry of Innovation, Business and Employment.

7) Symposium presented at the Fourth International Conference on Multifunctional, Hybrid and Nanomaterials, 9-13th March 2015, Sitges, Spain.

Haverkamp, R. G., Sizeland, K. H., ***Wells, H. C.,*** *Kayed, H. R., Edmonds, R. L., Kirby, N., Hawley, A., & Mudie, S.*

[1]*School of Engineering and Advanced Technology, Massey University, New Zealand*

[2]*Leather and Shoe Research Association, New Zealand*

[3]*Australian Synchrotron, Melbourne, Victoria, Australia*

ABSTRACT

Strength in Collagen Biomaterials

Natural collagen materials are used in industrial and medical applications; for example leather for shoes and garments, and extra cellular matrix materials for surgical scaffolds. For most applications the strength of the material is a critical performance property. Therefore, an improved understanding of how the structure of these natural and processed materials relates to strength is needed. A range of collagen based materials have been characterised using synchrotron based small angle X-ray scattering (SAXS). The distribution of collagen fibril orientation in a material can be determined from this technique. In leather, fibril orientation in the plane of the leather was found to correlate strongly with the tear strength of the leather. Highly aligned collagen fibrils lead to stronger leather. This is explained by a structural model. Mechanisms of nanostructural response to strain in leather, medical scaffold material and pericardium were also investigated by these techniques. Collagen fibrils rearrange and then stretch but these behaviours are governed by a number of factors and the response can be altered by chemical and physical treatments. A better understanding of the structure and strain characteristics of collagen biomaterials has resulted and this enables the design of stronger materials for industrial and medical applications.

8) Symposium presented at the 66th Annual Leather and Shoe Research Association Conference, 24th August 2015, Queenstown, New Zealand.

Hannah C. Wells & Richard G. Haverkamp.

School of Engineering and Advanced Technology, Massey University, New Zealand.

An Investigation into Looseness in Bovine Hides and Leather

No abstract required.

9) Poster presented at the Advanced Materials World Congress, 23-26 August 2015, Stockholm, Sweden.

Hannah C. Wells[1], Geoff Holmes[2], Richard G. Haverkamp[1]

[1] Massey University, New Zealand

[2]Leather and Shoe Research Association, Palmerston North, New Zealand

ABSTRACT

Microstructure and Looseness in Bovine Leather

Around 10% of bovine leather manufactured suffers from a condition known as looseness which makes it unsuitable for high value applications. Looseness is identified by the display of creases on the grain of concave folded leather. However, the microstructural basis for looseness is not known. Currently, looseness can only be found in leather after much of the processing has taken place, and therefore results not only in a much lower value item, but also a waste in chemical materials and labour. We have used ultrasonic imaging, small angle X-ray scattering, scanning electron microscopy, light microscopy, tensile and tear strength tests to characterize loose and tight (non-affected) leather. Loose leather was found to contain a more open structure with greater space between collagen fibres particularly around the grain-corium boundary, and more aligned collagen fibrils particularly in the corium. Loose leather, despite its lower value, is found to have a higher tensile strength than tight leather, which is likely to be due to the greater fibril alignment. While greater alignment leads to stronger leather and therefore leather of greater value, looseness occurs when this alignment is too great leading to a weak connection between the layers and a subsequent degradation in the value of the leather. This study has helped identify the nanostructural characteristics of loose leather, and may be useful for further studies into methods of preventing or reducing looseness occurring during leather manufacturing. Achieving this would lead to significant financial benefits for the leather industry worldwide.

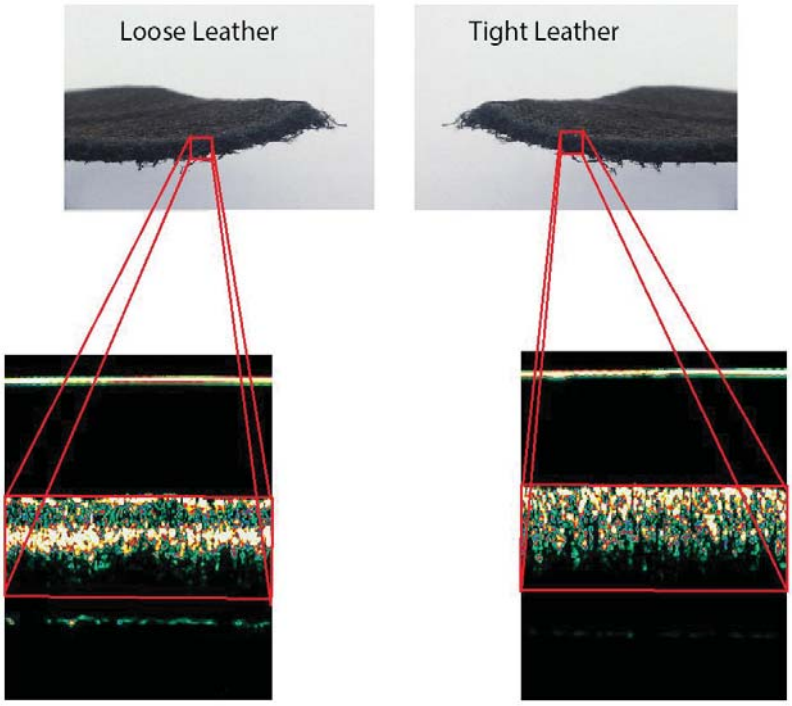
Loose Leather
Tight Leather

Microstructure and Looseness in Bovine Leather

Hannah C. Wells[1], Geoff Holmes[2], Richard G. Haverkamp[1]
[1]School of Engineering and Advance Technology, Massey University, New Zealand, [2]Leather and Shoe Research Association, New Zealand

Poster Presented at the Advanced Materials World Congress 23 – 26 August 2015, Stockholm, Sweden.

Introduction

Around 10% of bovine hides when processed into leather, produce poor quality 'loose' leather which is unsuitable for high value applications. Loose leather is identified by the presence of creases or wrinkles on the grain surface of concave folded leather , known as a break test (see figure 1).

The structural characteristics of looseness and how it develops in hides are not well understood. Therefore we have used a range of techniques such as ultrasonic imaging, SAXS, SEM, and TEM to try and understand the structural differences between loose and non-affected (or tight) leather.

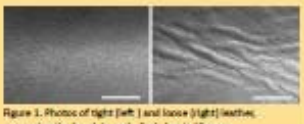

Figure 1. Photos of tight (left) and loose (right) leather, comparing the break in each. Scale bar is 10 mm.

Ultrasonic Testing

Ultrasonic images were recorded using a Dermascan C USB device (Cortex Technologies, Denmark). A 20MHz 2D scanning probe with an internal water chamber was used to carry out scans at 6-8 frames per second. The ultrasonic imaging was able to show a clear difference between the internal structure of loose and tight leather (see fig 2a and 1b). Loose leather has a band of lower intensity in the grain or grain-corium boundary region.

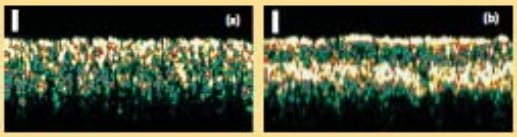

Figure 2. Ultrasonic images of a) tight leather and b) loose leather. Scale bar is 1 mm. Axial and lateral resolution of the scans in leather were 97 µm and 150 µm respectively.

This banding pattern suggests there is a difference in packing arrangement of collagen fibres in loose leather compared with tight leather, with larger gaps between fibres in the loose defected leather.

Scanning Electron Microscopy

Samples were fixed for 8 h in a modified Karnovsky's fixative, prepared, and gold sputter-coated before being viewed in the FEI Quanta 200 Environmental Scanning Electron Microscope (Manawatu Microscopy Centre, NZ) at an accelerating voltage of 20kV.

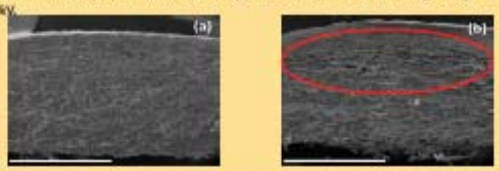

Figure 3. SEM images of cross sections of a) tight leather and b) loose leather. Scale bar is 2 mm.

The SEM images show that the loose leather samples appear to have a region below the grain that contains loosely packed collagen fibres (figure 3b), whereas the tight leather samples did not.

Transmission Electron Microscopy

Samples went through a multiple step preparation process before being cut with a glass knife into 1 µm sections and also a diamond knife into 100 nm sections and examined with a FEI Tecnai G2 Biotwin Transmission Electron Microscope.

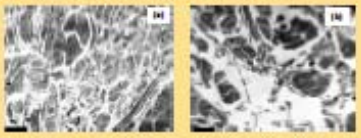

Figure 4. TEM images of the grain layer of a) tight leather and b) loose leather. Scale bar is 5 µm.

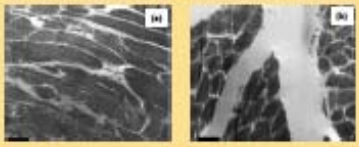

Figure 5. TEM images of the corium layer of a) tight leather and b) loose leather. Scale bar is 5 µm.

In both the corium and grain, there appears to be larger gaps in between the bundles of collagen fibres within leather.

Small Angle X-ray Scattering

Small angle X-ray scattering was carried out on loose and tight leather samples. A significant difference was found in the orientation or direction of collagen fibrils throughout the thickness of loose and tight leather samples. The fibrils in loose leather appear to be more orientated in one direction, where as tight leather appeared to have a structure of fibrils more varied in orientation.

Conclusions

The leather defect, known in the industry as looseness, appears to be the result of a poor connection between layers in the leather particularly in the lower grain or grain-corium boundary region. This poor connection is partly due to the aligned fibril structure of loose leather, and this results in a more open structure. This open structure of loose leather can be seen in the ultrasonic, SEM and TEM images.
Since this study we have been looking at the causes of looseness occurring in the leather manufacturing industry and possible solutions.

Acknowledgements
This research was supported by a grant from the Ministry of Business Innovation and Employment. Research was undertaken on the SAXS/WAXS beamline at the Australian Synchrotron.

10) **Poster presented at the Advanced Materials World Congress, 23-26 August, 2015, Stockholm Sweden. *This poster was chosen for the IAAM Young Scientist of the Year Award for 2015.***

Hannah C. Wells & Richard G. Haverkamp.

Massey University

ABSTRACT

Mechanical Behaviour of Collagen Fibrils with Strain

Type I collagen is the major component of tendon, skin and skin products such as leather. Type I collagen is a fibrous protein that provides most of the strength, stability and structure in biological tissues and therefore plays a major role in the overall behaviour of the bulk tissues. Despite many bulk tissues already being well studied and characterized themselves, little is understood about the mechanical behaviour of the individual collagen fibres that make up the bulk tissues.

A study has been carried out using SAXS on bovine pericardium to investigate how collagen fibrils behave while under stress. The diameter of the collagen fibrils and fibril elongation can be determined from SAXS diffraction patterns. The fibril elongation is calculated from the diffraction peaks that form in the SAXS diffraction patterns as a result of the collagen d-spacing.

When the bulk tissue was strained 25 %, a strain of 4.5 % was observed in the individual collagen fibrils. There appeared to be two phases of structural change in the fibrils while under increasing strain. In the first phase, when the strain is low, the fibril diameter decreases with a small increase in d-spacing and a large increase in OI. In this stage of low strain, it appears the strain is mostly taken up by the re-orientation and the removal of any crimp in the fibrils. The second stage, when strain is higher, involves a smaller change in OI, but the d-spacing increases significantly with decreasing fibril diameter. From the information collected on the fibril diameters and fibril extension or change in d-spacing, the Poisson ration can be determined. The Poisson ratio, corrected for a rod-shape, can be calculated using the equation:

$$v' = -\frac{\sqrt{\pi}/2(\frac{\Delta D}{D})}{\Delta L/L}$$

From a tissue strain from 0 to 25%, a Poisson ratio of 2.1 ± 0.7 was calculated, indicating a decrease in volume of the individual collagen fibrils as strain is increased. This is unlike most engineering materials and may be useful in explaining the unique characteristics and behaviour of collagen biomaterials.

Mechanical Behaviour of Collagen Fibrils with Strain

Hannah C. Wells, Richard G. Haverkamp.
School of Engineering and Advanced Technology, Massey University, New Zealand

Introduction

Type I collagen is the main structural component of biological tissues such as skin and tendon, and also skin products including leather and extracellular matrix scaffolds for surgical applications.

The primary function of type I collagen is to provide the majority of the strength, stability and structure of the material it forms. A significant amount of information has previously been collected on the bulk structural behaviour of each of collagen materials, however, little is known about the mechanical behaviour of the individual collagen fibrils that make up these tissues.

This study used small angle X-ray scattering (SAXS) to look at the individual collagen fibrils within the bulk materials while applying strain, in order to give a better understanding of one of the factors that contributes to the bulk properties of tissues during stress and strain.

Methodology

Fresh samples of bovine pericardium were cut, washed and stored in phosphate buffer solution for transportation to the Australian Synchrotron for data collection. SAXS diffraction patterns were recorded while the pericardium was subjected to strain in the beam line.

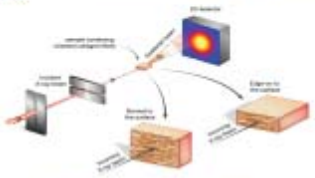

FIGURE 1: The SAXS experimental set-up.

From the scattering patterns, the average collagen fibril diameter, elongation and fibril orientation were determined.

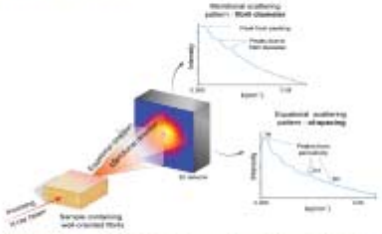

FIGURE 2 : Meridional and equatorial scattering from a sample containing well-oriented collagen fibrils.

Fibril elongation and fibril diameter were calculated from different parts of the scattering pattern. The fibril elongation was calculated from the shift in the diffraction peaks which result from the collagen d-spacing n the fibrils and these are prominent in the direction of strain. Fibril diameter was determined by fitting the SAXS scattering data in the meridional direction to a "cylinder AR" shape model using the Irena software package. From the fibril elongation and diameter the Poisson's ratio was calculated and corrected for a rod-shape model.

The orientation index, a measure of the how orientated the fibrils are, is defined as (90° - OA)/90°.OA is the minimum azimuthal angle range that contains 50% of the fibrils. Here it has been converted to an index where 0 is anisotropic and 1 is completely oriented. The azimuthal direction of the d-spacing diffraction peaks was used to determine orientation.

Results and Conclusions

The maximum strain obtained before rupture of the sample was 25%. There appeared to be two stages in the structural changes of collagen with increasing strain.

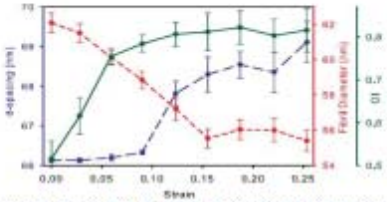

FIGURE 3: d-spacing (blue, long dash), fibril diameter (red, short dash) and OI (green, solid) changes with increasing strain.

In the initial stage (at low strain), we observe a large increase in the OI, with a small decrease in fibril diameter and small increase in d-spacing. It appears the strain is initially mostly taken up by the re-orientation of fibrils and removal of crimp. No significant strain is being taken up by the fibrils themselves at this stage.

The second stage (strain above 0.09) involves no significant change in OI but instead there is a large increase in d-spacing with a decrease in fibril diameter. It is during this stage that the individual fibrils undergo significant deformation due to strain.

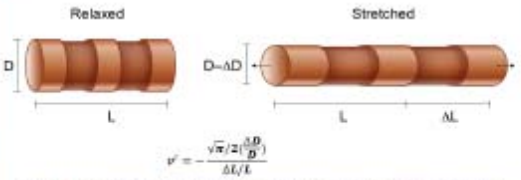

$$\nu' = -\frac{\sqrt{\pi}/2(\frac{\Delta D}{D})}{\Delta L/L}$$

FIGURE 4: Poisson's ratio, ν', from the change in collagen fibril diameter and fibril length upon stretching.

Using the fibril diameter and fibril elongation data, the Poisson's ratio was calculated to be 2.1 ± 0.7 for a tissue strain from 0 to 25%. This indicated a decrease in volume of the individual fibrils as strain increased. A Poisson's ratio of greater than 0.5 is not possible in anisotropic materials, so this behavior is unlike most engineering materials.

The collagen fibrils respond to strain (or resist strain) by compressing internally and this may contribute to the remarkable strength of the fibrils. This understanding may be useful in explaining some of the unique properties of collagen biomaterials.

ACKNOWLEDGEMENTS
This research was supported by a grant from the Ministry of Business and Innovation and Employment. This research was carried out on the SAXS/WAXS beamline at the Australian Synchrotron, Melbourne, Australia.

12) Poster presented at the 9th Annual CIGR Section VI International Technical Symposium, 16th – 20th November 2015, Massey University, Albany Campus, Auckland, New Zealand.

K. H. Sizeland[1], H. R. Kayed[1], H. C. Wells[1], N. Kirby[2], A. Hawley[2], S. Mudie[2], R. L. Edmonds[3], R. G. Haverkamp[1].

[1] Massey University, New Zealand

[2]Australian Synchrotron, Melbourne, Victoria, Australia

[3]Leather and Shoe Research Association, Palmerston North, New Zealand

ABSTRACT

Nanostructural Analysis of Bioengineered Tissues for Enhanced Performance

Collagen is the main structural component of a number of natural and processed biomaterials. The strength of these materials is often of crucial importance to their final applications. The structural foundation of strength in collagen biomaterials is not fully understood. We used synchrotron based small angle X-ray scattering to investigate the fibril structure of collagen in leather, pericardium, and surgical scaffolds. Samples were put under increasing strain so any structure-strength relationships could be investigated. Atomic force microscopy and histology compliment small angle X-ray scattering. Strong correlations between the strength of collagen biomaterials and fibril orientation have been found and are dependent on tissue type, tissue source, tissue age, and the chemical and mechanical processing of the tissue. These findings provide valuable insight into the basis of strength of bioengineered tissues and will inform future tissue selection and processing to maximise the value created from these animal bioresources.

Nanostructural Analysis of Bioengineered Tissues for Enhanced Performance

K. H. Sizeland,[1] H. R. Kayed,[1] H. C. Wells,[1] N. Kirby,[2] A. Hawley,[2] S. Mudie,[2] R. L. Edmonds,[3] R. G. Haverkamp.[1]

[1]School of Engineering and Advanced Technology, Massey University, [2]Australian Synchrotron, [3]Leather and Shoe Research Association.

Introduction

Collagen is the main structural component of a number of natural and processed biomaterials. The strength of these materials is often of crucial importance to their final applications. The structural foundation of strength in collagen biomaterials is not fully understood. We used synchrotron techniques to investigate the fibril structure of collagen in leather, pericardium, and surgical scaffolds. Samples were put under increasing strain so any structure-strength relationships could be investigated. These findings provide valuable insight into the basis of strength of bioengineered tissues and will inform future tissue selection and processing to maximise the value created from these animal bioresources.

SAXS Analysis

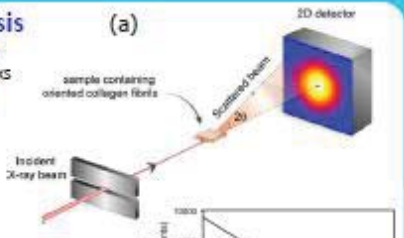

Figure 1. Example of SAXS analysis: (a) SAXS sample setup; (b) integrated intensity profile.

$$OI = (90^\circ - OA)/90^\circ$$

Where OA is the minimum azimuthal angle range containing 50% of the fibrils.

OI = 1 → perfectly aligned fibrils
OI = 0 → isotropic fibril arrangement

Leather

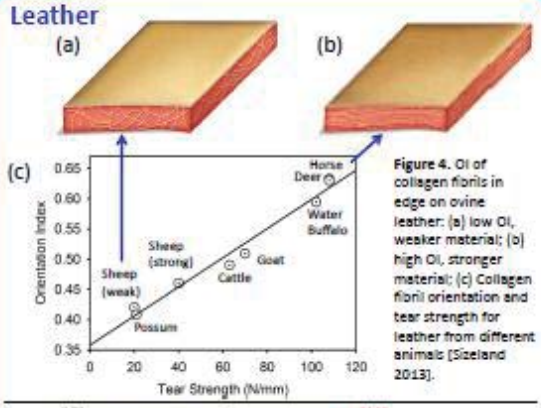

Figure 4. OI of collagen fibrils in edge on ovine leather: (a) low OI, weaker material; (b) high OI, stronger material; (c) Collagen fibril orientation and tear strength for leather from different animals [Sizeland 2013].

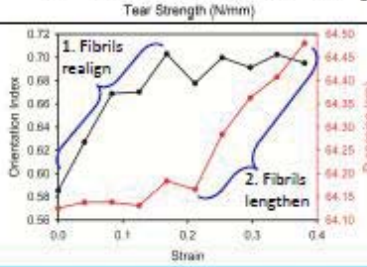

Figure 5. D-spacing and OI versus strain measured edge-on for ovine leather: (•) D-spacing; (•) OI [Basil-Jones 2012].

Pericardium

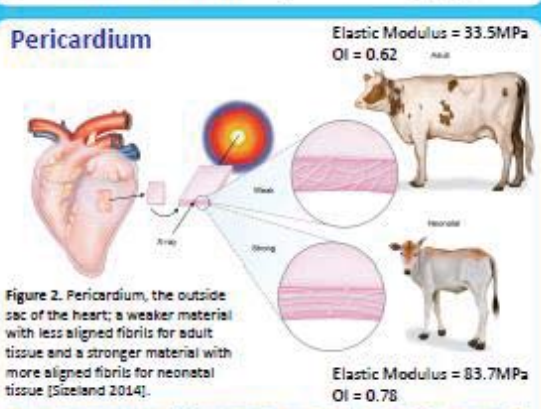

Figure 2. Pericardium, the outside sac of the heart; a weaker material with less aligned fibrils for adult tissue and a stronger material with more aligned fibrils for neonatal tissue [Sizeland 2014].

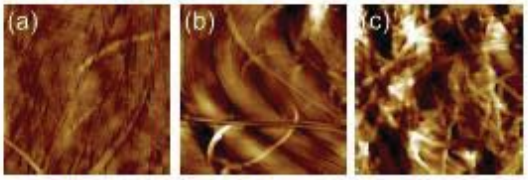

Figure 3. Atomic force microscopy images for (a) native pericardium; (b) chondroitinase ABC treated pericardium; (c) glutaraldehyde treated pericardium [Kayed 2015].

Surgical Scaffolds

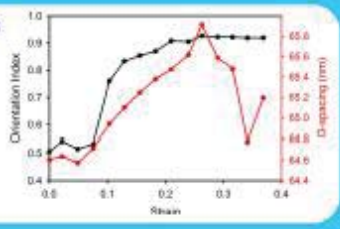

Figure 7. OI and D-spacing versus strain for ovine forestomach surgical scaffold material.

References

1. Sizeland, K. H., Wells, H. C., Higgins, J. J., Cuanan, C. M., Kirby, N., Hawley, A., & Haverkamp, R. (2014). Age Dependent Differences in Collagen Fibril Orientation of Glutaraldehyde Fixed Bovine Pericardium. *BioMed Research International* Volume, Article ID 189197.
2. Kayed, H. R., Sizeland, K. H., Kirby, N., Hawley, A., Mudie, S. T., & Haverkamp, R. (2015). Collagen Cross Linking and Fibril Alignment in Pericardium. *RSC Advances*, 5(5), 3611-8.
3. Sizeland, K. H., Basil-Jones, M. M., Edmonds, R. L., Cooper, S. M., Kirby, N., Hawley, A., & Haverkamp, R. G. (2013). Collagen Orientation and Leather Strength for Selected Mammals. *Journal of Agricultural and Food Chemistry*, 61(4), 887-892.
4. Basil-Jones, M. M., Edmonds, Norris, G., & Haverkamp, R. G. (2012). Collagen Fibril Alignment and Deformation During Tensile Strain of Leather: A Small Angle X-ray Scattering Study. *Journal of Agricultural and Food Chemistry*, 60(5), 1201-1208.

Acknowledgements

This research was supported by grants from the Ministry of Business ,Innovation, and Employment. LASRA, Mesynthes, and Southern Lights Biomaterials supplied the samples. This research was undertaken on the SAXS/WAXS beamline at the Australian Synchrotron, Victoria, Australia.

MASSEY UNIVERSITY
TE KUNENGA KI PŪREHUROA

Ministry of Business, Innovation & Employment

LASRA

13) Poster presented at the 9th Annual CIGR Section VI International Technical Symposium, 16th – 20th November 2015, Massey University, Albany Campus, Auckland, New Zealand.

Hannah C. Wells[1], Katie H. Sizeland[1], Nigel Kirby[2], Adrian Hawley[2], Stephen Mudie[2] & Richard G. Haverkamp[1]

[1]Massey University, New Zealand

[2]Australian Synchrotron, Melbourne, Victoria, Australia

ABSTRACT

A Comparison of Strength and Collagen Structure in Bovine, Porcine and Human Acellular Dermal Matrix Materials for Surgical Applications

Acellular dermal matrix (ADM) materials are scaffold materials used in surgical applications to reconstruct or replace tissue. The materials need to be immunologically compatible, strong and elastic. These properties make dermal tissues an ideal raw material for the synthesis of ADM materials, through methods of decellurization. Bovine and porcine dermal tissues are readily available as by products from the meat industry, and can offer another means of income for meat industries. Human dermal tissue is also used to synthesize ADM materials. Here we aim to compare physical properties of bovine, porcine and human origin ADM materials, and relate these properties to strength. The relationship between age in bovine species and ADM material strength is also studied.

Small angle X-ray scattering (SAXS) and scanning electron microscopy (SEM) were used to observe the ADM structures. An instron was used to carry out multiple tear and tensile tests on each material.

Tear analysis test showed that bovine and human had similar thickness normalised tear strengths (75-124 N/m and 79 N/m respectively). Porcine was weaker, with an average tear strength of 43 N/m. Tensile strengths were similar for all species (18-34 N/mm^2 for bovine, 18 N/mm^2 for human and 21 N/mm^2 for porcine). SEM images of the three materials showed that bovine ADM has a more open structure than the others when viewed under magnification. SAXS showed that the collagen fibril arrangement in the materials when viewed perpendicular to the surface varied among species. Human had an isotropic unimodal arrangement of fibrils (OI = 0.08), porcine was strongly bimodal and highly orientated (OI = 0.61) and the bovine was in between with a bimodal distribution, becoming more isotropic with age (OI = 0.14 - 0.24). The specific structural properties of each of these materials may determine which are more suitable for particular surgical applications.

Strength and Collagen Structure in Bovine, Porcine and Human Acellular Dermal Matrix Materials for Surgical Applications

Hannah C. Wells[1], Katie H. Sizeland[1], Nigel Kirby[2], Adrian Hawley[2], Stephen Mudie[2], and Richard G. Haverkamp[3].

[1]School of Engineering and Advanced Technology, Massey University, Albany, Auckland, New Zealand; [2]Australian Synchrotron, 800 Blackburn Road, Clayton, Melbourne, Victoria, Australia; [3] School of Engineering and Advanced Technology, Massey University, Palmerston North, New Zealand.

9th CIGR Section VI International Technical Symposium 2015, Auckland New Zealand

Introduction

Acellular dermal matrix (ADM) materials are scaffold materials used in the reconstruction and replacement of tissues in surgery. ADM materials are produced through the decellularization of dermal tissues,. Commonly used dermal tissues used include bovine, porcine and human tissue. The advantage of using biomaterial tissues as scaffold materials over synthetic materials is that they are more immunologically compatible. Other important properties for successful surgical application include material strength and elasticity. These physical properties vary depending on the source material used. Here we compare collagen structures and strength of ADM materials produced from three common biomaterials; bovine, porcine and human dermal tissue. The correlation between age of the animal and tissue strength is also studied for bovine ADM.

SAXS and SEM have been used to investigate collagen structure and tear and tensile tests were carried out on each type of ADM material.

Materials and Methods

Commercial materials were sourced, including Strattice Firm porcine ADM (LifeCell Corporation, US), Alloderm human ADM (LifeCell Corporation, US) and a range of SurgiMend bovine ADM (TEI Biosciences, US). The SurgiMend bovine materials included a third trimester fetal ADM sample and four neonatal ADM samples with varying thicknesses (approx 1.7, 2.0, 3.0 and 4.0 mm).

Synchrotron based SAXS was carried out at the Australian Synchrotron on the SAXS/WAXS beamline. The details of the experimental set-up and parameters used are given in detail in Wells et al. (2015). The data processing was carried out using Scatterbrain Software.

SAXS patterns were recorded in two directions through the samples (flat to the surface and normal to the surface).

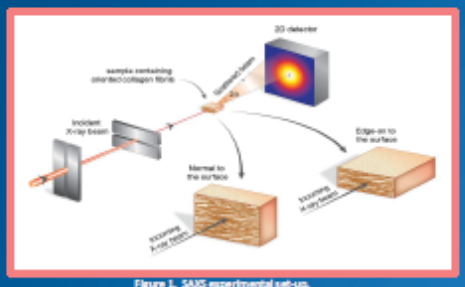

Figure 1. SAXS experimental set-up.

From the SAXS data it was possible to determine the average collagen fibril diameter , collagen d-spacing, and the average fibril orientation (or orientation index (OI)). Orientation Index (OI) was used as a quantification of the spread of fibril orientation and was calculated from:

$$OI = \frac{90^\circ - OA}{90^\circ}$$

Where OA = orientation angle = the minimum azimuthal angle range containing 50% of the fibrils, converted to an index using the spread in azimuthal angle of the diffraction peaks.

Tear and tensile strength was also measured for each sample. This was done using standard methods on an Instron device. Duplicate tests were run for each sample and results were averaged.

Results

Tear test

Thickness normalised, the strongest material was the thicker bovine neonatal material, followed by the other neonatal bovine materials , the fetal bovine material and human material, and porcine was the weakest overall. No correlation was found between tear strength and OI, d-spacing or fibril diameter.

Table 1. Tear results for ADM materials

Sample	Thickness (mm)	Force at rupture (N)	Thickness-normalized force at rupture (N/mm)
Bovine Fetal	0.98	76.1	78.0
Bovine Neonatal 1.7	1.67	127.0	76.0
Bovine Neonatal 2.0	2.01	172.0	85.6
Bovine Neonatal 3.0	3.02	227.0	75.1
Bovine Neonatal 4.0	3.98	494.3	124.2
Porcine	1.69	73.0	43.2
Human	1.01	79.5	79.0

Tensile test

Tensile tests were performed in to directions for each sample. Thickness normalised, fetal bovine had the highest cross-sectional tensile strength of 39.3 N/mm^3. Human was the weakest at 17N/mm^3 and the bovine materials ranged from 18.5 – 23.8 N/mm^3.

Collagen structure

SEM revealed a more open structure in bovine ADM than human and porcine (fig 2).

Fig 2. SEM images through the thickness of the ADM materials: a) bovine; b) porcine; c) human. Bar is 500 µm.

From the SAXS data, it was determined that d-spacing and fibril diameter did not vary significantly across species or show any correlation to strength. However the arrangement of the fibrils, when viewed perpendicular to the material surface, did vary between species. The variation between species in fibril arrangement is illustrated in figure 3 below. Porcine has a fibril arrangement as seen in (a), bovine is best represented by (b) and human by (c).

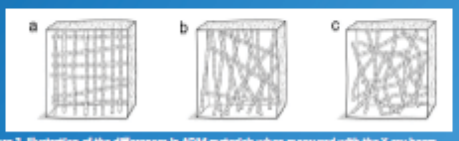

Figure 3. Illustration of the differences in ADM materials when measured with the X-ray beam perpendicular to the materials top surface. (a) is highly aligned in two orthogonal directions, (b) partly orientated and (c) largely isotropic.

Conclusion

The strongest material was bovine ADM, followed by human and porcine was the weakest.

Bovine ADM has a more open structure than human and porcine ADM, we speculate that this could be useful that this open structure may be advantageous for the integration of the ADM in vivo.

The different species have different fibril arrangements and those that are bimodal, such as porcine and bovine (a and b in figure 3), may have differing properties depending on direction. These differing properties, if known for each material, could be useful when selecting materials for specific surgical applications.

Acknowledgements

This research was supported by a grant from the TEI Biosciences. Bret Jessee and Vladimir Russakovsky of TEI Biosciences provided the samples. Research was undertaken on the SAXS/WAXS beamline at the Australian Synchrotron, Melbourne, Australia. The NZ synchrotron Group Ltd .is acknowledged for travel funding and accommodation. SEM was carried out at the Manawatu Microscopy Centre, Palmerston North.

14) Poster presented at the XXXIII International Congress of IULTCS 2015, 24-27th November, Novo Hamburgo, Brazil.

H. C. Wells[1], G. Holmes[2], R. G. Haverkamp[1]

[1]Massey University, New Zealand

[2]Leather and Shoe Research Association, Palmerston North, New Zealand

ABSTRACT

Microstructural Characterisation of Looseness in Bovine Leather using Ultrasound

Looseness is defect that affects the quality of a significant proportion of leather, particularly bovine and deer leather. This defect causes a lumpy appearance on the leather surface and results, greatly reducing the leathers value. The structural mechanism and causes of looseness in leather are not well understood; therefore this study aims to gain a better understanding of this. We have used small angle X-ray scattering, ultrasonic imaging, electron microscopy and tensile testing to characterize and compare the structures of loose and tight bovine leather. Loose leather can be characterized by highly aligned fibrils, resulting in weaker connections between the layers in leather. Loose leather also has a looser fibre packing arrangement, with larger gaps in between fibre bundles, particularly in the lower grain region of leather. We are able to see this characteristic loose, low density region using in-situ ultrasonic imaging and electron microscopy. We have used a range of techniques to gain a better understanding of the physical basis of looseness. This knowledge will be useful for further studies into the cause and prevention of looseness from developing during leather production.

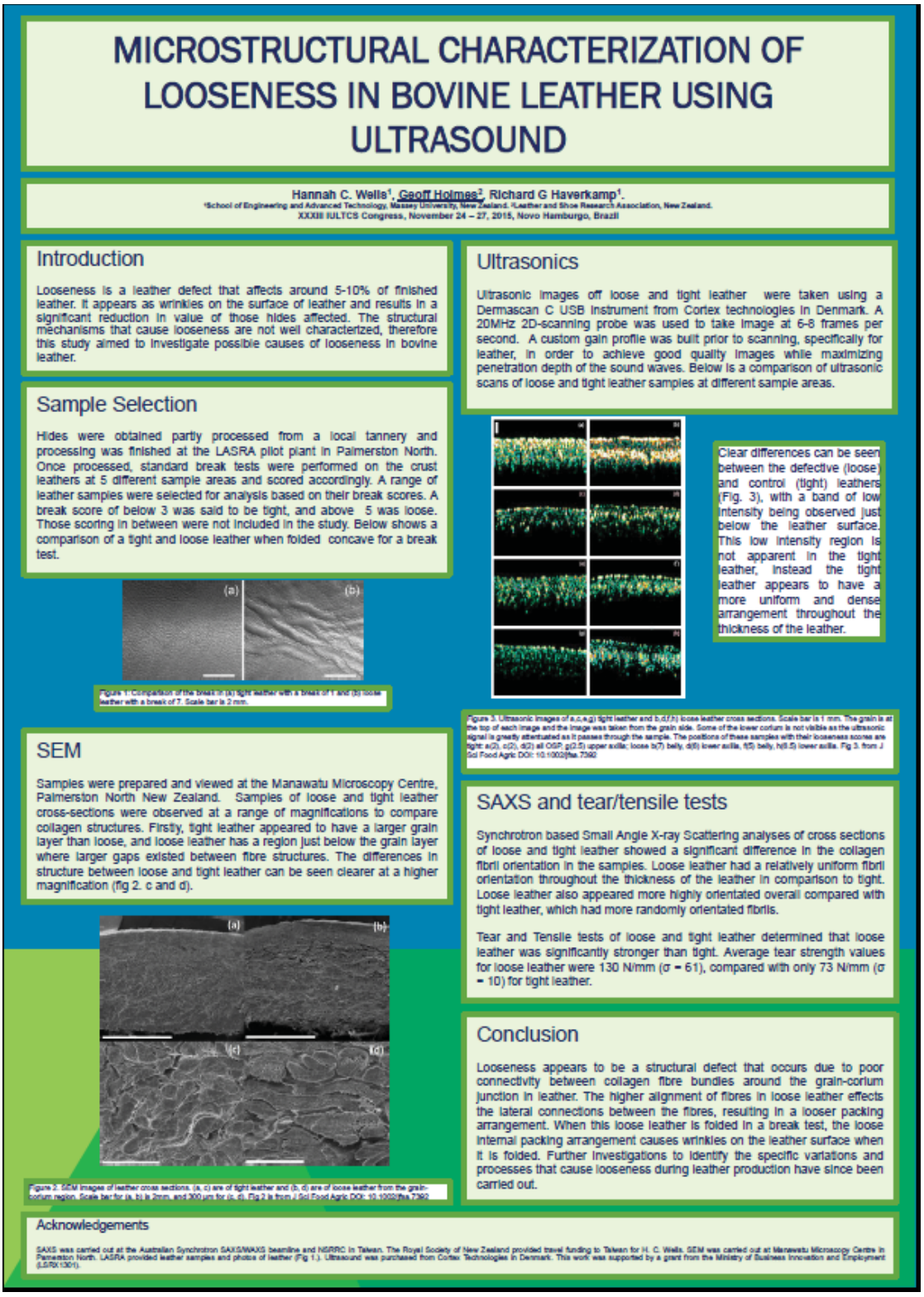

16) Poster presented at The International Chemical Congress of Pacific Basin Societies, 15-20th December 2015, Honolulu, Hawaii.

Hannah C. Wells[1], Katie H. Sizeland[1], Hanan Kayed[1], Nigel Kirby[2], Adrian Hawley[2], Stephen Mudie[2], Richard G. Haverkamp[1]

[1]*School of Engineering and Advanced Technolofy, Massey University, New Zealand*

[2]*Australian Synchrotron, Melbourne, Victoria, Australia*

ABSTRACT

Poisson Ratio of Collagen Fibrils under Tension

Tendon, pericardium, and skin are all primarily composed of type I collagen. Collagen is a fibrous protein that provides strength and stability to biological tissues. Therefore understanding the mechanical properties of collagen based materials is important for their natural and industrial uses. The properties of these bulk tissues have been widely studied, however the behaviour of the individual collagen fibrils that make up these tissues has not yet been studied.

In order to characterise the mechanical properties of individual collagen fibrils, we carried out measurements using small angled X-ray scattering (SAXS) on bovine pericardium tissue while applying stress. From the generated SAXS diffraction patterns we were able to calculate the diameter and elongation of the fibrils, which we could then use to calculate the Poisson ratio of collagen, and the orientation (OI) of the fibrils.

The tissue was strained up to 25% during data collection, which resulted in an observed strain of 4.5% (0.045) in the collagen fibrils. There appeared to be two distinct stages of changes in fibril structure during tissue strain. Initially, the strain was taken up by the reorientation of the collagen fibrils within the tissue. Secondly, above a strain of 0.09, the stress was mostly taken up by the individual fibrils, causing them to elongate.

From the information generated from SAXS, we determined a Poisson ratio of 2.1 ± 0.7 for collagen. The high Poisson's ratio (> 0.5) indicates a decrease in volume during strain. Previous studies on bulk collagen based materials have also shown high Poisson ratios. This study suggests that the unusual property of collagen based materials of a high Poisson ratio during stress may largely be due to the behaviour of the individual fibrils that make up the tissues.

Poisson Ratio of Collagen Fibrils Under Tension

Hannah C. Wells[1], Katie H. Sizeland[1], Hanan R. Kayed[1], Nigel Kirby[2], Adrian Hawley[2], Stephen T. Mudie[2] and Richard G. Haverkamp[1]
[1]School of Engineering and Advance Technology, Massey University, New Zealand. [2]Australian Synchrotron, 800 Blackburn Road, Melbourne, Victoria, Australia.
Poster presented at Pacifichem 2015 Conference, Honolulu, Hawaii. Poster area [8] Materials and Nanoscience #309

Introduction

Type I collagen is the primary structural component in biological tissues such as skin, tendon and heart pericardium. Due to collagens unique properties and strength, it is widely used in the cosmetic and surgical industries for reconstruction and wound healing, as well as being the structural foundation in leather, produced from skin and hides. The bulk properties of collagen materials have been widely studied, however little is known about the mechanical properties of individual collagen fibres that make up these tissues. Here we aim to study this.

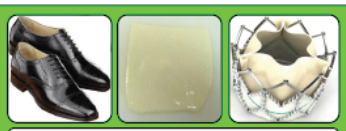

Figure 1. Examples of industrial uses of collagen based biomaterials. (a) shoes made from bovine leather, (b) acellular dermal matrix materials used for surgical applications and wound healing, (c) bovine pericardium used for heart valve transplants.

Methods

Synchrotron based small angle X-ray scattering (SAXS) was used to characterize the structure and mechanical behaviour of collagen fibrils . Samples of bovine heart pericardium were used as the subject material. SAXS data was collected while the sample were subjected to tension and scattering patterns were recorded at 1 mm increments until the sample failed.
A similar SAXS set up to that shown below in figure 2 was used.

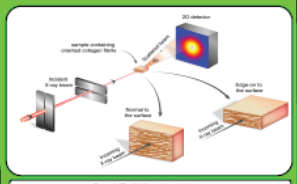

Figure 2. The SAXS experimental set-up

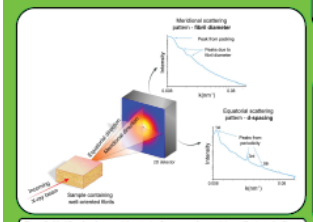

Figure 3. Meridional and equatorial scattering from a sample containing well-oriented collagen fibrils.

The average collagen fibril diameter, fibril elongation and fibril orientation were determined from integrated intensity plots from the SAXS scattering patterns. An example of an integrated scattering pattern in shown in figure 4.
The fibril d-spacing was used as a measure of fibril elongation.

From the change in fibril diameter (D) and length (L), the Poisson ratio was calculated for a rod shape from the formula:

$$\nu' = -\frac{\sqrt{R/2}\frac{\Delta D}{D}}{\Delta L/L}$$

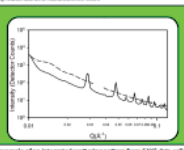

Figure 4. An example of an integrated scattering pattern from SAXS data collected for pericardium. Solid line is at an azimuthal angle centered 90°, which is used to determine the d-spacing. The dashed line is at an azimuthal angle of 0° which is used for fibril diameter.

Results

The maximum strain recorded before tissue rupture was 25%. There appeared to be two distinct stages in the behaviour of the collagen fibrils during strain (figure 5).
The first stage, up to a strain of around 0.09, there is a large increase in OI, indicating the fibrils are moving to become more aligned. During the initial change there are only small changes in fibril diameter and d-spacing.

The second stage, at a strain above 0.09, the d-spacing increases significantly along with a decrease in fibril diameter, indicating stress is now on the individual fibrils causing them to stretch out.

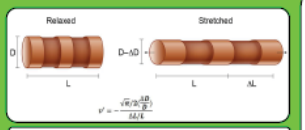

Figure 6. Illustration demonstrating the calculation of the Poisson ratio (ν') from the change in fibril diameter and fibril length when strain is applied.

Acknowledgments

This research was carried out at the SAXS/WAXS beamline at the Australian Synchrotron, Melbourne, Victoria, Australia. Nigel Kirby, Stephen Mudie and Adrian Hawley are thanked for their assistance in the beam line set-up . The NZ Synchrotron Group Ltd., is acknowledged for providing travel funding to the synchrotron.

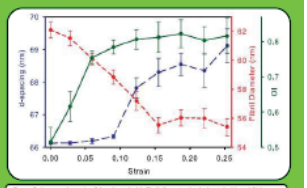

Figure 5. Average d-spacing (blue, long dash), fibril diameter (red, short dash) and OI (green, solid) changes with increasing strain.

The Poisson ratio was calculated from the change in fibril diameter and d-spacing determined during strain. For a tissue strain from 0 to 25%, the Poisson ration was calculated to be 2.1 ± 0.7.

This high Poisson ratio indicates a decrease in volume in the fibrils as strain is increased. This behaviour is unlike most engineering materials.

Conclusion

We have provided experimental evidence that collagen fibrils may have a Poisson ratio that is above 0.5. A Poisson ratio of 2.1 ± 0.7 suggests there is a decrease in volume in the fibrils when strain is applied. The decrease in volume could be due to tighter packing within the fibril under strain, due to the compression of hydrogen bonding within either the tropocollagen molecule, microfibril or fibril. Another explanation could be that water is being excluded from the fibrils when they are stretched.

The behaviour of collagen fibrils seen here could be contributing to collagens remarkable strength and unique properties. This may be helpful for the wide range of current industrial applications of collagen, as well as for the discovery of new applications.

Australian Synchrotron

MASSEY UNIVERSITY
TE KUNENGA KI PŪREHURO
UNIVERSITY OF NEW ZEALAND

17) Symposium presented at The International Chemical Congress of Pacific Basin Societies, 15-20th December 2015, Honolulu, Hawaii.

Hannah C. Wells[1], Katie H. Sizeland[1], Richard L. Edmonds[2], William Aitkenhead[2], Peter Kappen[3], Chris Glover[3], Bernt Johannessen[3], Richard G. Haverkamp[1]

[1]School of Engineering and Advanced Technology, Massey University, New Zealand

[2]Leather and Shoe Research Association, Palmerston North 4446, New Zealand

[3]Australian Synchrotron, Melbourne, Victoria, Australia

ABSTRACT

Mitigating Environmental Risks of Chromium from Leather Waste

There are environmental concerns around the possibility of chromium leaching into the environment from the disposal of chromium containing leather waste. Waste from chrome-tanned leather, both post-consumer and tanning industry scrap, must therefore be disposed of in an acceptable manner. We considered the option of producing biochar from leather waste and using this as a soil amendment. Chrome tanned leather was heated in an oxygen deficient environment at temperatures ranging from 500–1000 °C to form a char. The leaching characteristics of this char in 1 M HCl was measured. The chemical form of Cr in the char was analysed by synchrotron based Cr K edge X-ray absorption spectroscopy. It is found that there is minimal leach of Cr biochar in contrast to leather scap. The Cr is present in the char as highly dispersed Cr carbide, an insoluble and very stable material, and this accounts for the insolubility of leather char. Biochar made from leather waste largely eliminates the environmental availability of chromium from the waste and may be beneficial to the environment as both a soil enhancer and for long term carbon sequestration.

18) Poster presented at The International Chemical Congress of Pacific Basin Societies, 15-20th December 2015, Honolulu, Hawaii.

Katie H. Sizeland[1], Hannah C. Wells[1], John Higgins[2], Crystal M Cunanan[3], Nigel Kirby[4], Adrian Hawley[4], Stephen T. Mudie[4], Richard G. Haverkamp[1]

[1]School of Engineering and Advanced Technology, Massey University, New Zealand

[2]Southern Lights Biomaterials, Palmerston North, New Zealand

[3]*Structural Heart Division, Boston Scientific, Los Gatos, USA*

[4]*Australian Synchrotron, Melbourne, Victoria, Australia*

ABSTRACT

Structure and Strength of Neonatal Pericardium for Heart Valve Applications

Malfunctioning heart valve leaflets are surgically repaired by percutaneous delivery of replacement leaflets bioengineered from pericardium tissue. Replacements for the heart valve leaflets can be constructed from bovine pericardium. The strength of the material for a long life in service is of crucial importance; the thickness of the replacement material is also important as the device must fit through the inner diameter of arteries, some of which may narrowed. Neonatal bovine pericardium is thinner than adult pericardium. This research aims to provide a greater understanding of the properties of this biomaterial and the structural basis for these properties. The nanostructure of neonatal and adult bovine pericardium tissues are characterised by synchrotron-based small angle X-ray scattering (SAXS) and compared with the mechanical properties of these materials. Significant differences in structure were found between neonatal and adult tissue. The neonatal tissue has a higher degree of collagen alignment (orientation index (OI) = 0.78) than adult pericardium (OI = 0.62). The neonatal tissue also has a higher elastic modulus of 83.7MPa (than adult of 19.1 MPa) and a higher normalised ultimate tensile strength of 32.9MPa (adult 33.5 MPa).The higher alignment of collagen fibrils in neonatal pericardium provides the material with its increased strength. The physical properties of neonatal pericardium indicate it would be a suitable material for the heart valve leaflet replacements.

Structure and Strength of Neonatal Pericardium for Heart Valve Applications

K. H. Sizeland,[1] H. C. Wells,[1] J. Higgins,[2] C. Cunanan,[3] N. Kirby,[4] A. Hawley,[4] S. Mudie,[4] R. G. Haverkamp.[1]

[1]School of Engineering and Advanced Technology, Massey University, [2]Southern Lights Biomaterials, [3]Boston Scientific, [4]Australian Synchrotron.

Introduction

Malfunctioning heart valve leaflets are surgically repaired by percutaneous delivery of replacement leaflets that have been bioengineered from pericardium tissue. For a long life in service the strength of the material is of crucial importance; the thickness of the replacement material is also important as the device must fit through the inner diameter of arteries, some of which may be narrowed. This research aims to provide a greater understanding of the properties of this biomaterial and the structural basis for these properties. The nanostructure of neonatal and adult bovine pericardium tissues has been characterised by synchrotron-based small angle X-ray scattering (SAXS) and compared with the mechanical properties of these materials.

Methods

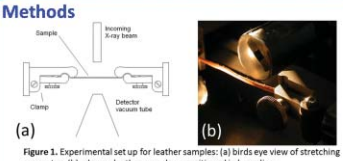

Figure 1. Experimental set up for leather samples: (a) birds eye view of stretching apparatus; (b) edge on leather sample as positioned in beamline.

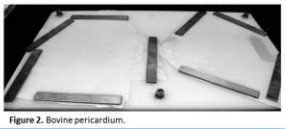

Figure 2. Bovine pericardium.

SAXS Analysis

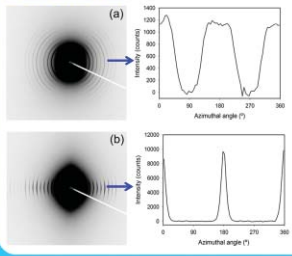

Figure 3. SAXS spectra of pericardium and plots of the intensity of a selected collagen peak at varying azimuthal angles for bovine pericardium samples: (a) A poorly aligned tissue; (b) a highly aligned tissue.

Strength Results

Table 1. Mechanical properties of adult and neonatal glutaraldehyde fixed bovine pericardium.

Test	Neonatal (n = 11) †	Adult (n = 13) †	P†
Small strain (<0.2) elastic modulus (MPa)	71.9 (11.6)	4.8 (2.0)	<0.0001
Large strain (>0.2) elastic modulus (MPa)	83.7 (10.6)	33.5 (3.2)	<0.0001
Ultimate tensile strength	32.9 (4.1)	19.1 (2.2)	0.0050
Strain at failure	0.48 (0.03)	0.80 (0.06)	0.0002

Orientation Index

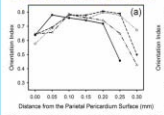

Figure 4. Variation of orientation index (OI) through the thickness of pericardium: (a) neonatal pericardium; (b) adult pericardium.

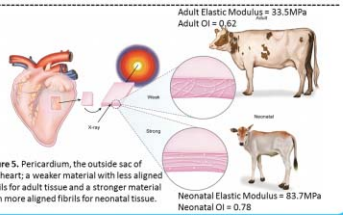

Figure 5. Pericardium, the outside sac of the heart; a weaker material with less aligned fibrils for adult tissue and a stronger material with more aligned fibrils for neonatal tissue.

Conclusions

Significant structural differences were found between neonatal and adult tissue. The neonatal tissue has a higher degree of collagen alignment, a higher elastic modulus , and a higher ultimate tensile strength than adult pericardium. This research shows that the higher alignment of the collagen fibrils provides the structural foundation for the superior strength of the neonatal pericardium. The physical properties of neonatal pericardium indicate it would be a suitable material for the heart valve leaflet replacements.

Acknowledgements

This research was supported by grants from the Ministry of Business, Innovation, and Employment. Southern Lights Biomaterials supplied the samples. This research was undertaken on the SAXS/WAXS beamline at the Australian Synchrotron, Victoria, Australia.

Appendix Two – Conference Papers

1) Symposium and conference paper presented at 65th Annual Leather and Shoe Research Association Conference, 13th August 2014, Wellington, New Zealand.

Hannah C. Wells[1], Katie H. Sizeland[1], Richard L. Edmonds[2], William Aitkenhead[2], Peter Kappen[3], Chris Glover[3], Bernt Johannessen[3], Richard G. Haverkamp[1].

[1] School of Engineering and Advanced Technology, Massey university, New Zealand

[2]Leather and Shoe Research Association, Palmerston North, New Zealand

[3]Australian Synchrotron, Melbourne, Victoria,Australia

Forming Biochar from Leather Waste to Reduce Leaching of Chromium into the Environment

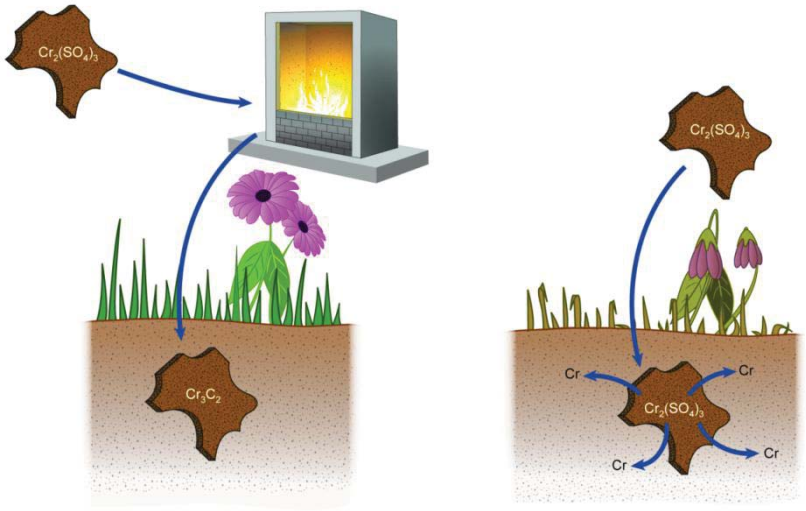

INTRODUCTION

Most leather is produced from skins and hides by tanning with chromium salts. Leather is used in upholstery (car and home), shoes and clothing but at the end of the life of these goods, the leather needs to be disposed of in an environmentally benign manner. Leather manufacture and production of goods from leather also produces leather scrap which requires disposal. Annual global leather production is about 6.8 million tonnes [7], around 80% of which contains Cr.

The main concern in the disposal of leather is the leaching from leather of Cr. Soluble Cr in a hexavalent oxidation state is considered to be undesirable in the environment [12, 17] and sites where Cr(VI) is present can require remediation [18].

Current and proposed leather disposal methods include: extraction of Cr before disposal [3, 5, 14]; disposal to wetlands for vegetation to absorb the Cr [9]; production of other reconstituted structural materials to bind the Cr in new products [2, 22]; and heating leather in an oxidizing environment to create a residue with soluble Cr [10, 28]. Cr contained in or on particulates from the burning of coal and biomass (in the presence of oxygen) can produce Cr(VI) [27]. Therefore, it is possible that burning leather may also generate Cr(VI), which is undesirable.

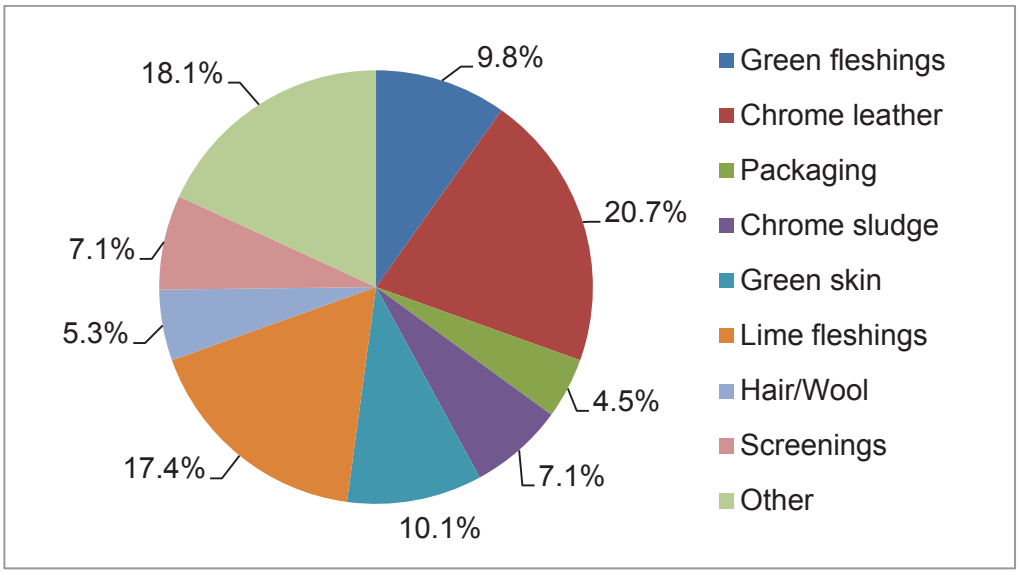

Figure 2: Breakdown of waste dumped in New Zealand landfills by the leather industry[29].

We have proposed that the production of biochar, carbonized organic matter, from waste leather may be a better alternative to other disposal methods[1]. Biochar is produced by heating organic matter in an oxygen deficient environment. The application of leather biochar is a way of sequestering carbon, thereby reducing the amount of carbon that may have otherwise become atmospheric CO_2. Biochar also has the demonstrated benefit of improving agricultural soil productivity[6]. Carbonized leather has previously been considered as a disposal option, with the suggestion of producing an activated carbon product for filtration applications [11, 21, 25].

Ideally, a leather biochar product could be produced that does not leach Cr. Exposing leather that has been "heat stablised" in a non-oxidising environment to leaching indicates that the material has a low solubility of Cr. Specifically, when leather was stablised at 350 °C or higher in a CO_2 environment, no soluble Cr is detected over a wide pH range in contrast to untreated, chrome-tanned leather [11]. It is also important that the Cr is resistant to oxidation, since both Cr oxidation and reduction between the Cr(III) and Cr(VI) couple [4] can occur in soils, depending on the nature and condition of the soils, and other factors that control the redox environment. This led to interest in the analysis of soils for the type of Cr contamination present [19, 20].

The chemical nature of Cr in leather has been characterised: Cr sulfate is used during tanning, and Cr bonds to the leather's collagen[8, 23] and is well dispersed. However, the form of Cr present in biochar is unknown, as are its stability and dispersion. In an earlier study of the leaching of leather after heat treatment in a non-oxidising environment, the chemical state of the Cr was not determined, despite some interest in doing so[11].

The purpose of the work reported here is to investigate the speciation and structure of the Cr in biochar produced from chrome-tanned leather as a function of the heating conditions. We wish to confirm the earlier reports of decreased solubility of Cr from leather heated in a non-oxidising environment and determine that the samples we are studying for Cr speciation do in fact exhibit low Cr solubility. Developing and understanding of the nature of entrapment of Cr in leather biochar may enable us to predict the likely stability of the Cr in the char in the

longer term. For the determination of the chemical speciation and structure of Cr, we use X-ray Absorption Spectroscopy (XAS) which is known to exhibit obvious spectral differences for different oxidation states and chemical environments.

EXPERIMENTAL

Standard, commercial chrome-tanned bovine leather was used for all experiments. The biochar was produced from leather by pyrolysis. Two pyrolysis reactors were used: a larger unit with no purge gas for the lower-temperature samples (up to 600 °C) and a smaller unit with the sample held under argon for higher-temperature samples (600–1000 °C). The temperatures were held for 1 hr before being cooled for analysis. Below is an overview of the experimental process carried out.

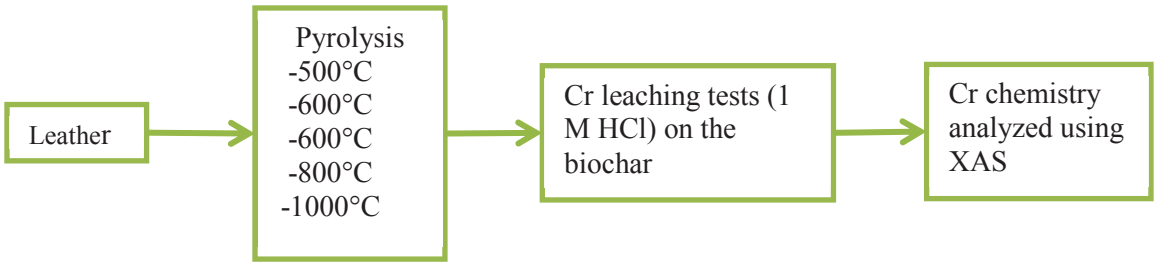

After pyrolysis, the char was measured for Cr content and leachable chromium. The Cr content of the char and leather samples was measured using a standard industry test method[15]. The leachable Cr was measured with duplicate samples of char (5 g) leached in 100 mL of 1 M HCl while shaken for 15 hours at room temperature. The Cr content of the aqueous HCl leachate was then assessed in duplicate with a Varian 220 SpectrAA using a standard industry test method[16].

XANES and EXAFS spectroscopic techniques were used to determine the chemical speciation and structure of the Cr in the leather and biochar samples from X-ray adsorption spectra recorded on the XAS beam line at the Australian synchrotron.

RESULTS

We found that a small amount of Cr can be leached from leather that has not been heat treated (Table 1), as has been reported previously[11]. After heating of the leather, the leachability of Cr diminishes. At 600 °C where the leather is clearly char no leaching of Cr could be detected (Table 1). In an earlier leaching study it was found that at 350 °C the Cr was found no longer able to be leached from the heated leather[11].

Table 1. Initial chromium content and leachable chromium of leather and of biochar samples produced under various heat treatments. No leachable Cr was detected in biochar samples formed at 600 °C or above.

Sample	**Initial % Cr (SD)**	**Leachable Cr, as % of initial Cr**
Leather	0.99 (0.01)	2.45
300 °C*	2.60 (0.02)	0.69

600 °C*	7.39 (0.04)	0.0007
600 °C†	11.8 (0.8)	0.08
800 °C†	12.5 (0.1)	0.06
1000 °C†	15.4 (0.1)	0.03

*Larger reaction vessel. †Finely ground, from small reaction vessel.

X-ray absorption near edge structure (XANES) is a spectroscopic technique carried out on the XAS beam line, that is element specific and is local bonding sensitive. XANES was carried out on both the chrome leather and biochar samples. The XANES spectrum of chrome leather is very similar to that of $Cr_2(SO_4)_3.xH_2O$. This is the salt that is used in chrome tanning, so clearly some structural aspects of this salt are retained in the tanned leather. The XANES spectrum of the biochar indicated significant differences with each 200°C increase. As the treatment temperature increases, the amount of carbide increases. The calculated proportions of carbide and Cr sulfate (represented as the dry leather spectrum) are listed in Table 2.

Table 2. Chemical components of linear combination fitting to the XAS energy spectrum. Uncertainty in mol% Cr in $Cr_2(SO_4)_3.xH_2O$ and Cr_2C_3 is around ± 5 %.

Sample	$Cr_2(SO_4)_3.xH_2O$ (mol % Cr)	Cr_2C_3 (mol % Cr)	R factor ($\times 10^{-4}$), χ^2
Biochar 500°C*	93	7	1.7, 0.027
Biochar 600°C*	77	23	3.4, 0.051
Biochar 600°C	59	41	5.6, 0.081
Biochar 800°C	35	65	5.8, 0.081

Biochar 1000°C	12	88	2.2, 0.031

*Larger reaction vessel.

Information about the structural environment of the Cr in the leather biochar is obtained from an analysis of the EXAFS range of the data acquired. The bond lengths obtained from the modelling of Fourier transform for EXAFS spectra of the biochar samples are given in table 3. The EXAFS analysis supports the XANES interpretation and confirms that Cr carbide is formed at higher temperatures.

Table 3. Bond lengths obtained from the modelling of Fourier transform of EXAFS spectra of leather biochar. Six scattering paths were combined for Cr-C, 12 paths for Cr-Cr in total (in two groups).

Sample	Cr-C (Å), coordination number	Cr-Cr (Å), coordination number	Cr-Cr (Å), coordination number
Biochar 800 °C	2.07, 3.6	2.58, 0.7	2.94, 3.0
Biochar 1000 °C	2.05, 1.7	2.70, 4.3	2.92, 1.8

Cr carbide is a very stable material, and is resistant to oxidation or reduction[26]. The charcoal or biochar matrix within which the Cr is contained is also known to be very stable in soils[24]. The addition of charcoal to soil enhances the agricultural productivity of the soil, for example in the traditional terra preta soils from South America[13] but also in more recent studies of soil productivity[6].

While we have found that using acid to produce biochar leachate does not remove Cr from the biochar, we have not performed long-term stability tests of the material in soil

environments. These would be desirable to ensure the safety of the material for use in agricultural settings.

CONCLUSION

We have shown that there may an environmental benefit in making biochar from chrome-tanned leather waste. The char does not release Cr with acid leaching, unlike untreated leather. We have also shown that the Cr becomes chemically reduced by a carbothermic reaction on charing, at high temperatures forming Cr carbide. Cr carbide is an inherently stable compound and its stability is further enhanced by being highly dispersed in a stable carbon medium. Biochar has the added benefits of enhancing agricultural production from soil and providing long-term sequestration of carbon from the environment. This strategy may turn a large-scale, potentially troublesome waste into an economic resource.

REFERENCES

1 W. Aitkenhead, and R. L. Edmonds, 'Biochar: A Possibility for Solid Waste Disposal', *Leather International,* 215 (2013), 28-30.

2 M. Ashokkumar, P. Thanikaivelan, K. Krishnaraj, and B. Chandrasekaran, 'Transforming Chromium Containing Collagen Wastes into Flexible Composite Sheets Using Cellulose Derivatives: Structural, Thermal, and Mechanical Investigations', *Polymer Composites,* 32 (2011), 1009-17.

3 J. C. Beltran-Prieto, R. Veloz-Rodriguez, M. C. Perez-Perez, J. L. Navarrete-Bolanos, E. Vazquez-Nava, H. Jimenez-Islas, and J. E. Botello-Alvarez, 'Chromium Recovery from Solid Leather Waste by Chemical Treatment and Optimisation by Response Surface Methodology', *Chemistry and Ecology,* 28 (2012), 89-102.

4 D. A. Brose, and B. R. James, 'Oxidation-Reduction Transformations of Chromium in Aerobic Soils and the Role of Electron-Shuttling Quinones', *Environmental Science & Technology,* 44 (2010), 9438-44.

5 L. F. Cabeza, M. M. Taylor, G. L. DiMaio, E. M. Brown, W. N. Mermer, R. Carrio, P. J. Celma, and J. Cot, 'Processing of Leather Waste: Pilot Scale Studies on Chrome Shavings. Isolation of Potentially Valuable Protein Products and Chromium', *Waste Management,* 18 (1998), 211-18.

6 K. Y. Chan, L. Van Zwieten, I. Meszaros, A. Downie, and S. Joseph, 'Agronomic Values of Greenwaste Biochar as a Soil Amendment', *Australian Journal of Soil Research,* 45 (2007), 629-34.

7 F.A.O. Commodities and Trade Division, United Nations, 'World Statistical Compendium for Raw Hides and Skins, Leather and Leather Footwear 1990-2011', (Rome: 2012).

8 Anthony D Covington, Graham S Lampard, Ozlem Menders, Alan V Chadwick, Georgios Rafeletos, and Paul O'Brien, 'Extanded X-Ray Absorption Fine Structure Sudies of the Role of Chromium in Leather Tanning', *Polyhedron,* 20 (2001), 461-66.

9 G. Dotro, S. Castro, O. Tujchneider, N. Piovano, M. Paris, A. Faggi, P. Palazolo, D. Larsen, and M. Fitch, 'Performance of Pilot-Scale Constructed Wetlands for Secondary

Treatment of Chromium-Bearing Tannery Wastewaters', *Journal of Hazardous Materials,* 239 (2012), 142-51.

10 M. Erdem, 'Chromium Recovery from Chrome Shaving Generated in Tanning Process', *Journal of Hazardous Materials,* 129 (2006), 143-46.

11 M. Erdem, and A. Ozverdi, 'Leaching Behavior of Chromium in Chrome Shaving Generated in Tanning Process and Its Stabilization', *Journal of Hazardous Materials,* 156 (2008), 51-55.

12 Y. Gao, and J. Xia, 'Chromium Contamination Accident in China: Viewing Environment Policy of China', *Environmental Science & Technology,* 45 (2011), 8605-06.

13 B. Glaser, L. Haumaier, G. Guggenberger, and W. Zech, 'The 'Terra Preta' Phenomenon: A Model for Sustainable Agriculture in the Humid Tropics', *Naturwissenschaften,* 88 (2001), 37-41.

14 E. Heidemann, 'Disposal and Recycling of Chrome-Tanned Materials', *Journal of the American Leather Chemists Association,* 86 (1991), 331-33.

15 ISO, 'Leather -- Chemical Determination of Chromic Oxide Content -- Part 1: Quantification by Titration', (2007).

16 'Leather -- Chemical Determination of Chromic Oxide Content -- Part 3: Quantification by Atomic Absorption Spectrometry', ISO 5398-3:2007 (IULTCS/IUC 8-3) (2007).

17 J. A. Izbicki, T. D. Bullen, P. Martin, and B. Schroth, 'Delta Chromium-53/52 Isotopic Composition of Native and Contaminated Groundwater, Mojave Desert, USA', *Applied Geochemistry,* 27 (2012), 841-53.

18 B. R. James, 'The Challenge of Remediating Chromium-Contaminated Soil', *Environmental Science & Technology,* 30 (1996), A248-A51.

19 P. Kappen, E. Welter, P. H. Beck, J. M. McNamara, K. A. Moroney, G. M. Roe, A. Read, and P. J. Pigram, 'Time-Resolved Xanes Speciation Studies of Chromium on Soils During Simulated Contamination', *Talanta,* 75 (2008), 1284-92.

20 R. R. Martin, S. J. Naftel, T. K. Sham, B. Hart, and M. A. Powell, 'Xanes of Chromium in Sludges Used as Soil Ameliorants', *Canadian Journal of Chemistry-Revue Canadienne De Chimie,* 81 (2003), 193-96.

21 L. C. A. Oliveira, M. C. Guerreiro, M. Goncalves, D. Q. L. Oliveira, and L. C. M. Costa, 'Preparation of Activated Carbon from Leather Waste: A New Material Containing Small Particle of Chromium Oxide', *Materials Letters,* 62 (2008), 3710-12.

22 A. Przepiorkowska, K. Chronska, and M. Zaborski, 'Chrome-Tanned Leather Shavings as a Filler of Butadiene-Acrylonitrile Rubber', *Journal of Hazardous Materials,* 141 (2007), 252-57.

23 T. Reich, A. Rossberg, C. Hennig, and G. Reich, 'Characterization of Chromium Complexes in Chrome Tannins, Leather, and Gelatin Using Extended X-Ray Absorption Fine Structure (Exafs) Spectroscopy', *Journal of the American Leather Chemists Association,* 96 (2001), 133-47.

24 M. W. I. Schmidt, M. S. Torn, S. Abiven, T. Dittmar, G. Guggenberger, I. A. Janssens, M. Kleber, I. Kogel-Knabner, J. Lehmann, D. A. C. Manning, P. Nannipieri, D. P. Rasse, S. Weiner, and S. E. Trumbore, 'Persistence of Soil Organic Matter as an Ecosystem Property', *Nature,* 478 (2011), 49-56.

25 G. Sekaran, K. A. Shanmugasundaram, and M. Mariappan, 'Characterization and Utilisation of Buffing Dust Generated by the Leather Industry', *Journal of Hazardous Materials,* 63 (1998), 53-68.

26 S. Sen, O. Ozdemir, A. S. Demirkiran, and U. Sen, 'Oxidation Kinetics of Chromium Carbide Coating Produced on Aisi 1040 Steel by Thermo-Reactive Deposition Method During High Temperature in Air', in *Materials and Manufacturing Technologies Xiv*, ed. by F. Yigit and M. S. J. Hashmi (2012), pp. 649-54.

27 A. F. Stam, R. Meij, H. T. Winkel, R. J. van Eijk, F. E. Huggins, and G. Brem, 'Chromium Speciation in Coal and Biomass Co-Combustion Products', *Environmental Science & Technology,* 45 (2011), 2450-56.

28 S. Tahiri, A. Albizane, A. Messaoudi, M. Azzi, J. Bennazha, S. A. Younssi, and M. Bouhria, 'Thermal Behaviour of Chrome Shavings and of Sludges Recovered after Digestion of Tanned Solid Wastes with Calcium Hydroxide', *Waste Management,* 27 (2007), 89-95.

2) Conference paper presented at the XXXIII International Congress of IULTCS 2015, 24-27th November, Novo Hamburgo, Brazil.

H. C. Wells[1], G. Holmes[2], R. G. Haverkamp[1]

[1]Massey University, New Zealand

[2]Leather and Shoe Research Association, Palmerston North, New Zealand

Microstructural Characterization of Looseness in Bovine Leather using Ultrasound

INTRODUCTION

Around 5-10% of bovine leather produced displays a defect known as looseness[1]. The defect looseness appears as undesirable wrinkles on the leather surface and results in a significant reduction of value of the affected hide. An entire finished leather is deemed rejected when looseness appears more than half-way up one side of the leather, and the leather becomes waste. The test for looseness involves a simple break test that occurs in the latter stages of the processing line, where an operator folds a piece of leather with the grain side in to observe and rank the surface wrinkles. The significant proportion of reject leather in the late stages of processing results in a significant waste of processing time and resources for leather tanneries. Despite the substantial loss in profit due to looseness, the industry has little understanding of the structure of loose leather and the causes. This work aims to gain more of an understanding of this.

MATERIALS AND METHODS

Leather preparation

Hides, weighing around 35kg, were obtained part-processed from either a local tannery or a pilot tannery. They had been green fleshed and processed using a conventional recipe based on sodium sulphide, sodium hydrosulfide and lime, where they were added to a 4 m diameter by 3.8 m wide drum along with the chemicals to depilate and open up the structure in order to removal of non-collagenous proteins. Around 8500 kg of hides were processed at a time and hides were removed from the rotating drums after 8 h of liming. They were then lime split to a thickness of 2.5-4.0 mm. It was through the lime splitter that the hides with more “draw” than others were selected for further processing at the LASRA pilot tannery with the hope of selecting some hides that produced loose leather for analysis. A conventional recipe for shoe leather production was used for onward processing at the LASRA pilot tannery. Selected hides were sammed and sett, toggle dried at 40°C and conditioned prior to Molissa staking.

Looseness Evaluation

The standard break test method was used to evaluate looseness in the crust leather[2]. This test involves folding the leather inwards grain side up and scoring the size of the surface wrinkles against a standard break scale. From the prepared leather, three crust leathers were selected and divided into five regions. Samples were taken from each region. Two operators measured and scored each leather sample and the results were averaged. From these scores the samples were deemed either loose or tight. Samples were considered tight if a break score of three or less was given, and loose if they had a break score of five or greater. Samples between 3 and 5 were not evaluated in this study.

Ultrasonic Imaging

A Dermascan C USB instrument (Cortex Technology, Denmark) was used for the ultrasonic measurements. A 20 MHz 2D-scanning probe with an internal water chamber was used to carry out the scanning at 6-8 frames per second. To achieve good image quality and minimize signal attenuation the scans were carried out under water and after the leather had been soaked for at least 24 h. Calibration of the sound velocity in leather was carried from the time of signal reflection and found to be 2561 m/s. The set bandwidth is 0.75 which results in an axial resolution of 97μm. The lateral resolution is set according to the mechanical scanning of the transducer at 150 μm. The focal point sits at a depth of 13 mm which falls approximately within the leather sample. A custom gain profile was created and the gain level was used for smaller adjustments of the signal amplification to improve signal penetration and image quality. The custom gain profile had a minimum sound intensity of 21 dB near the grain surface, increasing steadily to 42 dB within the corium.

Scanning electron microscopy

Samples were fixed for 8 h in a modified Karnovsky's fixative at room temperature. This was followed by three washes in phosphate buffer and dehydration in a graded ethanol series. Samples were critical point dried using the Polaron E3000 series II critical point drying apparatus with liquid CO_2 and ethanol. Samples were then mounted on to aluminium stubs and sputter-coated with gold (Baltec SCD 050 sputter coater) before being viewed in the FEI Quanta 200 Environmental Scanning Electron Microscope at an accelerating voltage of 20kV.

Small angle X-ray scattering

The Australian Synchrotron SAXS/WAXS beamline was used to record diffraction patterns. The beamline has an energy resolution of 10^{-4} from an undulator source and a cyro-cooled Si (III) double-crystal monochromator. The beam size is 250 x 150 μm full width half maximum (FWHM) at the sample, and has a photon flux of around 2 x 10^{12} ph/s. Diffraction patterns were recorded with an exposure time of 1-2 s and an X-ray energy of 11 keV. A

Pilatus 1M detector was used with an area of 981 x 1043 pixels, a sample-to-detector distance of 3371 mm and an active area of 170 x 170 mm. To calibrate the energy at 9.659keV, the zinc-K edge from zinc foil was used and maintained within 2 eV of the nominal energy.

For data collection, the samples were mounted individually on a remotely controlled sample plate and placed in the path of the X-ray beam. Spectra were recorded from the grain to the corium at 0.2 mm increments under constant humidity conditions. The SAXS diffraction data was processed using SAXS15ID software.

To measure the spread of orientation of the collagen fibrils within samples the Orientation Index (OI) was calculated. OI was calculated from the range in azimuthal angle of the most intense Bragg's peak at around 0.058-0.060 $Å^{-1}$, and is defined as (90° - OA)/90° where OA is the minimum azimuthal angle range that contains 50% of the fibril scattering intensity centred around the maximum peak intensity. An OI value of 0 indicates a completely isotropic orientation of fibrils within a material, where as an OI of 1 indicates completely parallel fibrils to each other.

Tear and tensile test

A standard method for double-edge tear testing was used to determine tear strengths[3, 4]. After being cut to size, samples were stored at 20°C and 650 g kg^{-1} relative humidity for 24 h before tear tests were carried out using an Instron 4467. Thickness was recorded using method BS EN ISO 2589:2002. Six measurements were taken on both loose and tight leather, 3 being parallel and 3 being perpendicular to the line of the backbone of the animal.

RESULTS AND DISCUSSION

Looseness in leather results from a structural deficiency which weakens the connections between layers within the leather structure. Until now, the details on the structure, and the region that the structural weaknesses occur, have not been known. Therefore we have investigated cross sections of leather with multiple structural characterisation techniques in

order to gain a better understanding of looseness and how it occurs. Below are the results and structural characteristics observed from each technique:

Break and Looseness

Loose leather displays larger wrinkles than tight when folded inwards towards the grain. An example of break for a loose (break of 7) and tight (break of 1) is shown in Figure 1. below.

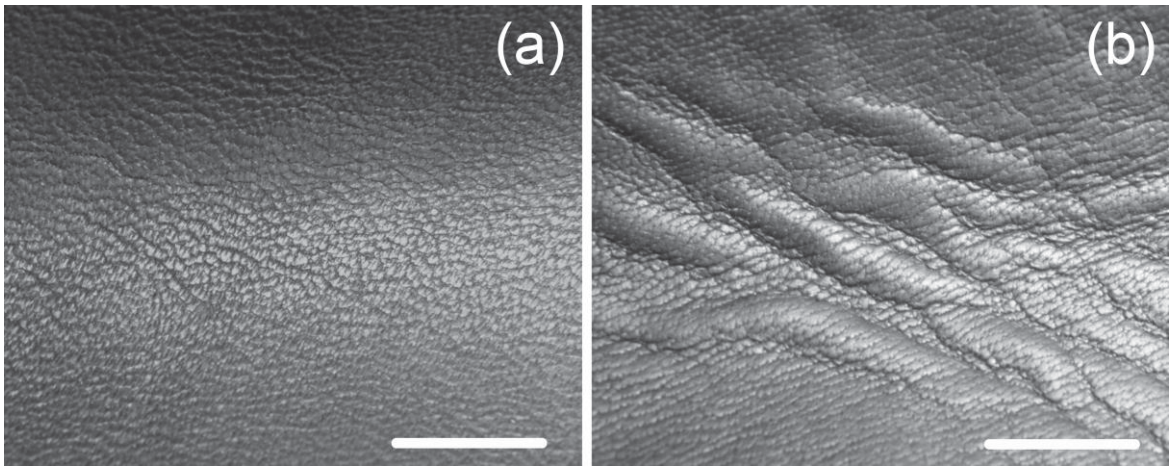

Figure 1: Comparison of the break in a) tight leather (break = 1) and b) loose leather (break = 7). Photos were taken of the concave surface of the grain while simulating the break test. Scale bar 10 mm. Figure 1 from J Sci Food Agric DOI: 10.1002/jfsa.7392.

Small Angle X-ray Scattering

SAXS analyses of cross sections of loose and tight leather showed a difference in fibril OI. Loose leather had a relatively uniform OI throughout the thickness of leather in comparison to tight leather, which showed a larger change in OI between the grain and corium regions. In tight leather, the corium had a much lower OI, suggesting a more isotropic fibril arrangement. Overall, loose leather had a higher average OI throughout the entire thickness of 0.61 ($\sigma = 0.01$) compared with 0.43 ($\sigma = 0.03$) for tight leather, $P < 0.001$ for $\alpha = 0.05$).

Ultrasonic Imaging

Clear differences can be seen between the ultrasonic images of tight and loose leather, as demonstrated in Figure 2.

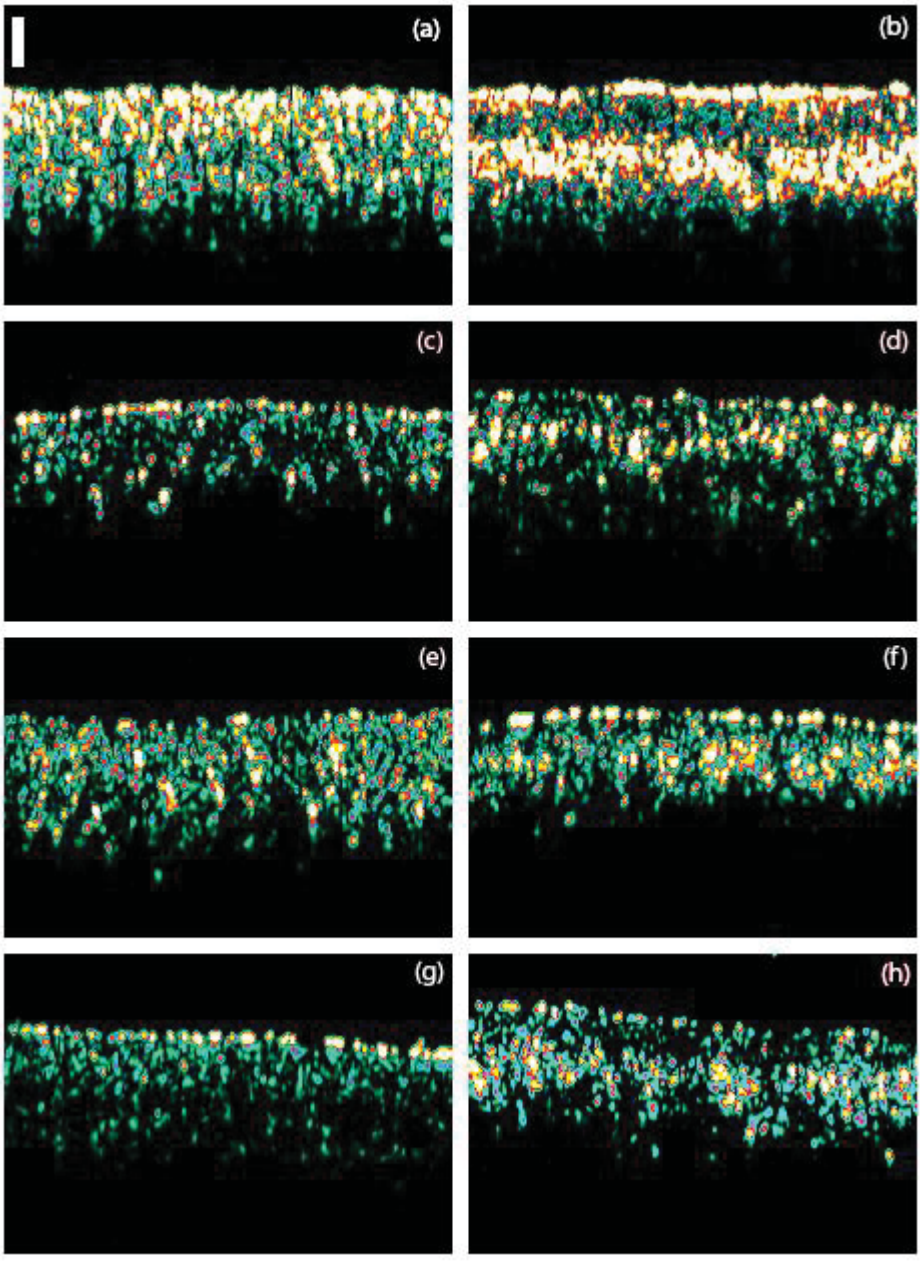

Figure 2: Ultrasonics image of a,c,e,g) tight leather and b,d,f,h) loose leather (scale bar 1 mm). The grain is at the top of each image and the image was taken from the grain side. Some of the corium (bottom of the leather) is not visible as the ultrasonic signal is greatly attenuated as it passes thought the sample positions of these samples with their looseness

scores are tight: a(2), c(2), d(2) all OSP, g(2.5) upper axilla; loose b(7) belly, d(6) lower axilla, f(5) belly, h(6.5) lower axilla. Figure 2 from J Sci Food Agric DOI: 10.1002/jfsa.7392.

We observe a band region of low intensity in the scans taken of loose leather that is not apparent in the tight leather. This band region could represent a less dense region of collagen fibres, with space or gaps existing between collagen fibres. The gap regions shown in the images would be filled with water due to the images being taken while the samples were submerged under water, however usually these gaps would be air gaps. Tight leather appears to have a very uniform and dense packing of fibres in the grain and grain-corium regions.

SEM

Scanning electron microscope images of tight and loose leather samples show also show a number differences between sample types.

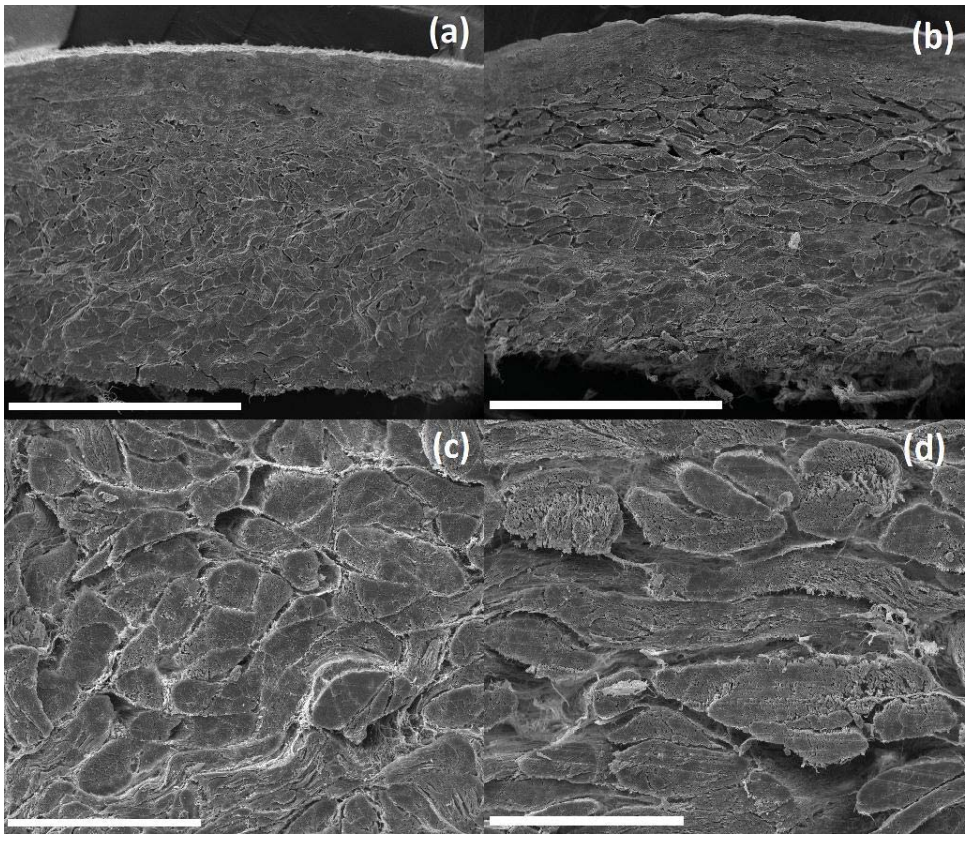

Figure 2: SEM images of leather cross sections. (a, c) are of tight leather and (b, d) are of loose leather from the grain-corium boundary region. Scale bar for (a, b) is 2 mm, and 300 μm for (c, d). Figure 3 from J Sci Food Agric DOI: 10.1002/jfsa.7392.

Firstly, tight leather appears to have a larger grain structure region than loose (Figure 3 a,b). This grain layer contains densely packed fibrils in both the tight and loose samples; however the loose samples appear to contain a region just below the grain where there are larger gaps between fibre structures. When viewed under a higher magnification, the difference in structure between the loose an tight samples around the grain-corium junction area is more obvious (Figure 3 c,d). The loose leather has larger cavities around the grain-corium boundary, whereas the tight leather does not appear to have these larger cavities and instead contains more uniform densely packed fibres.

Tear and tensile strength

Tear and tensile tests determined that loose leather was significantly stronger than tight with an average tear strength of 130 (σ = 61) N/mm, compared with 73 (σ = 10) N/mm (t = 16, $P < 0.001$ for $\alpha = 0.05$).

From the results collected from ultrasonic imaging, electron microscopy and SAXS it appears that loose leather has poorer inter-layer connections due to less over-lap of collagen fibre layers, resulting in a looser packing arrangement around the grain-corium junction region. This looser packing arrangement causes larger gaps in the structure and means the loose leathers are not as well held together as the tight, causing the grain to come apart slightly from the corium. The separation of the two layers causes the wrinkled appearance on the grain surface of loose leather in a break scale test.

The ultrasonic imaging is able to pick up on this looser packing arrangement, displaying a less dense band around the grain-corium boundary. This characteristic is similar to what is seen below the dermis of aged or sun damaged skin[5].

SEM images also reveal the larger gaps between fibre bundles in the looser sample, and images taken under a higher magnification also confirms this on a finer scale, with evidence of loose packing not only between fibre bundles but within fibre bundles of loose leather.

The SAXS OI profiles of loose and tight leather showed quite different results with loose leather having a much more aligned and uniform packing arrangement throughout the thickness of the leather. In studies carried out previously, OI profiles of strong tight bovine leather typically show a dip in OI around the middle layers of the leather, similar to what is

shown here for tight leather[6]. It appears that the absence of this feature in loose leather could be contributing to the lack of interconnections between layers of fibres, since fibres are not crossing over each other as much.

According to the tear and tensile tests, loose leather is stronger than tight, initially this may seem surprising. However an explanation can be provided that is consistent with the rest of the analytical results and previous work on the strength of leather and other collagen materials[7, 8, 9]. It is known that fibril orientation has a large influence on a material's strength since collagen fibrils are strong along the length of the fibril, however a much weaker bonding strength exists between fibrils. Therefore strong leather results when fibrils are highly aligned in the plane of the leather and the direction of stress in a tensile test. However, if the fibrils become too aligned, the fibrils are unable to maintain connections between each other and gaps are able to form, causing loose leather. Therefore, it can be said that optimal leather structure exists when the collagen fibres are aligned to give sufficient strength, but not so aligned that interconnecting layers are compromised and gaps or looseness is able to form.

CONCLUSION

Looseness appears to be a structural leather defect that is due to poor connectivity between layers of collagen fibres near the grain-corium boundary of leather. The higher alignment of the fibres in loose leather effects the lateral connections between fibre layers, and results in a loose packing arrangement. When loose leather is folded during a break test, the grain and corium layers become separated and wrinkles appear on the surface, giving poor break scores. A separate study is looking into whether looseness varies among different animals – for example, varying breed, age, condition, sun exposure and feed composition. Further investigation into why variations may cause looseness would then be an interesting topic to investigate.

REFERENCES

1) Thiele C, Tasman Tanneries, Personal communication, Wanganui, New Zealand (2014).
2) ASTM, D2941-13, Standard test method for measuring break pattern of leather
3) (break scale), Ed, ASTM International, West Conshohocken, PA. (2013).
4) Williams JMV, IULTCS (IUP) test methods - Measurement of tear load-double edge tear. *J Soc Leather Tech Ch* 84:327-329 (2000).
5) IULTCS, Leather - Physical and mechanical tests - Determination of tear load - Part 2: Double edge tear, Ed. ISO, Switzerland (2002).
6) Crisan D, Lupsor M, Boca A, Crisan M and Badea R, Ultrasonographic assessment of skin structure according to age. *Indian J Dermatol Venerol Leprol* 78:519 (2012).
7) Basil-Jones MM, Edmonds RL, Norris GE and Haverkamp RG, Collagen fibril alignment and deformation during tensile strain of leather: A SAXS study. *J Agric Food Chem* 60:1201-1208 (2012).
8) Sizeland KH, Basil-Jones MM, Edmonds RL, Cooper SM, Kirby N, Hawley A and Haverkamp RG, Collagen Alignment and Leather Strength for Selected Mammals. *J Agric Food Chem* 61:887-892 (2013).
9) Basil-Jones MM, Edmonds RL, Norris GE and Haverkamp RG, Collagen fibril alignment and deformation during tensile strain of leather: A SAXS study. *J Agric Food Chem* 60:1201-1208 (2012).
10) Sizeland KH, Wells HC, Higgins JJ, Cunanan CM, Kirby N, Hawley A and Haverkamp RG, Age Dependant Differences in Collagen Fibril Orientation of Glutaraldehyde Fixed Bovine Pericardium. *BioMed Res Int* 2014:189197 (2014).

3) Conference Paper presented at the XXXIII International Congress of IULTCS 2015, 24-27th November, Novo Hamburgo, Brazil.

Richard G. Haverkamp[1], Hannah C. Wells[1], Katie H. Sizeland[1], Richard L. Edmonds[2], Nigel Kirby[3], Adrian Hawley[3], Stephen Mudie[3]

[1]School of Engineering and Advanced Technology, Massey University, New Zealand.

[2] Leather and Shoe Research Association, Palmerston North, New Zealand

[3]Australian Synchrotron, Melbourne, Victoria, Australia

Collagen structure and strength in leather

ABSTRACT

Strength is an important property of leather. However the structural basis of strength in leather is not well understood. We have used synchrotron based small angle X-ray scattering combined with atomic force microscopy and electron microscopy to learn about the structure and strength of collagen materials under a variety of conditions. We have found that collagen alignment in the plane of the leather correlates strongly with strength in bovine and ovine leather and across a range of other mammals. Collagen fibril diameter has a weak correlation with strength in bovine leather. Changes in thickness and dryness during processing affect fibril orientation. Fat liquor modifies the native collagen structure in a systematic way. Strong leather is better able to distribute applied stress across the full thickness of leather than weak leather. These factors provide a better understanding at the nanostructural level of strength in leather.

INTRODUCTION

A large portion of leather produced globally is used for the production of footwear, upholstery and clothing, and many of these applications require good quality leather. One important property of leather is its strength. The strength of leather is largely dependent upon the properties and behaviour of the fibres that make up the material. Leather consists of long collagen fibres that interlink to form a mesh-like structure. The collagen fibres are held together in the mesh-like structure through cross-links, either natural or synthetic.

Small angle X-ray scattering has been used to determine structural characteristics of various leather materials with ranging strengths. The manner in which collagen provides strength to leather and the reason strength varies in different leather materials is the subject of this paper.

MATERIALS AND METHODS

Ovine, bovine and other animal leathers were prepared using conventional beamhouse and tanning processes with chrome tanning.

Synchrotron based small angle X-ray scattering was used to investigate the collagen structural arrangement [3]. This enables changes in the extent of orientation of the collagen fibrils to be quantified and the internal stress on the individual collagen fibrils to be measured [4]. Diffraction patterns were recorded on the Australian Synchrotron SAXS/WAXS beamline, utilizing a high-intensity undulator source. Energy resolution of 10^{-4} was obtained from a cryo-cooled Si (111) double-crystal monochromator and the beam size (FWHM focused at the sample) was 250 x 80 μm, with a total photon flux of about 2 x 10^{12} ph·s^{-1}. All diffraction patterns were recorded with an X-ray energy of 11 keV using a Pilatus 1M detector with an active area of 170 x 170 mm and a sample-to-

detector distance of 3371 mm. Exposure time for diffraction patterns was 1 s and data processing was carried out using the SAXS15ID software [11]. The partially processed leather samples were mounted onto a sample plate and sealed using kapton tape to prevent drying during X-ray analysis.

Orientation Index (OI) is used to measure the spread of orientation of the collagen fibrils. It is calculated from the azimuthal angle spread of the most intense Bragg's peak at around 0.058–0.060 $Å^{-1}$. OI is defined as (90° – OA)/90° where OA is the minimum azimuthal angle range, centered at maximum peak intensity, that contains 50% of the fibril scattering intensity. An OI value of 1 indicates that the fibrils are completely parallel to each other, while a value of 0 indicates orientation of the fibrils is completely isotropic.

Tear strengths were determined using standard methods for double-edge tear testing [21, 41]. Samples were cut and stored at 20 °C and 65% relative humidity for 24 hr before the tear strength was measured using an Instron 4467. Thickness was measured using method BS EN ISO 2589:2002.

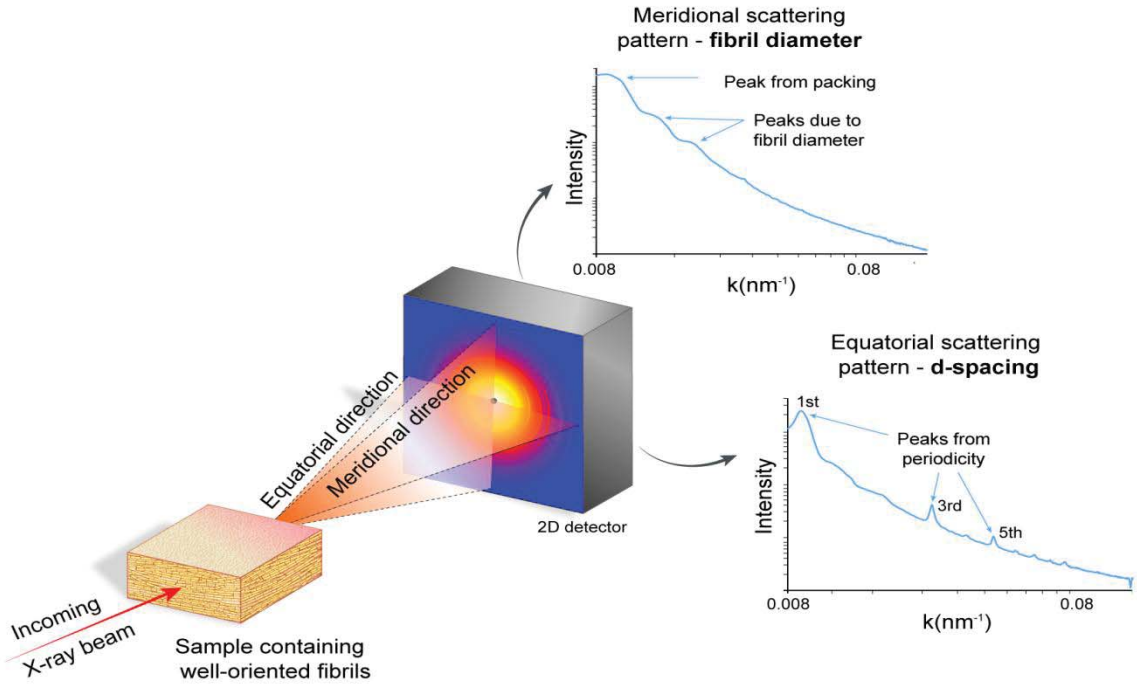

Figure 1. The SAXS experimental setup. Meridional and equatorial scattering from a sample containing well-oriented collagen fibrils.

RESULTS AND DISCUSSION

The collagen alignment in the plane of the leather is found to correlate strongly with strength in bovine and ovine leather [4] and across a range of other mammals [35] (Figure 2). Collagen fibrils are strong in the direction of the length of the fibril but connections between fibrils determine the strength of a collagen based material in the direction at right angles to the fibrils. These connections are relatively weak. These connections in green hide are largely glycosaminoglycans but these are removed during tanning and cross-links between fibrils are probably chromium complexes. The strength of these linkages is apparently much less than the strength of the collagen fibrils, and therefore

collagen materials are stronger in the direction in which the majority of fibrils are oriented.

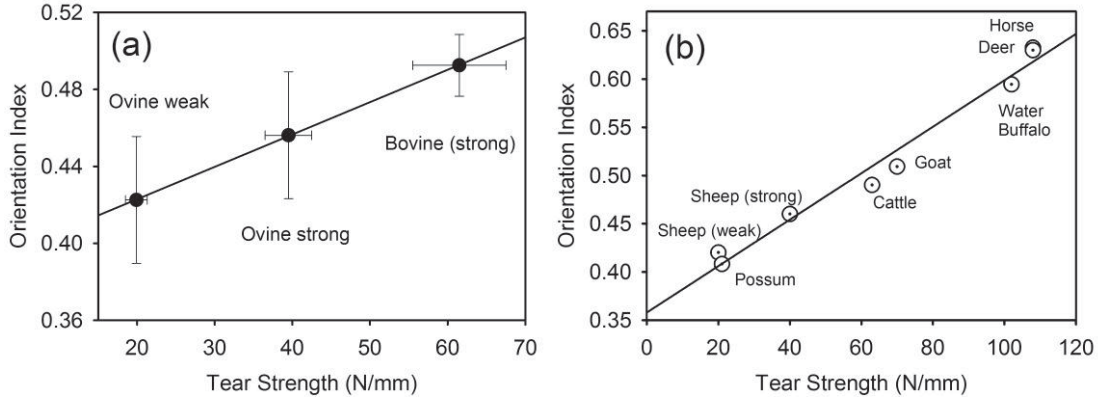

Figure 2. a) Orientation index versus tear strength for the averages of each of the leather types measured through the edge parallel to the backbone. Error bars for one standard deviation.; b) Orientation index versus tear strength for a range of animals. a) from *J. Agric. Food Chem.* 59(18) 9972-9979 ©American Chemical Society; b) from *J. Agric. Food Chem.* 61(4) 887-892 ©American Chemical Society.

It is possible with SAXS analysis to take points through the thickness of leather and observe the behavior of the collagen fibril orientation and strain during strain of the leather. We have found that there is a difference in the response to strain of strong and weak leather. Strong leather is better able to distribute applied stress across the full thickness of leather, and the load is taken up fairly evenly by the collagen fibrils throughout, whereas in weak leather there are points of high and of low stress within the leather. Failure therefore is likely in weak leather at lower overall stress because it will be initiated at the regions where stress is concentrated [5].

Collagen fibril diameter has been shown to have some influence on strength in tendons [27]. We have found a correlation of collagen fibril diameter with strength in bovine leather

where for larger diameter fibrils are present in stronger leather [39] although the correlation is not very strong (Figure 3).

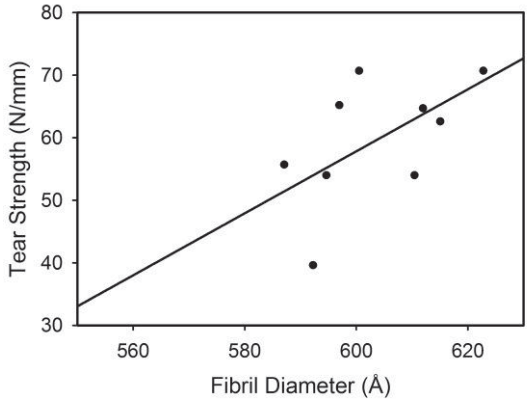

Figure 3. Collagen fibril diameter versus tear strength for bovine leather r^2 = 0.59, t = 3.4, P = 0.009 (for slope). Each point is the average value from 12–20 diffraction patterns. From *J. Agric. Food Chem.* 61(47) 11524-11531 ©American Chemical Society

Other factors have been shown to affect the orientation of collagen fibrils in leather. In particular, changes in thickness during processing results in a change in measured orientation index, with thicker stages having lower OI, but without fundamentally altering the structural arrangement of the collagen [33].

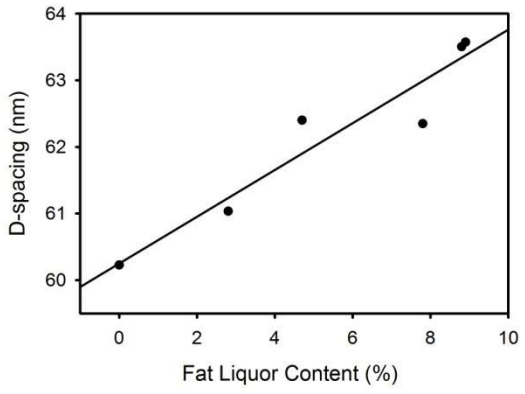

Figure 4. Collagen D-spacing versus measured fat liquor content for ovine leather. Each point is taken from the average of about 20 scattering patterns. Adapted from data presented in *J. Am. Leather Chem. Assoc.* , 110(3) 66-71 with the difference that here we show measured fat content rather than offered fat.

One of the final stages of leather manufacture is the addition of fat liquor to increase strength and impart suppleness to leather. We have investigated the action of fat liquor and find that it penetrates to the level of collagen fibrils and penetrates the fibrils to alter the structure of individual fibrils. This is evident in linear change in D-spacing with fat liquor content (Figure 4) [34]. However, despite the penetration within the collagen fibrils, the lubrication action of fat liquor appears to apply only at a structural level of fibers not fibrils [36]

The contribution of the mechanical properties of individual collagen fibrils to the mechanical properties of the tissue which they comprise has also been studied [40]. It was found that the collagen fibrils under tension exhibit a high Poisson's number, greater than 0.5 (Figure 5). This means that as a fibril is stretched the diameter contracts at an unusually high rate, resulting in a diminishing overall volume of the fibril. This is likely to impart a particular resistance to strain and could be a contributing mechanism to the strong an elastic properties of collagen.

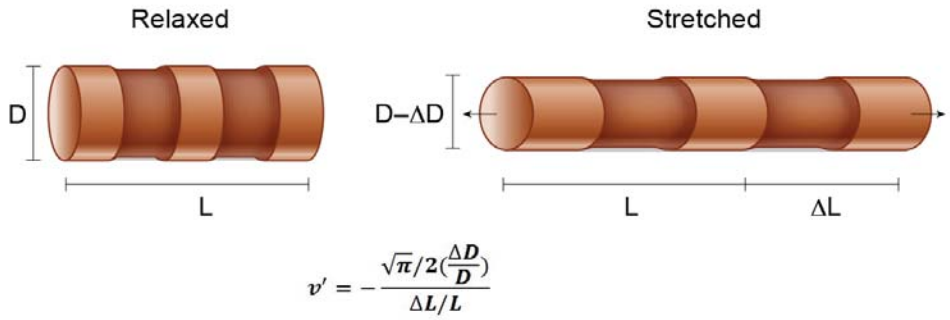

Figure 5. Schematic of a collagen fibril when stretched.

CONCLUSION

Fibril orientation was found to have a significant influence on the overall strength of leather, with higher fibril alignment in the plane of the leather leading to higher strength in that direction. Weak interactions exist between fibrils at right angles to the length of fibrils. Strong leather, with highly aligned fibrils in the plane of the leather, distributes an applied load more evenly through the thickness of the material compared with weak leather. Weak leather tends to have regions of high and low stress, which leads to failure at a lower load. Collagen fibril diameter was also shown to have a small influence on overall strength in bovine leather. When fibril diameters were combined with d-spacing values to calculate the Poisson's ratio, it was found that collagen exhibits a high Poisson ratio under stress, a characteristic that is unlike most engineering materials. By studying the collagen fibril component of leather including the orientation of the fibrils, the diameter, the changes with processing and chemistry and the behaviour under strain, it has been possible to understand better some of the strength and mechanical properties of leather.

References

1 W. Aitkenhead, and R. L. Edmonds, 'Biochar: A Possibility for Solid Waste Disposal', *Leather International,* 215 (2013), 28-30.

2 M. Ashokkumar, P. Thanikaivelan, K. Krishnaraj, and B. Chandrasekaran, 'Transforming Chromium Containing Collagen Wastes into Flexible Composite Sheets Using Cellulose Derivatives: Structural, Thermal, and Mechanical Investigations', *Polymer Composites,* 32 (2011), 1009-17.

3 Melissa M. Basil-Jones, Richard L. Edmonds, Timothy F. Allsop, Sue M. Cooper, Geoff Holmes, Gillian E. Norris, David J. Cookson, Nigel Kirby, and Richard G. Haverkamp, 'Leather Structure Determination by Small-Angle X-Ray Scattering (Saxs): Cross Sections of Ovine and Bovine Leather', *J. Agric. Food Chem.,* 58 (2010), 5286-91.

4 Melissa M. Basil-Jones, Richard L. Edmonds, Sue M. Cooper, and Richard G. Haverkamp, 'Collagen Fibril Orientation in Ovine and Bovine Leather Affects Strength: A Small Angle X-Ray Scattering (Saxs) Study', *J. Agric. Food Chem.,* 59 (2011), 9972-79.

5 Melissa M. Basil-Jones, Richard L. Edmonds, Gillian E. Norris, and Richard G. Haverkamp, 'Collagen Fibril Alignment and Deformation During Tensile Strain of Leather: A Small-Angle X-Ray Scattering Study', *J. Agric. Food Chem.,* 60 (2012), 1201-08.

6 J. C. Beltran-Prieto, R. Veloz-Rodriguez, M. C. Perez-Perez, J. L. Navarrete-Bolanos, E. Vazquez-Nava, H. Jimenez-Islas, and J. E. Botello-Alvarez, 'Chromium Recovery from Solid Leather Waste by Chemical Treatment and Optimisation by Response Surface Methodology', *Chemistry and Ecology,* 28 (2012), 89-102.

7 D. A. Brose, and B. R. James, 'Oxidation-Reduction Transformations of Chromium in Aerobic Soils and the Role of Electron-Shuttling Quinones', *Environmental Science & Technology,* 44 (2010), 9438-44.

8 L. F. Cabeza, M. M. Taylor, G. L. DiMaio, E. M. Brown, W. N. Mermer, R. Carrio, P. J. Celma, and J. Cot, 'Processing of Leather Waste: Pilot Scale Studies on Chrome

Shavings. Isolation of Potentially Valuable Protein Products and Chromium', *Waste Management,* 18 (1998), 211-18.

9 K. Y. Chan, L. Van Zwieten, I. Meszaros, A. Downie, and S. Joseph, 'Agronomic Values of Greenwaste Biochar as a Soil Amendment', *Australian Journal of Soil Research,* 45 (2007), 629-34.

10 F.A.O. Commodities and Trade Division, United Nations, 'World Statistical Compendium for Raw Hides and Skins, Leather and Leather Footwear 1990-2011', (Rome: 2012).

11 D. Cookson, N. Kirby, R. Knott, M. Lee, and D. Schultz, 'Strategies for Data Collection and Calibration with a Pinhole-Geometry Saxs Instrument on a Synchrotron Beamline', *J. Synchrotron Radiat.,* 13 (2006), 440-44.

12 Anthony D Covington, Graham S Lampard, Ozlem Menders, Alan V Chadwick, Georgios Rafeletos, and Paul O'Brien, 'Extanded X-Ray Absorption Fine Structure Sudies of the Role of Chromium in Leather Tanning', *Polyhedron,* 20 (2001), 461-66.

13 G. Dotro, S. Castro, O. Tujchneider, N. Piovano, M. Paris, A. Faggi, P. Palazolo, D. Larsen, and M. Fitch, 'Performance of Pilot-Scale Constructed Wetlands for Secondary Treatment of Chromium-Bearing Tannery Wastewaters', *Journal of Hazardous Materials,* 239 (2012), 142-51.

14 M. Erdem, 'Chromium Recovery from Chrome Shaving Generated in Tanning Process', *Journal of Hazardous Materials,* 129 (2006), 143-46.

15 M. Erdem, and A. Ozverdi, 'Leaching Behavior of Chromium in Chrome Shaving Generated in Tanning Process and Its Stabilization', *Journal of Hazardous Materials,* 156 (2008), 51-55.

16 Y. Gao, and J. Xia, 'Chromium Contamination Accident in China: Viewing Environment Policy of China', *Environmental Science & Technology,* 45 (2011), 8605-06.

17 B. Glaser, L. Haumaier, G. Guggenberger, and W. Zech, 'The 'Terra Preta' Phenomenon: A Model for Sustainable Agriculture in the Humid Tropics', *Naturwissenschaften,* 88 (2001), 37-41.

18 E. Heidemann, 'Disposal and Recycling of Chrome-Tanned Materials', *Journal of the American Leather Chemists Association,* 86 (1991), 331-33.

19 ISO, 'Leather -- Chemical Determination of Chromic Oxide Content -- Part 1: Quantification by Titration', (2007).

20 ———, 'Leather -- Chemical Determination of Chromic Oxide Content -- Part 3: Quantification by Atomic Absorption Spectrometry', ISO 5398-3:2007 (IULTCS/IUC 8-3) (2007).

21 IULTCS, 'Leather - Physical and Mechanical Tests - Determination of Tear Load - Part 2: Double Edge Tear', (Switzerland: ISO, 2002).

22 J. A. Izbicki, T. D. Bullen, P. Martin, and B. Schroth, 'Delta Chromium-53/52 Isotopic Composition of Native and Contaminated Groundwater, Mojave Desert, USA', *Applied Geochemistry,* 27 (2012), 841-53.

23 B. R. James, 'The Challenge of Remediating Chromium-Contaminated Soil', *Environmental Science & Technology,* 30 (1996), A248-A51.

24 P. Kappen, E. Welter, P. H. Beck, J. M. McNamara, K. A. Moroney, G. M. Roe, A. Read, and P. J. Pigram, 'Time-Resolved Xanes Speciation Studies of Chromium on Soils During Simulated Contamination', *Talanta,* 75 (2008), 1284-92.

25 R. R. Martin, S. J. Naftel, T. K. Sham, B. Hart, and M. A. Powell, 'Xanes of Chromium in Sludges Used as Soil Ameliorants', *Canadian Journal of Chemistry-Revue Canadienne De Chimie,* 81 (2003), 193-96.

26 L. C. A. Oliveira, M. C. Guerreiro, M. Goncalves, D. Q. L. Oliveira, and L. C. M. Costa, 'Preparation of Activated Carbon from Leather Waste: A New Material Containing Small Particle of Chromium Oxide', *Materials Letters,* 62 (2008), 3710-12.

27 D. A. D. Parry, G. R. G. Barnes, and A. S. Craig, 'Comparison of Size Distribution of Collagen Fibrils in Connective Tissues as a Function of Age and a Possible Relation between Fibril Size Distribution and Mechanical-Properties', *P. Roy. Soc. B-Biol. Sci.,* 203 (1978), 305-21.

28 A. Przepiorkowska, K. Chronska, and M. Zaborski, 'Chrome-Tanned Leather Shavings as a Filler of Butadiene-Acrylonitrile Rubber', *Journal of Hazardous Materials,* 141 (2007), 252-57.

29 T. Reich, A. Rossberg, C. Hennig, and G. Reich, 'Characterization of Chromium Complexes in Chrome Tannins, Leather, and Gelatin Using Extended X-Ray

Absorption Fine Structure (Exafs) Spectroscopy', *Journal of the American Leather Chemists Association,* 96 (2001), 133-47.

30 M. W. I. Schmidt, M. S. Torn, S. Abiven, T. Dittmar, G. Guggenberger, I. A. Janssens, M. Kleber, I. Kogel-Knabner, J. Lehmann, D. A. C. Manning, P. Nannipieri, D. P. Rasse, S. Weiner, and S. E. Trumbore, 'Persistence of Soil Organic Matter as an Ecosystem Property', *Nature,* 478 (2011), 49-56.

31 G. Sekaran, K. A. Shanmugasundaram, and M. Mariappan, 'Characterization and Utilisation of Buffing Dust Generated by the Leather Industry', *Journal of Hazardous Materials,* 63 (1998), 53-68.

32 S. Sen, O. Ozdemir, A. S. Demirkiran, and U. Sen, 'Oxidation Kinetics of Chromium Carbide Coating Produced on Aisi 1040 Steel by Thermo-Reactive Deposition Method During High Temperature in Air', in *Materials and Manufacturing Technologies Xiv*, ed. by F. Yigit and M. S. J. Hashmi (2012), pp. 649-54.

33 K. H. Sizeland, R. L. Edmonds, M.M. Basil -Jones, N Kirby, A Hawley, S. Mudie, and R. G. Haverkamp, 'Changes to Collagen Structure During Leather Processing', *J. Agric. Food Chem.,* 63 (2015), 2499-505.

34 K.H. Sizeland, H.C. Wells, G.E. Norris, R.L. Edmonds, N. Kirby, A. Hawley, S. Mudie, and R.G. Haverkamp, 'Collagen D-Spacing and the Effect of Fat Liquor Addition', *J. Am. Leather Chem. Assoc. ,* 110 (2015), 66-71.

35 Katie H. Sizeland, Melissa M. Basil-Jones, Richard L. Edmonds, Sue M. Cooper, Nigel Kirby, Adrian Hawley, and Richard G. Haverkamp, 'Collagen Orientation and Leather Strength for Selected Mammals', *J. Agric. Food Chem.,* 61 (2013), 887-92.

36 Katie H. Sizeland, Geoff Holmes, Richard L. Edmonds, Nigel Kirby, Adrian Hawley, Stephen T. Mudie, and Richard G. Haverkamp, 'Fatliquor Effects on Collagen Fibril Orientation and D-Spacing in Leather During Tensile Strain', *J. Am. Leather Chem. Assoc.,* 110 (2015).

37 A. F. Stam, R. Meij, H. T. Winkel, R. J. van Eijk, F. E. Huggins, and G. Brem, 'Chromium Speciation in Coal and Biomass Co-Combustion Products', *Environmental Science & Technology,* 45 (2011), 2450-56.

38 S. Tahiri, A. Albizane, A. Messaoudi, M. Azzi, J. Bennazha, S. A. Younssi, and M. Bouhria, 'Thermal Behaviour of Chrome Shavings and of Sludges Recovered after

Digestion of Tanned Solid Wastes with Calcium Hydroxide', *Waste Management,* 27 (2007), 89-95.

39 H. C. Wells, R. L. Edmonds, N. Kirby, A. Hawley, S. T. Mudie, and R. G. Haverkamp, 'Collagen Fibril Diameter and Leather Strength', *J. Agric. Food Chem.,* 61 (2013), 11524-31.

40 Hannah C. Wells, Katie H. Sizeland, Hanan R. Kayed, Nigel Kirby, Adrian Hawley, Stephen T. Mudie, and Richard G. Haverkamp, 'Poisson's Ratio of Collagen Fibrils Measured by Saxs of Strained Bovine Pericardium', *J. Appl. Phys.,* 117 (2015), 044701.

41 J. Williams, 'Iultcs (Iup) Test Methods - Measurement of Tear Load-Double Edge Tear', *J. Soc. Leather Tech. Ch.,* 84 (2000), 327-29.

Appendix Three – Client Reports and Articles

Three reports have been written and presented. These were:

1) Katie. H. Sizeland, **Hannah. C. Wells**, Melissa. M. Basil-Jones, Richard. L. Edmonds, Richard. G. Haverkamp "Leather Nanostructure and Performance" *International Leather Maker* **2014** Sept/Oct p30-34

2) Richard G. Haverkamp, **Hannah C. Wells**, Katie H. Sizeland, "Preliminary Comparison of the Collagen Fibril Structure of Bovine and Porcine Derived Acellular Dermal Matrix Materials" Pilot report prepared for TEI Biosciences Inc., Boston, USA **2014.**

Leather Nanostructure and Performance

*Katie H. Sizeland[1], Hannah C. Wells[1], Melissa M. Basil-Jones[1], Richard L. Edmonds[2], Richard G. Haverkamp[1]**

[1]School of Engineering and Advanced Technology, Massey University, Palmerston North, New Zealand; [2]Leather and Shoe Research Association, Palmerston North, New Zealand.

*r.haverkamp@massey.ac.nz

One of the very important properties of leather is its mechanical robustness including the tensile strength, tear resistance and flexibility. If one had a deep understanding of how this natural material achieves these properties, it might be possible to modify and improve aspects of the mechanical performance of leather. Here we describe how we have used some of the most sophisticated tools and techniques available to learn more about the structure of leather at the nanoscale and to relate this structure to the physical properties of leather.

Leather composition

Finished leather is primarily composed of type I collagen but also contains a myriad of other components in smaller quantities such as fats or oils, other proteins such as elastin, and cross-linking agents such as tannins or chrome. Each of these components may make some contribution to the physical properties of the leather. Because the major component of leather is type I collagen, we have focused first on its structure and have investigated how the fibrils of collagen are arranged in leather. We have studied how this arrangement varies among leather that has different physical properties and in leather when it is strained.

Structural analysis of leather via synchrotron based SAXS

The technique we have employed to quantify the collagen structure at the nanoscale is small angle X-ray scattering (SAXS). This technique was invented in the late 1930's. However, only recently has the technique been able to provide the sort of precise and detailed information that is useful for understanding leather structure. This has been possible with the advent of synchrotron based SAXS. Synchrotrons are large and expensive facilities that cater for a wide range of scientific studies. At the heart of the synchrotron is a ring, typically over 100 metres in diameter (Figure 1), with a stainless steel pipe pumped free of air inside. Bundles of high energy electrons, contained by a series of magnets (figure 2), circulate inside the ring at close to the speed of light. This travelling bundle of electrons is the source of X-rays of whatever energy you require or of other electromagnetic radiation such as UV, visible light or infrared radiation. For SAXS we use X-rays. To create the X-rays a device called an undulator is placed at one point on the ring. This causes the electrons that pass through to change direction producing X-rays. These X-rays are directed to the SAXS analysis equipment contained in a radiation proof hutch where samples to be investigated are placed (Figure 3). The X-ray beam can be tightly focussed (0.15 x 0.08 mm) and is fired through the piece of leather to be analysed. Most of the X-rays pass straight through but

some X-rays are scattered by the structure of the collagen. It is these scattered X-rays that are collected by a detector and the position of these X-rays provides a wealth of information on the dimensions, arrangement and other features of collagen fibrils in the leather.

Figure 1. The Australian Synchrotron, like most synchrotrons, is housed in a round building because the electrons travel in a ring with a large diameter.

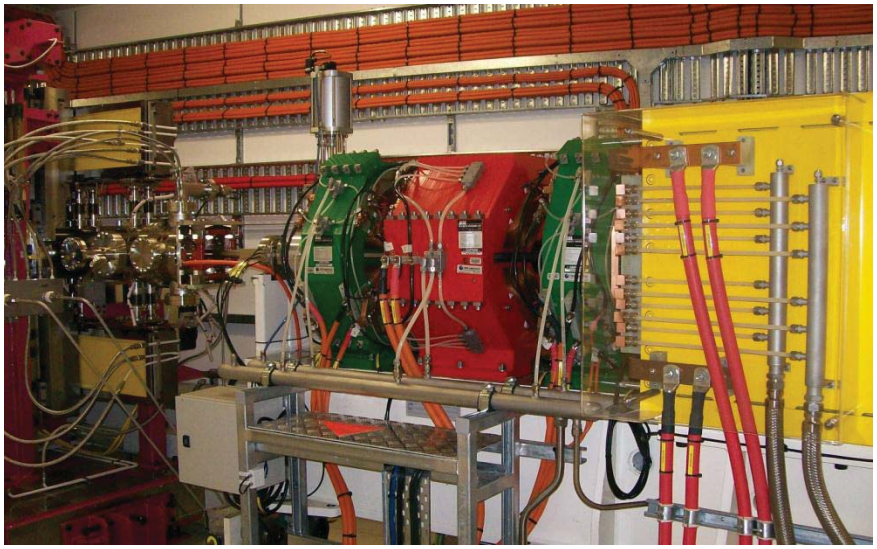

Figure 2. Magnets around the stainless steel pipe that contains the high energy electrons control the position of the electrons within the pipe as it goes around the synchrotron ring.

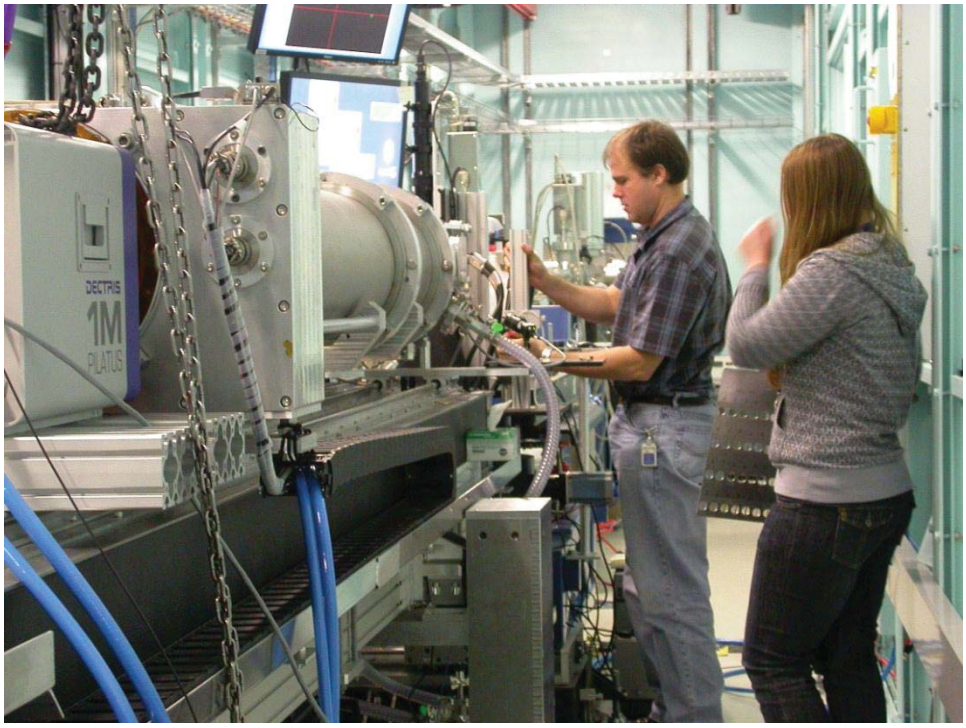

Figure 3. Mounting leather samples for analysis inside the SAXS hutch at the Australian Synchrotron.

What we can measure

From SAXS analysis of leather we have been able to extract four useful categories of information on the collagen structure. These are: 1) the average orientation of the collagen fibrils (which direction they are aligned in); 2) the spread of orientation of the fibrils (are they anisotropic or isotropic); 3) an accurate measure of the d-banding in the collagen (and this can tell us about the stress experienced by individual fibrils); and 4) the diameter of the collagen fibrils. Leather is of course a three dimensional material so measures of orientation can be in three orthogonal directions. By correlating some of these properties with mechanical tests of leather we can infer how changes in the structure of the collagen may affect the mechanical properties.

Collagen fibril orientation and tear strength

We looked at the variety of collagen structural factors we could measure and compared them with tear strength of leather to see if any were correlated. We did find a strong correlation in one of these. The tear strength for leather samples from about 600 ovine and bovine skins or hides (taken from the official sampling position) were measured using standard test methods. The collagen fibril orientations for these samples were measured using SAXS. We can quantify the collagen fibril orientation using an orientation index (OI) where an OI of 1 represents all fibrils are perfectly aligned (anisotropic) whereas an OI of 0 signifies a fully isotropic arrangement[13]. We found that there is a statistically very robust correlation between the tear strength and the fibril alignment in the direction edge on to the leather[14] (Figure 4a). Measured flat on (i.e. normal to the leather surface) there is not a strong correlation, it is only the edge on measurements that relate to tear strength. This correlation was also seen for a number of other mammals across a wider tear strength range[196] (Figure 4b). (Note that for the other mammals the figures do not necessarily represent average strength values for the species, but only for the samples we used.) In other words when the collagen is aligned in parallel planes the result is stronger leather. We have described a model to explain this relationship[196].

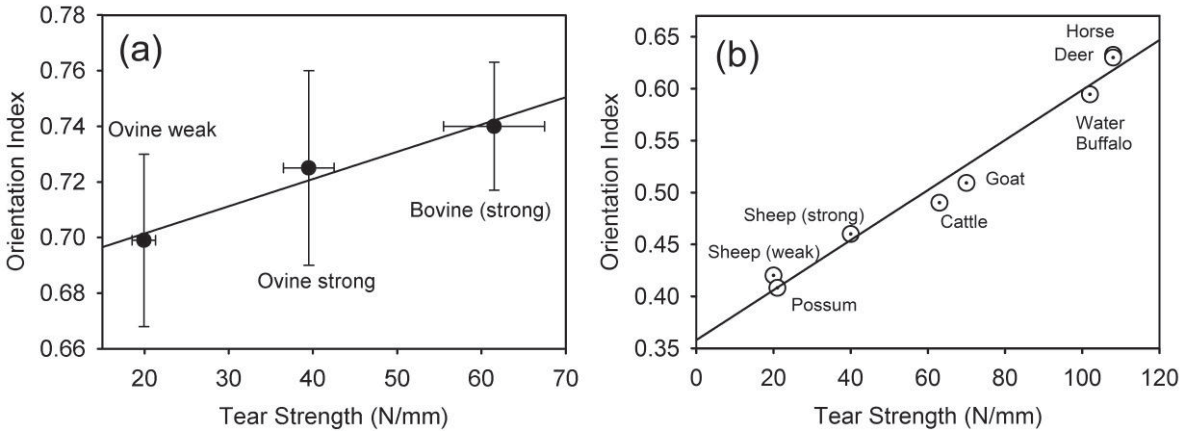

Figure 4. Leather tear strength and collagen fibril orientation. The orientation is measured edge on to the leather: a) Ovine and bovine leather (each point represents the analysis of samples from many skins); b) Other mammals (each point, excluding sheep weak, sheap strong and cattle, represents a sample from one skin). © American Chemical Society. Figure (a) from J. Agric. Food Chem. **59** (18), 9972-9979 (2011); Figure (b) from *J Agric Food Chem* **61** (4) 887-892 (2013).

What happens to the fibrils when leather is stretched?

It is possible with synchrotron based SAXS to measure the changes in the structure of the collagen fibrils in leather as a piece of leather is stretched. We built a stretching apparatus to measure the stress-strain on pieces of leather while simultaneously recording SAXS patterns. We found that when leather is stretched the first thing that happens is the fibrils begin to become more aligned in the direction of the applied force (this can be seen by an increase reduction in the OI). After about 15% extension, not much further alignment takes place but instead the individual collagen fibrils start to stretch (with little more alignment taking place)[12]. We can see the stretching because the change in d-spacing of collagen,

which is obtained from the SAXS, provides a measure of the force experienced by individual fibrils.

Differences through the thickness of leather

We also looked at how the arrangement and structure of collagen fibrils in leather varies through the grain and the corium both in a relaxed state and when under stress. The fibril orientation changes through the thickness of leather, as one would expect. We also found there are significant differences between bovine and ovine leather and especially between strong ovine leather and weak ovine leather. When strong leather is stretched, the tension is taken up by the fibrils through most of the thickness of the leather (which we can see from the d-spacing natural internal stress gauge), whereas when weak ovine leather is stretched the force is taken up unevenly. Hence it is not surprising that the leather with an uneven load distribution breaks at a lower force.

Fibril diameter and tear strength

There had been some suggestions for materials, such as tendon, that suggested fibril diameter is also important for strength with larger diameter collagen fibrils resulting in material with higher strength. We have also looked at this using SAXS to measure the fibril diameter and we did find a correlation for bovine leather, however it was only a weak correlation, and we did not find one for ovine leather[218].

Other aspects of leather structure and strength

There are many other aspects of leather structure and processing we can investigate with these techniques. We are now looking into changes to leather structure during processing. For example, when fat liquor is added to leather, what effect does it have on leather structure and how does it lubricate the fibres? How are the dynamics of leather stretching changed by the addition of fat liquor? We have discovered some interesting things and this work will shortly be submitted to the academic literature. What about the changes that take place in the processing of hide or skins to leather through each step of the conventional leathermaking process? It would be interesting to understand how each of these steps alters the collagen fibril arrangement and structure and why. We have nearly completed this work and are preparing a contribution for publication. We have also looked in more detail at what happens to collagen fibrils during stretching – how much thinner they get when they are stretched – and what implications this might have for the properties of the materials they form.

How can we use this information?

We hope that these fundamental investigations into collagen will ultimately be useful to the craft of leathermaking. If we understand how the arrangement of collagen differs in different leathers, how collagen behaves under stress, and what chemical processing does to the structure of collagen we may have the ability to control and manipulate these changes to produce improved or more consistent leather products.

References

1. Basil-Jones, M. M.; Edmonds, R. L.; Allsop, T. F.; Cooper, S. M.; Holmes, G.; Norris, G. E.; Cookson, D. J.; Kirby, N.; Haverkamp, R. G., Leather structure determination by small angle X-ray scattering (SAXS): Cross sections of ovine and bovine leather. *J. Agric. Food Chem.* **2010,** *58*, 5286-5291.
2. Basil-Jones, M. M.; Edmonds, R. L.; Cooper, S. M.; Haverkamp, R. G., Collagen fibril orientation in ovine and bovine leather affects strength: A small angle X-ray scattering (SAXS) study. *J. Agric. Food Chem.* **2011,** *59*, 9972-9979.
3. Sizeland, K. H.; Haverkamp, R. G.; Basil-Jones, M. M.; Edmonds, R. L.; Cooper, S. M.; Kirby, N.; Hawley, A., Collagen Alignment and Leather Strength for Selected Mammals. *J. Agric. Food Chem.* **2013,** *61*, 887-892.
4. Basil-Jones, M. M.; Edmonds, R. L.; Norris, G. E.; Haverkamp, R. G., Collagen fibril alignment and deformation during tensile strain of leather: A SAXS study. *J. Agric. Food Chem.* **2012,** *60*, 1201-1208.
5. Wells, H. C.; Edmonds, R. L.; Kirby, N.; Hawley, A.; Mudie, S. T.; Haverkamp, R. G., Collagen Fibril Diameter and Leather Strength. *J. Agric. Food Chem.* **2013,** *61*, 11524-11531.

MASSEY UNIVERSITY
GRADUATE RESEARCH SCHOOL

STATEMENT OF CONTRIBUTION TO DOCTORAL THESIS CONTAINING PUBLICATIONS

(To appear at the end of each thesis chapter/section/appendix submitted as an article/paper or collected as an appendix at the end of the thesis)

We, the candidate and the candidate's Principal Supervisor, certify that all co-authors have consented to their work being included in the thesis and they have accepted the candidate's contribution as indicated below in the *Statement of Originality*.

Name of Candidate: Hannah Wells

Name/Title of Principal Supervisor: Professor Richard Haverkamp

Name of Published Research Output and full reference:
H. C. Wells, G. Holmes, R. G. Haverkamp "Looseness in bovine leather: microstructural characterisation" (2015) J. Sci. Food Agric. DOI: 10.1002/jsfa.739

In which Chapter is the Published Work:

Please indicate either:

- The percentage of the Published Work that was contributed by the candidate: 90%
  and / or
- Describe the contribution that the candidate has made to the Published Work:

Candidate's Signature — 14/1/16 Date

Principal Supervisor's signature — 21/12/15 Date

MASSEY UNIVERSITY
GRADUATE RESEARCH SCHOOL

STATEMENT OF CONTRIBUTION TO DOCTORAL THESIS CONTAINING PUBLICATIONS

(To appear at the end of each thesis chapter/section/appendix submitted as an article/paper or collected as an appendix at the end of the thesis)

We, the candidate and the candidate's Principal Supervisor, certify that all co-authors have consented to their work being included in the thesis and they have accepted the candidate's contribution as indicated below in the *Statement of Originality*.

Name of Candidate: Hannah Wells

Name/Title of Principal Supervisor: Professor Richard Haverkamp

Name of Published Research Output and full reference: Early Detection of Looseness in Bovine Hides Using Ultrasonic Imaging.

→ Hannah C. Wells, Geoff Holmes, Richard G. Haverkamp. "Early Detection of Looseness in Bovine Hides using Ultrasonic Imaging." J. Am. Leather Chem. Assoc. (2015) 111 (2)

In which Chapter is the Published Work:

Please indicate either:

- The percentage of the Published Work that was contributed by the candidate: 90%

  and / or
- Describe the contribution that the candidate has made to the Published Work:

Candidate's Signature — 14/1/16 Date

Principal Supervisor's signature — 21/12/15 Date

MASSEY UNIVERSITY
GRADUATE RESEARCH SCHOOL

STATEMENT OF CONTRIBUTION TO DOCTORAL THESIS CONTAINING PUBLICATIONS

(To appear at the end of each thesis chapter/section/appendix submitted as an article/paper or collected as an appendix at the end of the thesis)

We, the candidate and the candidate's Principal Supervisor, certify that all co-authors have consented to their work being included in the thesis and they have accepted the candidate's contribution as indicated below in the *Statement of Originality*.

Name of Candidate: Hannah Wells

Name/Title of Principal Supervisor: Prof. Richard Haverkamp

Name of Published Research Output and full reference:

H. C. Wells, G. Holmes, H. Jeng, W-R Wu, N. Kirby, A. Hawley, S. Mudie, R.G. Haverkamp. "A Small Angle X-ray Scattering Study of the Structure and Development of Looseness in Bovine Hides and Leather"

In which Chapter is the Published Work:

Please indicate either:

- The percentage of the Published Work that was contributed by the candidate: 90%

  and / or
- Describe the contribution that the candidate has made to the Published Work:

Candidate's Signature — 14/1/16 Date

Principal Supervisor's signature — 21/12/15 Date

MASSEY UNIVERSITY
GRADUATE RESEARCH SCHOOL

STATEMENT OF CONTRIBUTION TO DOCTORAL THESIS CONTAINING PUBLICATIONS

(To appear at the end of each thesis chapter/section/appendix submitted as an article/paper or collected as an appendix at the end of the thesis)

We, the candidate and the candidate's Principal Supervisor, certify that all co-authors have consented to their work being included in the thesis and they have accepted the candidate's contribution as indicated below in the *Statement of Originality*.

Name of Candidate: Hannah Wells

Name/Title of Principal Supervisor: Prof Richard Haverkamp

Name of Published Research Output and full reference: H. C. Wells, K. H. Sicland, R. L. ~~Aitkenhead~~ Edmonds, W. Aitkenhead, P. Kappen, C. Glover, B. Johannessen, R. G. Haverkamp, "Stabilising Chromium from Leather Waste in Biochar." ACS Sustainable Chem Eng. 2: 1864-1870.

In which Chapter is the Published Work:

Please indicate either:

- The percentage of the Published Work that was contributed by the candidate: 80%

  and / or
- Describe the contribution that the candidate has made to the Published Work:

Candidate's Signature — 14/1/16 Date

Principal Supervisor's signature — 21/12/15 Date

MASSEY UNIVERSITY
GRADUATE RESEARCH SCHOOL

STATEMENT OF CONTRIBUTION TO DOCTORAL THESIS CONTAINING PUBLICATIONS

(To appear at the end of each thesis chapter/section/appendix submitted as an article/paper or collected as an appendix at the end of the thesis)

We, the candidate and the candidate's Principal Supervisor, certify that all co-authors have consented to their work being included in the thesis and they have accepted the candidate's contribution as indicated below in the *Statement of Originality*.

Name of Candidate: Hannah Wells

Name/Title of Principal Supervisor: Prof Richard Haverkamp

Name of Published Research Output and full reference:

H.C. Wells, R.L. Edmonds, N. Kirby, A. Hawley, S. Mudie, R.G. Haverkamp (2013) "Collagen Fibril Diameter and Leather Strength" J. Agric. Food. Chem. 61: 11524-11531.

In which Chapter is the Published Work:

Please indicate either:

- The percentage of the Published Work that was contributed by the candidate: 90%
  and / or
- Describe the contribution that the candidate has made to the Published Work:

Candidate's Signature — 14/1/16 Date

Principal Supervisor's signature — 21/12/15 Date

MASSEY UNIVERSITY
GRADUATE RESEARCH SCHOOL

STATEMENT OF CONTRIBUTION TO DOCTORAL THESIS CONTAINING PUBLICATIONS

(To appear at the end of each thesis chapter/section/appendix submitted as an article/paper or collected as an appendix at the end of the thesis)

We, the candidate and the candidate's Principal Supervisor, certify that all co-authors have consented to their work being included in the thesis and they have accepted the candidate's contribution as indicated below in the *Statement of Originality*.

Name of Candidate: Hannah Wells

Name/Title of Principal Supervisor: Professor Richard Haverkamp

Name of Published Research Output and full reference:

H.C. Wells, K.H. Sixeland, H.R. Kayed, N. Kirby, A. Hawley, S. Mudie, R.G. Haverkamp. "Poisson's Ratio of collagen Fibrils Measured by Small Angle X-ray Scattering of Stained Bovine Pericardium" (2015) J. Appl. Phys. 117 (4)

In which Chapter is the Published Work:

Please indicate either:

- The percentage of the Published Work that was contributed by the candidate: 90%

  and / or
- Describe the contribution that the candidate has made to the Published Work:

Candidate's Signature — 14/1/16 Date

Principal Supervisor's signature — 21/12/15 Date

MASSEY UNIVERSITY
GRADUATE RESEARCH SCHOOL

STATEMENT OF CONTRIBUTION TO DOCTORAL THESIS CONTAINING PUBLICATIONS

(To appear at the end of each thesis chapter/section/appendix submitted as an article/paper or collected as an appendix at the end of the thesis)

We, the candidate and the candidate's Principal Supervisor, certify that all co-authors have consented to their work being included in the thesis and they have accepted the candidate's contribution as indicated below in the *Statement of Originality*.

Name of Candidate: Hannah Wells

Name/Title of Principal Supervisor: Professor Richard Haverkamp.

Name of Published Research Output and full reference:
H.C. Wells, K.H. Sizeland, N. Kirby, A. Hawley, S. Mudie, R.G. Haverkamp. "Collagen Fibril Structure and Stength in Acellular Dermal Matrix Materials of Bovine, Porcine and Human Origin" (2015) ACS Biomat. Sci. Eng 1(10) 1026-1038

In which Chapter is the Published Work:

Please indicate either:

- The percentage of the Published Work that was contributed by the candidate: 80%
  and / or
- Describe the contribution that the candidate has made to the Published Work:

Candidate's Signature — 14/1/16 Date

Principal Supervisor's signature — 21/12/15 Date